THE UNIVERSITY
of EDINBURGH

This thesis has been submitted in fulfilment of the requirements for a postgraduate degree (e.g. PhD, MPhil, DClinPsychol) at the University of Edinburgh. Please note the following terms and conditions of use:

This work is protected by copyright and other intellectual property rights, which are retained by the thesis author, unless otherwise stated.
A copy can be downloaded for personal non-commercial research or study, without prior permission or charge.
This thesis cannot be reproduced or quoted extensively from without first obtaining permission in writing from the author.
The content must not be changed in any way or sold commercially in any format or medium without the formal permission of the author.
When referring to this work, full bibliographic details including the author, title, awarding institution and date of the thesis must be given.

Characterisation of the Active Site of Kynurenine 3-Monooxygenase

Helen B. Bell

Supervised by Dr Chris Mowat

Doctor of Philosophy

The University of Edinburgh

2016

Acknowledgements

I would like to acknowledge my supervisor Dr Chris Mowat for his advice and support throughout this project. I would also like to thank him for the opportunity to work in his group. I would also like thank my second supervisors Dr Simon Daff and Professor Steve Chapman. I would also like to acknowledge all the members of the Mowat group, past and present, particularly Dr Martin Wilkinson, Mark Taylor and Lindsay McGregor.

I would like to acknowledge Dr Gavin Milne for synthesising the inhibitor compounds used in this work. I would like to thank Dr Julia Richardson and the structural biology groups led by Professor Walkinshaw, Dr Marles-Wright and Dr Arulanandam for organising and including me in the beamtime allocations at the Diamond Light Source.

I would also like to thank Dr David Dryden for the use of the GraFit software. I would like to acknowledge Professor Dominic Campopiano and his group for use of the PCR machine and valuable discussions. I would also like to thank Graham Moran for the generous gift of the *Pf*KMO plasmid.

I also thank the University of Edinburgh for the award of a Principal's Career Development Scholarship which partly funded my studies.

I would like to thank all my colleagues, friends, and family (particularly my mother, Irene) for their continued enthusiasm and encouragement over the last four years.

Declaration

I declare that the work presented in this thesis is my own except where clearly indicated. This work has not been submitted for any other degree and has not yet been published. The results are in preparation for publication.

Lay Summary

Kynurenine 3-monooxygenase (KMO) is an enzyme that converts L-kynurenine to 3-hydroxykynurenine as part of the kynurenine pathway. In humans this pathway metabolises over 95% of dietary L-tryptophan, an essential amino acid. KMO has been implicated in a number of diseases including Alzheimer's disease, Huntington's disease and acute pancreatitis. In these conditions, a raised level of KMO occurs causing an increase in the level of 3-hydroxykynurenine present in cells to a potentially toxic level. As studies in animal models of disease and examination of samples from patients have implicated KMO, there is significant interest in understanding both the chemistry of this enzyme and also in developing effective inhibitors that could potentially provide drugs to treat these conditions. The KMO enzyme studied in this thesis is from the bacterium *Pseudomonas fluorescens,* as the human enzyme is insoluble.

The reaction catalysed by KMO occurs in the active site of the enzyme which contains a number of amino acids involved in recognising and binding L-kynurenine. By altering the identity of specific amino acids and studying the difference in the properties of the enzyme it is possible to determine the role of a particular amino acid in the original enzyme. Four amino acids in the active site have been investigated using kinetic experiments, which show changes in binding affinity of L-kynurenine or in the catalytic efficiency, and crystallography experiments, from which structural changes are observed. Three of the active site residues were shown to contribute to substrate binding, although changing two of these to structurally similar amino acids did not have a major effect on the chemistry of KMO whereas the slight change to the other caused the enzyme to become inactive.

There is only one difference in the active site amino acids present in *Pseudomonas fluorescens* and human KMO, and kinetic studies demonstrated that this amino acid does not have a major effect on substrate binding and therefore suggest that this enzyme is a good model for the human enzyme.

The ability of a set of inhibitor molecules to bind to the active site of the enzyme has also been investigated using kinetic and crystallographic methods. These inhibitors have been shown through kinetic assays to bind tightly but reversibly to the enzyme and provide useful insights both into the potential development of drugs targeting this enzyme and also into the interactions formed in the active site between the enzyme and small molecules.

Abstract

Kynurenine 3-monooxygenase (KMO) is a flavoprotein which has been implicated in Huntington's disease, Alzheimer's disease and acute pancreatitis. Recently there has been important research published about this enzyme including the structure of a truncated *Saccharomyces cerevisiae* KMO enzyme and KMO inhibition studies in animal models of disease. In previous work from this research group the complete *Pseudomonas fluorescens* KMO enzyme has been successfully crystallised both with and without the substrate, L-kynurenine, from which significant insights were gained into function and the potential role of domain movement.

To examine substrate binding in KMO and to consolidate previous structural studies, key residues in the active site have been investigated using site directed mutagenesis, crystallography and kinetic analysis using steady-state techniques. This analysis has identified the interactions between the enzyme and the substrate and provides a basis for inhibitor design. The residues implicated in substrate binding are N369, Y404 and R84. For N369 and Y404, minor changes to the amino acid in the mutations N369S and Y404F were shown to cause a decrease in binding affinity of the substrate but the enzyme remained active. For the mutations Y404A and R84K enzyme activity was significantly affected. Crystal structures of N369S, Y404F and R84K were also obtained.

Another residue in the active site studied was H320 which is the only amino acid to differ in the active sites of the human and *Pseudomonas fluorescens* enzymes. This residue was therefore of interest to determine whether the bacterial enzyme used in this work is likely to be a good model for the human enzyme, which has not yet been successfully isolated in significant quantities for *in vitro* research. Modifying this residue to obtain H320F KMO revealed that this residue does not have a significant role in substrate binding.

Potent inhibitor molecules have been studied with this enzyme and shown in kinetic assays to have nanomolar K_i values. These inhibitors are the most potent inhibitors studied with *Pseudomonas fluorescens* to date and continue previous inhibitor studies carried out with this enzyme. This group of inhibitors contain different substituents in the part of the molecule shown to bind closest to the C-terminal domain of the protein. These novel inhibitors do not allow the flavin to be reduced by NADPH (which results in unwanted peroxide production) unlike a number of previously studied molecules and therefore have the potential to be clinically useful.

This research therefore answers many questions about this enzyme, in particular about the role of particular residues in the active site, substrate recognition and inhibition of this important drug target.

Abbreviations

Amino acids:

Amino Acid Name	Three letter code	One letter code
Alanine	Ala	A
Asparagine	Asn	N
Aspartic Acid	Asp	D
Arginine	Arg	R
Cysteine	Cys	C
Glutamic Acid	Glu	E
Glutamine	Gln	Q
Glycine	Gly	G
Histidine	His	H
Isoleucine	Ile	I
Leucine	Leu	L
Lysine	Lys	K
Methionine	Met	M
Phenylalanine	Phe	F
Proline	Pro	P
Serine	Ser	S
Threonine	Thr	T
Tryptophan	Trp	W
Tyrosine	Tyr	Y
Valine	Val	V

Nucleotides:

Adenine	A
Cytosine	C
Guanine	G
Thymine	T

General Abbreviations:

AMPA	α-amino-3-hydroxy-5-methyl-4-isoxazolepropionic acid
BLAST	basic local alignment search tool
DMSO	dimethyl sulfoxide
DNA	deoxyribonucleic acid
dNTPs	deoxyribonucleotides
DTT	dithiothreitol

E. coli	*Escherichia coli*
EDTA	ethylenediaminetetraacetic acid
FAD	flavin adenine dinucleotide
FPLC	fast protein liquid chromatography
g/mg/µg	grams/milligrams/micrograms
HEPES	4-(2-Hydroxyethyl)piperazine-1-ethanesulfonic acid
IDO	indoleamine 2,3-dioxygenase
IFN-γ	interferon-γ
KAT	kynurenine aminotransferase
k_{cat}	turnover number
K_M	Michaelis-Menten constant
KMO	kynurenine 3-monooxygenase
l/ml/µl	litre/millilitre/microlitre
LB	Luria broth
LDS	lithium dodecyl sulfate
MES	2-(N-morpholino)ethanesulfonic acid
MHPCO	2-methyl-3-hydroxypyridine-5-carboxylic acid oxygenase
M/mM/µM/nM	molar/millimolar/micromolar/nanomolar
MW	molecular weight
NAD	nicotinamide adenine dinucleotide
NADPH	nicotinamide adenine dinucleotide phosphate
NMDA	N-methyl-D-aspartate
^oC	degrees Celsius
PCR	polymerase chain reaction
PDB	Protein Data Bank
PEG	polyethylene glycol
*Pf*KMO*	C252S C461S *Pseudomonas fluorescens* kynurenine 3-monooxygenase
PHB	para-hydroxybenzoate
PHBH	para-hydroxybenzoate hydroxylase
PLP	pyridoxal 5´-phosphate
PMSF	phenylmethylsulfonyl fluoride
RNA	ribonucleic acid
rpm	revolutions per minute
s	seconds
S. cerevisiae	*Saccharomyces cerevisiae*

SDS-PAGE	sodium dodecyl sulfate – polyacrylamide gel electrophoresis
SOC	Super optimal broth with catabolite repression
TAE	tris-acetate-EDTA buffer
TDO	tryptophan 2,3-dioxygenase
TNF-α	tumour necrosis factor - α
µm	micrometre
UV	ultraviolet
V/mV	volts/millivolts
w/v	weight/volume

Contents

Chapter 1: Introduction

1.1 The kynurenine pathway

1.1.1 Overview of the kynurenine pathway

The kynurenine pathway in mammals metabolises over 95% of dietary L-tryptophan, an essential amino acid. [1] This pathway has been implicated in numerous diseases including Huntington's disease, Alzheimer's disease, cancer, Parkinson's disease, acute pancreatitis and schizophrenia resulting in considerable interest in identifying new therapeutic strategies targeting this pathway. [1-4]

L-Tryptophan is converted to N-formyl-L-kynurenine by either indoleamine 2,3-dioxygenase (IDO) or tryptophan 2,3-dioxygenase (TDO) in the rate-limiting step of the pathway (Figure 1.1). This is then converted to L-kynurenine which can be metabolised by three different enzymes at the key branching point in the pathway.

L-kynurenine is a substrate for kynureninase, kynurenine aminotransferase (KAT) and kynurenine 3-monooxygenase (KMO). KAT converts L-kynurenine to kynurenic acid which is one of the three main neuroactive metabolites of the kynurenine pathway. KMO converts kynurenine to 3-hydroxykynurenine, a neuroactive metabolite, which can then metabolised further to quinolinic acid which is also neuroactive and implicated in disease. The conversion of quinolinic acid to nicotinamide adenine dinucleotide (NAD) is the end of the pathway.

The pathway is split into two separate and independent branches in the brain as different cells contain different pathway enzymes. Kynurenine is metabolised to kynurenic acid in astrocytes and to 3-hydroxykynurenine and further metabolites in microglia. [5,6] Kynurenine is metabolised to quinolinic acid in macrophages which, when treated with interferon (IFN)-γ, release enough harmful kynurenine pathway metabolites to cause death to surrounding neuronal tissue. [7] This may affect kynurenine pathway metabolite levels in the brain under inflammatory conditions as macrophages infiltrate the brain. [1]

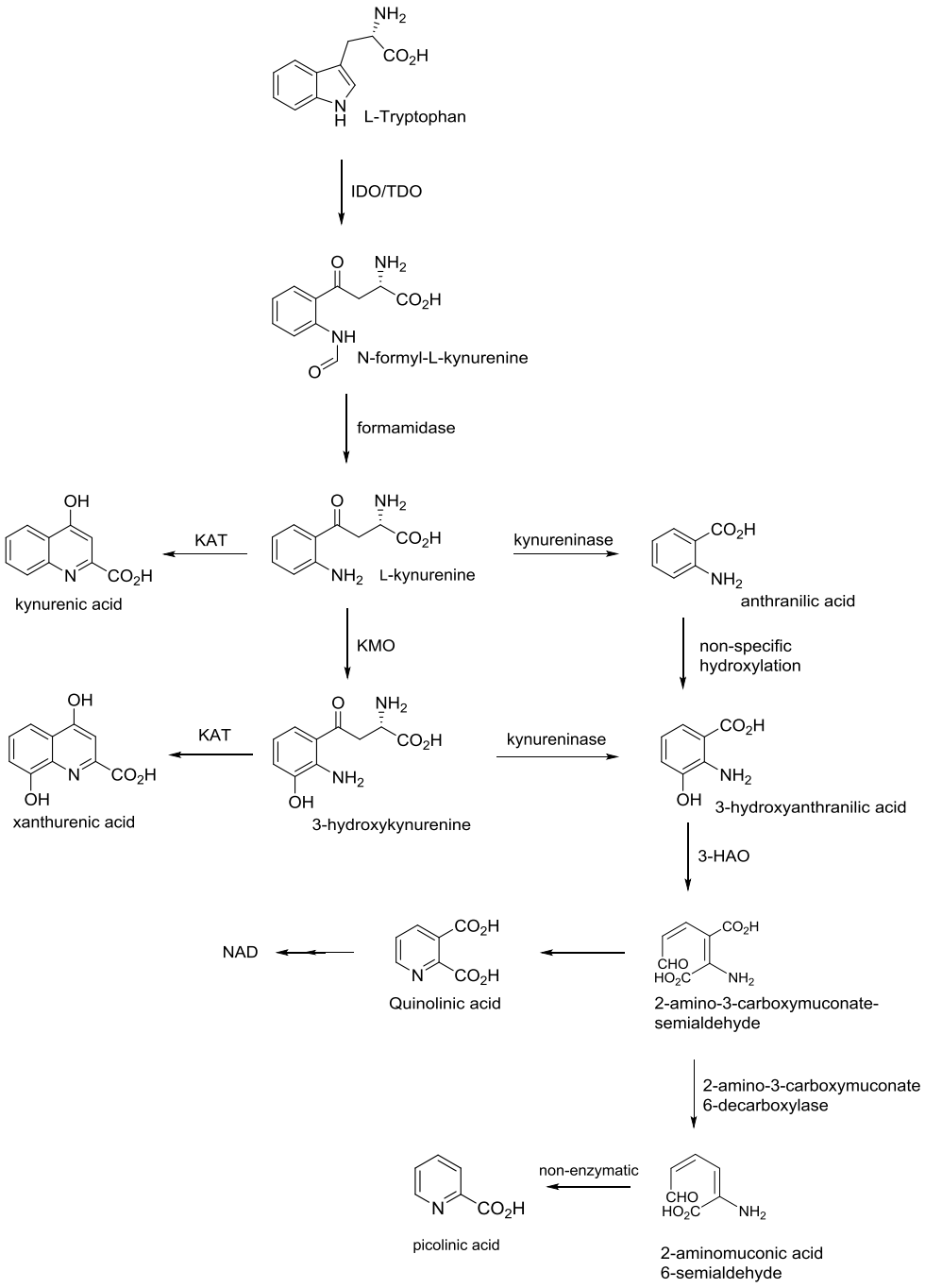

Figure 1.1: The major steps in the kynurenine pathway. Abbreviations used are IDO, indoleamine 2,3-dioxygenase; TDO, tryptophan 2,3-dioxygenase; KAT, kynurenine aminotransferase; KMO, kynurenine 3-monooxygenase; 3-HAO, 3-hydroxyanthranilic acid oxidase; and NAD, nicotinamide adenine dinucleotide.

1.1.2. Kynurenine pathway metabolites

Kynurenic acid is an antagonist at glutamate receptors including the NMDA (N-methyl-D-aspartate), AMPA (α-amino-3-hydroxy-5-methyl-4-isoxazolepropionic acid) and kainite receptors. [1] At the NMDA receptor it binds competitively at the glycine binding site and counteracts the action of quinolinic acid, an agonist at this receptor. [1,8,9] Kynurenic acid is recognised as a non-competitive inhibitor at the AMPA receptor although some researchers argue that in low (nanomolar to micromolar) concentrations kynurenic acid does not inhibit but instead acts as a "positive allosteric modulator", an effect also reported at the NMDA receptors at nanomolar concentrations. [10,11]

Kynurenic acid also binds to the α7 nicotinic acetylcholine receptor at concentrations found in healthy cell conditions (reported as low nanomolar to micromolar levels). [3,12,13] These receptors are more sensitive to the non-competitive binding of kynurenic acid than the glutamate receptors, suggesting that these receptors are more important for understanding the effects of kynurenic acid. [12]

While increased levels of kynurenic acid have been considered beneficial in some diseases (for example in Huntington's disease where it can counteract the harmful effects of other kynurenine pathway metabolites), increased levels of kynurenic acid have harmful effects. [1] Kynurenic acid has been implicated in Alzheimer's disease and schizophrenia through its inhibitory effect on glutamate and α7 nicotinic acetylcholine receptors, resulting in cognitive problems. [2,14,15] Kynurenic acid-related cognitive deficits have also been identified in patients post-surgery as imbalances in the immune system cause changes to kynurenine pathway metabolite levels with increased levels of tumour necrosis factor (TNF)-α causing increases in kynurenic acid levels. [16]

Kynurenic acid is also reported to be an agonist at the aryl hydrocarbon receptor. [17,18] This receptor was known for some time to bind toxins including 2,3,7,8-tetrachlorodibenzo-p-dioxin but endogenous ligands have recently been discovered. [17] Activation of this receptor increases the production of interleukin-6 which has been linked to cancer and potentially to a positive feedback mechanism as interleukin-6 increases IDO levels. [18] Recent research into this receptor has shown that L-kynurenine is an agonist and is implicated in the mechanism of immune escape of cancer. [19,20]

Another receptor that kynurenic acid has recently been shown to bind to is G coupled-protein receptor (GPR) 35. [21] The concentrations of kynurenic acid required to observe this effect

were higher than found under normal physiological conditions (micromolar compared to nanomolar concentrations) but it is argued that levels of kynurenic acid are raised in some circumstances and tagging of proteins in research studies have affected the levels of affinity observed. [17,21] The effects of kynurenic acid binding to this receptor are not fully understood but are thought to potentially include an increase in calcium concentrations. [21] In addition to its action at receptors, kynurenic acid can also scavenge hydroxyl and superoxide radicals and prevent lipid peroxidation, suggested to be particularly important for its role in neuroprotection. [8]

Quinolinic acid is a potent agonist at the NMDA glutamate receptor and through this action causes toxicity. [22,23] High levels of quinolinic acid cause cell death by necrotic processes thought to involve the generation of nitric oxide via induction of nitric oxide synthase. [23,24] Quinolinic acid has also been shown to cause lipid peroxidation through complex formation with Fe(II). [25,26] Through its actions at the NMDA receptor, increased levels of quinolinic acid have been reported to indirectly cause increases in tau phosphorylation measured in neuronal tissue which could have implications for understanding Alzheimer's disease. [27] Other reported toxic effects of quinolinic acid include affecting the blood brain barrier, death of neurons and microglia, and mitochondrial dysfunction. [23,28] Therapeutic strategies to combat increased levels of quinolinic acid have focussed on KMO inhibition as this alters the balance of kynurenine metabolites to favour increased levels of kynurenic acid, which can counteract the effect of quinolinic acid. [3,29]

The toxicity of 3-hydroxykynurenine is thought to arise through an oxidation reaction producing significant quantities of superoxide radicals and hydrogen peroxide. [30] Cell death is observed in the presence of high levels of this metabolite that can be decreased by blocking apoptotic pathways. [24] It has also been found that 3-hydroxykynurenine toxicity arises from the direct action of H_2O_2 formed in the presence of Cu(II) ions that may damage DNA. [31-33] 3-hydroxykynurenine is found in the lens of the eye and is thought to contribute to the formation of cataracts through cross-linking of crystallin proteins. [30,32] It was recently reported that 3-hydroxykynurenine is able to oxidise methionine residues of α-crystallin resulting in aggregation. [34]

In contrast to the detrimental effects outlined above, other researchers have suggested that 3-hydroxykynurenine may have antioxidant properties and be a potent nitric oxide and hydroxyl radical scavenger. [35,36] To reconcile the different theories about 3-hydroxykynurenine, it has been suggested that many studies look at phenomena observed at concentration ranges not found in healthy cells and that at normal levels

3-hydroxykynurenine may play a positive role as an antioxidant. [30] A recent study has investigated these two effects of 3-hydroxykynurenine using striatal tissue and has shown that it does not cause cell death even in high quantities, perhaps because the necessary enzymes to degrade kynurenine pathway metabolites are present in this tissue and therefore 3-hydroxykynurenine should perhaps be considered as a redox modulator rather than as a cytotoxic molecule. [37] 3-hydroxyanthranilic acid has also been reported to have similar toxic effects to 3-hydroxykynurenine including damaging proteins, generating hydrogen peroxide and the potentially beneficial scavenging of NO radicals. [32,35]

KMO knock-out mice have been used to investigate pathway regulation. In these animals the levels of kynurenic acid is increased significantly in the periphery but only by 20% in the brain. [38] In the brain the levels of anthranilic acid were increased resulting in only a moderate decrease of quinolinic acid in the brain that may have major implications for KMO inhibition as a strategy to treat neurological conditions where quinolinic acid is implicated. [38]

1.1.3 Key kynurenine pathway enzymes

TDO is mainly expressed in the liver and was first discovered in hepatic tissues from mammalian and avian species in the 1950s. [39] Although TDO and IDO catalyse the same reaction and are both heme-containing proteins they have less than 10% sequence identity. [40] TDO is a homotetrameric enzyme and has higher substrate specificity than monomeric IDO. [40] Expression of TDO has recently been found in tumours and it has been shown in glioma that TDO is responsible for producing L-kynurenine which acts on aryl hydrocarbon receptors resulting in tumour immune escape. [19,20] A study in mice showed that inhibiting TDO decreased tumour progression and targeting this enzyme could be useful in chemotherapy. [41] Antitumour agents which are specific inhibitors for TDO rather than IDO have since been identified. [42]

IDO is also expressed in a number of tumours as a mechanism of immune escape. [43] It has been shown in a mouse model that IDO expression protects the tumour against immune responses and IDO inhibition results in decreased tumour progression. [43] The Bin1 gene (which controls transcription of the indo gene which expresses IDO) is suppressed in breast cancer thus causing an increase in the expression of IDO. [44] The use of IDO inhibitors in combination with other drugs has been found to be effective in a mouse model. [44] The cytokine IFN-γ induces expression of IDO which links this pathway to inflammation. [45,46]

Lipopolysaccharide, a component of bacterial cell membranes, activates the pathway independently of IFN-γ suggesting the relationship between the pathway and immune system is complex and may differ in different cell types. [46,47] A study into the effect of the immune system on downstream enzymes of the pathway in rats found that immune activation also induces expression of KMO. [46]

Kynureninase is a pyridoxal-5´-phosphate (PLP)-dependent enzyme that converts L-kynurenine and 3-hydroxykynurenine to anthranilic acid and 3-hydroxyanthranilic acid respectively. [48] The preferred substrate of the human enzyme is 3-hydroxykynurenine, unlike the bacterial enzyme from *Pseudomonas fluorescens* which preferentially metabolises L-kynurenine. Studies with substituted kynurenines have shown that human kynureninase prefers substrates with polar substituents at the 3´ position of L-kynurenine but the substrate specificity can be changed from a preference for 3-hydroxykynurenine to only accepting L-kynurenine by mutating three of the active site residues to be the same as those found in *Pseudomonas fluorescens* kynureninase. [49,50]

There are four different KAT enzymes that have been identified from mammalian tissue, all of which are PLP-dependent. [51-53] KAT I and KAT II are the most important of these enzymes in the brain but although they catalyse the same reaction, they have only 15% sequence identity. [51,54] KAT II is responsible for the majority of kynurenic acid formation in the brain in rats and humans and is localised in astrocytes, particularly in those found close to neurons. [51,55] The crystal structures of KATs I, II and III have been solved and reveal that KAT I and III are highly similar. [54,56-58]

1.2 KMO in disease

Under normal physiological conditions the levels of kynurenine pathway metabolites in the brain are controlled by cytokines, growth factors and steroids but under inflammatory conditions, upregulation of enzymes including IDO and KMO significantly affect the levels of kynurenine pathway metabolites in the brain (Figure 1.2). These increased levels of 3-hydroxykynurenine and quinolinic acid can result in toxic effects as discussed above in Section 1.1.2.

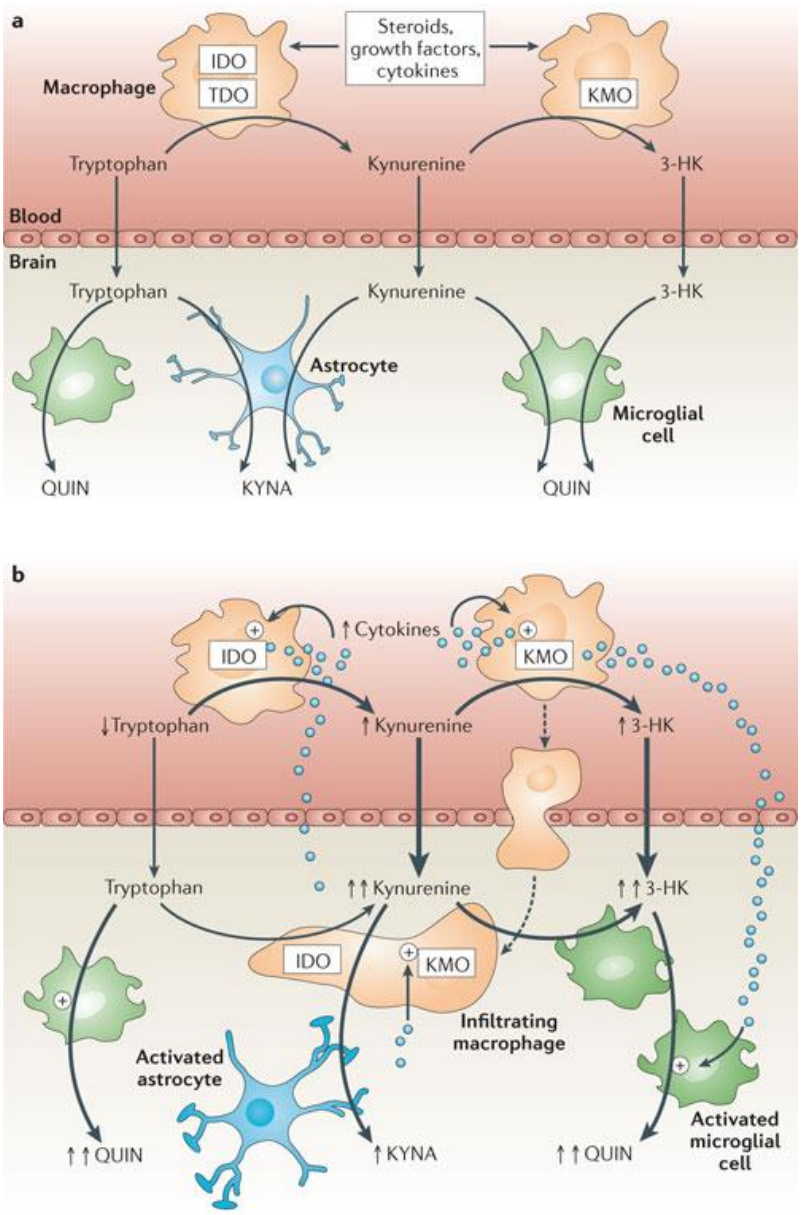

Figure 1.2: The kynurenine pathway in the mammalian brain under (a) normal physiological conditions and (b) when activated by the immune system. Under normal conditions the activity in the periphery of IDO, TDO and KMO is controlled by cytokines, growth factors and steroids. Tryptophan, kynurenine and 3-hydroxykynurenine can cross the blood brain barrier from the periphery. Astrocytes convert kynurenine to kynurenic acid and microglia convert tryptophan and kynurenine to 3-hydroxykynurenine and downstream metabolites, including quinolinic acid. Cytokines can induce both IDO and KMO in the periphery resulting in increased levels of kynurenine and 3-hydroxykynurenine which enter the brain resulting in a slight increase in kynurenic acid and a significant increase in quinolinic acid through the action of microglial cells that are activated by infiltrating macrophages which also have

upregulated KMO. Abbreviations used are IDO, indoleamine 2,3-dioxygenase; TDO, tryptophan dioxygenase; KMO, kynurenine 3-monooxygenase; 3-HK, 3-hydroxykynurenine; QUIN, quinolinic acid; and KYNA, kynurenic acid. Figure taken from Schwarcz *et al*. [1]

Imbalances in the kynurenine pathway and the relative levels of metabolites from this pathway have been implicated in a number of diseases including Huntington's disease and Alzheimer's disease. To counteract the harmful effects of increased levels of 3-hydroxykynurenine and quinolinic acid, there has been a focus on KMO inhibition as a potential strategy to treat these conditions. KMO is located at a key branching point of the kynurenine pathway and by inhibiting KMO, it is hoped both to decrease the levels of 3-hydroxykynurenine and quinolinic acid and to increase levels of kynurenic acid as more L-kynurenine will be available for metabolism by kynurenine aminotransferase. Some of the diseases in which this strategy is thought likely to be beneficial are discussed in more detail below.

1.2.1 Huntington's disease

Huntington's disease is caused by an increased number of CAG repeats in the IT15 gene resulting in expression of mutant huntingtin protein with extended glutamine repeats at the N-terminus. [59] Disease occurs in individuals with more than 35 CAG repeats and the onset of disease correlates with the degree of repetition. [59]

Growing evidence over the last thirty years has implicated the kynurenine pathway as causing the neurodegenerative effects observed in patients (Figure 1.3). Increased levels of the potentially harmful metabolites 3-hydroxykynurenine and quinolinic acid have been detected in tissue from early stage patients, particularly in the striatum, and decreased kynurenic acid concentrations have also been detected. [60,61] Increased activity of 3-hydroxyanthranilate oxygenase has also been reported in brain tissue from deceased patients although in a mouse model this increase was not found to be statistically significant. [62,63] One study examined 3-hydroxykynurenine levels from post-mortem tissue samples and found increases in the frontal and temporal cortex and the putamen. [64] Other researchers have also found increased levels of 3-hydroxykynurenine and recorded increased levels (although to a lesser extent) of kynurenic acid in samples from early stage patients and from mouse models. [65] As well as changes to the balance of metabolites, decreased levels of

the free radical scavenger glutathione have been detected, suggesting a possible role for radical toxicity although most research has focussed on toxicity caused by quinolinic acid acting through NMDA receptors, which are potentially present in increased levels. [61,66]

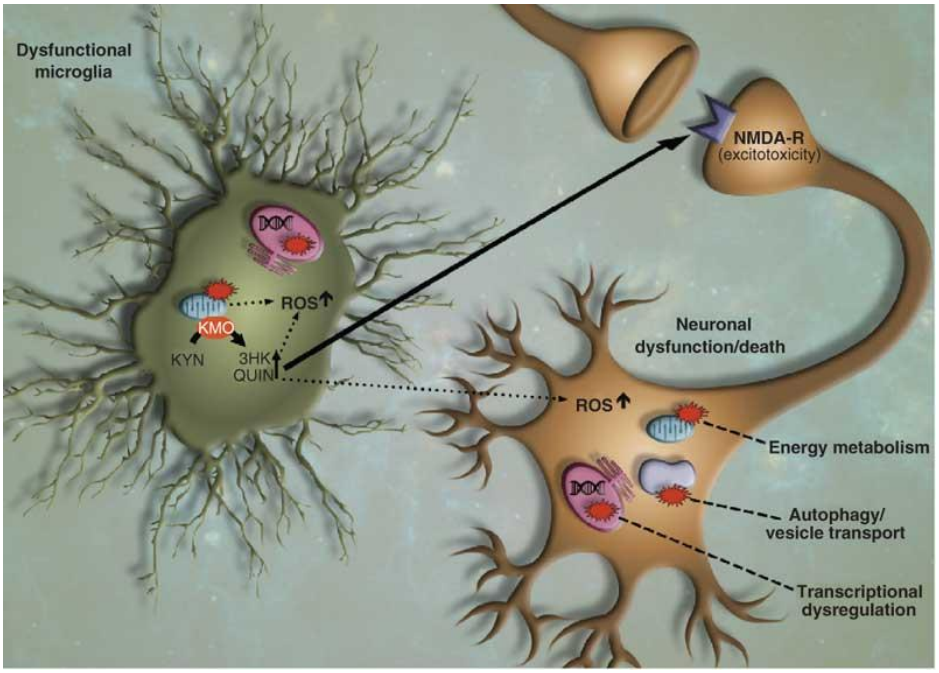

Figure 1.3: In Huntington's disease, the presence of mutant huntingtin protein in microglia (green) is thought to causes increases in the levels of 3-hydoxykynurenine and quinolinic acid leading to an increase in reactive oxygen species in both microglia and neurons (orange) and over-activation of the NMDA receptors. Other pathological symptoms observed in Huntington's disease including transcriptional dysregulation, mitochondrial impairment and changes to vesicle transport. [67] Abbreviations used are KYN, kynurenine; 3HK, 3-hydroxykynurenine; QUIN, quinolinic acid, NMDA-R, N-methyl-D-aspartate receptor; ROS, reactive oxygen species. Figure taken from Giorgini *et al*. [67]

These findings establishing a link between kynurenine pathway metabolites and Huntington's disease have been validated by genetic studies and animal models. In studies of different mouse models of disease, significantly increased levels of 3-hydroxykynurenine and quinolinic acid were detected shortly before neurodegenerative effects of disease were observed. [68] Another study on a mouse model found increased levels of 3-hydroxykynurenine due to increased KMO expression but no significant increase in quinolinic acid. [63] Increased levels of 3-hydroxykynurenine and quinolinic acid have also

been observed in *Drosophila* models and the ratio of 3-hydroxykynurenine and quinolinic acid has been shown to affect neurodegeneration. [69]

Other work carried out in *S. cerevisiae* has shown a link between suppression of the yeast gene expressing KMO and decreased toxicity caused by mutant huntingtin protein. [67] In this study of 28 yeast gene deletions that suppress mutant huntingtin toxicity, the majority caused a decrease in the levels of 3-hydroxykynurenine and quinolinic acid, suggesting that the kynurenine pathway is strongly linked to neurodegeneration in this disease. [70,71] Further work suggests ribosome activity is affected by mutant huntingtin although it is thought that there may be several pathways through which the protein acts in microglia to affect the kynurenine pathway. [70,72]

The increase in 3-hydroxykynurenine and quinolinic acid and the decrease in neuroprotective kynurenic acid have led to KMO inhibition being considered as a therapeutic strategy in the treatment of Huntington's disease. [3,73] This approach has been tested in different animal models including *Drosophila* where KMO inhibition has been shown to decrease neurodegeneration and increase the levels of kynurenic acid observed. [69] A further finding was that feeding 3-hydroxykynurenine to *Drosophila* reversed this effect, showing clearly the importance of the ratio between these two branches of the kynurenine pathway. [69]

Another study of KMO inhibition was carried out in mice models using a prodrug which increased the levels of kynurenic acid and increased the life span of the mice and decreased symptoms of neurodegeneration. [29] The prodrug is metabolised to form Ro 61-8048 (a KMO inhibitor discussed in Section 1.5.2) that inhibits KMO causing an increase in kynurenic acid that decreases the levels of glutamate and is an antagonist at NMDA receptors. [29] One of the interesting aspects of this study is that the prodrug and the KMO inhibitor are unable to cross the blood brain barrier, and instead act in the periphery. [29,74]

1.2.2 Alzheimer's disease

Microglia and macrophages, capable of producing significant quantities of quinolinic acid, have been known to surround amyloid plaque, and studies from the hippocampus of Alzheimer's disease patients show significantly increased levels of quinolinic acid (and an increase in IDO levels) in close proximity to plaque. [75,76] A decrease in the level of tryptophan in patients has also been recorded, and while this is partly due to aging it could be responsible for an increase in levels of kynurenine metabolites. [77] The increased levels of

quinolinic acid are proposed to increase tau phosphorylation which is implicated in neurodegeneration in Alzheimer's disease. [27] These findings support the hypothesis that in Alzheimer's disease there is oxidative stress leading to over-activation of glutamate receptors, perhaps exacerbated by quinolinic acid, resulting in damage to neurons. [1,78]

Significant increases in the levels of tumour necrosis factor-α (TNF-α) have been detected in serum samples from Alzheimer's disease patients and this, along with IFN-γ, is known to induce IDO. [45,79] In a mouse model of Alzheimer's disease it was found that when the IFN-γ receptor type 1 was suppressed there was decrease in gliosis and plaque formation and no induction of IFN-γ or TNF-α. [80] In comparison, the mice without the IFN-γ receptor suppression had significantly lower plaque degradation through the actions of these two cytokines. [80]

Studies in animal models have been used to validate these findings. Rats that have had quinolinic acid infused into the brain performed more poorly than control animals in maze tests, and exhibited impaired short-term memory but no other behavioural changes. [81] A recent study tested a KMO inhibitor on mouse models of Alzheimer's disease and Huntington's disease (as mentioned in Section 1.2.1). [29] The inhibitor increased the levels of kynurenic acid (from approximately 25 nM in the plasma of untreated model mice to over 150 nM in mice treated with the inhibitor where wild type mice had plasma concentrations of approximately 60 nM), prevented synaptic loss and improved spatial memory. [29] It is suggested that the beneficial effect of kynurenic acid is caused by both indirect effects at the glutamate receptors (due to levels of kynurenic acid being too low for direct effects) and by acting as an agonist at the GPR35 receptor that decreases production of TNF-α. [21,29,45]

1.2.3 Ischaemic stroke

Kynurenine pathway metabolites have also been implicated in brain damage following ischaemic stroke. One early study showed that in gerbils there is a delayed increase in quinolinic acid in some brain tissues after an ischaemic event which correlates with the degree of damage caused. [82] The levels of several kynurenine pathway enzymes were also found to be elevated, including IDO, KMO and 3-hydroxyanthranilate oxidase but not KAT. [82] An increase in KMO mRNA is detected after an increase of IDO mRNA but the levels of KAT mRNA are unaffected. [46] The levels of KAT are significantly higher than those of KMO in the brain. [46]

KMO inhibitors have been tested on animal models and tissues to determine whether shifting the balance of the kynurenine pathway towards kynurenic acid is beneficial. An *in vivo* study on gerbils and rats using Ro 61-8048 and m-nitrobenzoylalanine showed that KMO inhibition decreased damage and neuronal death. [83] These inhibitors were also used in an *in vitro* study of oxygen deprived tissue slices and were again found to prevent neuronal death. [84] The authors of this study were; however, unable to fully explain their results through the action of kynurenic acid. [84]

Further studies on human patients show that the levels of kynurenic acid are significantly increased in patients who die following a stroke. [85] The reasons for this increase are unclear but it is hypothesised that it is due to the overall activation of the kynurenine pathway. [71,85] In addition these samples showed a marked change in the ratio of 3-hydroxyanthranilic acid: anthranilic acid, and it has been suggested that the decrease in 3-hydroxyanthranilic acid is due to generation of reactive oxygen species by this metabolite. [85] This research may help fully explain some of the earlier findings with KMO inhibitors, as use of these compounds would decrease the levels of 3-hydroxyanthranilic acid which may be responsible for toxic effects as well as for increasing the levels of kynurenic acid.

1.2.4 Schizophrenia

Recent research has suggested that KMO expression is lower in patients with schizophrenia. [86,87] KMO expression and activity is also reduced in brain tissue samples taken from deceased patients with schizophrenia. [87] Some researchers have hypothesised that in this disease the kynurenine pathway produces greater quantities of kynurenic acid which leads to impairment of oculomotor response. [87]

There are reports of an increased occurrence of R452C KMO in patients which may cause the observed decrease in KMO activity and is proposed to interfere with the ability of KMO to interact with the outer mitochondrial membrane, although this has not been confirmed. [86] Other researchers were unable to find any significant link between schizophrenia and particular polymorphisms in the KMO gene and research in this area is ongoing. [88]

1.2.5 KMO in other conditions

Metabolites of the kynurenine pathway have also been implicated in the pathophysiology of acute pancreatitis, a condition in which there is inflammation of the liver, most commonly caused by gallstones or alcoholism. [89,90] In approximately 20% of cases, acute pancreatitis leads to multiple organ failure, which is fatal in 30-50% of these patients. [91] Increased levels of both kynurenine and 3-hydroxykynurenine have been found in mesenteric lymph tissue from patients and rat models of disease and it is hypothesised that 3-hydroxykynurenine causes some of the symptoms of acute pancreatitis through oxidative damage to cells. [89] KMO inhibition is therefore seen as a potential therapeutic strategy to decrease mortality rates by decreasing the level of 3-hydroxykynurenine.

Increased levels of kynurenine and significantly higher levels of 3-hydroxykynurenine and quinolinic acid have been identified in experimental chronic renal failure leading to the hypothesis that oxidative stress caused by kynurenine pathway metabolites is connected to renal disease. [92] Significant changes in kynurenine pathway metabolites were later observed in samples from patients with end stage renal disease and a correlation was shown between the levels of kynurenine, 3-hydroxykynurenine and quinolinic acid and those of von Willebrand factor and thrombodulin, known to be markers for endothelial dysfunction. [93]

Another use of KMO inhibitors is to increase the concentration of kynurenic acid antagonising α7 nicotinic acetylcholine receptors to counteract the effect of tetrahydrocannabinol. [94] A study on squirrel-monkeys and rats showed that the KMO inhibitor Ro 61-8048 resulted in a decrease in self-administration of cannabinoid compounds and the authors hope that this may have an application in prevention of drug use relapse. [94]

Ro 61-8048 has also been reported to decrease the severity of paroxysmal dyskinesia in mice models by inhibiting KMO and increasing kynurenic acid levels, resulting in potential antagonism of glutamate receptors. [95]

1.3 Flavoprotein aromatic hydroxylases

Flavoproteins that catalyse a monooxygenation reaction have been divided into six categories. KMO is characterised as Class A flavoprotein aromatic hydroxylase as it fulfils

the following criteria: it is transcribed from a single gene, it contains a flavin adenine dinucleotide (FAD) cofactor, it uses NADPH for flavin reduction and then releases $NADP^+$ and it contains a Rossmann fold. [96,97]

Class A	Encoded by one gene FAD cofactor Use either NADPH or NADH Release $NADP^+$/NAD^+ after flavin reduction One dinucleotide binding domain
Class B	Encoded by one gene FAD cofactor Uses NADPH $NADP^+$ released when reaction is completed Two dinucleotide binding domains Hydroxylation of atoms other than carbon possible
Class C	Encoded by more than one gene Reduced FMN cofactor Use NADPH and/or NADH Monooxygenase subunit has a TIM-barrel fold Example enzymes include bacterial luciferases
Class D	Monooxygenase and reductase components each encoded from one gene Reduced FAD cofactor Use NADPH and/or NADH
Class E	Monooxygenase and reductase components each encoded from one gene Reduced FAD cofactor Use NADPH and/or NADH Thought to have some structural similarities with Class A enzymes The known Class E enzyme is styrene monooxygenase
Class F	Monooxygenase and reductase components each encoded from one gene Reduced FAD cofactor Use NADPH and/or NADH One FAD binding domain and a helical domain Known Class F enzymes are halogenases

Table 1.1: Overview of the general characteristics of the six classes of flavin-dependant monooxygenases summarised from van Berkel *et al*. [97]

1.3.1 Class A flavoprotein aromatic hydroxylases

The typical reaction mechanism for this family of enzymes has the following steps: reduction of the FAD cofactor by NADH or NADPH; NAD^+ or $NADP^+$ is released by the enzyme; the reduced flavin reacts with oxygen to form a peroxyflavin which is immediately protonated to form a hydroperoxyflavin which hydroxylates the substrate, typically an aromatic molecule with an amino or hydroxyl substituent. [97,98] In Class A enzymes the reaction with oxygen is thought to be carefully controlled, with a small cavity holding O_2 close to the isoalloxazine moiety of the FAD cofactor to ensure formation of a peroxyflavin. [99] Conserved motifs have been identified in this family for binding NADPH and FAD. [100] Class A enzymes have been widely studied for their catalytic potential in regioselective oxidation of aromatic substrates using molecular oxygen. [97,98,101]

A number of Class A flavoprotein aromatic hydroxylase enzymes have been well characterised and KMO has been considered in the context of these enzymes especially as structural information about KMO has only recently been obtained. An overview of some of these enzymes is given below to explore some of the details of the mechanism and chemistry of these enzymes.

1.3.2 p-Hydroxybenzoate hydroxylase

One of the most extensively characterised enzymes related to KMO is p-hydroxybenzoate hydroxylase (PHBH, EC 1.14.13.2). Both the *Pseudomonas fluorescens* and *Pseudomonas aeruginosa* enzymes have been used in these studies as they are extremely similar, differing only in two surface residues. [102] The overall structure of the enzyme is shown below as well as the active site environment (Figure 1.4).

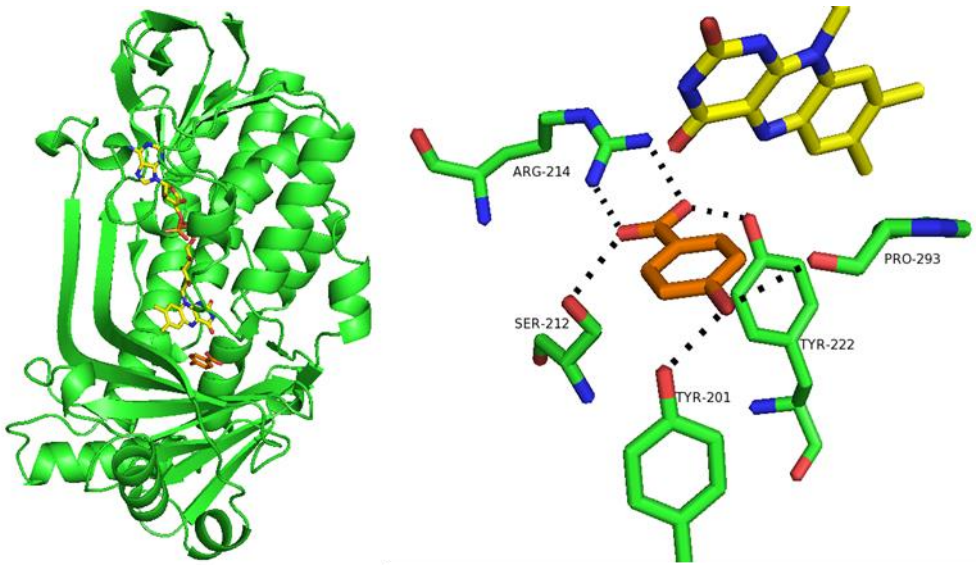

Figure 1.4: Structure of *Pseudomonas fluorescens* PHBH (left) and main interactions in the active site (right) between PHBH residues (green) and para-hydroxybenzoate (orange) with the isoalloxazine moiety of the FAD cofactor (yellow) also shown. Coordinates used are from PDB ID 1PBE. [103]

Residues in the active site important for substrate recognition and for conformational dynamics have been identified. Y222 forms a hydrogen bond to the carboxylate of p-hydroxybenzoate (PHB) important for conformational control. [104] Y201 forms a hydrogen bond to the hydroxyl group and is part of a hydrogen-bonding network stretching to the protein surface. [105] S221 forms a hydrogen bond to the carboxylate group of PHB but this interaction is not critical for catalysis. [106] R214 forms an ion-pair interaction with the carboxylate group of PHB without which the affinity of PHBH for PHB significantly decreases. [107]

A schematic of the mechanism of PHBH below (Figure 1.5) suggests the major intermediates formed indicating the conformation of the protein in each step. There are three conformations observed in PHBH and understanding control of conformational change is one of the reasons for the significant interest in this enzyme.

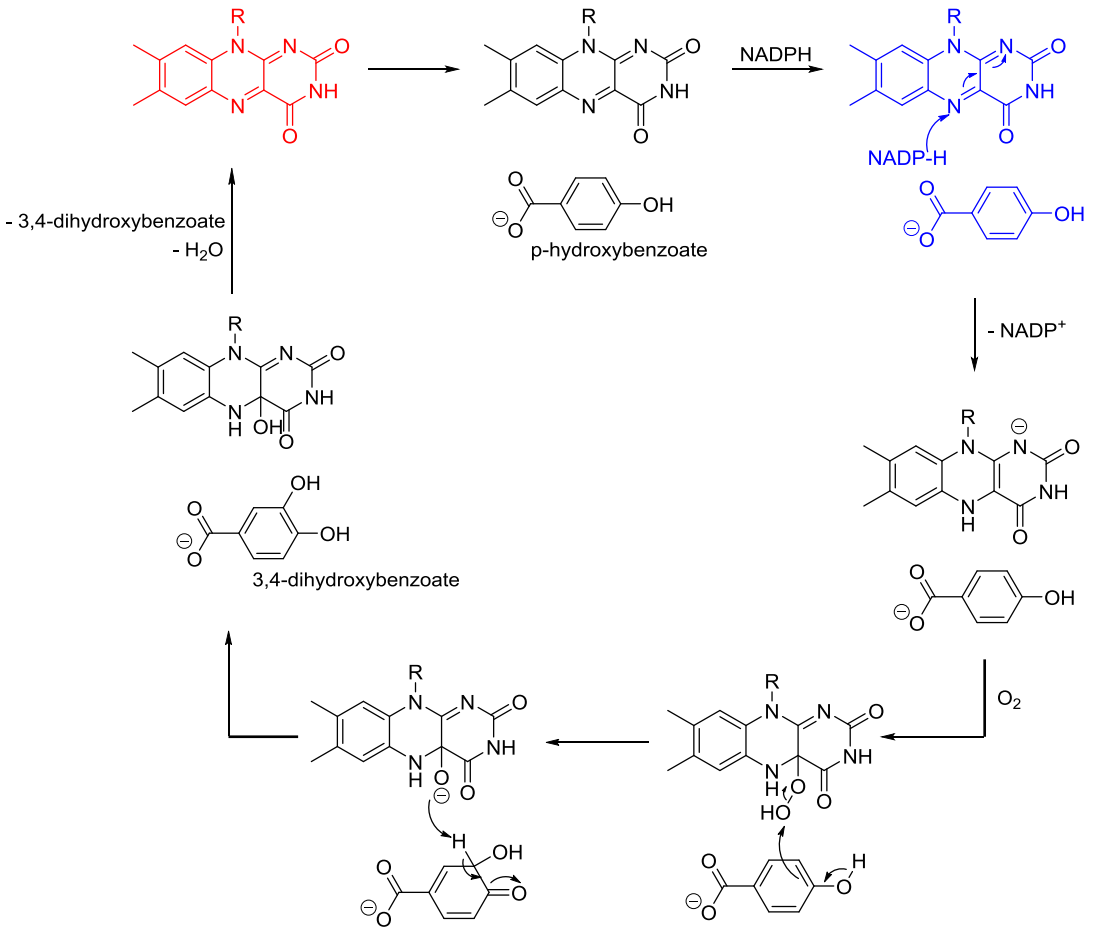

Figure 1.5: Overview of the mechanism of the hydroxylation of p-hydroxybenzoate to 3,4-dihydroxybenzoate catalysed by PHBH. The isoalloxazine moiety of the FAD cofactor is shown, with the rest of the cofactor represented by R. The *open* (red), *in* (black) and *out* (blue) conformations observed at each stage are indicated in the mechanism.

The substrate binds to the enzyme in the *open* conformation when the active site is solvent accessible. [108] This conformation was first observed in R220Q PHBH and the crystal structure showed that the substrate-binding β-sheets rotate away from the FAD-binding domain (Figure 1.6). [109] The conversion to the *open* conformation is thought to be driven by relieving of conformational strain around R44 and neighbouring residues that are part of a conserved loop close to the active site. [110] Another mutation, A45V, causes stabilisation of the *open* conformation and work on both mutated enzymes has shown that they have lower affinities for the substrate but binding occurs more rapidly. [111] The crystal structure of R220Q variant PHBH showed that the residue R214 (shown in Figure 1.4) is rotated out of the active site resulting in fewer interactions between PHBH and the substrate. [108,112] R220Q

and A45V PHBH are inactive due to their inability to change conformation rapidly which is necessary for further steps in the catalytic cycle. [111]

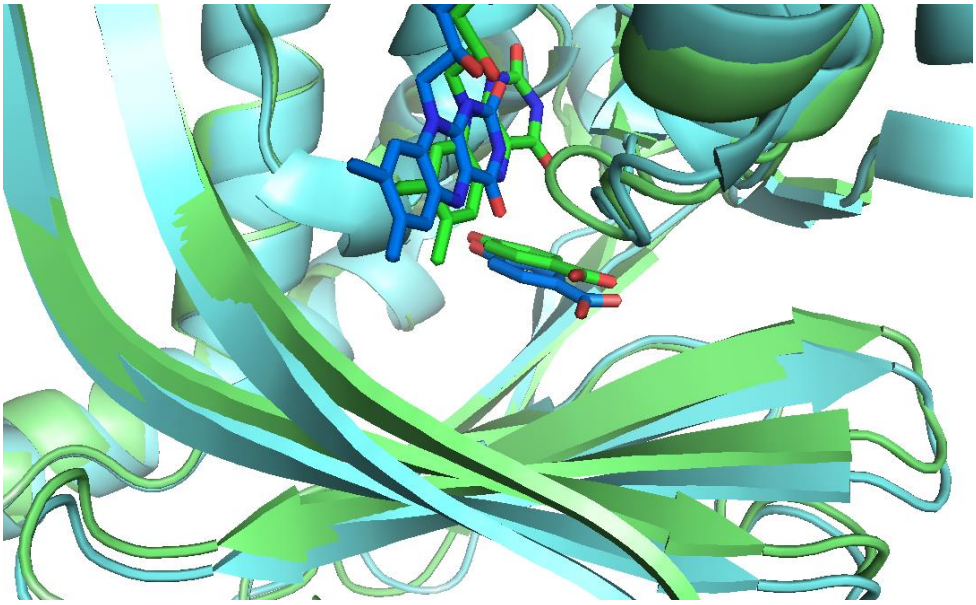

Figure 1.6: Overlay comparing *in* (green) with *open* (blue) conformation. The *open* conformation has the β-sheets positioned further from the FAD binding domain. The *in* structure is *Pseudomonas fluorescens* wild-type PHBH and the *out* is *Pseudomonas aeruginosa* R220Q PHBH constructed from PDB IDs 1PBE [103] and 1K0I [109] respectively.

Once PHB is in the active site the conformation changes to *in*, a solvent-inaccessible active site environment. In this conformation all the possible interactions between the substrate and enzyme have formed. [112] For catalysis to proceed, the FAD must be reduced by NADPH which requires a solvent accessible environment for the isoalloxazine ring. [111] In the change to the *out* conformation (Figure 1.7) the isoalloxazine ring of the FAD cofactor moves 7 to 8 Å, a phenomenon known as the "wavin' flavin". [113]

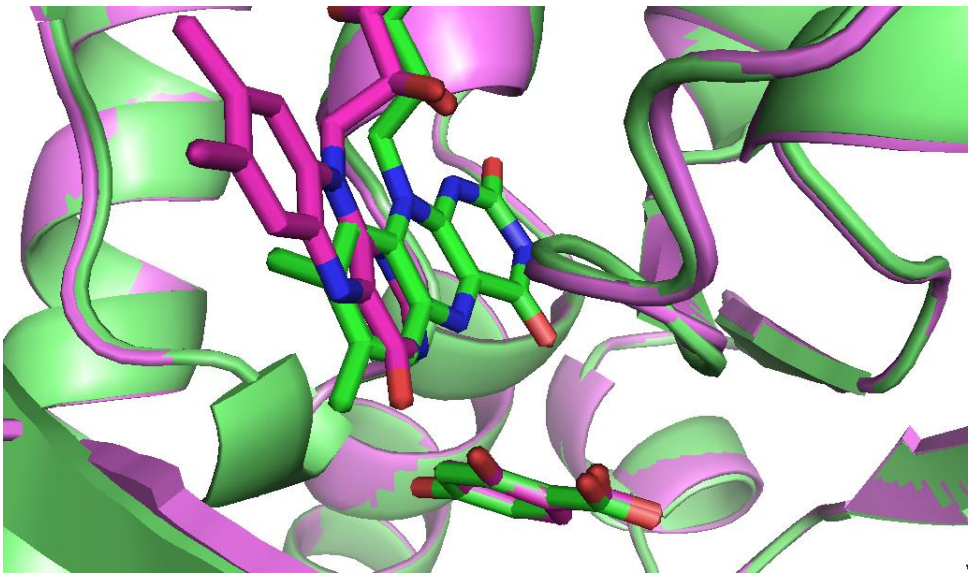

Figure 1.7: Overlay showing the active site in the *in* and *out* conformations. The *in* conformation (green) is the wild-type *Pseudomonas fluorescens* enzyme with PHB bound from PDB 1PBE, [103] the *out* conformation (purple) is wild-type *Pseudomonas aeruginosa* PHBH with 2,4-dihydroxybenzoic acid from PDB 1DOD. [104]

PHB is deprotonated by a proton-transfer network extending from H72 at the protein surface to the active site (Y201). [114,115] This network appears to be unique for PHBH among the Class A FAH enzymes. [116] The deprotonated substrate repels the carbonyl of P293 which is a rigid residue in a loop near the active site. [102] This repulsion of a rigid residue in the loop causes a global conformational change to the *out* conformation.[102] The requirement for a substrate to be deprotonated increases the specificity of the catalytic cycle and has been described as "substrate recognition by password" and loss of the hydrogen-bonding network significantly decreases the rate of hydroxylation. [105,117] This tight control is thought to be necessary for PHBH to avoid hydroxylating a similar metabolite, 4-aminobenzoate, which has been observed in the active site by crystallography. [108,118] The mutation P293S increased flexibility which reduces the ability of PHB to repel this residue and uncoupled the conformational change, thus significantly slowing the reduction of the FAD cofactor. [102] In addition this flexibility increased the accessibility of the active site to solvent and decreased hydroxylation efficiency. [102]

Once in the *out* conformation, FAD is reduced by NADPH. [113] The enzyme then returns to the *in* conformation which forces the release of $NADP^+$. [108] The reduced FAD cofactor reacts

with a molecule of oxygen to form a peroxyflavin which must occur in a solvent inaccessible environment to prevent the loss of H_2O_2. [113] PHB is deprotonated by the peroxyflavin to form a more electrophilic hydroperoxyflavin and also results in a more nucleophilic substrate. [112] The deprotonated substrate is hydroxylated and re-aromatises to form the product, 3,4-dihydroxybenzoate. These steps of the catalytic cycle are stabilised by the positive environment of the active site and rate of hydroxylation can be modified by changing the electrostatic environment. [119] Mutations made to PHBH which increase its positive charge increase the rate of hydroxylation, and those that decrease the positive environment decrease the rate. [119,120] The product, 3,4-dihydroxybenzoate, is released upon conversion to the *open* conformation and the catalytic cycle is complete.

1.3.3 Phenol hydroxylase

Phenol hydroxylase differs from PHBH as it is a far larger protein and has lower substrate specificity. Phenol hydroxylase converts phenol to catechol but also accepts substituted phenols as substrates. [121] While there are similarities in the active site residues between this enzyme and PHBH, there is no evidence from kinetic studies to suggest that they play the same role in substrate deprotonation or that there is a proton transfer network in phenol hydroxylase. [122]

The enzyme from *Trichosporon cutaneum* has been crystallised and the crystal structure showed two separate conformations of the enzyme (Figure 1.8). [123] There is a major conformational change that is associated with the movement of the FAD cofactor from an *in* to an *out* conformation, the largest difference in residue position is reported as 30 Å. [124] The region of the protein involved in this change is described as a "lid" and is thought to control access to the active site for substrate and solvent, the mechanism controlling this change is still unknown. [124]

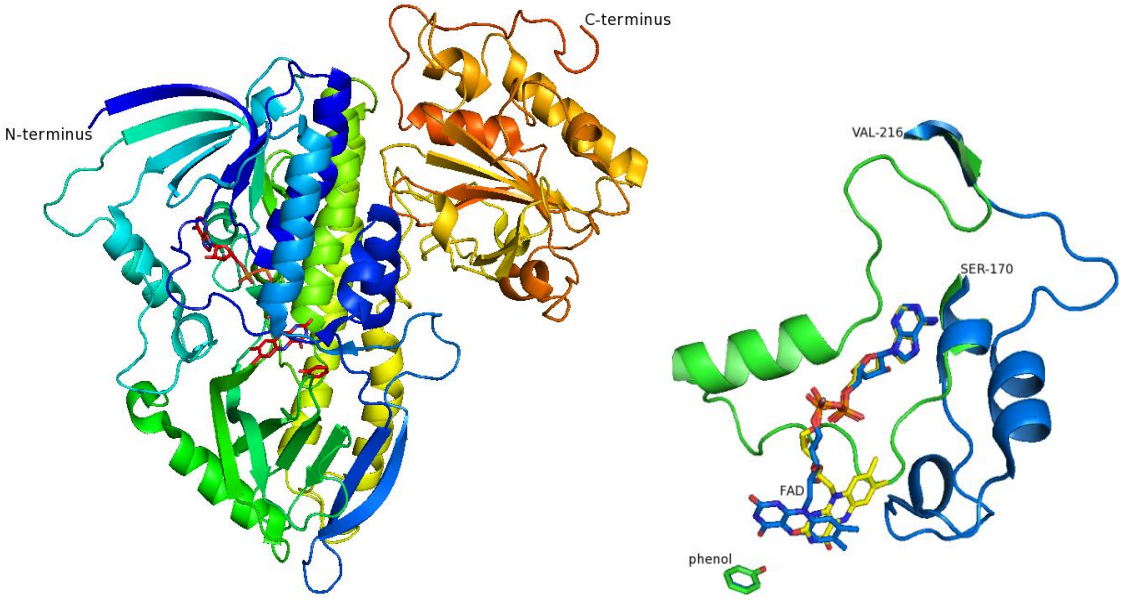

Figure 1.8: The structure of the *in* conformation of phenol hydroxylase (left) coloured from N-terminus (blue) to C-terminus (orange) with FAD cofactor and phenol hydroxylase (red). On the right is an overlay of the *in* (blue) and *out* (green with FAD cofactor in yellow) conformations, showing the phenol substrate and residues 170 – 216, the region of phenol hydroxylase where there is significant conformational change when the FAD cofactor moves between the *in* and *out* conformations. Images generated from PDB 1PN0. [123]

1.3.4 MHPCO

2-methyl-3-hydroxypyridine-5-carboxylic acid oxygenase (MHPCO) is a tetrameric Class A flavoprotein aromatic hydroxylase containing one FAD cofactor per monomer. [125] The reaction catalysed by this enzyme is unusual for this family as, after the substrate is hydroxylated, the molecule formed undergoes a ring opening reaction to form the final product. [101,126]

The structure of the *Mesorhizobium loti* enzyme has been obtained and shows that the active site is large (15 by 12 by 10 Å) and interactions between residues and the substrate are mediated through water molecules. [127] The substrate gains access to the active site through a 17 Å tunnel from the surface, visible in the crystal structure (Figure 1.9). [127]

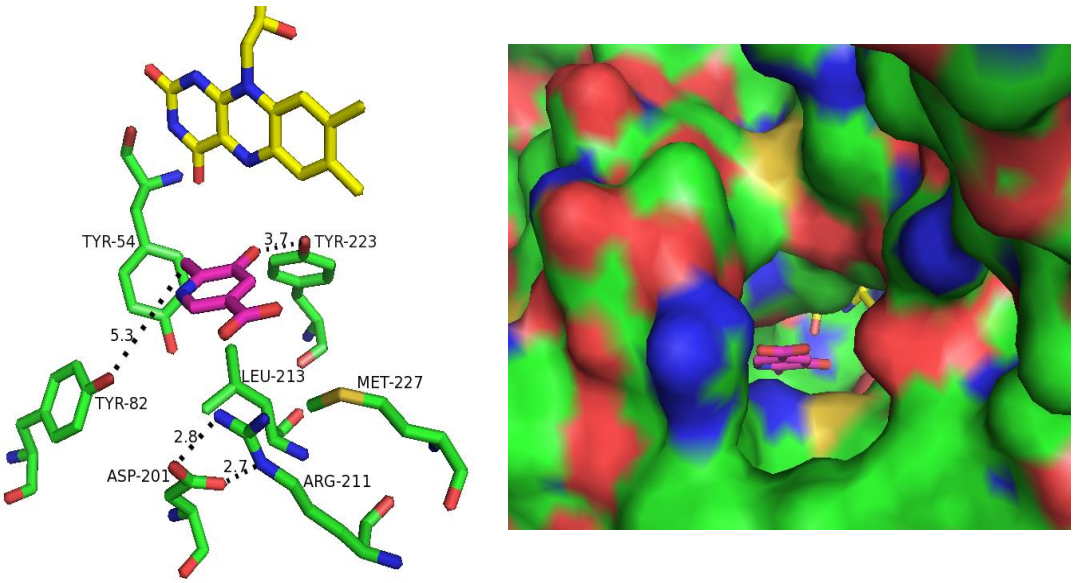

Figure 1.9: A view of the active site of MHPCO showing most of the active site residues (left) and the tunnel leading from the protein surface to the active site (right) with the substrate in magenta and FAD cofactor in yellow. Two tyrosine residues interact with the substrate through water-mediated hydrogen bonding interactions (distances indicated in the figure in Å) in the active site. The interaction between Asp201 and Arg211 is thought to prevent Arg211 interacting with the substrate due to its orientation in the active site. Figure constructed using PDB 3GMC. [127]

In contrast to PHBH, no evidence from structural studies or using substituted FAD cofactor analogues has been found to support the idea of a "wavin flavin" in this enzyme as the FAD cofactor is observed in the *in* conformation only. [127,128] The hydroxylation reaction is thought to proceed by the same mechanism common to Class A flavoprotein aromatic hydroxylases but the mechanism of the ring-opening reaction has been debated in the literature. [129] It is currently thought that that the mechanism involves a Baeyer-Villiger rearrangement before the ring cleavage occurs with a second oxygen atom incorporated into the product from a water molecule. [126,129,130]

1.3.5 Other enzymes in this family

Other enzymes in this class which have been structurally characterised have shown similar properties of flavin movement, control of substrate access to the active site, and overall

structural folds to the proteins described above although the high level of catalytic control achieved with three conformations and a hydrogen transfer network appears to be unique to PHBH. A summary of the features of some of these characterised Class A enzymes is given below (Table 1.2)

Aklavinone-11-hydroxylase	Crystallised with flavin in the *out* conformation, modelling suggests movement to *in* does not require major conformational change. [131] Route for substrate access to the active site unconfirmed. [131] C-terminal domain has a thioredoxin fold with no known biological function. [131]
RebC	Accepts a highly reactive substrate as part of an eight-electron oxidation reaction in the biosynthesis of rebeccamycin. [132,133] Active site is accessed via a disordered region which folds into a helix once the substrate is bound. [132] Substrate binding causes movement of the flavin from an *out* conformation to *in*.[132]
Pyocyanin biosynthetic protein (PhzS)	Part of a protein complex that produces pyocyanin in *Pseudomonas aeruginosa*. [134] Substrate (unconfirmed identity) enters the active site through a tunnel from the surface of the protein. [134] C-terminal domain is disordered in the substrate-unbound structure, its function has not yet been determined. [134]
3-hydroxybenzoate hydroxylase (*Comamonas testosteroni*)	Substrate enters the active site through a tunnel which is thought to increase substrate specificity. [135]
3-hydroxybenzoate-6-hydroxylase (*Rhodococcus jostii*)	Binds a lipid molecule with the hydrophilic end on the protein surface and the hydrophobic end in the active site which in the crystal structure appears to be involved in substrate binding. [136]

Table 1.2: Summary of observed conformational changes and features of substrate access to the active site occurring in examples of Class A flavoprotein aromatic hydroxylases.

1.4 Kynurenine 3-monooxygenase

1.4.1 Efforts to isolate and characterise KMO

Despite extensive characterisation of other Class A flavoprotein aromatic hydroxylases, KMO has not been well-characterised even though it has been implicated in disease. Like other enzymes in this family, KMO hydroxylates the substrate in a redox reaction requiring a non-covalently bound FAD cofactor, NADPH and oxygen (Figure 1.10). [137]

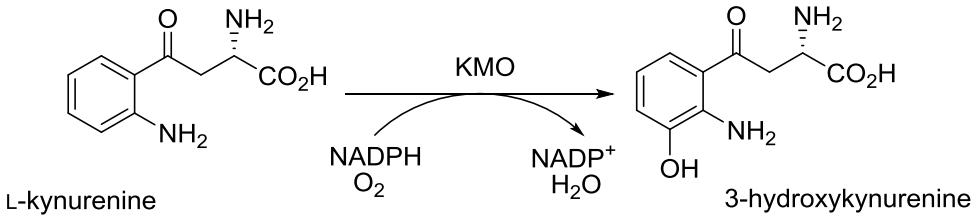

Figure 1.10: The hydroxylation of L-kynurenine catalysed by KMO

One of the major challenges in obtaining active mammalian KMO enzyme is overcoming solubility problems. Work with mammalian KMO enzymes has mostly been carried out with recombinant enzymes expressed in cell lines. Active human KMO has been expressed in HEK (human embryonic kidney)-293 cells and later in COS-1 cells where it was confirmed that the human enzyme contains one non-covalently bound FAD cofactor per enzyme monomer. [138,139] The pig KMO enzyme has been expressed in COS-7 cells where it was shown that the C-terminal domain was essential for activity and that residues in the last twenty amino acids of this domain are necessary for localisation of the enzyme in the outer mitochondrial membrane which is thought to cause the insolubility of KMO. [140]

Significant amounts of recombinant protein for *in vitro* work have been obtained using recombinant *Pseudomonas fluorescens* KMO (*Pf*KMO), which has 36% sequence identity with human KMO. [96] This construct (a kind gift from Graham Moran, University of Minnesota) was also used for the work described here on *Pf*KMO, using a similar purification method (Section 2.4). *Pf*KMO was successfully purified in sufficient levels to allow stopped-flow kinetic experiments to be carried out, demonstrating that the enzyme mechanism is broadly similar to that of related flavoprotein aromatic hydroxylase enzymes

such as PHBH. [137] The efficacy of a number of KMO effector molecules was also tested against this enzyme as discussed in Section 1.5.

In the last year, an attempt to purify human KMO was published although the full-length protein was insoluble and efforts to remove it from the insoluble fraction during purification were unsuccessful. [141] A truncated protein was prepared which, although soluble, lacked activity supporting previous work showing that the C-terminus is necessary for activity. A FLAG-tagged fusion protein was prepared and partially purified by the same group and has been shown to be active. [141]

Another KMO enzyme to be successfully purified is from *Saccharomyces cerevisiae* which was expressed in *E. coli* and from which the first published KMO structure was obtained. [142] The crystal structure of *S. cerevisiae* KMO was of a truncate (truncated at residue 394) without the C-terminal domain that nevertheless was reported to retain activity, in contrast to earlier findings with human and pig KMO discussed above. [142]

1.4.2 KMO mechanism and properties

The proposed reaction mechanism for KMO was developed after studying *Pf*KMO with pre-steady-state kinetic techniques. The mechanism (Figure 1.11) is consistent with those of previously characterised Class A flavoprotein aromatic hydroxylases such as PHBH.

In the reductive half-reaction, L-kynurenine and NADPH bind to *Pf*KMO and the FAD cofactor is reduced by NADPH which then dissociates from the enzyme as $NADP^+$. The dissociation constant for the KMO·L-kynurenine complex was measured and determination of the reduction potential of the FAD cofactor both in the presence and absence of L-kynurenine showed that the reduction potential was unaffected by substrate binding. The dissociation constant for the KMO·NADPH complex was shown to be unaffected by the presence or absence of L-kynurenine but the rate of reduction of *Pf*KMO by NADPH was increased in the presence of L-kynurenine by a factor of 2500. This suggests that while L-kynurenine does not affect the ability of NADPH to bind to *Pf*KMO, it has to be present for rapid reduction to occur. After the FAD cofactor is reduced, there is rapid release of $NADP^+$.

The evidence from stopped flow kinetic experiments studying absorbance changes on mixing the anaerobic reduced *Pf*KMO·L-kynurenine complex with oxygen suggests that the reduced

flavin reacts with a molecule of oxygen, resulting in its one-electron reduction to superoxide; the two radical species rapidly react to form a peroxyflavin which is protonated to form a hydroperoxyflavin. The hydroperoxyflavin can then hydroxylate the substrate resulting in hydroxyflavin that re-forms the oxidised flavin independent of product release. The release of 3-hydroxykynurenine is the rate-limiting step of the mechanism and causes a change in the spectrum of the oxidised enzyme and it was hypothesised that the release of 3-hydroxykynurenine requires a conformational change. [137]

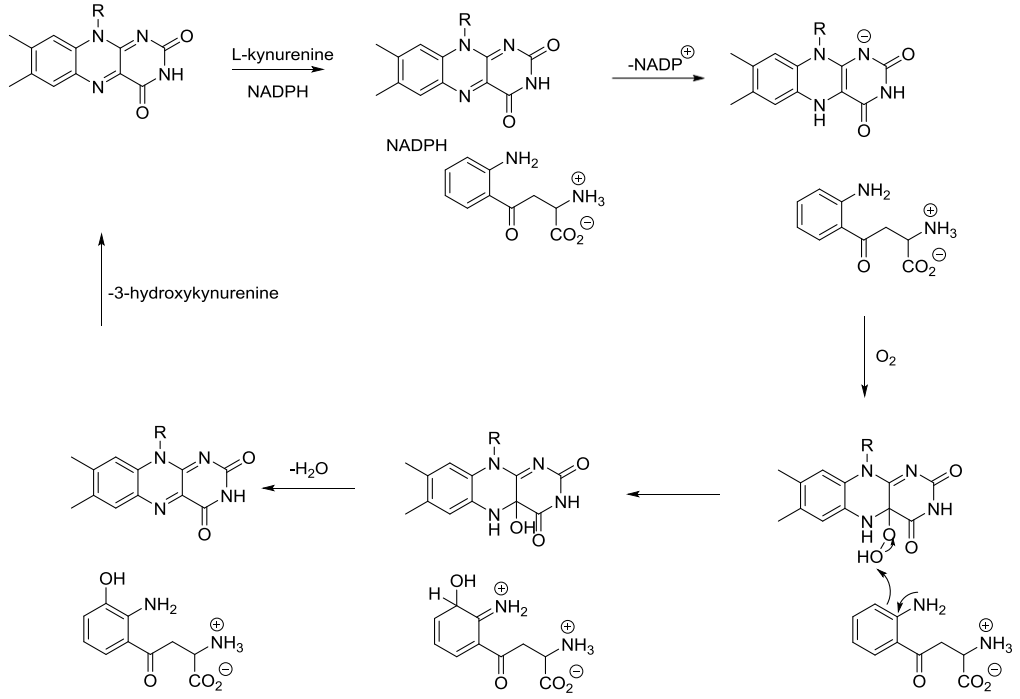

Figure 1.11: Overview of the proposed mechanism of KMO, figure adapted from work by Crozier-Reabe *et al*. [137]

These kinetic investigations also studied the effects of 3,4-dichlorobenzoylalanine and m-nitrobenzoylalanine, molecules that are structurally similar to L-kynurenine. It was found that these molecules are able to bind to *Pf*KMO and increase the rate of flavin reduction, although not to the same extent as L-kynurenine, but are not hydroxylated. [137] This suggests that the activating substituent on the aromatic ring (in this case NH_2) required by most flavoprotein aromatic hydroxylases is necessary for hydroxylation to proceed but is not vital to the recognition of substrate that controls FAD reduction.

In earlier work on *Pf*KMO, enzyme activity was observed to decrease with time in the absence of a reductant. Using a DNTB assay with Ellman's Reagent (5,5′-dithio-bis-[2-nitrobenzoic acid]) it was shown that this was related to the number of free thiols suggesting that in the absence of a reducing agent, cysteine residues in different monomers form disulfide bonds leading to aggregation and loss of activity. [96] *Pf*KMO has four cysteine residues and to stabilise the enzyme and successfully obtain crystal structures, two of these were mutated to serine residues. The C252S C461S *Pf*KMO (*Pf*KMO*) had similar kinetic properties to the wild-type enzyme (Table 1.3) and was used throughout this work. [143]

	K_M (μM)	k_{cat} (s^{-1})	k_{cat}/K_M ($s^{-1}\mu M^{-1}$)
*Pf*KMO	14.5 ± 2.5	9.1 ± 1.6	0.63
C252S C461S *Pf*KMO (*Pf*KMO*)	8.8 ± 1.5	8.9 ± 1.1	1.01

Table 1.3: Kinetic parameters of wild-type *Pf*KMO and *Pf*KMO* which contains two cysteine to serine mutations. Both enzymes have similar values of K_M and k_{cat} which were determined using a kinetic assay that monitored NADPH consumption. [143]

1.4.3 Structure of *Pf*KMO* with L-kynurenine

Until recently there was no structural information about KMO which has made attempts to design potent inhibitors challenging. In 2013 the first structure of KMO was published in *Nature* of a truncated *S. cerevisiae* enzyme (PDB entries include 4J36 and 4J33). [142] In addition to this structure, there is significant work on *Pf*KMO including solved structures with no ligand in the active site, with L-kynurenine bound and with inhibitors bound. [143]

Crystals of *Pf*KMO with L-kynurenine bound in the active site were successfully grown after two mutations, C252S and C461S, had been introduced in the enzyme (*Pf*KMO*). The structure had a high solvent content of approximately 84% and diffracted poorly resulting in a resolution of 3.4 Å for this structure. [143,144]

The main domain contains the Rossmann fold common to all Class A flavoprotein aromatic hydroxylases. [97] This domain non-covalently binds the FAD cofactor and also contains the active site of the enzyme. In the active site, the substrate and the isoalloxazine moiety of the cofactor are in close proximity (Figure 1.12).

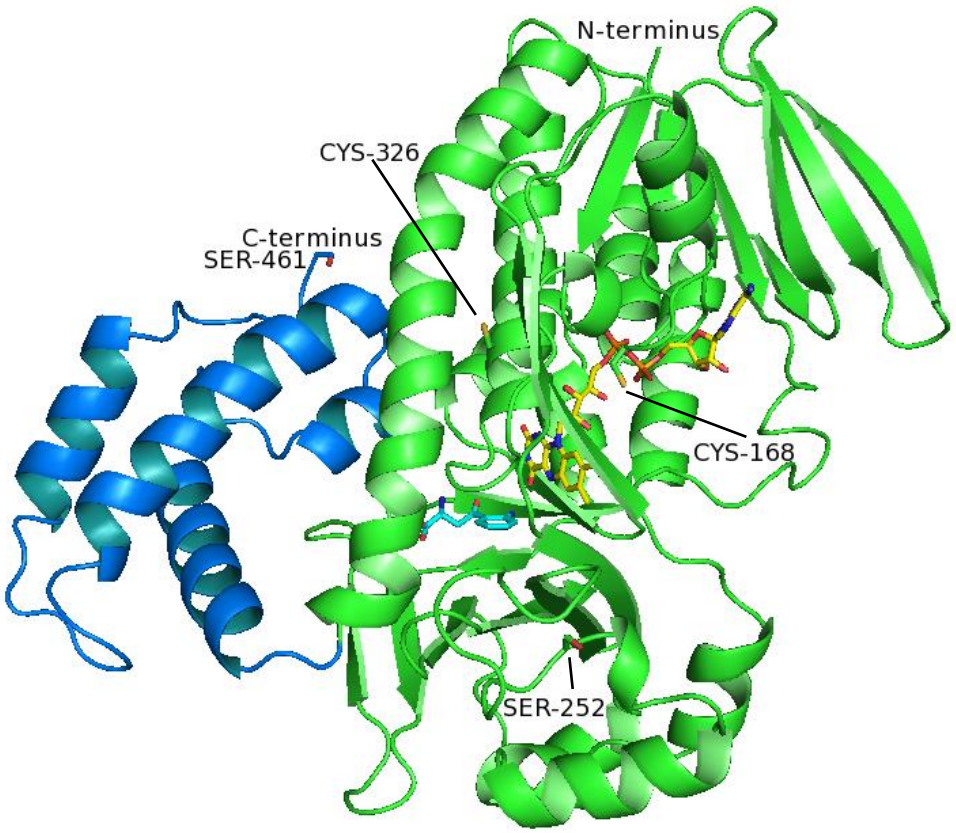

Figure 1.12: Structure of *Pf*KMO* with FAD cofactor (yellow) and L-kynurenine (cyan) bound in the active site. The main domain of the protein is shown in green and the C-terminal domain in blue. The two cysteines mutated to serines (S252 and S461) are labelled as are the two remaining cysteine residues (C168 and C326).

The active site contains a number of residues that are thought to be important in substrate binding and recognition. Close to the carboxylate group of the substrate there are a number of hydrophilic residues including R84, Y98, N369 and Y404 (Figure 1.13). Also present closer to the aromatic ring of the substrate are hydrophobic residues including L213, I224, L226, F238 and M373. An understanding of the key interactions between the substrate and the protein, based both on structural information and also kinetic data, will be necessary to validate this structure and also to understand substrate binding and to apply this knowledge to the design of effective inhibitors. The key interactions between *Pf*KMO* and L-kynurenine appear from this structure to include potential interactions between the carboxylate group of the substrate and R84, Y98, N369 and Y404.

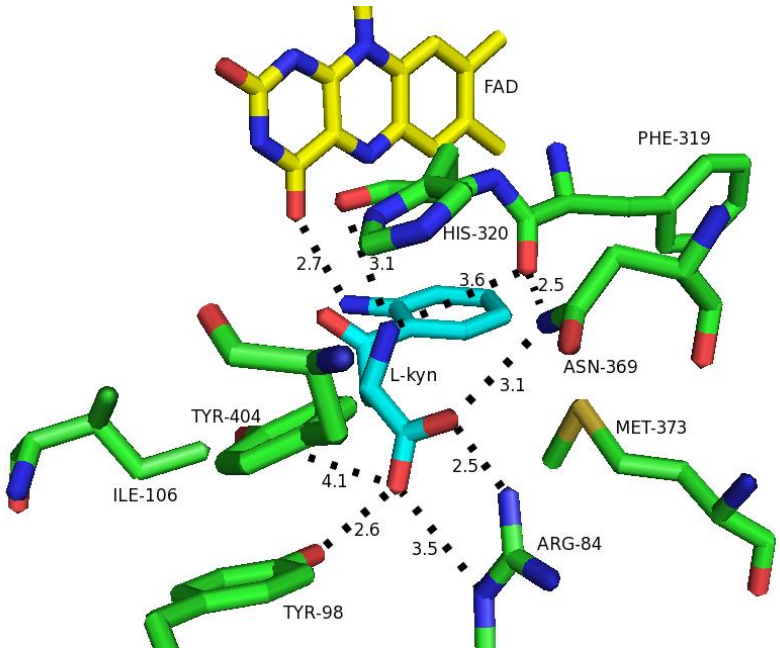

Figure 1.13: View of some of the active site residues of *Pf*KMO* with L-kynurenine (L-kyn, cyan) and the FAD cofactor (yellow) with approximate distances indicated are in Å. The carboxylate moiety of L-kynurenine is hypothesised to interact with R84, Y98, N369 and potentially Y404 although this residue appears to be over 4 Å from the substrate. The carbonyl of H320 is 3.1 Å from the amine of L-kynurenine. There is also a possible interaction between N369 and the carbonyl of F319.

1.4.4 Structure of *Pf*KMO* in the absence of substrate

A crystallographic model of the structure of *Pf*KMO* was also obtained in the absence of substrate in the space group $P2_122_1$ and at a higher resolution of 2.26 Å. [143] This structure also consisted of two domains with the main domain containing the Rossmann fold, the active site and the non-covalently bound FAD cofactor and a C-terminal domain (Figure 1.14). The main domain of both *Pf*KMO* structures is similar in both the presence and absence of substrate but there is a significant conformational change in the position of the C-terminal domain.

This significant movement of the C-terminal domain is thought to play an important role in substrate binding. [143] The substrate free form of *Pf*KMO* is an *open* conformation hypothesised to allow rapid substrate binding and product release. The C-terminal domain

moves in the event of substrate binding in the active site resulting in the *closed* conformation observed in the L-kynurenine bound structure.

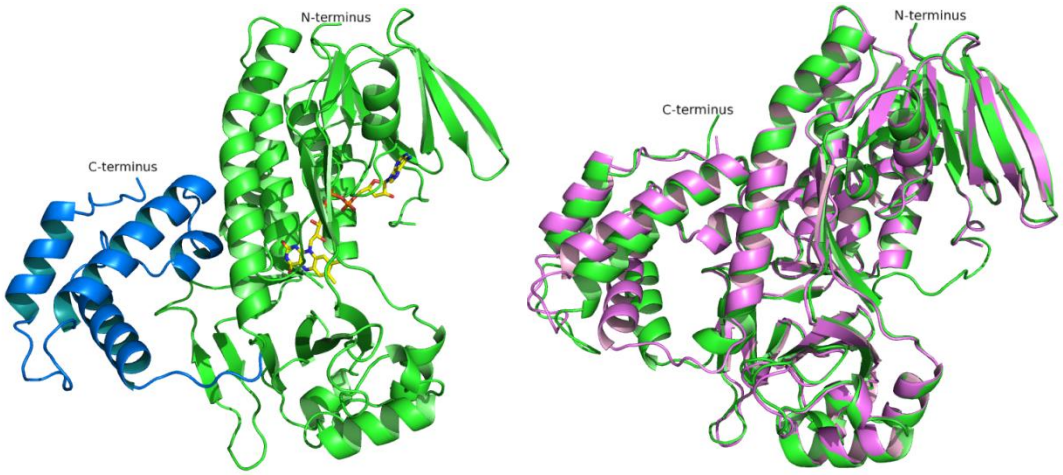

Figure 1.14: On the left is *Pf*KMO* with FAD (yellow) bound in the main domain (green) and the C-terminal domain (blue) in the absence of substrate, on the right is a comparison of the L-kynurenine bound (green) and substrate free (purple) structures.

The residues that are thought to control this movement of the C-terminal domain (Figure 1.15) are R84, E372, Y382 and R386. Three of these residues have been investigated in previous work using site-directed mutagenesis, crystallography and steady-state kinetics to elucidate their importance for conformational change. [143]

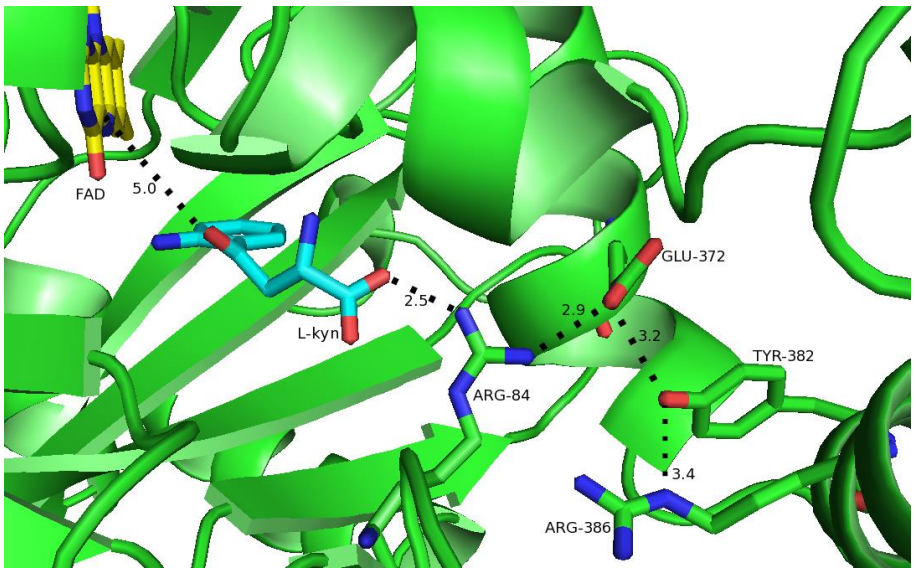

Figure 1.15: Proposed network of interactions resulting in the *closed* conformation, where the C-terminal domain is in closer proximity to the active site with distances indicated in Å. The residues thought to be involved in this interaction are Arg84, Glu372 and the C-terminal domain residues Tyr382 and Arg386. The distance between the site of hydroxylation in L-kynurenine (L-kyn) and the FAD cofactor is also indicated.

The mutations E372T, R386K, R386T and Y382F were made in *Pf*KMO* and the resulting proteins were successfully crystallised. The disruption of this network of interactions at any of these three residues resulted in a mixed conformation in the L-kynurenine bound structure and no conformational changes in the structures in the absence of substrate relative to that obtained for *Pf*KMO*. [143]

In the structure of Y382F with L-kynurenine bound, the C-terminal domain was moved further from the main domain resulting in a more *open* conformation although the extent of this movement is not as great as is observed in the substrate free structure of *Pf*KMO* (Figure 1.16). The C-terminal domain residues F382 and R386 are orientated towards the active site in the Y382F *Pf*KMO* structure although the distances between these residues and E372 are too large to maintain the network of interactions responsible for the *closed* conformation. The interactions between L-kynurenine, R84 and E372 are maintained in Y382F *Pf*KMO* and the positions of these residues are closer to those in the *Pf*KMO* with L-kynurenine than the structure in the absence of substrate. [143]

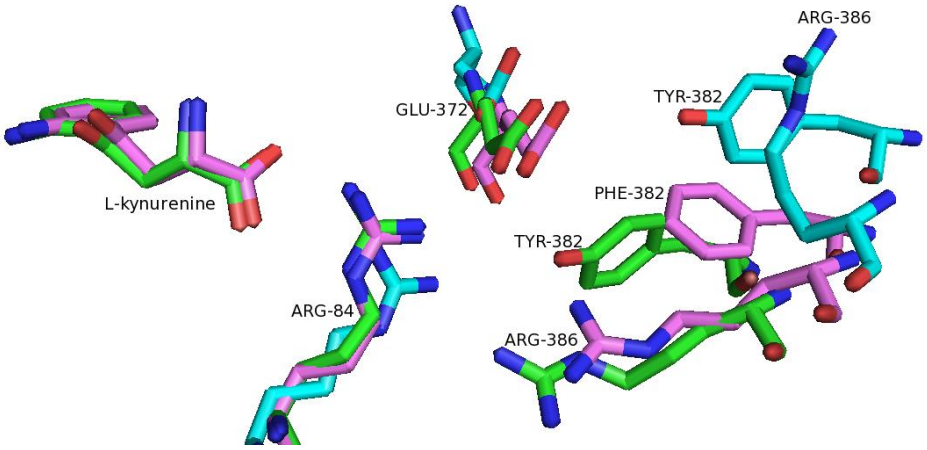

Figure 1.16: The positions of the substrate and residues implicated in the movement from the *open* to *closed* conformation in the structures of *Pf*KMO* with L-kynurenine bound (green), Y382F *Pf*KMO* with L-kynurenine bound (purple) and *Pf*KMO* in the absence of substrate (cyan). In the structures of Y382F *Pf*KMO* and *Pf*KMO* with L-kynurenine bound, the positions of L-kynurenine, R84 and E372 are similar but the mutation Y382F results in a loss of the interactions between this residue and both E372 and R386. The movement of F382 and R386 in this structure, compared to *Pf*KMO* with L-kynurenine bound and in the absence of substrate shows that Y382 *Pf*KMO* is in neither the *open* nor the *closed* conformation. The loss of interactions between these residues appears to prevent the *closed* conformation occurring, but in the presence of L-kynurenine, the interactions between the substrate, R84 and E372 prevent the structure from being in the *open* conformation.

1.4.5 *S. cerevisiae* KMO

S. cerevisiae KMO has been expressed in *E. coli* and purification resulted in the isolation of truncated KMO thought to be due to proteolysis at residue 396. [142] This KMO was shown in an HPLC-based assay to convert L-kynurenine to 3-hydroxykynurenine even though it has no C-terminal domain, in contrast to previous work on truncated pig KMO. [140,142]

Both the proteolysed form of *S. cerevisiae* KMO and an engineered truncate (truncated at residue 394) have been crystallised and the solved structures were the first published structures of a KMO enzyme. The structure of *S. cerevisiae* KMO truncated at residue 394

with no ligand bound in the active site (Figure 1.17) has been solved as a putative dimer with a resolution of 1.82 Å (PDB 4J33) and is the highest resolution KMO structure published to date. *S. cerevisiae* KMO has been co-crystallised with UPF 648 (Figure 1.19) in the active site of one monomer of the dimer at a resolution of 2.13 Å (PDB 4J36). [142]

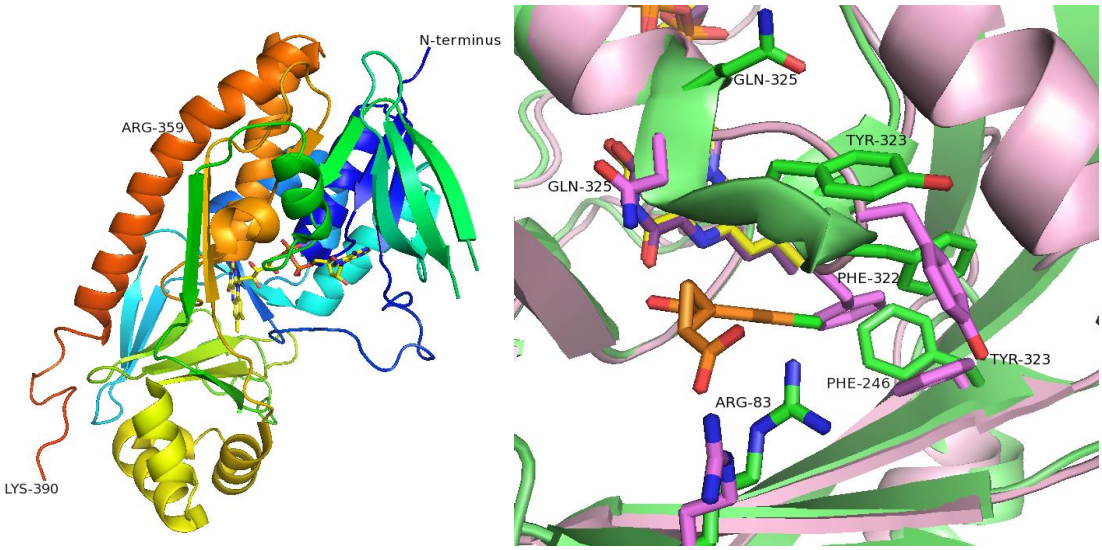

Figure 1.17: The structure of *S. cerevisiae* KMO (PDB 4J33) in the absence of ligand from N-terminus (dark blue) to Lys390 (orange), the last residue present in the structure. In the presence of UPF 648, residues Arg359 to Lys390 are disordered and their position could not be determined in PDB 4J36. On the right the secondary structures of *S. cerevisiae* KMO with no ligand (lilac) with FAD cofactor (purple) is compared with *S. cerevisiae* KMO with UPF 648 bound (green) with FAD cofactor (yellow) and UPF 648 (orange) from PDB 4J33 and 4J36 respectively. [142] In the presence of UPF 648 there is a conformational change resulting in a change of position of residues 322 – 325, Arg83 and Phe246.

When UPF 648 is bound in the active site of *S. cerevisiae* KMO, there is a conformational change with active site residues 322 – 325 forming a helix rather than a loop. In the absence of ligand, Y323 occupies space in the active site and the position of F322 causes displacement of F246, which is in a different orientation when UPF 648 is bound. The position of R83 is different in the two structures, probably due to a possible interaction with the carboxylate of UPF 648. This is similar to R84 from *Pf*KMO* suggesting that perhaps this residue might play a similar role in ligand binding and conformational control.

In the active site R83 and Y97 interact with the carboxylate group of UPF 648, the aromatic ring of UPF 648 is surrounded by hydrophobic residues and the carbonyl of P231 located about 3.2 Å from the aromatic ring of UPF 648. [142] An alignment of KMO sequences shows that many of these active site residues are conserved across different species including residues A53, R83, Y97, I104, M230, I232, L234, P321 and F322. Y323 is not conserved, and in *Pf*KMO the equivalent residue is H320. In the absence of any structural data for the C-terminal domain it is not possible to determine whether there are equivalents to the interactions observed between L-kynurenine and N369 and Y404 in *Pf*KMO* or whether there is a similar movement of the C-terminal domain occurring when ligands bind in the active site and how it is controlled in *S. cerevisiae* KMO.

1.5 KMO inhibitors

1.5.1 KMO inhibition by substrate analogues

Interest in developing KMO inhibitors for clinical use has been hindered by the lack of structural information. Assays for finding inhibitors have developed from measuring tritiated water released after hydroxylation to high-throughput assays combining liquid chromatography techniques with mass spectrometry using mitochondrial membrane fractions of human KMO which can rapidly identify potential lead compounds. [145,146]

In the absence of structural information early inhibitors of KMO were based on analogues of L-kynurenine (Figure 1.18). Early work showed that nicotinylalanine was a weak non-specific inhibitor of both KMO and kynureninase and was capable of causing an *in vivo* increase in kynurenic acid levels in rat brain tissue. [147,148]

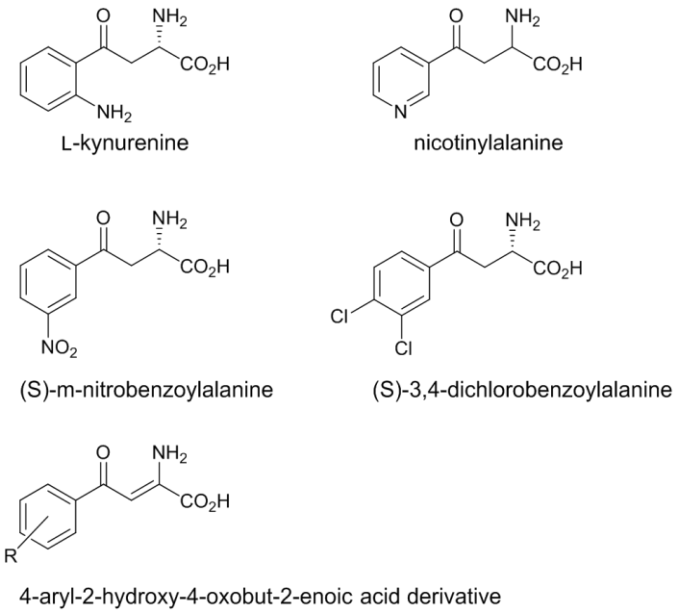

Figure 1.18: Chemical structures of L-kynurenine and KMO inhibitors developed from structural analogues.

The first inhibitor specific for KMO was m-nitrobenzoylalanine which increased levels of kynurenic acid and had anticonvulsant properties in rats. [148-150] Reports of an enantiopure sample were published soon after showing that the S-enantiomer was the active component. [151] This competitive inhibitor was used in a few studies of disease, particularly ischaemia, but more potent inhibitors have since been discovered. [83,84]

(R,S)-3,4-dichlorobenzoylalanine (FCE 28833A) has an increased affinity for KMO and causes a longer-lasting increase in kynurenic acid levels in rat brain tissue. [152] Structure-activity relationship analysis of 3,4-dichlorobenzoylalanine has shown that 3,4-dichloro substitution of the aromatic ring results in the most potent inhibitors, although 3,4-difluoro and 3-chloro derivatives are also potent. [153] Removing the carboxylic acid group results in an inactive molecule but the amine group is not necessary and substituting the amine with a (S)-hydroxyl or (S)-benzyl group can decrease the IC_{50} value observed in an assay using rat KMO from mitochondrial extracts. [153]

Incorporation of a double bond resulted in further derivatives that maintained an inhibitory effect and similar compounds were further investigated in a later study on 4-aryl-2-hydroxy-4-oxobut-2-enoic acids and esters. [154] The effect of the substitution pattern on the aromatic ring was investigated with these compounds and again it was observed that 3,4-difluoro or

3,4-dichloro compounds were the most potent and that 2-substituted compounds were not good inhibitors. The ester derivatives were active but were always slightly less potent than the acid derivatives. This study also demonstrated that some derivatives were able to decrease quinolinic acid formation in human macrophage tissue cultures. [154]

While these inhibitors were among the first molecules found to inhibit KMO it was also later found that they act as not as inhibitors but as effector molecules. It has been shown that 3,4-dichlorobenzoylalanine and m-nitrobenzoylalanine bind in the active site of KMO and stimulate NADPH reduction resulting in the formation of the unstable hydroperoxyflavin which is unable to hydroxylate these molecules resulting in release of H_2O_2 when the hydroperoxyflavin decomposes. [137]

1.5.2 Development of potent KMO inhibitors

A significant breakthrough in the development of potent KMO inhibitors was the development of *N*-(4-phenylthiazol-2-yl)benzenesulfonamide derivatives developed from the substrate analogue m-nitrobenzoylalanine by researchers at Hoffman-La Roche. In this series of inhibitors the carboxylic acid moiety was replaced by sulfonamides to improve the ability of the compound to pass through the blood brain barrier as well as to improve potency. [155]

Some inhibitors in this series were found to be significantly more potent than either m-nitrobenzoylalanine or 3,4-dichlorobenzoylalanine (FCE 28833) particularly the patented Ro 61-8048 (Figure 1.19) that has been used extensively in research with animal models of disease (Section 1.2). In developing Ro 61-8048, it was found that for potent inhibition, the best substitution on the aromatic ring near the sulfonamide was 3,4-diOMe and that the inclusion of 4-^{i}Pr, a large hydrophobic substituent, lead to significantly reduced inhibition. While this was thought to be due to combination of factors including substituent size, in view of our work with novel inhibitors, the loss of potency is probably due to the hydrophobic nature of the substituent as large substituents are tolerated by *Pf*KMO*. In this series, 3-NO_2 substitution resulted in more potent compounds than the 3,4-dichloro substitution unlike the research summarised above on substrate analogue derivatives; however, this group could result in toxic side-effects. [155]

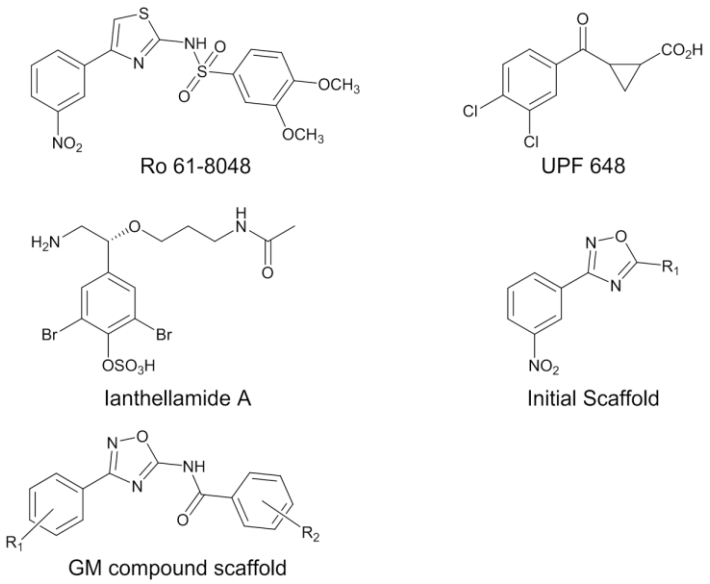

Figure 1.19: Chemical structures of further KMO inhibitors.

Other KMO inhibitors include UPF 648 which has been used to study the kynurenine pathway in the rat brain, inhibit KMO in a model of Huntington's disease, and was crystallised in the active site of *S. cerevisiae* KMO. [5,69,142] UPF 648 is also an effector rather than a true inhibitor and increases the production of H_2O_2 by a factor of 20. [142] A recent publication reported the discovery of Ianthellamide A, a naturally occurring KMO inhibitor isolated from the sponge *Ianthella quadrangulata*. [156]

The development of Ro 61-8048 and UPF 648 resulted in more potent KMO inhibitors being available for studying the kynurenine pathway in animal models of disease; however, it was still necessary to design inhibitors that would not stimulate FAD reduction by NADPH. A new scaffold was designed and tested *in vitro* in collaboration with Gavin Milne, a PhD student supervised by Nigel Botting and David O'Hagan at St Andrews University. A series of molecules were synthesised by G. Milne and optimisation has resulted in the development of extremely promising inhibitor molecules which do not cause H_2O_2 production. Study of most of the early molecules in this series was carried out by other members of the Mowat research group but kinetic and crystallographic data for the latest series of potent compounds is contained in Chapter 3.

The inhibitors designed on the GM compound scaffold are significantly larger than L-kynurenine and while the 3,4-dichloro substituted ring binds in the same position as the aromatic ring of L-kynurenine, the other aromatic ring of the inhibitor extends beyond the

active site. [143] This causes changes in the position of active site residue sidechains to accommodate the inhibitor and the interactions responsible for connecting the two domains in the *closed* conformation are disrupted. In the structure of *Pf*KMO* with inhibitors bound, the main domain is similar to the L-kynurenine bound structure but the C-terminal domain has moved to the same position occupied in the *open* conformation observed in the *Pf*KMO* structure in the absence of ligands in the active site (Figure 1.20). [143]

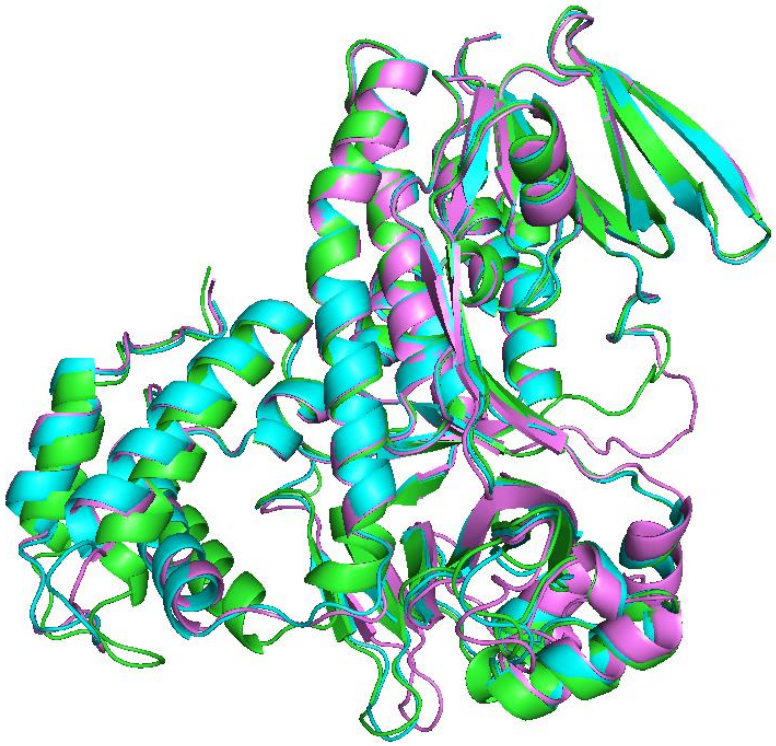

Figure 1.20: Representation of the secondary structure elements of the protein chain in the structure of *Pf*KMO* with inhibitor GM303 (magenta), *Pf*KMO* with L-kynurenine (green) and *Pf*KMO* in the absence of substrate (cyan).

The inability of *Pf*KMO* to form the *closed* conformation when the inhibitors are bound is the proposed reason for these compounds not acting as effector molecules. In the presence of these inhibitors and in the absence of L-kynurenine, no consumption of NADPH can be detected suggesting that the FAD cofactor is not being reduced and therefore cannot form a hydroperoxyflavin. These compounds represent a very interesting and potentially clinically relevant development in KMO inhibition.

1.5.3 Characterisation of enzyme inhibition

The Michaelis-Menten equation is used to describe enzyme reactions where the enzyme and substrate reversibly interact to form an enzyme-substrate complex that can then irreversibly react resulting in free enzyme and product (Equation 1.1). [157] By graphically plotting the observed rate of reaction against substrate concentration, this equation is used to determine the values of V_{max} and the Michaelis-Menten constant which indicates the affinity of the enzyme for the substrate.

$$v = \frac{V_{max}\,[S]}{K_M + [S]} + S \qquad \mathrm{E} + \mathrm{S} \rightleftharpoons \mathrm{ES} \rightarrow \mathrm{E} + \mathrm{P}$$

Equation 1.1: The Michaelis-Menten equation and a general formula for the reaction described where ν is reaction rate, V_{max} is the maximum rate, [S] is substrate concentration, K_M is the Michaelis-Menten equation, E is the enzyme, S is the substrate and P is the product.

Inhibitors can interact with the enzyme or enzyme-substrate complex to inhibit the reaction in different ways that affect the values of K_M and V_{max} as summarised below:

- Competitive inhibitors reversibly compete with the substrate for binding to the enzyme, usually in the active site, resulting in an unchanged V_{max} and an increased K_M
- Non-competitive inhibitors bind to an allosteric site decreasing the catalytic activity of the enzyme but not its affinity for the substrate resulting in an unchanged K_M and a decreased V_{max}
- Mixed inhibitors can bind both to the enzyme and the enzyme-substrate complex and decrease the catalytic activity of the enzyme and the affinity of the enzyme for the substrate resulting in a decreased V_{max} and increased K_M
- Uncompetitive inhibitors bind to the enzyme-substrate complex and increase the affinity of the enzyme for the substrate and decrease the catalytic activity of the enzyme resulting in a decreased K_M and V_{max}

The *in vitro* effect of an inhibitor on an enzyme can be investigated by determining the rate of reaction at various substrate concentrations at a series of inhibitor concentrations. The Dixon plot can be used to determine the value of K_i by plotting the reciprocal of reaction rate against the inhibitor concentration. [158] A disadvantage of this method is that it does not

always clearly show the difference between competitive and mixed inhibition so it is often complemented by a graph of substrate concentration divided by reaction rate plotted against inhibitor concentration. [159] This combination allows the determination of both K_i and the type of inhibition observed (Figure 1.21). The Dixon plot is also known to be less reliable than other methods such as simultaneous non-linear regression methods. [160]

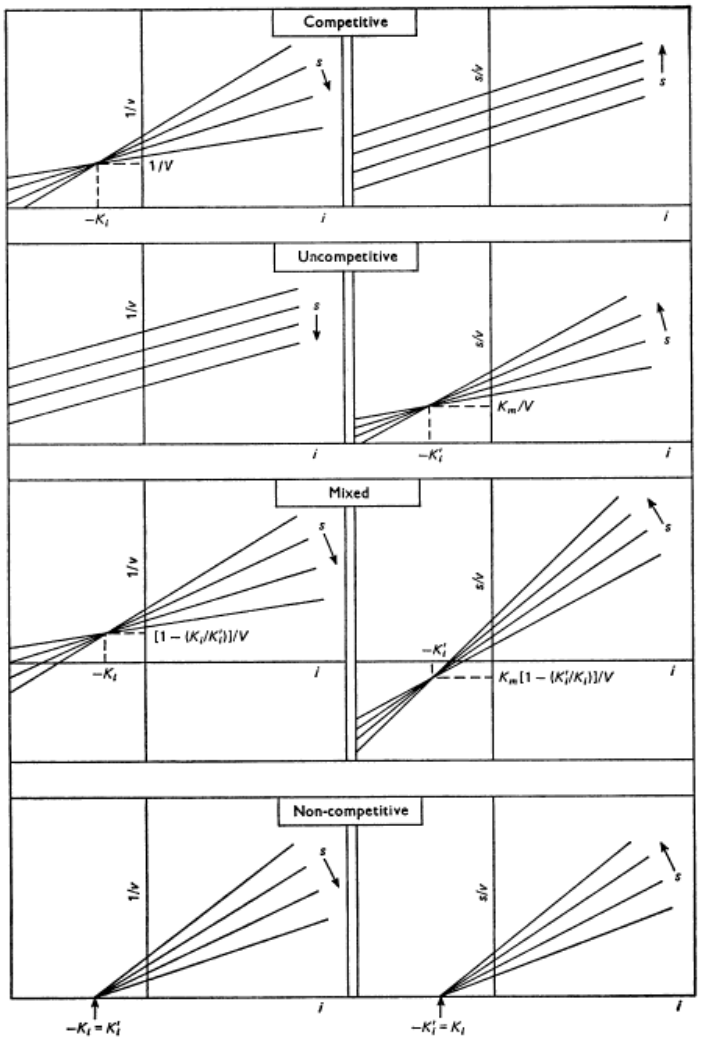

Figure 1.21: Dixon plots (left) and s/v against i (right) for each type of enzyme inhibition where s is substrate concentration, v is reaction rate and i is inhibitor concentration. Taken from Cornish-Bowden, 1974. [159]

1.6 Protein crystallisation

1.6.1 Protein crystals

Protein crystals have long-range order as they consist of identical repeating units called *unit cells*. Unit cells can contain multiple protein molecules which are related to each other by symmetry elements that can include translational, rotational and screw axes. The space group assigned to a crystal denotes the symmetry elements that relate the molecules in the unit cell as well as the relative dimensions and angles of the unit cell.

A common method to crystallise proteins is vapour diffusion in which a drop containing the protein and well solution is either suspended above a well solution on a glass coverslip (hanging drop vapour diffusion) or placed on a bridge surrounded by the well solution (sitting drop vapour diffusion) in a sealed environment. Vapour diffusion results in water from the drop transferring to the well solution over time increasing both the protein and precipitant concentration in the drop until equilibrium is reached. For successful crystallisation this results in conditions changing from the undersaturation zone to the nucleation zone (Figure 1.22). In the nucleation zone, a nucleus from which crystal growth can occur is formed. As protein crystals start to form, the concentration of protein in the drop decreases, causing the conditions to move into the metastable zone if crystallisation is sufficiently slow and controlled.

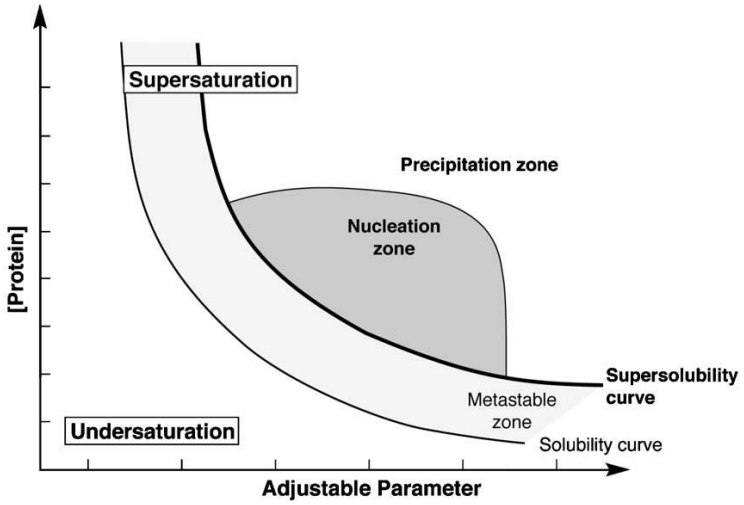

Figure 1.22: Phase diagram representing conditions in which nucleation, crystallisation and precipitation can occur with protein concentration plotted against an adjustable experimental parameter e.g. precipitant concentration. Taken from N. E. Chayen. [161]

Protein crystals are, on average, 50% solvent with ordered water molecules close to the protein interacting specifically with the protein molecule that will be seen in the electron-density maps and disordered water molecules further from the protein molecule. [162]

1.6.2 The phase problem

When x-rays are diffracted by the electron density of atoms in the crystal, the reflected x-rays are detected by the detector which measures both the position and intensity of the reflection. Detectable reflections in the diffraction image require the constructive interference of diffracted x-rays. This only occurs when Bragg's Law (Equation 1.2) is fulfilled for a set of Miller indices (Figure 1.21). Parallel planes in the unit cell are described by using the Miller indices, hkl, where the values of h, k and l indicate the number of planes that intersect the x, y and z axes of the unit cell.

$$2d_{hkl} \sin\theta = n\lambda \quad (1.2)$$

Equation 1.2: Bragg's Law where θ is the diffraction angle, d_{hkl} is the spacing between the hkl planes, n is an integer and λ is the wavelength of the x-ray radiation.

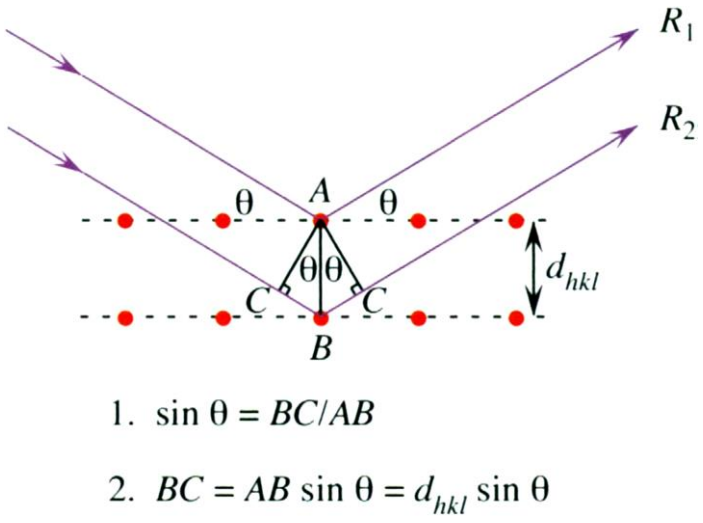

Figure 1.21: The relationship between d_{hkl} and θ, taken from G. Rhodes p56.[162] The red dots are lattice points located on parallel planes indicated by the black dots. The purple arrows represent x-rays R_1 and R_2 and the spacing between the planes, d_{hkl}, is equal to vector AB. When $2d_{hkl}\sin\theta$ (where θ is the diffraction angle) is equal to an integer multiplied by the wavelength of the x-rays, then the x-rays interfere constructively.

The diffracted x-rays are periodic waves with amplitude, frequency and phase. Any periodic function can be described as a sum of terms in the form below (Equations 1.3 – 1.5). [162]

$$f(x) = \sum_{h=0}^{n} F_h \left[\cos 2\pi\,(hx) + i \sin 2\pi\,(hx)\right] \quad (1.3)$$

$$f(x) = \sum_{h} F_h\, e^{2\pi i(hx)} \quad (1.4)$$

$$f(x,y,z) = \sum_{h}\sum_{k}\sum_{l} F_{hkl}\, e^{2\pi i(hx+ky+lz)} \quad (1.5)$$

Equation 1.3 describes a general periodic function as the sum of Fourier terms dependant on cos and sin where F is amplitude and h is frequency. **Equation 1.4** is a simplification of **1.3** using complex number theory. **Equation 1.5** is a general formula for a periodic function in three dimensions.

The square root of the intensity of a reflection in the diffraction image is proportional to the structure factor. The structure factor is the sum of the contribution to each reflection from each atom in the unit cell (Equations 1.6 and 1.7). [162]

$$f_{hkl} = f_j\, e^{2\pi i(hx_j+ky_j+lz_j)} \quad (1.6)$$

$$F_{hkl} = \sum_{j=1}^{n} f_j e^{2\pi i(hx_j+ky_j+lz_j)} \quad (1.7)$$

Equation 1.6 describes the contribution of an atom, j, to a reflection in the diffraction pattern where f_j is the atomic scattering factor of atom j which depends on the chemical identity of the atom and (x_j, y_j, z_j) are the coordinates in real space of atom j. **Equation 1.7** defines the structure factor, F_{hkl} as the sum of the contributions of each atom in the structure to the reflection.

As the structure factor, F_{hkl}, is dependent on the identity and position of atoms within the unit cell (Equation 1.7), it can also be described in terms of electron density per unit volume. By considering the electron density in infinitesimally small units of volume, this relationship can

be expressed as a Fourier transform (Equation 1.8). The electron density can then be expressed in the reverse Fourier transform (Equation 1.9) using a triple sum rather than an integral because the structure factor is a sum of contributions from discrete atoms to the reflections. [162]

To calculate the electron density and create an electron density map of the protein molecule from Equation 1.9 it is necessary to know the amplitude, frequency and phase of the diffracted waves but the phase is unknown and cannot be experimentally determined. This is the phase problem which must be solved for every reflection.

$$F_{hkl} = \int_V \rho(x,y,z)\ e^{2\pi i(hx+ky+lz)}\, dV \quad (1.8)$$

$$\rho(x,y,z) = \frac{1}{V}\sum_h \sum_k \sum_l F_{hkl}\ e^{-2\pi i(hx+ky+lz)} \quad (1.9)$$

Equation 1.8 expresses the structure factor as the integral of the electron density where ρ(x,y,z) is the electron density at coordinates (x,y,z), F_{hkl} is the structure factor and V is unit cell volume. **Equation 1.9** expresses electron density as the Fourier transform of the structure factor.

The phase problem can be solved either by isomorphous replacement methods with heavy atoms e.g. mercury, or by using anomalous scattering by an element such as selenium. In multiple isomorphous replacement, a heavy atom that diffracts strongly is incorporated, often by soaking, into the protein crystal. The intensities of spots in the diffraction image differ in the data sets of the protein and the protein with heavy atom incorporated. This difference is used to determine the structure factors for the heavy atoms.

The difference in the structure factors of the data set of the protein with heavy atoms and the native protein is used to calculate the difference Patterson function. This function is used to make the Patterson map which contains peaks corresponding to vectors between atoms. As there are only a few heavy atoms in each unit cell, it is possible for the position of the heavy atoms to be determined computationally from the peaks in the Patterson map. This process often has to be repeated with another heavy atom that binds at a different position and from all the information calculated from the data sets, only one possible solution for the phases remains. Multiwavelength anomalous dispersion is a similar process but all the data required can be generated from one crystal using synchrotron radiation where the wavelength can be

changed. Some atoms, including selenium, can absorb x-rays, but this absorption drops at a wavelength specific to that element called the absorption edge.

Molecular replacement methods can be used to solve a structure if there is a homologous structure that has previously been solved. Molecular replacement programs use the previously solved structure as a model inserted into the unit cell of the unsolved data to attempt to find a solution that fits the experimental data. [162] The molecular replacement program *Molrep* uses translation and rotation functions to find the correct position of protein molecules in the unit cell using model of a previously solved homologous protein. The solution is found when the calculated and observed structure factors are in agreement. [163]

1.7 Aims

Inhibition of KMO has been identified as a potentially beneficial therapeutic strategy in diseases including Huntington's disease, Alzheimer's disease and acute pancreatitis. There is therefore a need to develop potent inhibitors of KMO that do not act as effectors. In this work a set of novel KMO inhibitors is assayed with *Pf*KMO* to investigate the effects of substituents on the K_i value. Crystallisation of *Pf*KMO* with some of these inhibitors was undertaken to further understand how they bind and what important interactions are formed between the inhibitor and the protein to gain insights useful for developing more potent inhibitors that may lead in the future to the development of KMO inhibitors that can be used clinically.

Recently crystal structures of *Pf*KMO* and *S. cerevisiae* KMO have been obtained. These structures have provided valuable insights into the chemistry of KMO but a thorough characterisation of residues in the active site has not yet been completed. In this work, residues in the active site of *Pf*KMO* are investigated using kinetic and crystallographic techniques to investigate proteins that have mutations in the active site. The information gained in this work will complement the previously obtained structures and be useful in confirming whether the hypotheses made about the roles and importance of residues in the active site are correct.

A further aspect of this work is to characterise the role of residues in the active site of *Pf*KMO* that are not conserved in the human KMO enzyme. The only residue not conserved is H320, which is a phenylalanine in the human enzyme. Characterisation of this residue may provide insights into potential differences in the active site properties of the two enzymes and indicate whether *Pf*KMO* is a good model for understanding the human enzyme and also whether the inhibitors shown to be effective in inhibiting *Pf*KMO* are likely to be potent inhibitors of the human enzyme.

Chapter 2: Materials and Methods

2.1 Site-directed mutagenesis using megaprimer PCR

The megaprimer method contains two rounds of PCR. [164] In the first round the primer for the mutation and the flanking primer for the end of the gene closest to the mutation site are added to the PCR mixture. The result is a megaprimer which is then used as a primer for the second round of PCR in which the whole of the gene is amplified. After each round of PCR the DNA product is purified before being used in further steps. After the gene is amplified with the mutation introduced, it is digested with restriction enzymes and then ligated into a pET17b plasmid. The plasmid is then transformed into competent cells and sequenced to confirm that the desired mutation has been achieved.

2.1.1 Primer design

The primers used for the megaprimer PCR are given in Table 2.1. The combination of these individual primers used to obtain each desired mutation is listed in Table 2.2.

T7 Promoter	TAATACGACTCAGTATAGGG
T7 Terminator	GCTAGTTATTGCTCAGAGG
N Terminator (F) primer	GAAGAGATATACATATGACTGCTACAGACAAGGC
R84K	GTGATGATGCGTGGGAAAATGGTGCATGTG
Y98A	CTGCAGCCAGCCGGACGTGATGAC
N369S (reverse complement)	CTCCACGTAGCTTTCCAGGGC
Y404F (reverse complement)	GACCATGCTGAAACGCGGGATAAAACG

Table 2.1: Primer sequences used for megaprimer PCR. The bases highlighted in yellow are those changed to make the mutation in the amino acid sequence, those underlined were changed to optimise primer properties.

Mutation	Mutation primer	Flanking Primer in PCR 1	Flanking Primer in PCR 2
R84K	R84K	T7 Promoter	T7 Terminator
N369S	N369S	T7 Terminator	T7 Promoter
Y404F	Y404F	T7 Terminator	T7 Promoter

Table 2.2: Combination of primers used for each mutation made using megaprimer PCR.

2.1.2 PCR 1

The composition of a typical PCR 1 reaction is given in Table 2.3. The reactions were set up in a 0.2 ml sterile tube and were made to a volume of 50 µl using elution buffer (from a QIAprep® Spin Miniprep kit). The flanking primer used was either the T7 promoter or terminator primer depending on which site was nearer to the mutation site.

2.5 µl 10× ThermoPol buffer
0.25 mM dNTPs
1 µl template plasmid
0.4 µM flanking primer
0.4 µM mutation primer
1 Unit Vent polymerase

Table 2.3: Typical PCR 1 composition

The typical reaction conditions are given below in Table 2.4. Vent polymerase was added during the first 50 ºC step.

	Temperature (ºC)	Time (s)	No. of Cycles
Stage One	96	60	1
Stage Two	96 50 + 0.2 per cycle 72	60 60 60 +1 per cycle	30
Stage Three	72	300	1

Table 2.4: Typical conditions for PCR 1

2.1.3 Purification of PCR product

The PCR product was purified by extraction from a 1% w/v agarose gel. The gel was prepared by heating genetic analysis grade agarose in TAE (0.04 M Tris, 0.05 M EDTA pH 8.0 and 0.02 M glacial acetic acid) buffer. Ethidium bromide was added to the cooled buffer to allow visualisation of the DNA bands under UV light.

Samples were prepared by adding 6× Bromophenol Blue loading dye to the PCR mixture. The samples were loaded into the gel once it had been set and the gel was run in TAE buffer at 110 mV. The DNA band was separated from the gel using a PureLink Quick Gel Extraction Kit (Life Technologies) and was eluted in 40 µl of Elution Buffer. This was stored at -20 ºC until required.

The yield from the gel was often low so for some reactions the PCR mixture was directly purified using either a gel extraction kit or a QIAquick® PCR Purification Kit (QIAgen). A few µl of the PCR product was reserved to run on a gel to check that only one DNA band could be observed.

2.1.4 PCR 2

The typical composition of a PCR 2 reaction is given in Table 2.5. The reaction was made to final volume of 50 µl using elution buffer. The megaprimer volume was often varied to achieve a successful reaction.

2.5 µl of 10× ThermoPol Buffer
0.25 mM dNTPs
2 mM $MgCl_2$ or $MgSO_4$
0.4 µM flanking primer
2 µl plasmid template
15 µl megaprimer
1 Unit of Vent polymerase.

Table 2.5: Typical composition of PCR 2

The typical conditions for a PCR 2 are given in Table 2.6. The reaction was purified as described above for PCR 1 and stored at -20 ºC until required.

	Temperature (ºC)	Time (s)	Number of Cycles
Stage One	96	60	1
Stage Two	96 75 68	60 45 45	4
Stage Three	96 55 + 0.25 per cycle 72	60 90 60 + 1 per cycle	25
Stage Four	72	300	1

Table 2.6: Typical conditions for PCR 2

2.1.5 Digestion

Prior to ligation into a pET17b plasmid, the PCR product had to be digested with Type II restriction enzymes. The purified PCR product was incubated at 37 ºC for 3 hours with 5 µl of 10× NEB (New England Biolabs) Buffer 4 and 0.04 Units each of Nde1 and Xho1.

The digestion reaction was quenched either by running the reaction mixture on a 0.8% w/v agarose gel followed by an extraction kit as described above in Section 2.1.3 or by heating the reaction mixture to 80 ºC for ten minutes.

The pET17b plasmid was also digested before the ligation reaction, using the same procedure described above. The plasmid was extracted using a QIAprep® Spin Miniprep kit (QIAgen) from 10 ml cultures of *E. coli* cells that had been grown for 16 hours at 37 ºC (as described in section 2.3.2) before harvesting by centrifugation.

2.1.6 Ligation

The digested PCR product was ligated into a digested pET17b plasmid prepared as described in Section 2.1.5. The reactions were carried out at 4 ºC overnight. A typical ligation reaction contained 1 µl pET17b, 4 µl insert, 2 µl T4 DNA ligase buffer and 1 µl T4 DNA ligase made to a final volume of 10 µl using elution buffer (from a QIAprep® Spin Miniprep kit).

2.1.7 Transformation of high efficiency cloning cells

The ligation product was used to transform NEB 5-alpha Competent *E. coli* (High Efficiency) Cells. The cells were defrosted on ice before 30 µl was transferred to a sterile 15 ml polypropylene tube and incubated on ice with 5 µl of ligation product. The cells were heat-shocked at 42 ºC for 40 seconds before a further 5 minutes on ice. Approximately 950 µl LB or SOC (Table 2.10) was added and the cells were incubated at 37 ºC for 1 hour. 100 µl of cells were spread onto a warm sterile agar plate (prepared as described in Section 2.3.1) which was incubated at 37 ºC overnight.

2.1.8 Submission of samples for Sanger Sequencing

Cells were grown from an individual colony in 10 ml LB with 50 µg/ml ampicillin (as described in Section 2.3.2) overnight at 37 ºC with shaking at 200 rpm. The cells were harvested by centrifugation and the plasmids were extracted using a QIAprep® Spin Miniprep kit (QIAgen).

Samples containing 5 µl plasmid and 1 µl of 3.2 µM primer were submitted for sequencing. One sample with each flanking primer (T7 promoter or terminator) was submitted for sequencing. The Sanger Sequencing was performed by The Genepool at the University of Edinburgh and the data obtained is listed in Appendix 1.

2.1.9 Transformation of BL21 (DE3) *E. coli* cells

Plasmids which were found to contain the desired mutation were used to transform BL21 (DE3) *E. coli* cells in order to express active *Pf*KMO protein.

The competent cells were defrosted on ice and 30 µl of cells was mixed with 5 µl plasmid in a sterile 1.2 ml Eppendorf tube. The tubes were gently tapped to mix and then heat-shocked in a 42 ºC water bath for 20 seconds before returning to ice. Approximately 1 ml of SOC or LB was added (as described in Table 2.10) and the cells were incubated at 37 ºC for 1 hour. 100 µl of the cells was spread onto a dry warm agar plate which was then incubated overnight at 37 ºC.

2.2 Site Directed Mutagenesis using a Quikchange protocol

Other mutations were made using a Quikchange II Site-Directed Mutagenesis kit (Agilent technologies) with an adapted primer design strategy using primers that have long overhang regions. [165] The primers were designed to contain the mutations near the 5′ end and to have long overhanging regions in 3´ end. The pairs of primers for each mutation were therefore not complimentary. The primers used in this protocol are listed below in Table 2.7.

Primer	Primer Sequence (5´ – 3´)
R84A forward	CGCGGGGCTATGGTTCATGTGCCGGGCACG
R84A reverse	CACCATGGCCCCACGCATCATCACCGCTTC
H320F forward	CCGTTCTTTGGCCAAGGCATGAACTGTGCA
H320F reverse	CTGGCCAAAGAAGGGTACCATGGGATGGGC
Y404A forward	CCGCGTGCCAGCATGGTCACCTTCAGCCGC
Y404A reverse	CATGCTGGCACGTGGGATAAAACGCGTCGG

Table 2.7: Primers designed for the Quikchange protocol written from 5´ to 3´. The bases highlighted in yellow indicate the changes made to obtain the required mutation and those underlined show changes made to improve primer properties but that do not affect the amino acid sequence.

2.2.1 PCR Conditions

The PCR was a one-pot process set up in a 0.2 ml sterile tube using the reagents provided in the Agilent QuikChange II Site-Directed Mutagenesis kit. The typical composition is given in Table 2.8 below and was made to a final volume of 50 µl using sterilised H_2O. The only varied parameters were the volumes of plasmid and primer used.

5 µl 10× reaction buffer
1 µl dNTPs (proprietary mix)
2 µl template plasmid
2.5 µl forward primer
2.5 µl reverse primer
2.5 Units *PfuUltra* High-Fidelity DNA polymerase

Table 2.8: Typical composition of QuikChange PCR.

The typical reaction conditions are given in Table 2.9 below. The reaction was performed in a Techne TC3000 thermal cycler.

	Temperature (ºC)	Time (minutes)	Number of cycles
Stage One	95	5	1
Stage Two	95 55 72	1 1 10	12
Stage Three	45 72	1 30	1

Table 2.9: Typical conditions for QuikChange PCR.

2.2.2 Digestion of template plasmid

To remove the template plasmid which would not contain the desired mutation, the PCR mixture was then incubated with a Type 1 restriction enzyme.

5 Units of DpnI were added directly to the reaction mixture. The tube was centrifuged briefly to thoroughly mix the contents and the digest was incubated at 37 ºC for 1 hour.

2.2.3 Transformation of competent cells

After incubation with DpnI, the PCR mixture was used to transform competent cells, either the XL-1 Blue Supercompetent cells provided in the kit, as described below, or into NEB 5-alpha *E. coli* (High Efficiency) cells as described above in Section 2.1.7.

The transformation into XL-1 Blue Supercompetent cells was carried out in a cold, sterile 14 ml polypropylene tube. 50 µl of cells were mixed with 1 µl PCR product on ice. The tubes were gently rotated to mix the contents and were incubated on ice for 30 minutes. The cells were then heat-shocked at 42 ºC for 40 seconds before the tubes were returned to ice.

After 2 minutes on ice, 0.5 ml LB was added to the transformations and the tubes were incubated for 1 hour at 37 ºC. 100 µl of the cells were spread onto agar plates as described in Section 2.1.7 and plasmids were submitted for Sanger sequencing as described in Section 2.1.8.

2.3 Cell growth and protein expression

2.3.1 Media

The media used are listed in Table 2.10 below. All media was adjusted to pH 7.0 with NaOH and autoclaved at 121 ºC for 20 minutes before use.

LB media	10 g/l tryptone 5 g/l yeast extract 5 g/l NaCl
LB Agar	LB media with 15 g/l agar
SOC media	20 g/l tryptone 5 g/l yeast extract 8.56 mM NaCl 2.5 mM KCl 10 mM $MgCl_2$ 20 mM glucose

Table 2.10: Media used to grow cells for cloning and protein expression

LB agar plates were prepared with autoclaved LB agar cooled to 40 ºC before 50 µg/ml ampicillin was added. The media was poured into sterile Petri plates and stored at 4 ºC until shortly before use when the plates were incubated at 37 ºC for 1 hour.

2.3.2 BL21 (DE3) *E. coli* cells

*Pf*KMO protein was produced in BL21 (DE3) *E. coli* cells containing a pET17b vector with the KMO gene. The cell growth was initiated in 30 ml sterile tubes containing 10 ml LB and 50 µg/ml ampicillin. Once inoculated with the BL21 (DE3) *E. coli* cells, the tubes were incubated for approximately 20 hours at 37 ºC with shaking at 180 rpm.

To produce active protein, cells were grown slowly in a second overnight step. 1 l of LB with 50 µg/ml ampicillin in a 1 l Nalgene flask was inoculated with 10 ml cell culture. Cells were grown at 22 ºC with shaking at 180 rpm for 16 hours.

Cells were harvested by centrifugation in at 8289 *g* for 7 minutes and the cell mass obtained was stored at -20 ºC until required.

2.4 Protein purification

2.4.1 *Pf*KMO purification

The compositions of the buffers used in the purification are listed in Table 2.11. The buffers were made using deionised water and the pH was adjusted using NaOH. Before use the buffers were filtered through a 0.22 µm filter.

The BL21 (DE3) *E. coli* cells were defrosted on ice and resuspended in 10 ml (per gram cell weight) lysis buffer supplemented with 0.2 mM PMSF. Cells were lysed by sonication for an approximate total of 1-2 minutes on ice in bursts of 20 seconds each followed by a minimum of one minute to cool on ice. Sonicated cells were centrifuged at 38759 *g* for 1 hour. The supernatant was filtered, before further purification, using 0.22 µm syringe-driven filters.

The filtered protein solution was loaded onto a 60 ml FPLC Q-Sepharose 26/10 column pre-equilibrated with lysis buffer. The column was connected to an Akta FPLC pump. A yellow band was observed on the column. The column was washed with 400 ml wash buffer before *Pf*KMO was eluted using 500 ml elution buffer. Fractions were collected in an automated fraction collector. The elution of *Pf*KMO was monitored using UV absorbance at 280 nm and a kinetic assay (as described in Section 2.5.1) and fractions found to contain *Pf*KMO were pooled.

*Pf*KMO in the pooled fractions was precipitated by slow addition of 300 ml ammonium sulfate buffer on ice. After 30 minutes the mixture was centrifuged at 38759 *g* for 20 minutes at 4 ºC. The supernatant was discarded and the yellow pellets could be stored at -20 ºC prior to further purification.

*Pf*KMO was further purified using size exclusion chromatography. The column and buffer used depended on whether the protein sample was required for crystallisation or for kinetic assays.

Lysis buffer	20 mM HEPES, pH 7.5 10 mM NaCl 1 mM DTT
PMSF stock	0.2 M PMSF in ethanol
Wash buffer	20 mM HEPES, pH 7.5 50 mM NaCl 1 mM DTT
Elution buffer	20 mM HEPES, pH 7.5 110 mM NaCl 1 mM DTT
Ammonium sulfate buffer	20 mM HEPES, pH 7.5 75% (saturated) ammonium sulfate 1 mM DTT
Size exclusion buffer 1	20 mM HEPES, pH 6.8 10 mM NaCl 1 mM DTT
Size exclusion buffer 2 (for crystallography)	20 mM HEPES, pH 6.8 110 mM sodium acetate 1 mM DTT

Table 2.11: Composition of buffers used for in purification

*Pf*KMO purified for kinetic assays was purified using either G25 Sephadex column using gravity at 4 ºC or a 120 ml S75 column connected to an Akta FPLC pump. This protocol used size exclusion purification buffer 1.

*Pf*KMO was resuspended in a minimum volume of size exclusion buffer 1 and concentrated to a total volume of 2 ml using VIVASPIN MW 30000 concentrators. When the G25 column was used, the protein was loaded onto the pre-washed column and eluted as a single fraction judged by eye. Alternatively, the protein could be loaded onto the S75 column using a 2 ml loop and eluted in a single fraction using the absorbance at 280 nm as a guide for fraction collection. After size exclusion chromatography, *Pf*KMO was adjusted to the required concentration and flash frozen in liquid nitrogen before being stored at -80 ºC.

Highly pure samples were required for crystallography and this was achieved using the S75 column pre-equilibrated in size exclusion buffer 2. *Pf*KMO was resuspended in a minimum volume of size exclusion buffer 2 and concentrated to a total volume of 2 ml as described above. Pure *Pf*KMO was collected as a single fraction. The protein was concentrated again and then diluted to adjust the concentration of sodium acetate to approximately 10 mM. *Pf*KMO was concentrated to 240 µM and stored in 50 µl aliquots at -80 ºC after flash freezing in liquid nitrogen.

2.4.2 SDS-PAGE

The success of the purification was confirmed using SDS-PAGE. Protein samples were denatured by heating in boiling water for 5 minutes. The samples were then mixed with an equal volume of 2x NuPAGE® LDS sample buffer and then loaded into a pre-cast NuPAGE® Novex® 4-12% Bis-Tris SDS-PAGE gel run in NuPAGE® MES SDS running buffer. A protein marker (SeeBlue® or SeeBlue® Plus 2 Pre-Stained Standard) was also loaded into the gel to allow determination of approximate molecular weight.

Once the gel had run for 1 hour, it was removed from the plastic casing and stained using Coomassie Blue stain (Table 2.12) for 45 minutes with gentle shaking. The gel was then gently shaken in a destain solution (Table 2.12) for one hour and then overnight in water. An image of the destained gel was obtained before disposal.

Coomassie Blue Stain	0.1% Coomassie Brilliant Blue 40% methanol 10% acetic acid
Destain solution	40% methanol 10% acetic acid

Table 2.12: Staining and destaining solutions used for SDS-PAGE

2.5 Kinetic Assays

2.5.1 Purification assay

A kinetic assay was used during purification to check for the presence of active *Pf*KMO in fractions eluted from the Q-Sepharose anion-exchange column. This 1 ml cuvette assay monitored absorbance at 340 nm for 0.5 minutes using a Varian Cary 50 Probe UV-visible spectrophotometer. The typical composition of the assay is given in Table 2.13 below made to a total volume of 1 ml using 20 mM HEPES buffer, pH 8.0. The wavelength was chosen because NADPH absorbs at 340 nm but $NADP^+$ does not so that as NADPH reduces the FAD cofactor, the absorbance detected at this wavelength decreases with decreasing concentration of NADPH.

220 µM NADPH
200 µM L-kynurenine
50 µl *Pf*KMO sample

Table 2.13: Composition of purification cuvette assay

2.5.2 Michaelis-Menten Kinetics

The Michaelis-Menten parameters, K_M and k_{cat}, were determined using a 1 ml cuvette assay monitored at 340 nm for 0.5 minutes using a Varian Cary 50 Probe UV-Vis spectrophotometer. The typical composition of the assay is given in Table 2.14. Each sample had a different concentration of L-kynurenine while NADPH was held in excess.

20 mM HEPES buffer, pH 8.0
250 µM NADPH
20 µl L-kynurenine (various concentrations)
10 µl *Pf*KMO (10 – 30 µM)

Table 2.14: Typical composition of Michaelis-Menten kinetic assay

The measured change in absorbance at 340nm is converted to enzyme turnover using the equation below:

$$Turnover = \frac{\Delta Absorbance(340nm)}{60 * \varepsilon(NADPH\ at\ 340\ nm) * [enzyme]}$$

Equation 2.1: Calculation of enzyme turnover (s^{-1}) where ΔAbsorbance is the change in absorbance at 340 nm (min^{-1}) and ε is the molar absorption coefficient of NADPH at 340 nm which is 6200 $M^{-1}cm^{-1}$.

The Michaelis-Menten parameters were obtained by plotting the turnover values against L-kynurenine concentration in Origin 8.5.1. Assays were performed in triplicate to obtain accurate values.

2.5.3 Inhibition assays

A similar kinetic assay was used to determine the K_i values for a range of inhibitor compounds. Data were collected exactly as in Section 2.5.2 but both the kynurenine and inhibitor concentrations were varied. The composition of a typical assay sample is given below in Table 2.15.

935 µl 25 mM HEPES, pH 8.0
25 µl 10 mM NADPH
20 µl kynurenine (concentration varies)
10 µl inhibitor (concentration varies)
10 µl *Pf*KMO (10 – 30 µM)

Table 2.15: Composition of typical inhibition assay

A typical assay consisted of 25 measurements combining 5 kynurenine concentrations and 5 inhibitor concentrations. The inhibitor and kynurenine concentrations were combined randomly during the assay to decrease statistical error. As the inhibitor stocks were prepared using DMSO to solubilise the organic compounds, the samples containing 0 µM inhibitor contained an equal volume DMSO to replace the inhibitor as a control

Assays were performed in triplicate and the data were analysed using the Erithacus Software program GraFit which calculated the K_i value with single non-linear regression methods.

2.7 Crystallography

2.7.1 Hanging drop vapour diffusion

The hanging drop vapour diffusion method was used to grow crystals of *Pf*KMO either with no ligands in the active site or with kynurenine, substrate analogues or inhibitors bound in the active site.

Crystals were grown in 24 well plates, either Linbro or VDX, with 0.5 ml well solution in each well. The well solutions were varied to find the optimum conditions but typically contained 1.0M HEPES buffer pH 7.0, PEG 4K, isopropanol, glycerol and a salt, usually either NaCl or sodium tartrate.

Hanging drops consisting of a 1:1 mixture of 240 µM *Pf*KMO and well solution were suspended from a siliconized glass cover-slip over the well solution. The slide was sealed to the edges of the well using soft white paraffin. The trays were wrapped in aluminium foil to block out light. The trays were stored at 4 ºC and left undisturbed for at least 24 hours before being checked for crystals.

2.7.2 Sitting drop vapour diffusion

The sitting drop vapour diffusion method was used to grow *Pf*KMO crystals with inhibitor molecules bound in the active site. The sitting drops were set up in Greiner Bio-one CrystalBridge™ in 24 well plates using a 1:1 mixture of 240 µM *Pf*KMO and well solution. The well solutions were set up as described above in Section 2.7.1. The trays were wrapped in aluminium foil and stored at 4 ºC. Crystals were usually observed within one week.

2.7.3 Data collection

All data were collected on the macromolecular beamlines at the Diamond Light Source at Harwell Campus, Didcot, Oxfordshire. The crystals were transported to the Diamond Light Source in sample holders kept in liquid nitrogen.

Before the crystals were frozen in liquid nitrogen, they were cyroprotected using ethylene glycol. Crystals grown in hanging drops were picked up in cryoloops and exposed to 10%

and then 20% ethylene glycol solutions prepared using the appropriate well solution conditions. Crystals were flash-cooled in liquid nitrogen in a sample holder. Crystals grown in sitting drops were cryoprotected by adding 1 µl ethylene glycol directly to the drop before freezing on a loop.

2.7.4 Data processing

The diffraction images obtained from data collection were processed using *iMosflm* which determines the intensity of each reflection and the unit cell parameters. [166] The mtz files generated were processed further using programs supported by *CCP4i* (Collaborative Computer Project, number 4). [167] The Laue group was determined using *POINTLESS,* scaled using *SCALA* and the intensities were converted to structure factor amplitudes using *CTRUNCATE*. [168,169]

Molecular replacement was carried out using *MOLREP* which required the *SCALA* output and a model of a similar protein to obtain the phases (a PDB file of previously solved *Pf*KMO in the appropriate space group was used). [163] The model was refined using *REFMAC5* and after each round of refinement, the structure was validated using *Coot*. [170,171] Ligands were added to the model where appropriate in *Coot* after the dictionary and the three-dimensional coordinates in PDB format were generated from a two-dimensional representation using the *PRODRG* server. [172,173]

2.8 Presentation of data in figures and tables

Figures containing cartoon or stick representations of crystallographic structures throughout were made using Pymol (The PyMOL Molecular Graphics System, Version 1.5.0.5 Schrödinger, LLC). [174]

Figures of kinetic data fitted to the Michaelis-Menten equation were prepared using Origin 8.5.1 (Origin Lab, Northampton, MA). Accurate determination of K_i values by simultaneous non-linear regression analysis was carried out using GraFit 3.0, Erithacus software. [175]

Representations of chemical structures of small molecules were made using ChemDraw® Prime 15.0 (PerkinElmer software).

Chapter 3: Inhibition of *Pf*KMO*

3.1 Development of novel KMO inhibitors

A novel scaffold for KMO inhibitor compounds was developed in collaboration with Dr Gavin Milne, University of St Andrews, who synthesised this set of compounds as part of his PhD thesis (Figure 3.1). The initial scaffold has a number of similarities to the Ro 61-8048 compound as both contain an aromatic ring with a nitro-substituent and a heterocycle. Investigations into extending the structure of the initial scaffold led to the development of the final scaffold. The aim of developing this series of compounds was to make potent KMO inhibitors that did not contain the 3-NO_2 group thought to be associated with toxicity in Ro 61-8048. In addition, the aim was to develop compounds that would not act as effectors that allow reduction of the FAD cofactor by NADPH but cannot be hydroxylated resulting in the unstable hydroperoxyflavin decaying with release of H_2O_2.

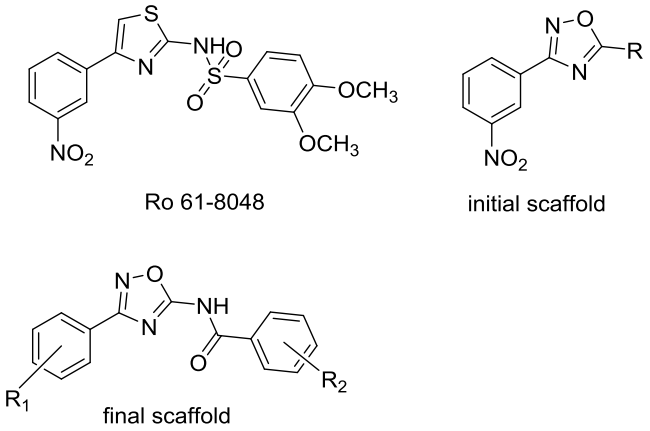

Figure 3.1: The structures of Ro 61-8048 and the initial and final scaffolds of the novel inhibitor compounds. *Pf*KMO* inhibition was obtained using compounds based on the initial scaffold. This was then developed to the final scaffold from which more potent *Pf*KMO* inhibitors were designed.

The aim of further developing this series of compounds was to investigate the effect of substituents on both of the aromatic rings to obtain potent inhibitors. The results for compounds with only a hydrogen atom at R2 or with a 3,4-diOMe substituent were

investigated in previous work (Table 3.1). Ro 61-8048 was assayed against *Pf*KMO* under the same conditions to provide a direct comparison with the novel series of inhibitor compounds. [143]

Compound Name	R1	R2	% activity decrease	K_i value (μM)
Ro 61-8048				1.03 ± 0.27
GM302	3-H	H	10.3 ± 9.5	
GM339	3-Me	H	8.4 ± 9.6	
GM348	3-OMe	H	7.0 ± 5.1	
GM342	3-F	H	1.3 ± 8.0	
GM304	3-CF_3	H	22.6 ± 12.1	
GM307	4-Br	H	21.3 ± 10.9	
GM340	3-Cl	H	22.0 ± 3.6	2.77 ± 0.43
GM308	3-Br	H	13.0 ± 9.2	1.581 ± 0.197
GM303	3,4-diCl	H	95.0 ± 3.2	0.115 ± 0.011
GM328	H	3,4-diOMe	5.4 ± 4.6	
GM366	3-Me	3,4-diOMe	2.2 ± 7.7	
GM467	3-OMe	3,4-diOMe	20.3 ± 5.1	
GM367	3-F	3,4-diOMe	17.7 ± 9.1	
GM457	3-CF_3	3,4-diOMe	39.7 ± 13.6	
GM469	4-Br	3,4-diOMe	44.3 ± 13.6	
GM466	3-Cl	3,4-diOMe	56.4 ± 9.6	0.782 ± 0.054
GM440	3-Br	3,4-diOMe	62.4 ± 10.9	1.330 ± 0.084
GM347	3,4-diCl	3,4-diOMe	94.4 ± 1.9	0.065 ± 0.020

Table 3.1: Table showing K_i assay results and activity tests using 10 μM inhibitor to measure the percentage decrease in activity for compounds based on the final scaffold of GM compounds quoted from previous work. The K_i assays were conducted in cuvettes with *Pf*KMO* as described in Section 2.5.3. [143]

Comparing the two sets of compounds in Table 3.1, it can be seen that the effects of R1 substitution are more significant than R2. Compounds with either no substituent or with electron-donating substituents at R1 (GM302, GM339, GM328 and GM366) were poor inhibitors of *Pf*KMO*. Chloro- and bromo-substitution at R1 can be used in place of the

3-NO_2 group, which is present in Ro 61-8048, while maintaining an inhibitory effect. It can be seen by comparing GM340, GM308, GM307 and GM303 that di-chloro substitution was particularly effective compared to monosubstitution with either chlorine or bromine in the 3- and 4- positions. GM303 was the first compound in this series shown to have greater potency than Ro 61-8048.

It can be seen that potency of the chloro/bromo-substituted compounds is also enhanced by di-OMe substitution on the other aromatic ring (GM compounds 340 and 466, 308 and 440, 307 and 469, and 308 and 347). This effect is particularly pronounced with R1 chloro-substituted compounds compared to the 3-Br substituted compounds. In the case of GM347, a compound had now been developed with a K_i value approximately 15× smaller than that of Ro 61-8048, and the subsequent compounds in this series were designed with 3,4-dichloro substitution and a series of R2 substituents to obtain even more potent compounds (Table 3.2). [143,176]

Compound Name	R1	R2	K_i value (μM)
GM303	3,4-diCl	H	0.115 ± 0.011
GM347	3,4-diCl	3,4-diOMe	0.065 ± 0.020
GM729	3,4-diCl	3,4-diOH	0.067 ± 0.018
GM760	3,4-diCl	3-$OPO(OEt)_2$, 4-OMe	0.020 ± 0.004
GM769	3,4-diCl	3-OMe, 4-$OPO(OEt_2)$	0.017 ± 0.002
GM854	3,4-diCl	3-OMe, 4-OCH_2CO_2H	0.029 ± 0.012

Table 3.2: Table containing K_i values for compounds with 3,4-dichloro substitution on the R1 aromatic ring. [143,176]

The compounds with 3,4-dichloro substituents at R1 were all potent inhibitors with R2 substitution contributing less to the degree of potency. 3,4-diOH and 3,4-diOMe substitution results in almost equally potent compounds (GM347 and GM729). Large substituents were tolerated in both meta- and para- positions with no significant differences in the measured K_i values observed between GM760, GM769 and GM854.

Four of these inhibitors, GM303, GM347, GM760 and GM769, have been crystallised with *Pf*KMO* in previous work in the $P6_122$ space group. [143] A comparison of the structures of *Pf*KMO* with L-kynurenine bound and with GM303 bound shows that the 3,4-dichloro substituted ring binds in the same position as the aromatic ring of L-kynurenine, in close

proximity to the isoalloxazine moiety of the FAD cofactor, but the large size of GM303 results in displacement of residues in the active site (Figure 3.2). All the inhibitors crystallised to date cause a displacement of R84 disrupting the interactions important for the *closed* conformation resulting in a movement of the C-terminal domain away from the active site. N369 is in a slightly different position able to interact with the carbonyl group of GM303. There is a slight conformational change affecting F319 and H320. With the displacement of R84, E372 and M373 are not held in close proximity to the active site and move further from the ligands. The positions of Y98, Y404 and the majority of the hydrophobic active site residues are unaffected.

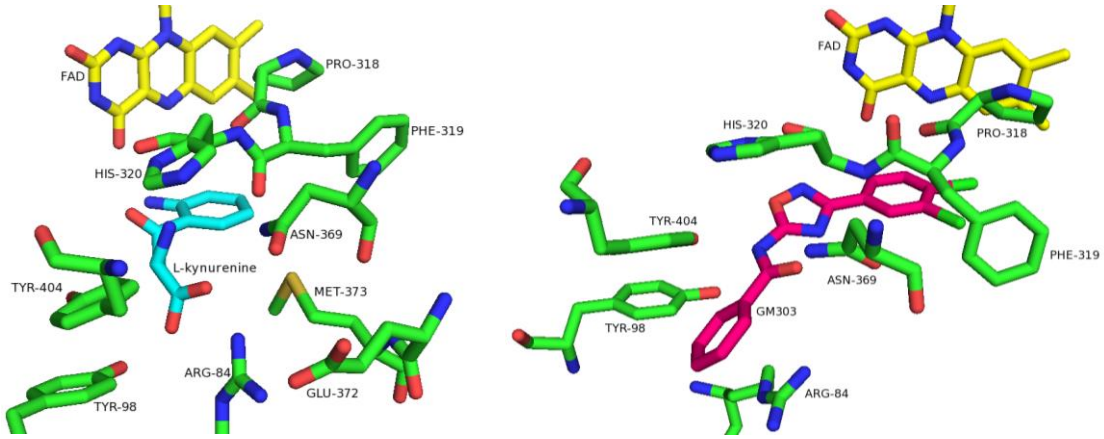

Figure 3.2: A comparison of some active site residues of *Pf*KMO* with L-kynurenine (left, cyan) and GM303 (right, pink) bound with the isoalloxazine moiety of the FAD cofactor (yellow). In the presence of GM303, Arg84 is displaced relative to its position in the presence of L-kynurenine, Asn369 and Tyr404 appears to interact with GM303. The displacement of Arg84 in the presence of GM303 prevents the formation of any interaction between Arg84 and Glu372, which is observed in the presence of L-kynurenine. [143]

The set of structures of *Pf*KMO*: inhibitor complexes have shown that there is more than one mode of inhibitor binding. The structure of *Pf*KMO* with GM760 bound shows the 3-OPO(OEt)$_2$, 4-OMe substituted aromatic ring in a different position than in the structure with GM303 causing movement of some active site residues (Figure 3.3). The change in the inhibitor position starts with the orientation of the carbonyl, which in GM303 is orientated towards N369 (Figure 3.3). In the structure containing GM760, the carbonyl is oriented in the opposite direction but the position of N369 is unaffected. The position of Y404 is

different in these structures with Y404 in the structure of *Pf*KMO* with GM760 able to interact with E372. [143]

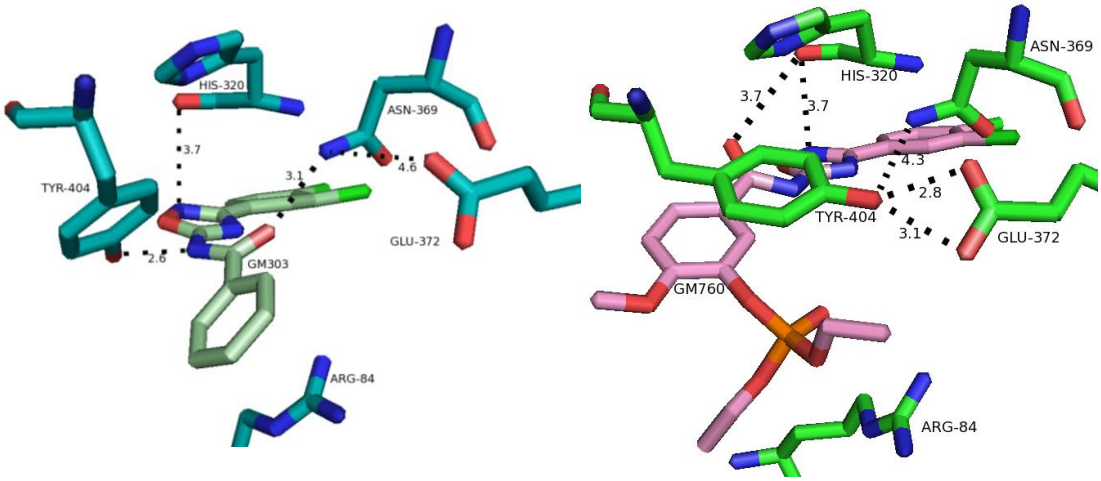

Figure 3.3: A comparison of the residues in close proximity to inhibitors bound in the active site in the structures of *Pf*KMO* with GM303 (left) and GM760 (right). In the structure of *Pf*KMO* with GM303 (teal) bound, the carbonyl of GM303 is able to interact with Asn369, the amide nitrogen is 2.6 Å from the hydroxyl group of Y404 and part of the heterocyclic ring is within 4 Å of the carbonyl of His320. In the structure of *Pf*KMO* with GM760 (pink) bound, the GM760 amide carbonyl is over 6 Å from Asn369. Y404 is significantly displaced and is able to interact with Glu372. The carbonyl of His320 is now within 4 Å of both the amide carbonyl and the heterocyclic moiety.

This series of novel inhibitors contains a number of promising compounds that are more potent than any previously reported inhibitors. In addition to this, they are true inhibitors in that they prevent the FAD cofactor from being reduced by NADPH, which results in H_2O_2 production observed with effector molecules. [143] This series also does not break Lipinski's "rule of five" for the following criteria: they have molecular weight of less than 500 Da, fewer than 5 hydrogen bond donors, fewer than 10 hydrogen bond acceptors. [177] The solubility of these compounds may present problems, as currently only GM760 and GM769 have been solubilised in water although the solubility of the newest series of compounds remains to be investigated. [143]

There are other compounds in this series which required characterisation to further explore the effect of substitution on the aromatic ring that, when the inhibitor is bound, is closest to

the C-terminal domain both to investigate the effect of any potential interactions between the substituents and *Pf*KMO* and also to understand the different modes of inhibitor binding. These inhibitors are studied in this work both with kinetic assays and by crystallisation with *Pf*KMO*.

3.2 Purification of *Pf*KMO*

The purification of *Pf*KMO*, prior to use in kinetic assays and crystallisation, was carried out as outlined in Section 2.4 with no differences in procedure required to obtain any of the *Pf*KMO* mutations discussed in this thesis. Typical chromatograms, SDS-PAGE and UV-visible spectrum obtained during the purification of *Pf*KMO* are presented below.

The first column used in *Pf*KMO* purification is a Q-Sepharose anion-exchange column. The supernatant obtained after centrifugation of cell debris was filtered and loaded onto the column with 10 mM NaCl present in the buffer (Section 2.4.1). The concentration of NaCl was increased to 50 mM before the elution of *Pf*KMO* in 110 mM NaCl to obtain fractions of higher purity. A typical chromatogram (Figure 3.4) shows the absorbance at 280 nm of the column eluent.

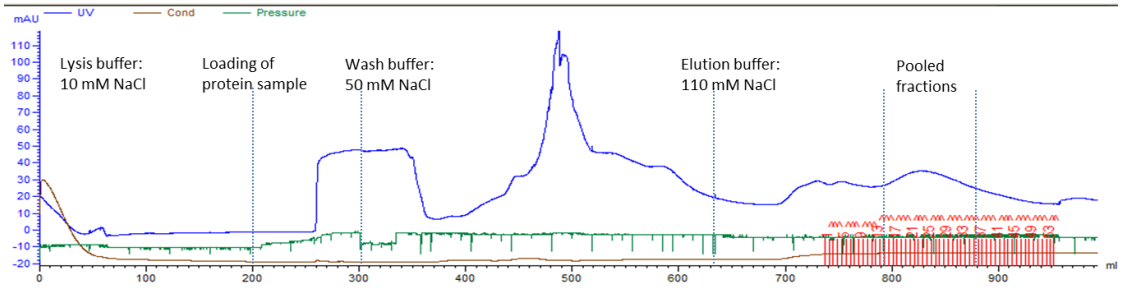

Figure 3.4: Typical chromatogram obtained showing absorbance at 280 nm of eluent from the Q-Sepharose column against volume in ml. The lysis buffer contained 20 mM HEPES, pH 7.5, 10 mM NaCl and 1 mM DTT. After the soluble fraction from cell lysis was loaded, the concentration of NaCl was increased to 50 mM NaCl. After other proteins had been eluted at this concentration of NaCl, the elution buffer, 110 mM NaCl, was used to elute the protein. Fractions containing active *Pf*KMO* were pooled prior to ammonium sulfate precipitation.

After ammonium sulfate precipitation, *Pf*KMO* was resuspended and concentrated before loading onto a S200 gel filtration column. The purified protein was collected as a single fraction when an increase in the UV-visible absorbance at 280 nm was observed at approximately 170 ml after column loading.

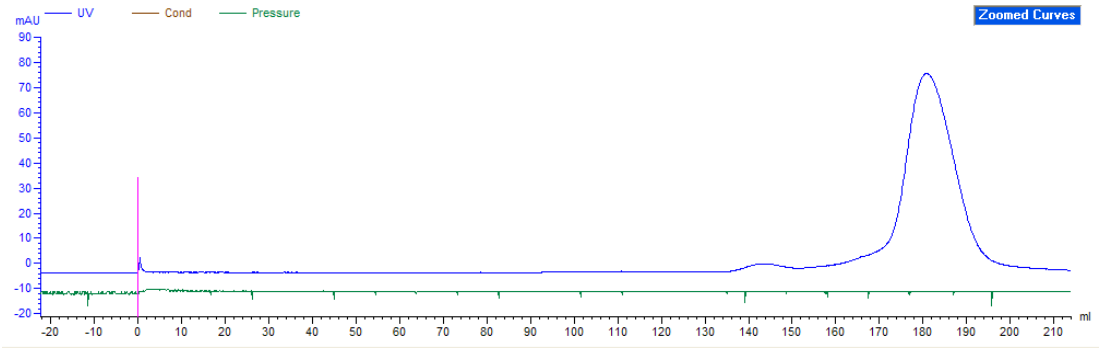

Figure 3.5: Typical chromatogram obtained showing absorbance at 280 nm of eluent from the S200 gel filtration column against volume in ml. The column was equilibrated in 2 column volumes buffer before the protein was loaded (at 0 ml). A single fraction of *Pf*KMO* was collected.

To determine the purity of *Pf*KMO* obtained, an SDS-PAGE gel of samples taken during the purification process was run (Section 2.4.2). A typical SDS-PAGE obtained is shown below with samples taken throughout the purification process (Figure 3.6).

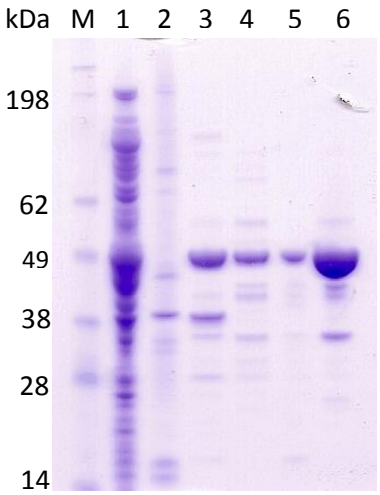

Figure 3.6: Typical SDS-PAGE gel of samples collected during *Pf*KMO* purification. The marker used is SeeBlue Pre-Stained Protein Standard (Invitrogen) with the weights of the

standards given in kiloDaltons; Lane 1 is supernatant obtained after centrifugation of lysed cells; Lane 2 is flow-through from the Q-Sepharose column; Lane 3 is the pooled fractions containing *Pf*KMO* from the Q-Sepharose column; Lane 4 is *Pf*KMO* after ammonium sulfate precipitation; Lane 5 is the fraction from the S200 column, Lane 6 is the concentrated fraction from the S200 column.

The UV-visible spectrum of a sample of purified *Pf*KMO* was obtained after each purification and the concentration determined using the known molar absorption coefficient of *Pf*KMO at 450 nm. [96] The concentration of the sample could then be adjusted as required, with protein used in crystallographic trials concentrated to 240 µM before storage at -20 ºC.

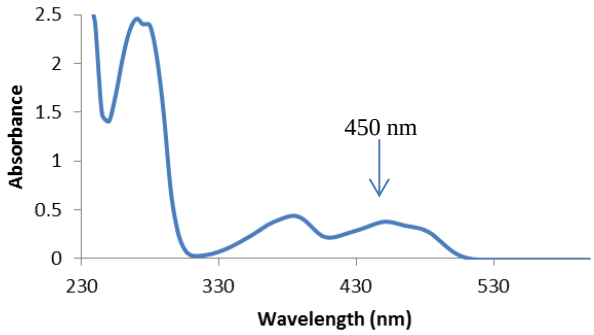

Figure 3.7: A typical UV-visible spectrum of a *Pf*KMO* sample. The FAD cofactor absorbs at 450 nm with a molar absorption coefficient of 12300 $M^{-1}cm^{-1}$ allowing determination of the concentration of *Pf*KMO*. This sample has a concentration of 30.7 µM.

3.3 Kinetic analysis of novel GM compounds

A final series of GM inhibitor compounds (Figure 3.4) were assayed with *Pf*KMO* using the method described in Section 2.5.3. All of the compounds investigated were expected to be good inhibitors of *Pf*KMO* as they had 3,4-dichloro substitution on the aromatic ring which binds close to the isoalloxazine ring which has shown to be important for potent inhibition. These compounds have different substituents on the aromatic ring furthest from the active site (assuming the same mode of binding seen for GM303) and were used to investigate the

importance of interactions between this moiety of the inhibitor and the residues of the C-terminal domain of the protein.

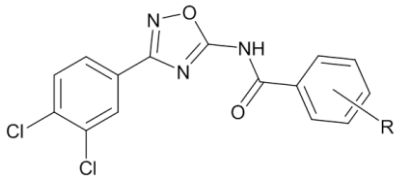

Compound Name	R
GM862	3-OMe, 4-OH
GM843	3-OH, 4-OMe
GM849	3-OCH_2CO_2Me, 4-OMe
GM855	3-OCH_2CO_2Et, 4-OMe
GM859	3-OSO_2NH_2, 4-OMe

Figure 3.8: General structure of inhibitors with a table listing the substituents of each inhibitor compound.

The inhibition assay monitored the formation of $NADP^+$ by measuring the decrease in absorbance at 340 nm as NADPH has a molar absorption coefficient $\varepsilon = 6200\ M^{-1}cm^{-1}$ at this wavelength. In the absence of L-kynurenine, no formation of $NADP^+$ was observed, indicating that these inhibitors are not effector molecules. The change in absorption at 340 nm was measured in the presence of different concentrations of each inhibitor and L-kynurenine. From this data it was possible to determine an approximate K_i value using a Dixon plot (Figure 3.5).

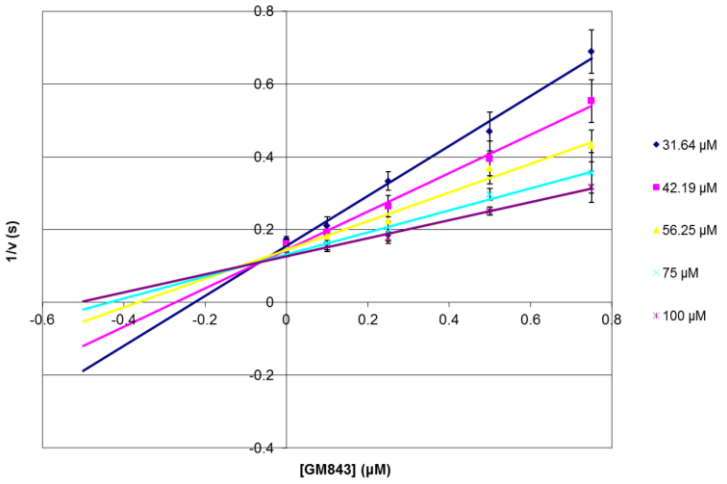

Figure 3.9: Dixon plot of the inhibition assay with *Pf*KMO* and GM843. The data show the reciprocal rate observed with different concentrations of both GM843 and L-kynurenine. A line of best fit is fitted to the data points for each L-kynurenine concentration. The lines intersect where $x = -K_i$.

To determine the type of inhibition behaviour for each compound assayed with *Pf*KMO*, the L-kynurenine concentration divided by the rate ([L-kynurenine/v] was plotted against the inhibitor concentration (Figure 3.10). Parallel lines plotted for data points at each concentration of L-kynurenine indicate competitive inhibition. [159]

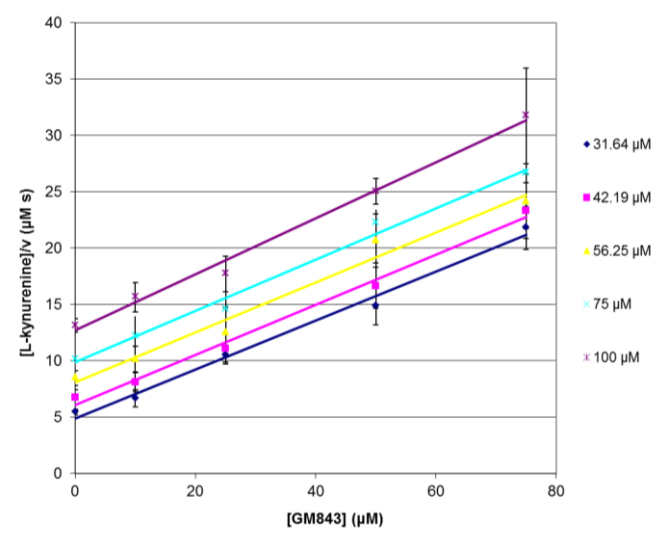

Figure 3.10: Graph of [L-kynurenine]/v against [GM843]. The parallel lines as seen above are indicative of competitive inhibition.

To obtain a more accurate K_i value, the inhibition assay results were analysed using simultaneous non-linear regression analysis methods in GraFit 3.0 (Erithacus Software), from which the K_i value was obtained for each compound (Table 3.3). [175] The graphical output from this program, together with the Dixon plots, is given in full for each compound in Appendix 3.

Compound Name	R substituent	K_i value (nM)
GM862	3-OMe, 4-OH	82.4 ± 10.0
GM843	3-OH, 4-OMe	73.3 ± 9.7
GM849	3-OCH_2CO_2Me, 4-OMe	-13.0 ± 8.9 *
GM855	3-OCH_2CO_2Et, 4-OMe	19.8 ± 8.7
GM859	3-OSO_2NH_2, 4-OMe	61.0 ± 12.8

Table 3.3: K_i assay results for final series of GM compounds. Values were calculated using GraFit with explicit weighting.

* The value obtained in GraFit for GM849 is a negative value. The reason for this is likely to be that the K_i value is very low and there may be some error so perhaps the program is unable to calculate a possible value. The value obtained for GM849 without weighting is 47.7 ± 7.8 nM.

While all the compounds in this series are potent inhibitors with K_i values in the nanomolar range, the more potent compounds are those with larger substituents at the *meta* position as can be seen comparing GM843 with GM859, GM849 and GM855. However, from the earlier data GM760 and GM769 have very similar K_i values showing that the large substituent could be at either the *meta* or *para* position. This trend suggests that a large substituent is required for the most potent inhibitors but its role is in disruption of the interactions between the C-terminal domain and the main domain of the protein. The identity of the large substituent does affect the potency observed as seen in the difference between the K_i value observed for GM859 and those of GM769, GM760, GM849 and GM855. The sulfonamide substituent present in GM859 results in a less potent inhibitor than the esters or phosphate esters.

3.4 Structure of *Pf*KMO* with GM862

Crystals of *Pf*KMO* with GM862 (Figure 3.11) bound in the active site were grown using sitting drop vapour diffusion at 4 ºC. The drop was set up in a Greiner Bio-One CrystalBridge™ and consisted of a 1:1 mixture of 240 μM *Pf*KMO* and well solution. The bulk well solution contained 0.1 M HEPES buffer pH 7.0, 12% PEG 4K, 6% glycerol, 10 mM sodium tartrate and 10% isopropanol. An aliquot of the bulk well solution, supplemented with 1 mM GM862, was used in setting up the drops as the inhibitor was not added to the bulk solution in order to minimise the amount of inhibitor used at this stage. The crystal was cryoprotected by adding 1 μl ethylene glycol directly to the drop before it was flash-frozen in liquid N_2. The data were collected on the i04 beamline at the Diamond Light Source, Oxfordshire. The images were collected with an oscillation of 0.2º with a total rotation of 120º with 0.2 s/image collected. The beam wavelength was 0.979 Å and intensity was 65.12%.

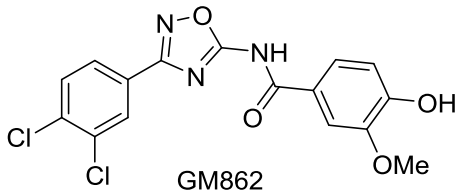

Figure 3.11: Structure of GM862

The diffraction images were processed using *iMosflm* and *Scala* as described in Section 2.7.4. The space group was found to be $P6_122$ and the resolution of the structure is 1.98 Å with R_{merge} of 0.213 (0.606 in the highest resolution shell). The unit cell dimensions were determined to be a = b = 117.0 Å, c = 418.1 Å with angles of $\alpha = \beta = 90^{o}$, $\gamma = 120^{o}$. The very large dimensions of the unit cell, particularly side c, resulted in small spot separation, which initially resulted in unsuccessful data processing. This was overcome by fixing the value of the mosaicity at 0.07 throughout processing in *iMosflm*, but this decreased value of the mosaicity could be responsible for the relatively high value of R_{merge} in the highest resolution shell. There were three *Pf*KMO* monomers in the asymmetric unit, each with one FAD cofactor bound non-covalently, one GM862 molecule was present in the active site of each *Pf*KMO* and 483 waters were found in the asymmetric unit.

The model of the GM862 bound structure was obtained using *Molrep* for molecular replacement with a previously obtained *Pf*KMO* inhibitor bound structure as a model. The structure was refined using *Refmac5* and manually edited in *Coot*. The final R_{factor} was 0.2183 and the R_{free} was 0.2561 (full data processing statistics are in Appendix 2 Table A2.1). The structure of *Pf*KMO* with GM862 bound was highly similar to that of *Pf*KMO* with GM303 with few differences (Figure 3.12) except that the residues of the loop from M373 leading to the C-terminal domain were not found in the GM862 bound structure and there are slight differences in the region of residues 372-373.

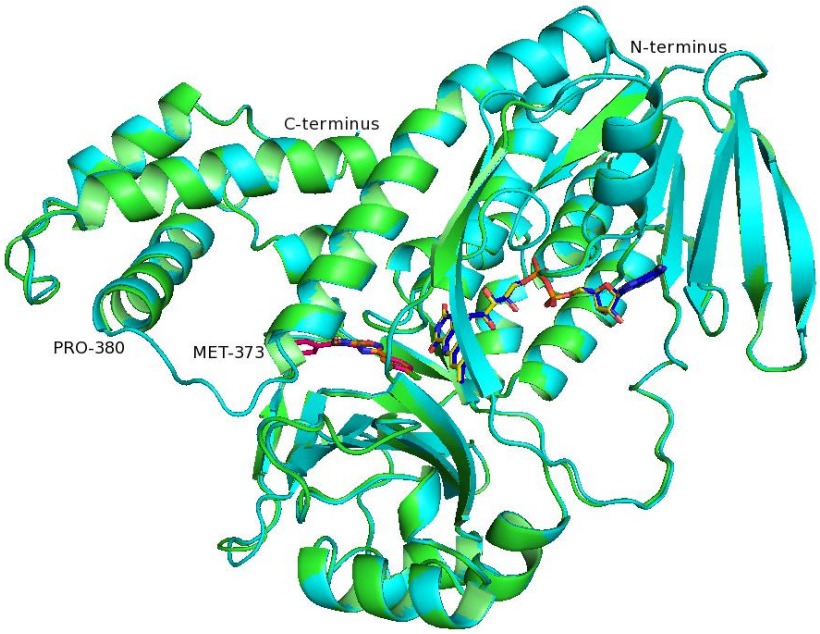

Figure 3.12: Representation of the structure of *Pf*KMO* Chain B (green) with GM862 (orange) with FAD cofactor (yellow) aligned with *Pf*KMO* (cyan) with GM303 (pink) with FAD cofactor (pink). Residues 374 – 379, which form the loop between the main domain and the C-terminal domain, are all absent in the structure of *Pf*KMO* with GM862.

The differences in the structure of *Pf*KMO* with GM862 bound in the active site compared to that of *Pf*KMO* with L-kynurenine are consistent with those observed previously with other of these novel inhibitor compounds. [143] The 3,4-dichloro substituted ring binds in close proximity to the isoalloxazine moiety of the FAD cofactor but the other aromatic ring extends out of the active site causing significant conformational change including disruption of the interactions important for the *closed* conformation to occur, resulting in movement of the C-terminal domain to the *open* conformation (Figure 3.13). The structure of *Pf*KMO* with GM862 bound is also similar to those with no substrate and with L-kynurenine bound (Table 3.4)

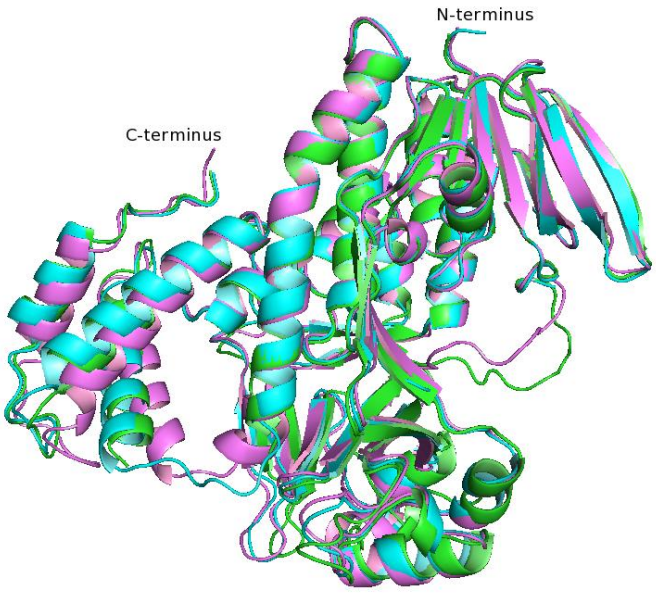

Figure 3.13: Comparison of the structures of *Pf*KMO* with GM862, Chain B (green) and those of *Pf*KMO* in the presence of L-kynurenine (lilac) and *Pf*KMO* in the absence of substrate (cyan). The position of the C-terminal domain of *Pf*KMO* with GM862 is similar to the *open* conformation observed in the structure of *Pf*KMO* in the absence of substrate.

	rmsd (Å)
*Pf*KMO* with no substrate (Chain A)	1.11
*Pf*KMO* with L-kynurenine	1.56
*Pf*KMO* with GM303 (Chain A)	0.24

Table 3.4: The rmsd values obtained in a pairwise comparison of *Pf*KMO* with GM862 bound Chain A with other *Pf*KMO* structures. The comparison was made using the protein structure comparison service PDBeFold at European Bioinformatics Institute (http://www.ebi.ac.uk/msd-srv/ssm), authored by E. Krissinel and K. Henrick. [178]

The GM862 ligand was prepared using the *PRODRG* server to generate three-dimensional PDB coordinates and a library file from the two-dimensional structure of the ligand and was added to the structure using *Coot* to position it in the active site. The electron density for the position of the 3,4-dichloro substituted ring and the heterocycle was clear in all three of the *Pf*KMO* monomers allowing for easy positioning of this part of the molecule into the model. Electron density that could accommodate the amide was also seen in all three chains

but there was little electron density for the 3-OMe, 4-OH substituted aromatic ring. After refining the model in the absence of GM862 to view the omit map, it was not possible to locate the 3-OMe, 4-OH substituted aromatic moiety in any of the three chains so a partial GM862 was modelled into the electron density (Figure 3.14).

In Chain A, there is the clearest suggestion of unmodelled density in close proximity to Y404 that may be caused by the presence of this ring but the evidence is not sufficiently clear to allow the complete ligand to be modelled into the active site. The reason for this aromatic ring not being clearly visible in the F_o-F_c map could be that it is mobile and is able to rotate or that the inhibitor has been hydrolysed.

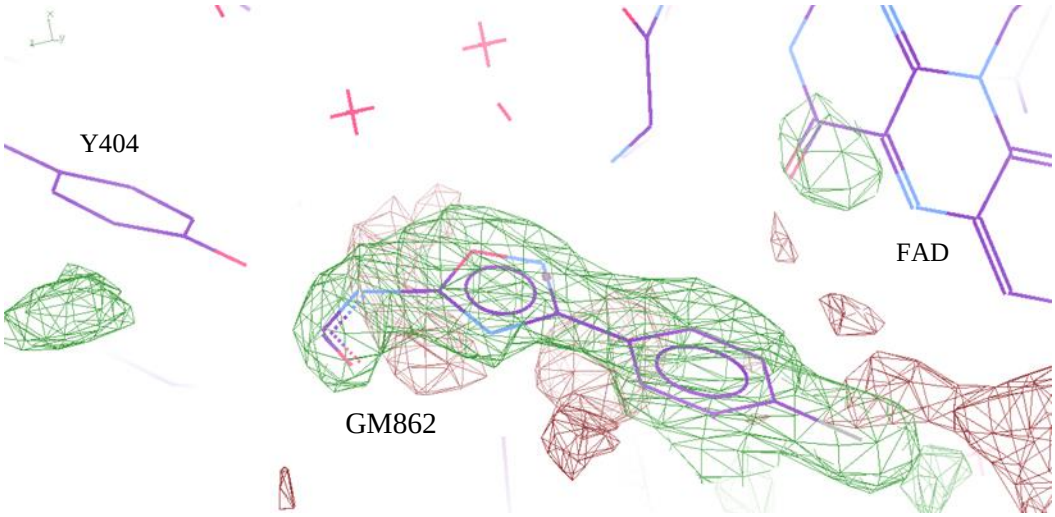

Figure 3.14: F_o-F_c map (green, positive; red, negative) for *Pf*KMO* Chain A with GM862 bound. The isoalloxazine moiety of the FAD cofactor is shown to the right and Y404 to the left of GM862 as shown. The map is contoured at 3.00 σ. Similar maps were obtained for Chains B and C but with less unmodelled density close to Y404 than observed with Chain A.

There are several residues within 4 Å of GM862 in the Chain B *Pf*KMO* active site, some of which are likely to form interactions with the inhibitor including N369 and Y404 (Figure 3.15). The carbonyl of GM862 is visible in all three protein chains and is oriented towards N369 in a potentially important interaction for ligand binding. The complete sidechain of E372 could not be observed in the electron density map so its exact orientation is not known. There are no residues likely to be in close proximity to the 3-OMe, 4-OH substituted aromatic ring except for Y404 and there is no obvious potential for interactions between the substituents on this ring and the residues of *Pf*KMO*.

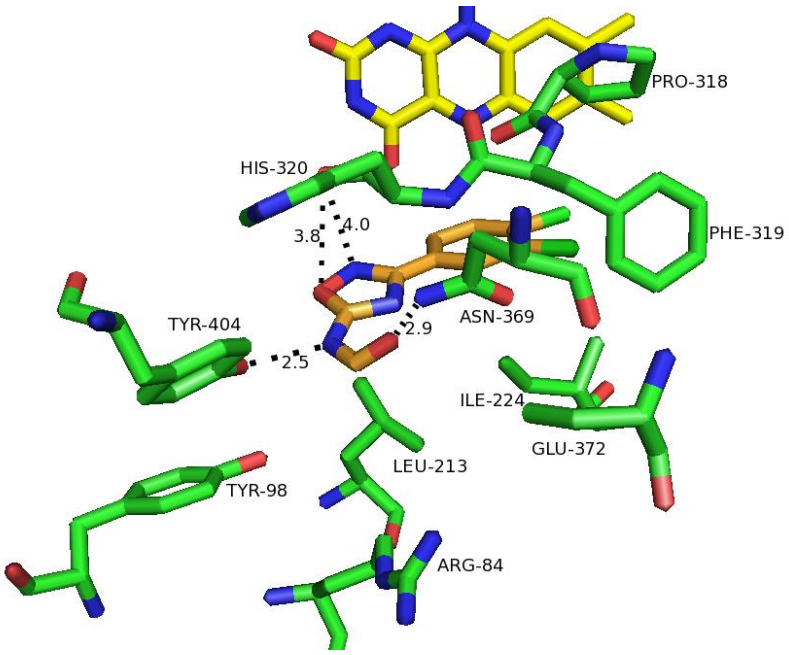

Figure 3.15: Residues in the active site of *Pf*KMO* (green) with GM862 (orange) with the isoalloxazine moiety of the FAD cofactor (yellow). Some residues have been omitted for clarity. Distances between active site residues and GM862 are shown with values in Å. Residues Tyr404 and Asn369 are in close proximity with GM862 and the carbonyl of His320 is within 4 Å of the heterocyclic moiety of GM862. The displacement of Arg84 away from the active site suggests that the other aromatic ring could be present although not observed in the electron density map. The whole of the Glu372 sidechain was not visible in the electron density map.

In the previously solved structure of *Pf*KMO* with GM347 bound in the active site, it was not possible to determine the position of this aromatic ring in any of the protein chains. GM347 is a very similar compound, but with 3,4-diOMe substitution rather than 3-OMe, 4-OH substitution on the aromatic ring. In the structure of *Pf*KMO* with GM347 the carbonyl is orientated towards N369, the same as is observed in all the protein chains in the structure of *Pf*KMO* with GM862. The reason that this area of the molecule is not visible has not been determined but it could be the result of freedom of movement or hydrolysis or decomposition of the inhibitor resulting in a lack of unambiguous electron density in the map and the cause of this in GM862 is likely to be similar. [143]

3.5 Structure of *Pf*KMO* with GM849

Crystals of *Pf*KMO* with GM849 (Figure 3.16) bound in the active site were obtained by sitting drop vapour diffusion at 4 ºC. The sitting drop was set up in a Greiner Bio-One CrystalBridge™ and consisted of a 1:1 mixture of 240 μM *Pf*KMO* and well solution. The bulk well solution contained 0.1 M HEPES buffer, pH 7.0, 14% PEG 4K, 6% glycerol, 10 mM sodium tartrate and 10% isopropanol. GM849 was not added directly to the bulk well solution but was added to a small aliquot of well solution to a final concentration of 1 mM which was used to set up the drop, in order to minimise the amount used in crystallisation trials. The crystal was cryoprotected prior to flash-freezing in liquid N_2 by adding 1 μl of ethylene glycol directly to the sitting drop. Data were collected on the i03 beamline at the Diamond Light Source, Oxfordshire. The images were collected with an oscillation of 0.2º with a total rotation of 120º with 0.2 s per image collected. The beam wavelength was 0.97 Å and intensity was 60%.

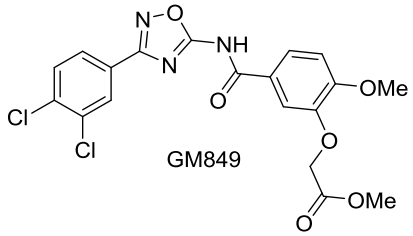

Figure 3.16: Structure of GM849

The diffraction images collected were processed using *iMosflm* and *Scala* as described in Section 2.7.4. The space group was found to be $P6_122$ and the unit cell dimensions were a = b = 116.7 Å, c = 419.2 Å with the angles α = β = 90º, γ = 120º (data processing statistics are listed in Appendix 2, Table A2.1). The value of the mosaicity was fixed at 0.1 throughout processing in *iMosflm* because the large cell dimensions resulted in very small spot separation. The maximum resolution that could be obtained in *Scala* was 3.26 Å with R_{merge} of 0.198 (0.421 in the highest resolution shell). Molecular replacement was carried out with *Molrep* using a previously solved inhibitor-bound structure of *Pf*KMO* as a similar model. The asymmetric unit contained three molecules of *Pf*KMO*, each with a non-covalently bound FAD cofactor. Only eight waters could be added to the model by *Coot*, probably due to the resolution. Rigid body and restrained refinement was carried out in *Refmac5* and the

resulting R_{factor} was 0.1904 and the R_{free} was 0.2858. Due to the resolution of the structure, a number of the residue sidechains could not be added to the model completely as their orientation could not be accurately determined.

The position of the entire GM849 ligand, prepared using the *PRODRG* server, could not be conclusively determined. In Chain B there is evidence in the F_o-F_c map for the presence of GM849 (Figure 3.17) although the position of the 3- OCH_2CO_2Me, 4-OMe substituted aromatic ring could not be determined. The carbonyl appears to be orientated in the same position as observed in the structure of *Pf*KMO* with GM303 and not like that of *Pf*KMO* with GM760, a hypothesis supported by the position of Y404, for which there is clear evidence in the $2F_o$-F_c map.

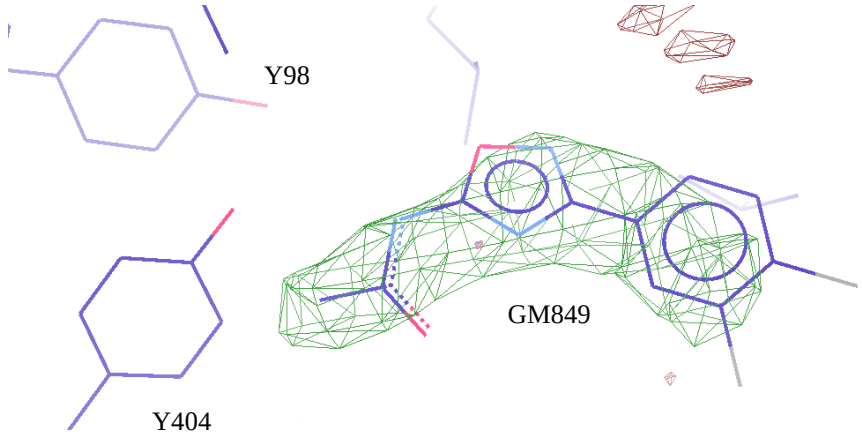

Figure 3.17: F_o-F_c map (green, positive; red, negative) contoured at 3.00 σ for the structure of *Pf*KMO* with GM849 bound, Chain B with residues Y98 (top left) and Y404 (bottom left) visible. The structure was refined with no ligand in the model to create the omit map. A partial fragment of GM849 was then modelled into the positive region of the F_o-F_c map. This chain had the clearest evidence for the position of GM849, with the 3,4-dichloro substituted aromatic ring and the heterocyclic moiety in close proximity to the FAD cofactor. It was not possible to determine the position and orientation of the 3-OCH_2CO_2Me, 4-OMe substituted aromatic ring in any of the three *Pf*KMO* molecules in the asymmetric unit.

In the other *Pf*KMO* molecules in the asymmetric unit, the evidence for the position of GM849 was weaker (Figure 3.18) although it was possible in Chain C to observed some evidence that the 3-OCH_2CO_2Me, 4-OMe substituted aromatic ring was present although it

was not possible to determine the orientation of this ring. Due to the poor resolution of this structure, the evidence for the position of GM849 is weak and a higher resolution structure of *Pf*KMO* with GM849 is required to provide more conclusive evidence.

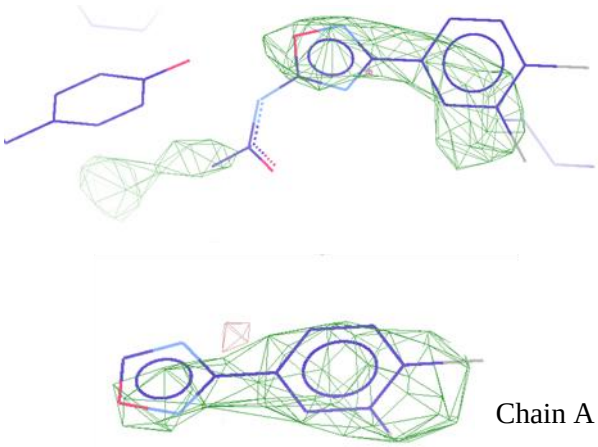

Figure 3.18: F_o-F_c maps (green, positive) for *Pf*KMO* with GM849 in Chains A and C, both contoured at 3.00 σ. In Chain C, there is evidence for the 3,4-dichloro and heterocyclic moiety as well as some evidence for the other aromatic ring although not evidence to accurately determine its position. There is no clear evidence for the position of the carbonyl of GM849 in this chain although Y404 (to the left of GM849) can be positioned accurately which suggests that the carbonyl is orientated in the direction of N369 otherwise it is too close to the hydroxyl group of Y404. In Chain A there is considerably less evidence for the position of GM849 and only a smaller fragment of GM849 could be modelled into the active site of *Pf*KMO*.

The overall structure was similar to that of *Pf*KMO* with GM303 with no major conformational changes observed as a result of GM849 binding (Table 3.5). There are slight differences between the two structures and there may be differences in the positions of GM849 and GM303 but a higher resolution structure of *Pf*KMO* with GM849 will be required to determine the exact position of this inhibitor.

	rmsd (Å)
*Pf*KMO* (no ligand) (Chain A)	1.04
*Pf*KMO* with L-kynurenine	1.46
*Pf*KMO* with GM303 (Chain A)	0.48

Table 3.5: The rmsd values obtained in a pairwise comparison of *Pf*KMO* with GM849 bound Chain A with other *Pf*KMO* structures. The structure of *Pf*KMO* with GM849 is most similar to that of *Pf*KMO* with GM303 and least similar to that with L-kynurenine bound, a structure in which *Pf*KMO* is in the *closed* conformation. The comparison was made using the protein structure comparison service PDBeFold. [178]

3.6 Structure of *Pf*KMO* with GM859

Crystals of *Pf*KMO* with GM859 (Figure 3.19) bound in the active site were obtained by sitting drop vapour diffusion at 4 ºC. The drop was set up in a Greiner Bio-One CrystalBridge™ and consisted of a 1:1 mixture of 240 µM *Pf*KMO* and well solution. The well solution consisted of 0.1 M HEPES buffer pH 7.0, 14% PEG 4K, 6% glycerol, 10 mM sodium tartrate and 10% isopropanol. GM859 was not added directly to the bulk well solution but was added to a small aliquot of well solution to a final concentration of 1 mM which was used to set up the drop to minimise the amount of GM859 used in crystallisation trials. The crystal was cryoprotected by adding 1 µl ethylene glycol directly to the drop and the crystal was flash-frozen in liquid N_2. Data were collected on the i04 beamline at the Diamond Light Source, Oxfordshire. The images were collected with an oscillation of 0.2º with a total rotation of 120º with 0.2 s per image collected. The beam wavelength was 0.979 Å and intensity was 65.12%.

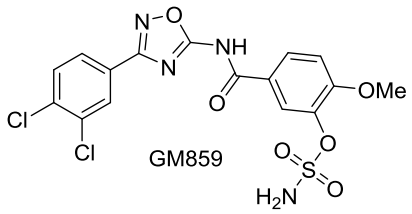

Figure 3.19: Structure of GM859

The diffraction images collected were analysed as described in Section 2.7.4 using *iMosflm* and *Scala*. The unit cell was found to have dimensions of a = 117.0, b = 117.0, c = 419.2 Å with angles $\alpha = \beta = 90^{o}$, $\gamma = 120^{o}$ and the space group was $P6_122$. The extremely large unit cell resulted in extremely small spot separation so the mosaicity was fixed at 0.07 to achieve successful processing of the data. The resolution was determined to be 2.6 Å and the R_{merge} is 0.224 overall but 0.543 for the highest resolution shell (data processing statistics are listed in Appendix 2 Table A2.1).

Molecular replacement was carried out with *Molrep* using a model of an inhibitor bound structure that had been solved in previous work. There were three protein monomers in the asymmetric unit, each with one non-covalently bound FAD cofactor and one GM859 molecule bound and 425 water molecules were identified. Refinement was carried out in *Refmac5* and *Coot* was used to inspect how the model fitted the map. The final value of R_{free} was 0.2025 and the R_{factor} was 0.2628. The GM859 ligand was added to the model after it had been prepared by submitting a two-dimensional version of the structure to the *PRODRG* server to generate the three-dimensional PDB coordinates and the .cif library file.

The structure of *Pf*KMO* with GM859 bound consists of the main domain of the protein and the C-terminal domain and is very similar to the structure of *Pf*KMO* with GM303 bound in the active site. The C-terminal domain is moved away from the main domain of the protein in the *open* conformation to accommodate the large GM859 which is bound partially in the active site consistent with other structures of *Pf*KMO* with related inhibitor compounds with the structure of *Pf*KMO* with GM859 being more similar to the structure of *Pf*KMO* in the absence of ligand than that of *Pf*KMO* with L-kynurenine (Table 3.6). The ligand can be observed with the 3,4-dichloro substituted aromatic ring located in close proximity to the isoalloxazine ring of the FAD cofactor.

	rmsd (Å)
*Pf*KMO* (no ligand) (Chain A)	1.00
*Pf*KMO* with L-kynurenine	1.49
*Pf*KMO* with GM303 (Chain A)	0.39

Table 3.6: The rmsd values obtained in a pairwise comparison of *Pf*KMO* with GM859 bound Chain A with other *Pf*KMO* structures. The comparison was made using the protein structure comparison service PDBeFold. [178]

The electron density map contained a large unoccupied volume of density located partially within the active site, into which GM859 was modelled prior to further refinement (Figure 3.20). GM859 could easily be modelled into this density which contained the 3,4-dichloro aromatic ring in close proximity to the isoalloxazine moiety of the FAD cofactor and the other aromatic ring extending out beyond the active site. The electron density for the sidechain of Y404 is also clear and shows the aromatic ring of this residue close to one of the aromatic rings of GM859.

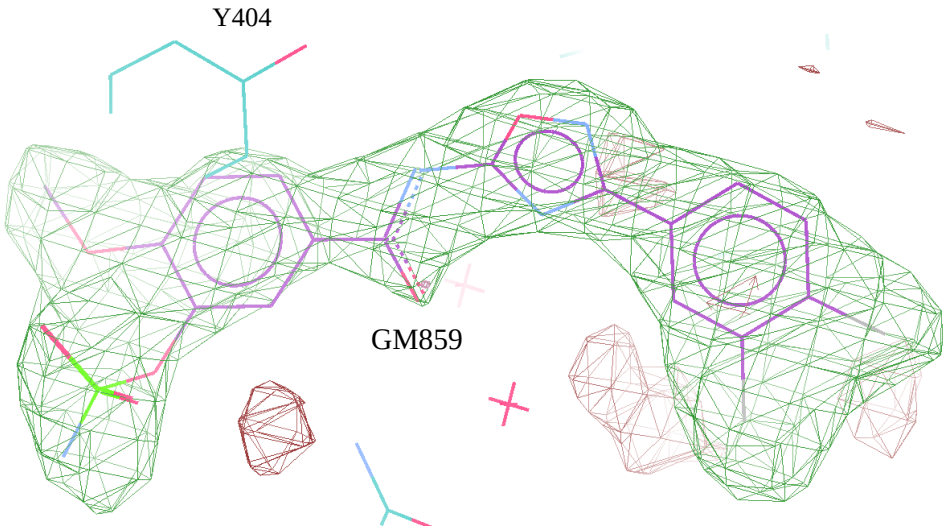

Figure 3.20: F_o-F_c map (green, positive; red, negative) for *Pf*KMO* (cyan) with GM859 (purple) after refinement in *Refmac5* with no ligand modelled in the active site. The whole of GM859 was then modelled into the active site. The sidechain of Y404 can be seen above GM859 in this view. The map is contoured at 3.06 σ.

Potential interactions between *Pf*KMO* and GM859 can be observed in the structure which are likely to contribute to the strong binding of GM859 observed in kinetic analysis as the K_i value is 61.0 ± 12.8 nM. The sulfonamide group of GM859 (Figure 3.21) is located out of the active site and appears to be sufficiently close to interact with the hydroxyl groups of E372, potentially forming hydrogen bonds with this residue. Y404 is also in close proximity to GM859 with the hydroxyl group of this residue 3 Å distant from the amide nitrogen. The position of this aromatic ring may potentially allow for a π-stacking interaction. The carbonyl of H320 is also within 4 Å of GM859.

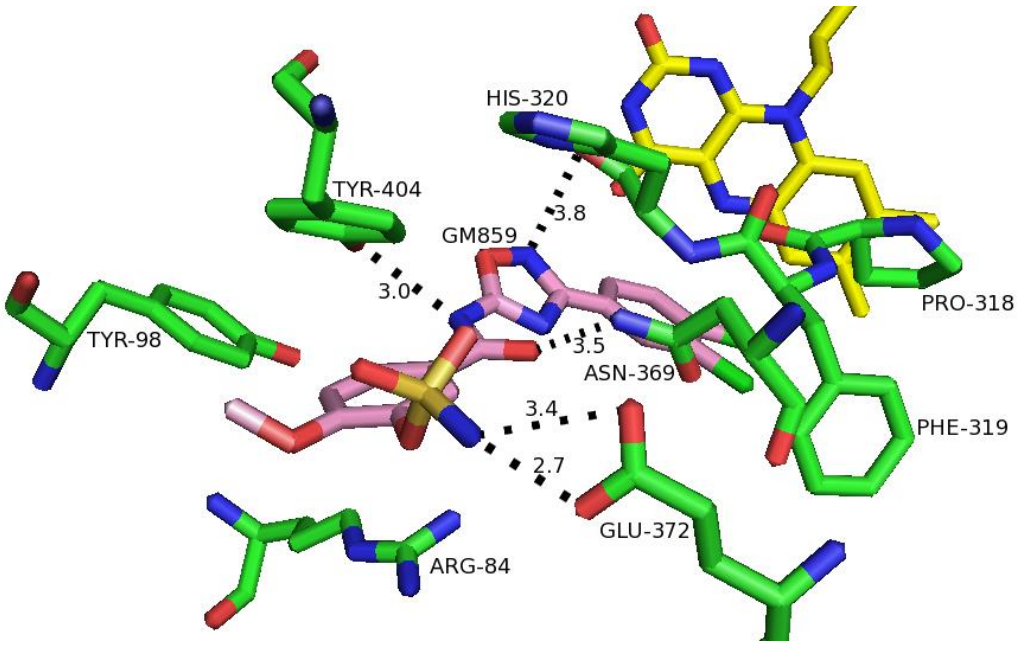

Figure 3.21: GM859 (pink) in the active site of *Pf*KMO* (green). The 3,4-dichloro substituted aromatic ring is in close proximity to the FAD cofactor (yellow). The sulfonamide substituent appears to be interacting with Glu372. The amide carbonyl is approximately 3.5 Å from Asn369 and the amide nitrogen is 3.0 Å from the hydroxyl group of Tyr404. The heterocycle is within 4 Å of the carbonyl of His320. All distances indicated in the figure are in Å.

The structure of *Pf*KMO* with GM859 bound is very similar to that of the *Pf*KMO* with GM303 bound, a structure obtained in previous work. [143] The active sites of these two *Pf*KMO*: inhibitor complexes show the residues in almost exactly the same positions which shows that the sulfonamide group can be incorporated into the available space without disruption to the structure of *Pf*KMO* (Figure 3.22). It is likely that the interactions between the sulfonamide of GM859 and E372 are an important contribution to the lower K_i observed with this inhibitor compared to GM303 which has a K_i value of 115 ± 11 nM.

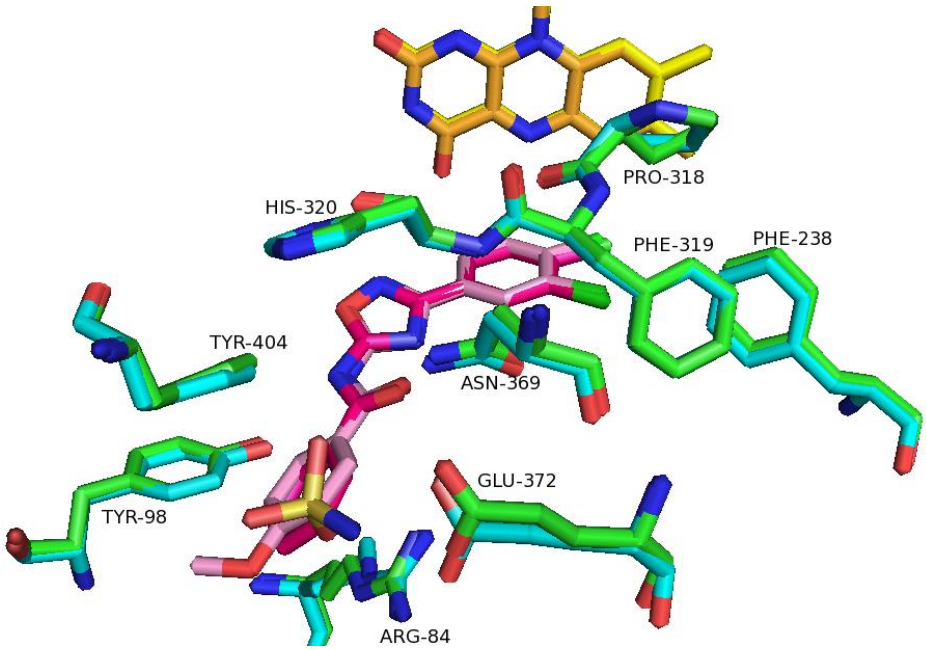

Figure 3.22: Comparison of residues in the active site of *Pf*KMO* (green) with GM859 (light pink) with FAD cofactor (yellow) with those in the structure of *Pf*KMO* (cyan) and GM303 (bright pink) and FAD cofactor (orange). Some of the active site residues have been omitted for clarity.

The other mode of binding observed in previous work with these novel inhibitors (Section 3.1) is seen with compounds with large substituents such as GM760, which has a phosphate group that cannot be accommodated in the space near E372. This results in a change in the orientation of the inhibitor, starting at the amide group and resulting in the aromatic ring outside of the active site displacing Y404. As GM859 also has a large substituent on the 3´ position of the aromatic ring, it was considered possible that it might bind in the same orientation as GM760; however, the sulfonamide substituent is located close to the helix containing E372. It is possible that this substituent on the aromatic ring of GM859 is one of the largest that can be accommodated sterically at this location and that any larger substituents would result in the structural change observed with GM760.

3.7 Conclusions

This novel series of inhibitor compounds is based on the structure of Ro 61-8048, but in assays with *Pf*KMO* have shown greater potency and do not contain the potentially toxic 3-NO_2 substituent observed in Ro 61-8048. In the absence of substrate, no consumption of NADPH by *Pf*KMO* could be observed in the presence of these inhibitors, demonstrating that these are true inhibitors rather than non-substrate effector molecules.

In this work, a small series of inhibitors was assayed against *Pf*KMO* to investigate the effect of substitution on an aromatic ring that has been shown not to fit completely within the active site. All the inhibitors in this series were potent and the K_i values were determined to be below 100 nM suggesting that the substitution on this ring is not critical for inhibition. The trend in the values obtained suggested that large substituents result in particularly potent inhibitors, particularly GM855. The structure of *Pf*KMO* with GM862 showed that the 3,4-dichloro-substituted aromatic ring binds in the active site in close proximity to the isoalloxazine moiety of the FAD cofactor but no electron density for the aromatic ring of GM862 located out of the active site was observed in the omit map. This could be the result of flexibility in this part of the ligand as this structure is similar to those of *Pf*KMO* with GM303 and GM347 from previous work with R84 displaced away from the active site and the C-terminal domain is in the *open* conformation. The structure of *Pf*KMO* with GM859 did contain the complete structure of the ligand and showed the inhibitor binding in a similar position and orientation to GM303 but with a potential interaction between the sulfonamide substituent and E372 that is likely to contribute to the lower K_i value obtained for GM859. From the structure of *Pf*KMO* with GM859, a schematic of GM859 binding in the active site illustrating the effect of inhibitor binding on the position of active site residues and the likely interactions formed between the inhibitor and *Pf*KMO* resulting in potent inhibition (Figure 3.23).

The other inhibitors studied in this thesis are likely to bind in a similar position, preventing the *closed* conformation from occurring, with *Pf*KMO* remaining in the *open* conformation when the inhibitors are bound in the active site. This is likely to be the main reason, rather than a specific interaction, why these inhibitors are not effectors like m-nitrobenzoylalanine and 3,4-dichlorobenzoylalanine. The previously studied effector molecules are smaller molecules that would be able to fit within the active site environment therefore allowing the *closed* conformation to occur. The inability of *Pf*KMO* to be in the *closed* conformation

when these novel inhibitors are bound could prevent the reduction of the FAD cofactor by NADPH. The series of novel inhibitors studied in this work are all larger molecules that extend beyond the active site displacing R84 and prevent the formation of interactions between R84, E372 and the C-terminal domain residues Y382 and R386 that are hypothesised to be necessary for the *closed* conformation to occur.

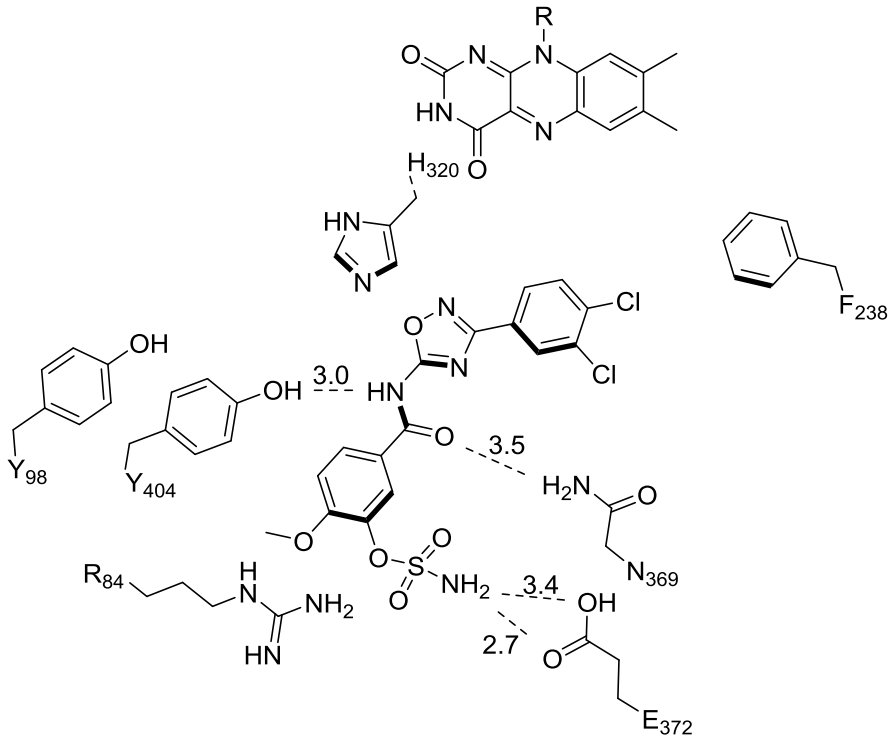

Figure 3.23: Schematic view of GM859 in the active site of *Pf*KMO*. When GM859 binds, the 3,4-dichloro substituted aromatic ring binds in the active site in a similar position and orientation to the aromatic ring of L-kynurenine in the substrate-bound structures. This inhibitor is large and forms interactions with active site residues including N369 and Y404. R84 is pushed downwards (in this perspective) away from the position it occupies in the structure of *Pf*KMO* with L-kynurenine. This allows the sulfonamide moiety of GM859 to interact with E372, a residue implicated in control of the movement between the *open* and *closed* conformations. This also results in the C-terminal domain being unable to move closer to the active site to form the *closed* conformation due to the size of GM859, which extends beyond the active site.

Unfortunately it was not possible to obtain the structure of *Pf*KMO* with either GM843 or GM855 bound or a high resolution structure with GM849 resulting in some uncertainty over

the position of the aromatic rings of GM855 and GM849 which contain particularly large substituents and could be binding in the same mode as GM760.

The series of compounds studied in this thesis are part of a larger group of compounds which contain particularly promising inhibitors including GM849, GM855, GM760 and GM769. In future work it would be particularly interesting to assay these inhibitors with human KMO to confirm that they inhibit the human enzyme and to identify potential lead compounds that could lead to the development of a drug that could be used for patients with conditions in which KMO inhibition is considered a useful therapeutic strategy.

Chapter 4: Characterisation of Substrate Binding

4.1: Residues involved in substrate binding

*Pf*KMO* active site residues thought to be important in substrate binding were initially proposed from sequence analysis and then identified in the *Pf*KMO* structure solved by M. Wilkinson. The roles of selected residues were investigated using site directed mutagenesis and then the resulting proteins were studied using steady-state kinetics and crystallography, thus allowing comparison with *Pf*KMO*.

From the L-kynurenine bound structure of *Pf*KMO* a number of residues in close proximity to the substrate were identified as potentially interacting with it (Figure 4.1). The distances indicated in the figure are approximations due to the low resolution (3.4 Å) of this structure; however, it is clear that Y98 and N369 are sufficiently close to be involved in hydrogen bonding interactions and R84 appears to be interacting with the carboxylate moiety of L-kynurenine. Y404 could also potentially be involved in interacting with the carboxylate even though the distance in this model is approximately 4 Å from the hydroxyl group of Y404 to the substrate carboxylate, which is likely to be too far, even given the positional error at this resolution.

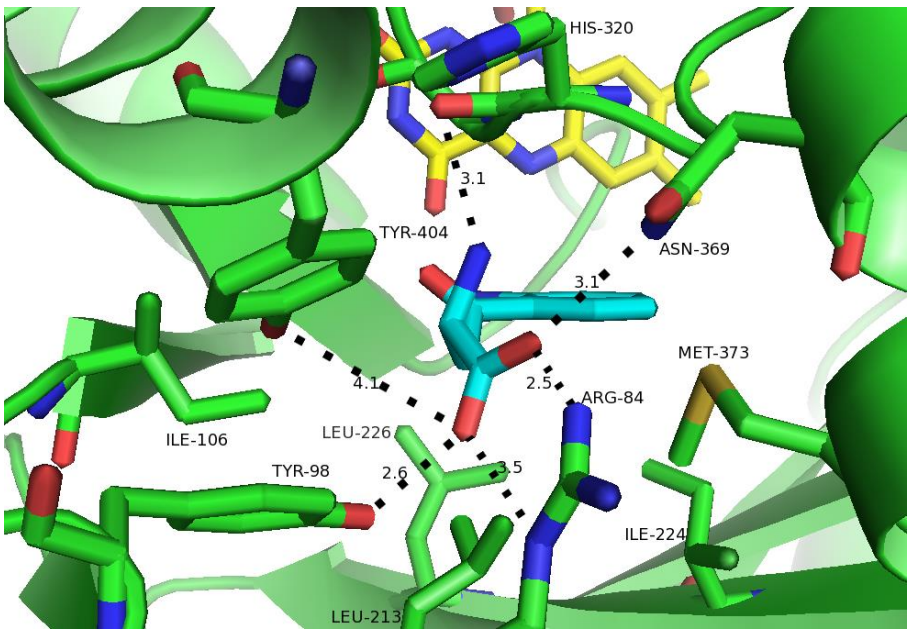

Figure 4.1: Residues in the active site of *Pf*KMO* with FAD cofactor (yellow) and L-kynurenine (cyan). Distances between L-kynurenine and some active site residues are indicated in Å. The carboxylate moiety of L-kynurenine could potentially interact with Arg84, Tyr98, Asn369 and Tyr404. The amine is 3.1 Å from the carbonyl of His320. The aromatic ring is in close proximity to the FAD cofactor.

Most of the residues in the active site of *Pf*KMO* are conserved in KMO enzymes from different species (Figure 4.2) with the exceptions of I106 and H320. The residues thought to be important in interactions with the substrate, including R84, Y404 and Y98, are conserved in all KMOs.

```
S.cerevisiae      ------------------------------------------------------------
C.albicans        ------------------------------------------------------------
Homo sapiens      ------------------------------------------------------------
R. norvegicus     ------------------------------------------------------------
Drosophila        MFVATPLHLVGFPQQHQTTIDTIYCPSDIISWLNISPASCLASISIPSSFRCQRASRTVM 60
PfKMO             ------------------------------------------------------------
Xant.sacchari     ------------------------------------------------------------

S.cerevisiae      ---MSES----------------------VAIIGAGLVGCLAALAFSKEGYNVTLYDFRQ 35
C.albicans        ---MSEEESQKT-----------------IGIVGAGLVGCLAALAFAKKGYDVTLFEYRP 40
Homo sapiens      ---MDSSVIQRK-----------------KVAVIGGGLVGSLQACFLAKRNFQIDVYEARE 41
R. norvegicus     ---MASSDTEGK-----------------RVVVIGGGLVGALNACFLAKRNFQVDVYEARE 41
Drosophila        SPGIVSQEVNGRQEPTEAARDERHGRRRRVAVIGAGLVGSLAALNFARMGNHVDLYEYRE 120
PfKMO             ---MTATDNA-------------------RQVTIIGAGLAGTLVARLLARNGWQVNLFERRP 40
Xant.sacchari     ---MNASP--------------------RSITLIGAGLAGSLLAILLSRQGWQVTVYERRG 38
                     :                         : ::*.**.* * *  ::: . .: ::: *

S.cerevisiae      DPRLDTTKNKNLKSINLAISARGIDALKSIDPDACEHILQDMIPMKGRMIHDLKG-RQES 94
C.albicans        DPRTVDSSKRNLRSINLAVSSRGIRALQYVDPAMADRILENVIPMKGRMIHDITGTKQES 100
Homo sapiens      DTRVATFTRG--RSINLALSHRGRQALKAVG--LEDQIVSQGIPMRARMIHSLSG-KKSA 96
R. norvegicus     DIRVANFMRG--RSINLALSYRGRQALKAVG--LEDQIVSKGVPMKARMIHSLSG-KKSA 96
Drosophila        DIRQALVVQG--RSINLALSQRGRKALAAVG--LEQEVLATAIPMRGRMLHDVRG-NSSV 175
PfKMO             DPRIETGARG--RSINLALAERGAHALRLAG--LEREVLAEAVMMRGRMVHVPGT-PPNL 95
Xant.sacchari     DPRVHDYERG--RSINLALAERGLHVLRQAG--ADAAVMAKAVMMRGRMVHFADG-HQQL 93
                  * *     .   :*****:: **  .*   .      ::   : *:.**:*       .

S.cerevisiae      QLYG-LHGEAINSINRSVLNNSLLDELEKS-TTELKFGHKLVKIEWTDDKQICHFAIGED 152
C.albicans        QVYG-LNGESINSIDRSFLNNCLLDELDKS-NVKILFKHKLVKLDTSN---ACRMTFIDG 155
Homo sapiens      IPYG-TKSQYILSVSRENLNKDLLTAAEKYPNVKMHFNHRLLKCNPEE----GMITVLGS 151
R. norvegicus     IPYG-NKSQYILSISREKLNKDLLTAVESYPNAKVHFGHKLSKCCPEE----GILTMLGP 151
Drosophila        VLYDPINNQCLYSVGRRQLNEVLLNACDKLPNIRCHFEHKLTSANLRE----GSMEFRNP 231
PfKMO             QPYGRDDSEVIWSINRDRLNRILLDGAEAA-GASIHFNLGLDSVDFAR----QRLTLSNV 150
Xant.sacchari     QRYGRDDSEVIWSVHRNDLNITLLQLAEQA-GARIHFYRRLHTVDFDAG---YARFIDDR 149
                    *.  ..:   *: *  **  **   :        *   * .            .

S.cerevisiae      LKAPHTEKYDFVIGCDGAYSATRSQMQRKVEMDFSQEYMNLRYIELYIPPTEEFKPNYGG 212
C.albicans        HNDAKTSTFDFVVGCDGAHSQFRYHLQKTMRMDYSQKYIDMQYLELYIPPSEDAN----N 211
Homo sapiens      DKVPKDVTCDLIVGCDGAYSTVRSHLMKKPRFDYSQQYIPHGYMELTIPP-------KNG 204
R. norvegicus     NKVPRDITCDLIVGCDGAYSTVRAHLMKKPRFDYSQQYIPHGYMELTIPP-------KNG 204
Drosophila        AKEAVAAHADLIVGCDGAFSSVRQXXVRLPGFNYSQEYIETGYLELCIPS-------KSG 284
PfKMO             SGERLEKRFHLLIGADGCNSAVRQAMASVVDLGEHLETQPHGYKELQITP------EASA 204
Xant.sacchari     DDQPHDIRFDSMIGADGAGSALRAAMQRKAPMAEHIEFLDHSYKELEIPP------GADG 203
                           . ::*.**. *  *        :    :     * ** *..

S.cerevisiae      NFAIAPDHLHIWPRHKFMLIALANSDGSFTSTFFGSKD---------QISDLITSKSRVR 263
C.albicans        KFSIDANHLHIWPRHNFMLIALANKDGSFTSTFFSPWS---------VIEGISSSQE-FV 261
Homo sapiens      DYAMEPNYLHIWPRNTFMMIALPNMNKSFTCTLFMPFE---------EFEKLLTSND-VV 254
R. norvegicus     EYAMEPNCLHIWPRNAFMMIALPNMDKSFTCTLFMSFE---------EFEKLPTHSD-VL 254
```

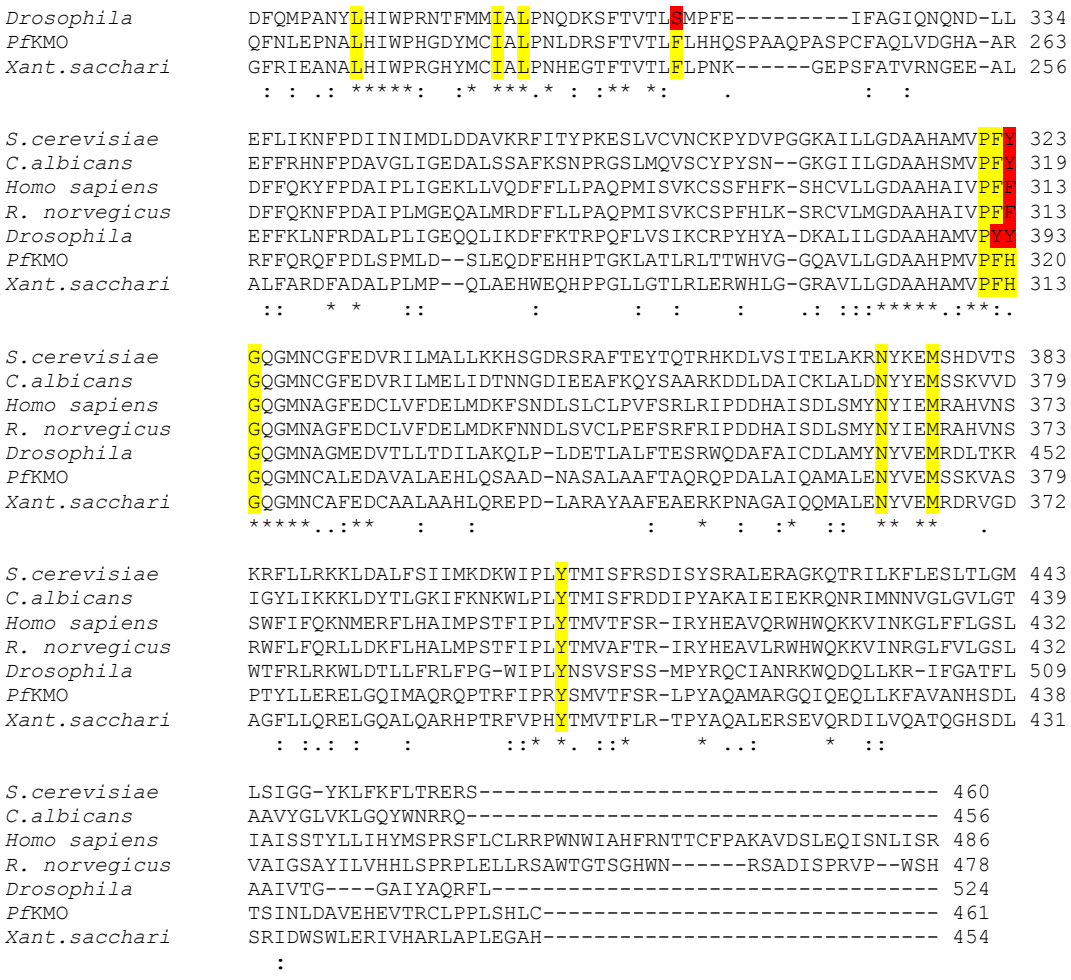

Figure 4.2: Alignment of KMO sequences generated using ClustalW. The highlighted residues are those with any atoms within 5 Å of L-kynurenine in the structure of *Pf*KMO* with yellow indicating those that are conserved in all of these sequences and residues that are not conserved are highlighted in red. Residues aligned with *Pf*KMO* H320 have a lesser degree of conservation across species than other active site residues. Sequences were obtained using BLAST. The accession numbers and UniProt codes respectively are *Saccharomyces cerevisiae* AJP85738.1, A0A0C5LRM7; *Homo sapiens* (human) CAA73613.1, O15229; *Drosophila melanogaster* AAC47351.1, A1Z746; *Rattus norvegicus* NP_067604.1, O88867; *Candida albicans* P87 KGU09898.1, A0A0A4AF15; *Xanthomonas sacchari* WP_043092154; A0A0A8DT66.

A comparison of the active site of *Pf*KMO* with that of *S. cerevisiae* KMO is useful as this structure (with the inhibitor UPF 648 bound) has a much higher resolution (2.14 Å) and can confirm the likely involvement of most of the residues listed above in substrate binding

(Figure 4.3). [142] A number of the residues in the active sites are not shown in this figure for clarity but these residues (I106, L213, I224, L226, P318, F319 using the *Pf*KMO* sequence for labelling) are in almost exactly the same position and orientation in both structures.

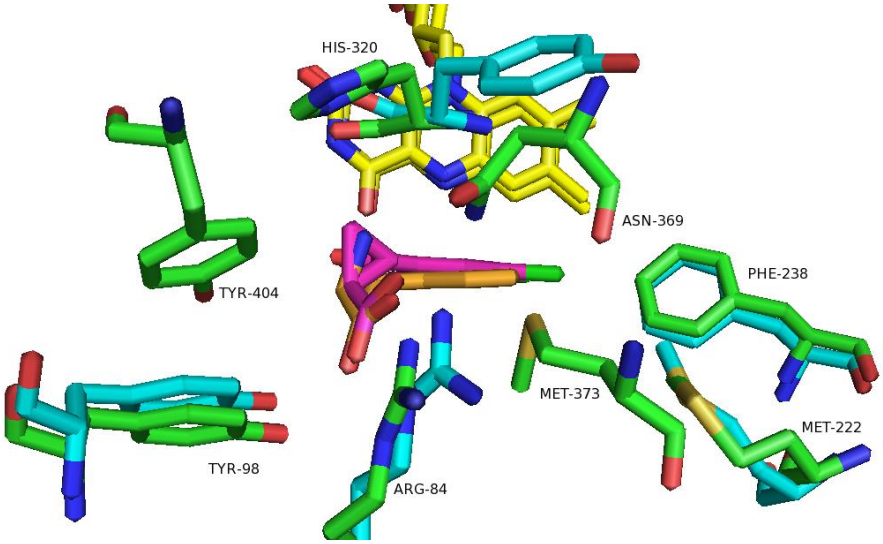

Figure 4.3: Some of the *Pf*KMO* active site residues (green) with FAD cofactor (yellow) and L-kynurenine (orange) are shown with *S. cerevisiae* KMO residues (cyan) with FAD cofactor (yellow) and UPF 648 (magenta). For clarity, only the *Pf*KMO* residues are labelled. Residues Arg84, Tyr98, Met222 and Phe238 are shown to be in very similar positions and orientations as the equivalent residues in the *S. cerevisiae* structure. Constructed using PDB 4J36 and *Pf*KMO* with L-kynurenine bound. [142,143]

The two active sites have many similarities including the position of the isoalloxazine moiety of the FAD cofactors and also residues R84 and Y98, both of which appear to be important in L-kynurenine/UPF 648 binding. As the *S. cerevisiae* KMO enzyme is disordered from residue 359 onwards when UPF 648 is bound and truncated at residue 394, there is no equivalent of the potential interactions between N369, M373 or Y404 and L-kynurenine observed in the *Pf*KMO* structure. [142] The main difference between the two structures is in the position of H320 in *Pf*KMO* and Y323 in *S. cerevisiae* KMO. The position of Y323 in *S. cerevisiae* KMO changes when ligand binds in the active site (Figure 1.17).

The mutations R83K and R83A (R83 is the equivalent residue to R84 in the *S. cerevisiae* enzyme) have been made in *S. cerevisiae* KMO and are reported to be inactive, which would support the theory that this residue is particularly important in substrate binding. [142]

Therefore it would be interesting to examine R84 in *Pf*KMO* as from the structures of *Pf*KMO* it is thought that this residue interacts both with the substrate and with N369, and is important in the movement of the C-terminal domain upon substrate binding. [143]

In the structure of *Pf*KMO* in the absence of substrate, small conformational changes are observed depending on the crystallisation conditions (Figure 4.4). In the presence of NaCl, the chloride anions bind to the protein close to the FAD cofactor and residues F319 and H320 resulting in conformational changes that cause two regions of the structure to resemble the structure in the presence of L-kynurenine. These are the loop from I44 – N54 which is not present in the structure in the absence of substrate crystallised using sodium tartrate rather than NaCl. In the structure with NaCl and no substrate, the loop is present and the residues are in a similar position to those in the structure of *Pf*KMO* in the presence of L-kynurenine. The other change is from Y370 where the end of the helix resembles that of the L-kynurenine bound structure, there is a flexible loop region from S375 – S379 in a different position than either of the other *Pf*KMO* structures and from P380 onwards the residues are the same as in the structure in the absence of both substrate and NaCl. This is a mix of features observed in the *closed* and *open* conformations even though no L-kynurenine is bound. [143] Most of the substrate-free structures obtained in this work were crystallised in the presence of NaCl and the significance of these conformational changes were only realised at a later date; however, valuable insights into the effects of the mutations on the structure of *Pf*KMO* were still gained.

In this chapter three active site residues were investigated to characterise important interactions between L-kynurenine and *Pf*KMO*. Y404 was investigated using the mutations Y404F and Y404A to ascertain whether this residue forms a hydrogen bond with the substrate. N369 was investigated using the conservative mutation N369S to examine the effect of this residue on binding. R84 was investigated with the conservative mutation R84K and also with R84A which was considered likely to cause major disruption to enzyme chemistry as it would disconnect substrate binding from the C-terminal domain.

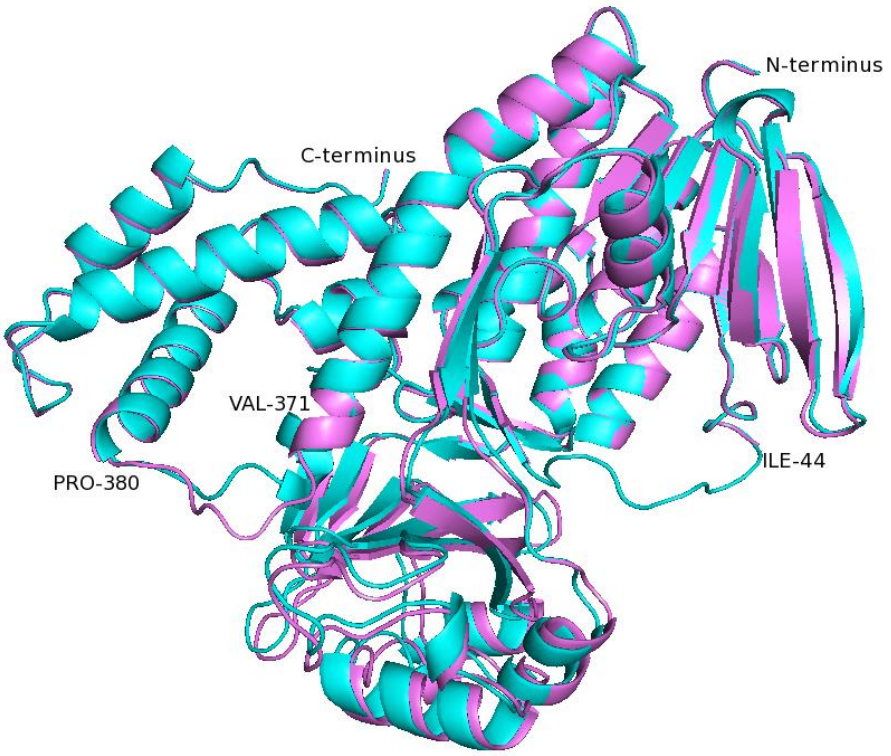

Figure 4.4: An overlay of the structure of *Pf*KMO* in the absence of substrate (lilac) with that of *Pf*KMO* in the absence of substrate crystallised in the presence of NaCl (cyan). [143]

4.2 Y404

In the active site of *Pf*KMO* with L-kynurenine bound, it is possible that Y404 could be involved in a hydrogen bonding interaction with the carboxylate moiety of L-kynurenine but this interaction is uncertain as the distance over which this interaction would occur is approximately 4 Å, while a hydrogen bond would not normally be expected to be longer than ~3 Å. The two mutations made to study this residue are Y404A and Y404F which will confirm whether there is an interaction between Y404 and L-kynurenine and determine the nature of this interaction and its importance for substrate binding in *Pf*KMO*.

4.2.1 Y404A *Pf*KMO*

The mutation Y404A was made using QuikChange II PCR methods (sequence data in Appendix 1) and Y404A *Pf*KMO* protein was expressed and purified using the methods in Chapter 2. The UV-visible absorbance scan of the protein is typical for *Pf*KMO* and indicates that the FAD cofactor is bound (Figure 4.5). The protein was not sufficiently active for determination of the K_M and k_{cat} values using the kinetic assay described in Section 2.5.2 which suggests that this residue is important for enzyme function although this does not provide any specific conclusions on the possible nature of the interaction of Y404 and the substrate.

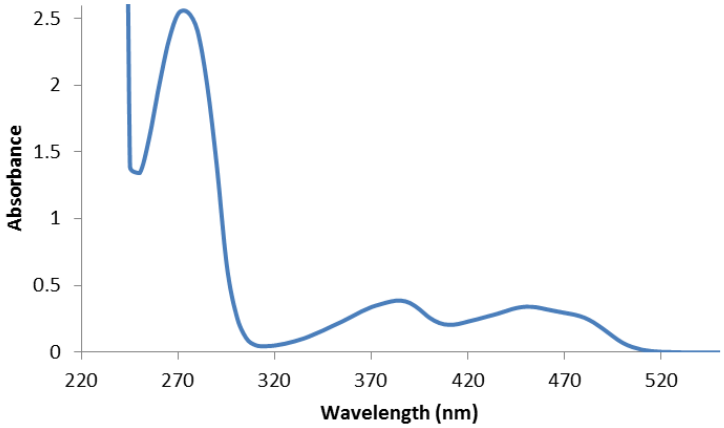

Figure 4.5: UV-visible spectrum of Y404A *Pf*KMO*. The molar extinction coefficient, ε, of *Pf*KMO* at 450 nm is 12300 $M^{-1}cm^{-1}$. The concentration of this sample is calculated to be 27.6 μM.

4.2.2 Kinetic analysis of Y404F *Pf*KMO*

The mutation Y404F was made using megaprimer PCR methods and the protein was expressed and purified as described in Chapter 2. A UV-visible scan of Y404F *Pf*KMO* confirmed that the FAD was bound (Figure 4.6).

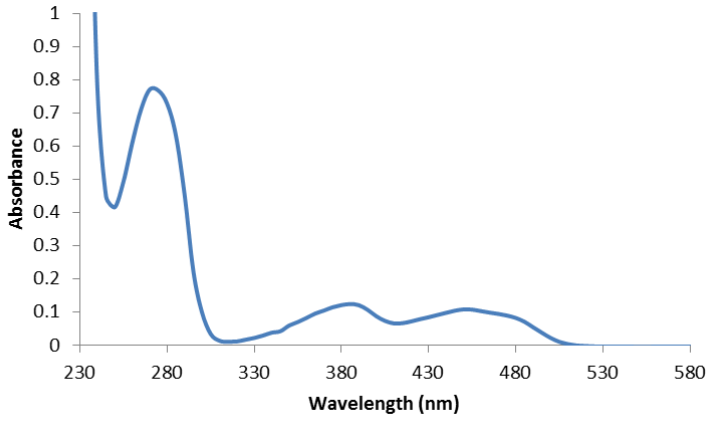

Figure 4.6: UV-visible spectrum of Y404F *Pf*KMO*. The concentration of this sample is 8.8 µM calculated from the *Pf*KMO* molar extinction coefficient at 450 nm of 12300 $M^{-1}cm^{-1}$.

The kinetic assay used to determine the kinetic parameters, K_M and k_{cat} (Section 2.5.2), was performed in triplicate and the parameters were determined using Origin 8.5.1 (Figure 4.7).

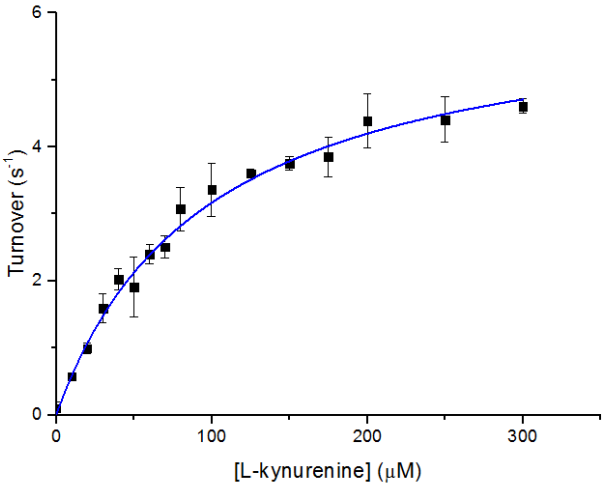

Figure 4.7: Plot of turnover vs L-kynurenine concentration for Y404F *Pf*KMO*. Data were fitted using the Michaelis-Menten equation.

The L-kynurenine K_M value determined for Y404F *Pf*KMO* is an order of magnitude greater than that of *Pf*KMO* confirming that the mutation has had an effect on substrate binding affinity, probably due to the loss of a hydrogen bond between Y404 and the carboxylate of the substrate (Table 4.1). The k_{cat} value for Y404F *Pf*KMO* is only slightly decreased

compared to that for *Pf*KMO*. [143] These kinetic data therefore suggest that Y404 forms a hydrogen bond to the substrate and that the loss of this interaction is responsible for the increase in K_M while k_{cat} is unchanged. This implies that while Y404 is not required for the ability of *Pf*KMO* to hydroxylate L-kynurenine, it is likely to be involved in substrate binding, suggesting that despite the apparent distance between the residue and L-kynurenine there is an interaction occurring.

	K_M (μM)	k_{cat} (s^{-1})	k_{cat}/K_M ($s^{-1}\mu M^{-1}$)
*Pf*KMO*	8.8 ± 1.5	8.9 ± 1.1	1.01
Y404F *Pf*KMO*	96.5 ± 4.0	6.2 ± 0.1	0.06

Table 4.1: The kinetic parameters, K_M and k_{cat}, and the catalytic efficiency determined for Y404F *Pf*KMO* from the results of the assay described in Section 2.5.2 compared to those values obtained for *Pf*KMO* in previous work. [143]

4.2.3 Structure of Y404F *Pf*KMO*

Crystals of Y404F *Pf*KMO* were grown by hanging drop vapour diffusion at 4 ºC. The drop contained a 1:1 mixture of 240 μM Y404F *Pf*KMO* and well solution. The well solution consisted of 0.1 M HEPES buffer pH 7.0, 10% PEG 4K, 8% glycerol, 10 mM NaCl, 10% isopropanol and 1 mM L-kynurenine. The crystal was cryoprotected by successive exposure to well solution containing 10% and then 20% ethylene glycol before it was flash-frozen in liquid N_2. Data were collected on the i03 beamline at the Diamond Light Source, Oxfordshire.

The diffraction images were processed using *iMosflm* and *Scala* as outlined in Section 2.7.4. The space group was fixed as $P2_122_1$ as the first screw axis was not detected to a sufficiently high degree by *POINTLESS*. The unit cell dimensions are a = 103.6 Å, b = 133.8 Å, c = 190.6 Å with angles $\alpha = \beta = \gamma = 90º$. *Molrep* was used for molecular replacement with the structure of *Pf*KMO* in the absence of substrate used to generate the model of the Y404F *Pf*KMO* structure. The resolution of the structure was determined to be 2.7 Å with an overall R_{merge} of 0.077 (data processing statistics listed in Appendix 2 Table A2.2). The asymmetric unit contained four Y404F *Pf*KMO* molecules, each with one non-covalently bound FAD cofactor per monomer. There was no electron density for a ligand found in the active site of any of the protein chains. Three chloride anions were found, binding close to the FAD cofactor in Chains A, B and D and 152 water molecules were added to the model.

The Y404F *Pf*KMO* structure was refined using *Refmac5* and manually edited using *Coot*. After the final round of restrained refinement in *Refmac5* the value of the R_{factor} was 0.2154 and R_{free} was 0.2853.

A comparison of the structures of Y404F *Pf*KMO* and *Pf*KMO* in the absence of substrate with and without NaCl (Table 4.2) shows that these structures are similar as expected as *Pf*KMO* is in the *open* conformation in all three of these structures.

	rmsd (Å)
*Pf*KMO* with NaCl and no substrate, Chain A	0.32
*Pf*KMO* with sodium tartrate and no substrate, Chain A	0.56
*Pf*KMO* with L-kynurenine	0.94

Table 4.2: The rmsd values obtained in a pairwise comparison of Y404F *Pf*KMO* Chain A with *Pf*KMO* in the absence of substrate crystallised both in the presence and absence of NaCl and the structure of *Pf*KMO* with L-kynurenine. The structure of Y404F *Pf*KMO* was most similar to that of *Pf*KMO* obtained in the absence of substrate with NaCl present in the crystallisation conditions. The comparison was made using the protein structure comparison service PDBeFold. [178]

At a resolution of 2.7 Å, most of the residue sidechains in Y404F *Pf*KMO* were visible in the $2F_o - F_c$ density map and could be included in the structure. In the active site of Y404F *Pf*KMO* many of the residues occupy similar positions to those in *Pf*KMO* in the absence of substrate, with and without NaCl (Figure 4.8) although residues I106, I224 and L226 are not shown in the figure for clarity and the sidechains of I224 and L226 are not fully visible in the map and are therefore not complete in the Y404F *Pf*KMO* structure. [143]

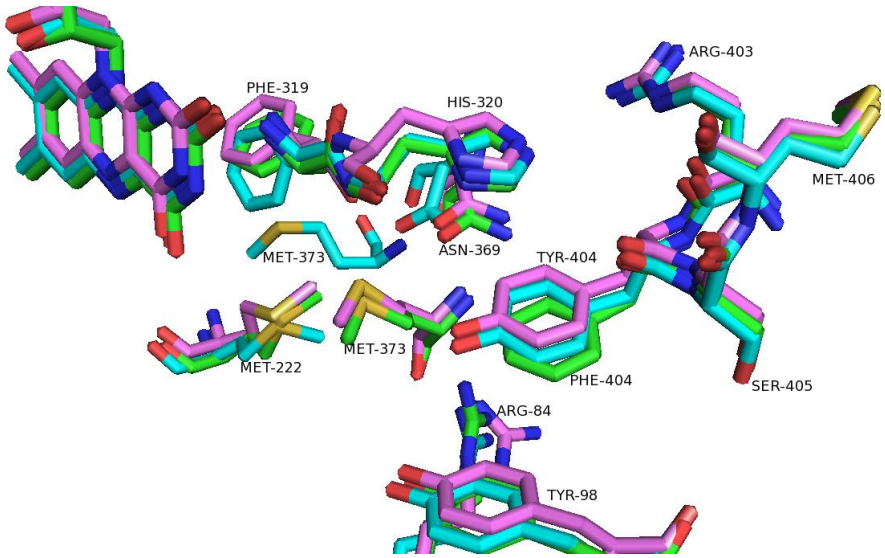

Figure 4.8: The residues in the active site and those close to residue 404 in the Y404F *Pf*KMO* structure (green) overlaid with those in the *Pf*KMO* structure in the absence of substrate (cyan) and *Pf*KMO* with NaCl in the absence of substrate (lilac). [143] From this the differences between the structure of the active site of Y404F *Pf*KMO* and *Pf*KMO* that are unrelated to the presence of NaCl can be identified. These include a movement of Phe404, the backbone near His320 and Arg84. Some of the active site residues including Ile106, Leu224 and Ile226 have been omitted for clarity.

The differences in the positions and orientations of the active site residues of Y404F *Pf*KMO* relative to *Pf*KMO* in the absence of substrate that are due to the presence of NaCl are a slight movement of N369 and F319 and significant displacement of residue M373 which is now in the active site. There are also changes that can be observed between the structure of Y404F *Pf*KMO* and *Pf*KMO* with NaCl that reflect changes which could be caused by the mutation. These include a slight movement of R84 and Y98 as well as movement of F404 relative to Y404. There is also a change in the positions of the sidechains of F319 and the amide bond between these residues in the structures of Y404F *Pf*KMO* and *Pf*KMO* in the absence of substrate with NaCl. The movement of F404 relative to Y404 in both the other structures suggests that in the position of Y404 is such that the interaction between the hydroxyl of Y404 and L-kynurenine can form and when F404 is present, the interaction cannot form so the residue can occupy a slightly different orientation.

Residues N369 and M373 are in the active site and are in a different position in the substrate-free structures obtained in the presence of NaCl compared to that of *Pf*KMO* in the absence

of both L-kynurenine and NaCl. These residues are located at the end of a helix which stops at residue 374 and becomes a loop leading to the C-terminal domain. The residues from N369 to S374 were visible in the electron density map for Y404F *Pf*KMO* but residues 375 – 378 were not. Residues from 379 onwards are in the same position in both the structures of Y404F *Pf*KMO* and *Pf*KMO* in the absence of substrate without NaCl. The positions of these residues are affected by the presence of NaCl and differ in the structures of Y404F *Pf*KMO* and *Pf*KMO* in the absence of substrate and NaCl (Figure 4.9), consistent with observations made in all the structures of *Pf*KMO* crystallised with NaCl in the absence of substrate to date. [143]

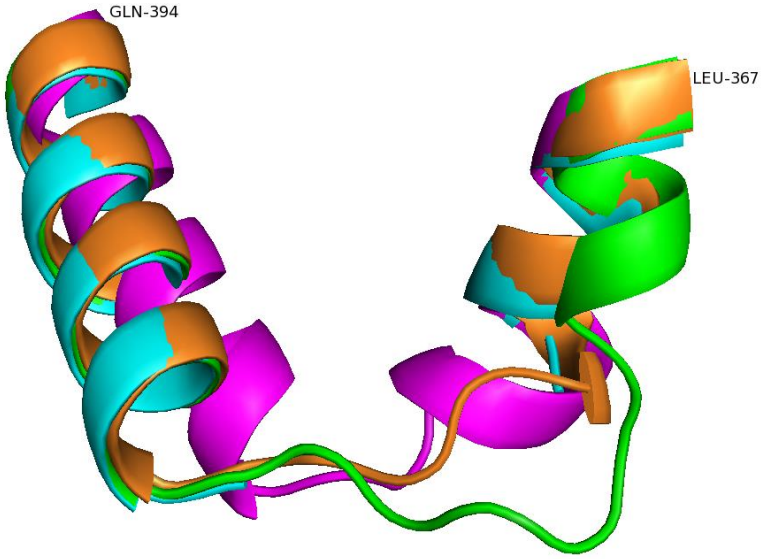

Figure 4.9: Cartoon representation showing the secondary structure of residues 367 – 394 in the structures of Y404F *Pf*KMO* (cyan), *Pf*KMO* in the absence of substrate (green), *Pf*KMO* in the absence of substrate crystallised in the presence of NaCl (orange) and *Pf*KMO* in the presence of L-kynurenine (magenta). Residues 375 – 378 are not present in the Y404F *Pf*KMO* electron density map.

Another area of difference between the structures of Y404F *Pf*KMO* and *Pf*KMO* in the absence of substrate caused by the presence of NaCl in the well solution is the loop consisting of residues I44 – N54 which is not present in the structure from the crystal grown with sodium tartrate. [143] The positions of these residues in the structures of Y404F *Pf*KMO* and *Pf*KMO* with NaCl are similar to those observed in the structure of *Pf*KMO* with L-kynurenine bound (Figure 4.10).

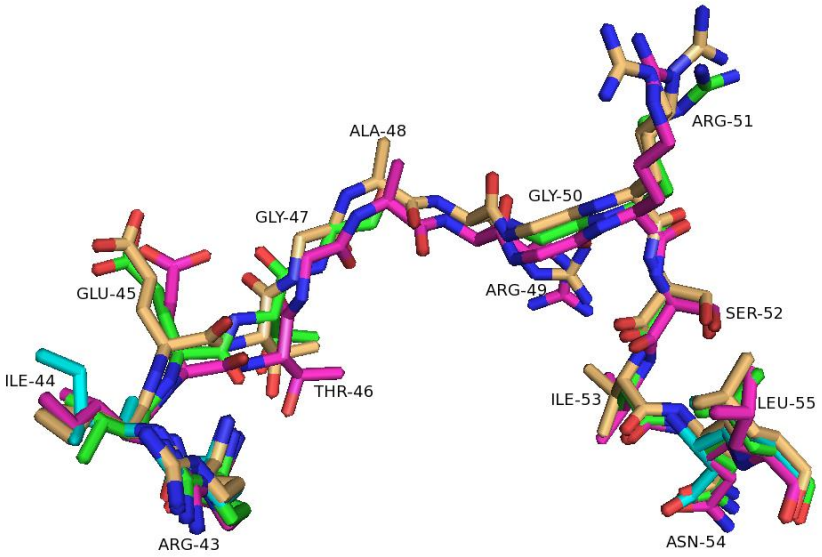

Figure 4.10: Residues in the loop from R43 – L55 for Y404F *Pf*KMO* (green), *Pf*KMO* in the absences of substrate (cyan), *Pf*KMO* with NaCl in the absence of substrate (light orange) and *Pf*KMO* in the presence of L-kynurenine (magenta). A48 and R49 are not visible in the electron density of Y404F *Pf*KMO* and Q45 – I53 are not visible in the *Pf*KMO* structure in the absence of substrate.

The mutation Y404F has not had a significant effect on the structure compared to that of *Pf*KMO*. There are no major conformational changes but there are a few small differences in the active site of Y404F with differences observed in the positions of F319, H320 and F404 which are not attributable to the presence of NaCl. These findings are consistent with the kinetic data obtained which indicate that Y404F *Pf*KMO* is capable of hydroxylating L-kynurenine although the K_M is slightly raised relative to *Pf*KMO*.

4.2.4 Structure of Y404F *Pf*KMO* with L-kynurenine

Crystals of Y404F *Pf*KMO* with L-kynurenine in the active site were obtained by hanging-drop vapour diffusion at 4 ºC. The drop contained a 1:1 mixture of purified protein and well solution. The well solution contained 0.1 M HEPES buffer pH 7.0, 10% PEG 4K, 8% glycerol, 10 mM NaCl, 10% isopropanol and 1 mM L-kynurenine, the same conditions as Y404F *Pf*KMO* in Section 4.2.3. The crystal was cryoprotected by successive exposure to well solution containing 10% and 20% ethylene glycol before being frozen in liquid N_2. Data

were collected on the i02 beamline at the Diamond Light Source, Oxfordshire with an oscillation of 0.3º over a rotation of 180º with a time of 0.3 s per image. The beam wavelength was 0.98 Å and the intensity was 60%. The data were processed using *iMosflm* and *CCP4i* as outlined in Section 2.7.4 and the processing statistics are listed in Appendix 2 Table A.2.

The space group of the Y404F *Pf*KMO* crystal was determined to be $I4_122$, the same as those for *Pf*KMO* with L-kynurenine bound, and there was one protein molecule in the asymmetric unit. The Matthews test showed that this Y404F *Pf*KMO* crystal was approximately 83% solvent. The Y404F *Pf*KMO* crystals grown in these conditions did not diffract to a high resolution and the best data set obtained had a resolution of 3.95 Å although attempts were made to obtain higher quality crystals by altering the growth conditions. Molecular replacement was carried out with *Molrep* using the *Pf*KMO* with L-kynurenine bound structure as a model. The Y404F *Pf*KMO* structure was refined using *Refmac5* and edited in *Coot* before further refinement.

This dataset had R_{factor} of 0.2602 and R_{free} of 0.2914 and B factors of 36.5 Å suggesting that these data are not particularly good quality and that further work refining this structure and editing it is unlikely to make significant valid improvements and is also problematic at this low resolution. The Ramachandran analysis in *Coot* showed that 10.5% of residues were outliers suggesting that the positions and angles of some residues in the structure are likely to be highly unreliable. These problems are likely to be due to the low resolution preventing accurate positioning of the atoms in the electron density map, presumably as a consequence of the high solvent content of the crystal.

The poor resolution of this structure means that many of the sidechains are not visible in the electron density and it is not possible to gain an understanding of subtle changes caused by the Y404F mutation; however, the main chain of the protein had clear electron density and the structure appeared to be very similar to that of *Pf*KMO* with L-kynurenine bound (Table 4.3). There are a few differences in the overall structure including a number of short regions where, in the structure of *Pf*KMO*, there are β-sheets as part of the Rossmann fold, unlike Y404F *Pf*KMO*. This is probably a result of the poor resolution and is unlikely to be a genuine difference in the two structures as the presence of a Rossmann fold is a key feature of Class A flavoprotein aromatic hydroxylases. [97] There are also a few residues in the Y404F *Pf*KMO* structure which did not have any electron density; these were 375-378 and 436-437, which are both loops in the *Pf*KMO* with L-kynurenine bound structure. There were very few differences in the sidechains of Y404F *Pf*KMO* that were visible in the electron

density map compared to those of *Pf*KMO* that were not likely to be the result of the poor resolution so the mutation appears to have had little effect that can be seen at this resolution on the overall structure in the presence of substrate.

	rmsd (Å)
*Pf*KMO* with L-kynurenine	0.77
*Pf*KMO* in the absence of substrate, Chain A	0.98

Table 4.3: The rmsd values obtained in a pairwise comparison of Y404F *Pf*KMO* with L-kynurenine with the structures of *Pf*KMO* in the presence and absence of L-kynurenine. The structure of Y404F *Pf*KMO* was more similar to that of *Pf*KMO* obtained in the presence of L-kynurenine, both structures in the *closed* conformation. The difference between the two rmsd values above is small, possibly a result of the poor resolution of the structure. The comparison was made using the protein structure comparison service PDBeFold. [178]

The exact position of L-kynurenine in the active site was ambiguous, and in the final round of refinement there was a small area of electron density in the active site which could potentially be from part of the substrate, but there was no density for the aromatic ring of L-kynurenine (Figure 4.11). By comparing this structure to that of *Pf*KMO* with substrate bound, this electron density could be from the carboxylate group of L-kynurenine and also part of the R84 sidechain but it is not sufficiently clear in the Y404F *Pf*KMO* structure to be certain of either the position of the substrate or the R84 sidechain at this resolution. The substrate is assumed to be present, due to the $I4_122$ space group and the overall similarity with the bound structure of *Pf*KMO*, especially as both structures are in the *closed* conformation with the C-terminal domain closer to the main domain and active site than is observed in substrate free structures of *Pf*KMO*.

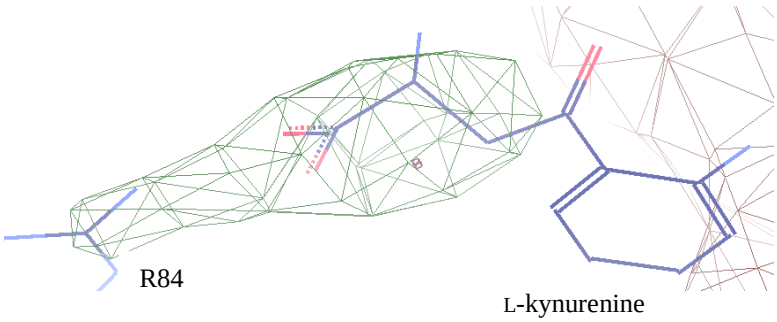

Figure 4.11: The F_o-F_c map of Y404F *Pf*KMO* with L-kynurenine bound (green, positive; red, negative) contoured at 3.00 σ with the superimposed model of *Pf*KMO* with L-kynurenine bound (blue) of which the substrate and the R84 sidechain are shown. The alignment of the two structures was made using the DALI server. [179] There is some unmodelled density in the active site which could be the result of the presence of the substrate and the R84 but as there is no evidence for the presence of the aromatic ring of L-kynurenine, it was not possible to add the substrate to the model of Y404F *Pf*KMO* with L-kynurenine bound.

Few of the residues in the active site of Y404F *Pf*KMO* have any electron density for the sidechains so it is difficult to make comparisons between *Pf*KMO* and Y404F *Pf*KMO*; however, there is density for F404 which shows the residue is in a similar position to that of Y404 (Figure 4.12) but the orientation is different. This could be due to the low quality of the structure and it is not possible to be certain of this slight difference; however it is could potentially represent a real difference in orientation that could be the result of the loss of the hydrogen bond interaction between Y404 and the substrate resulting in a different orientation for F404 becoming more favourable. The sidechains of H320 and N369 are present in the active site and are in similar positions in both structures. The position of the isoalloxazine ring of the FAD cofactors is also slightly different, but again this likely to be caused by the resolution of the Y404F *Pf*KMO* structure rather than represent a major difference between the two structures. The region around residue 404 appears to be highly similar in both structures suggesting that this mutation has not caused any local conformational changes in the protein structure. This is consistent with the kinetic data in Section 4.2.2, as the loss of the ability to form a hydrogen bond has an effect on K_M but barely any effect on the value of k_{cat}.

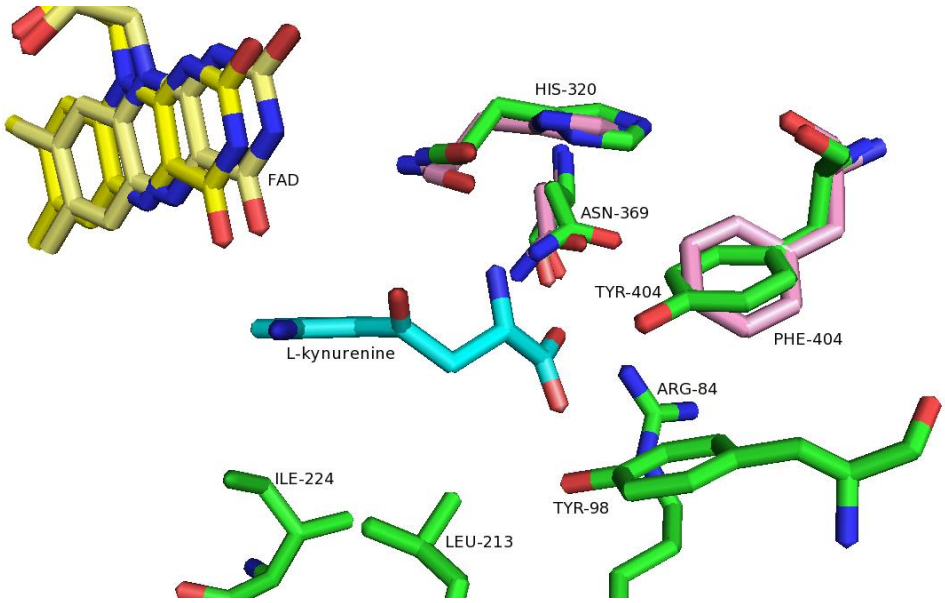

Figure 4.12: Active site residues of Y404F *Pf*KMO* (pink) overlaid with those from the structure of *Pf*KMO* (green) with L-kynurenine bound (cyan) with FAD cofactors (pale yellow and yellow respectively). Some of the residues with sidechains present in the model of the *Pf*KMO* structure only are not shown for clarity (Ile106, Met222, Leu224 and Met373). Slight differences in the orientation of His320, Asn369 and Tyr404/Phe404 can be observed although these could be due only to the poor resolution and quality of the Y404F *Pf*KMO* structure.

The resolution of the structure of Y404F *Pf*KMO* with L-kynurenine bound is 3.95 Å meaning that it is difficult to draw any reliable conclusions from the structure; however the structure is clearly similar to *Pf*KMO* with substrate bound as from the backbone, which can be observed from the electron density map, there are no observable conformational changes. This is consistent with the kinetic data and with the higher resolution structure of Y404F *Pf*KMO* in the absence of substrate, and would support the hypothesis that this residue is involved in a hydrogen-bonding interaction with L-kynurenine.

4.3 N369

In the structure of *Pf*KMO* with L-kynurenine bound, it appears that N369 may interact with the carboxylate moiety of the substrate. The mutation made to investigate the role of this residue is N369S and this protein was studied kinetically and crystallised both in the absence of ligand and with 3,4-dichlorobenzoylalanine, an effector molecule, in the active site.

4.3.1 Steady state kinetic analysis of N369S *Pf*KMO*

The mutation N369S was made in the gene of *Pf*KMO* using the megaprimer PCR method and was expressed and purified using the methods described in Chapter 2. The UV-visible spectrum of the N369S *Pf*KMO* was obtained (Figure 4.13).

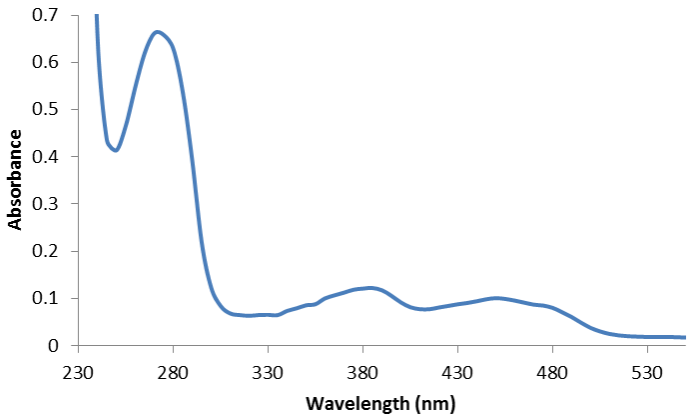

Figure 4.13: UV-visible spectrum of N369S *Pf*KMO*. The concentration was determined to be 8.2 µM.

N369S *Pf*KMO* was active and it was possible to obtain the kinetic parameters K_M and k_{cat} (Figure 4.16) using the kinetic assay (Section 2.5.2) performed in triplicate.

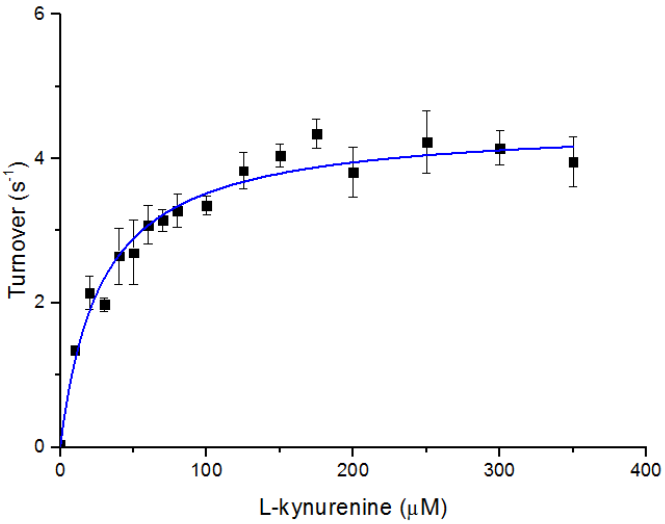

Figure 4.14: Graph of turnover plotted against L-kynurenine concentration fitted to the Michaelis-Menten equation using Origin 8.5.1.

The mutation N369S has caused a small increase in the K_M value (Table 4.4) which would suggest that this residue interacts with the substrate and the mutation affects this interaction but that it does not have a significant effect on the ability of the enzyme to bind L-kynurenine nor has this mutation had an effect on the k_{cat} value which is very similar for both N369S *Pf*KMO* and *Pf*KMO*. [143]

	K_M (μM)	k_{cat} (s^{-1})	k_{cat}/K_M ($s^{-1}\mu M^{-1}$)
*Pf*KMO*	8.8 ± 1.5	8.9 ± 1.1	1.01
N369S *Pf*KMO*	27.7 ± 3.3	4.5 ± 0.2	0.16

Table 4.4: The kinetic parameters, K_M and k_{cat}, and the catalytic efficiency determined for N369S *Pf*KMO* from the results of the assay described in Section 2.5.2 compared to those values obtained for *Pf*KMO* in previous work. [143]

4.3.2 Structure of N369S *Pf*KMO*

Crystals of *Pf*KMO* N369S were obtained by hanging drop vapour diffusion at 4 ºC. The drop was a 1:1 mixture of N369S *Pf*KMO* and well solution. The well solution contained 0.1 M HEPES pH 7.0, 9% PEG 4K, 10 mM NaCl, 10% glycerol, 10% isopropanol and 1

mM L-kynurenine. Although the substrate was present in the drop, there was no electron density for any substrate molecule in the active site. The crystal was cryoprotected in a well-solution containing 10% ethylene glycol and flash-frozen in liquid nitrogen.

Data were collected on the i03 beamline at the Diamond Light Source, Oxfordshire. Data was collected with an oscillation of 0.2º over a rotation of 120º and an exposure time of 0.2s/image, beam wavelength of 0.976 Å, and beam intensity of 25%. The images were processed using *iMosflm* and *Scala*. The space group was found to be $P2_122_1$, the same as the structure of *Pf*KMO* in the absence of substrate. The asymmetric unit contained four protein molecules, each with one non-covalently bound FAD cofactor and had cell dimensions of a = 104.85 Å, b = 133.96 Å, c = 188.32 Å, $\alpha = \beta = \gamma = 90^{o}$ (processing statistics are listed in full in Appendix 2 Table A2.3). One chloride anion was identified as binding close to the FAD cofactor for each *Pf*KMO* and 323 waters were found in the asymmetric unit. Molecular replacement was carried out using *Molrep* using the structure of *Pf*KMO* in the absence of substrate which was expected to be quite similar. The structure was refined using *Refmac5* and after refining and validation the R_{factor} was 0.2290 and R_{free} was 0.2752.

The resolution of the structure is 2.38 Å, which is sufficient to see most of the residues and their sidechains in the electron density map; however, there were residues for which the sidechain positions could not be determined and there were some residues for which there was no density in the $2F_o$-F_c map. Some of the missing regions, including residues 46 – 47, 207 – 209 and 245 – 246, correspond to loops in the *Pf*KMO* structure and could be flexible regions in the crystal structure of N369S *Pf*KMO* for reasons unrelated to the N369S mutation (Figure 4.15). The other missing regions including residues 203 – 206 and 373 – 380 are potentially more significant and are discussed below.

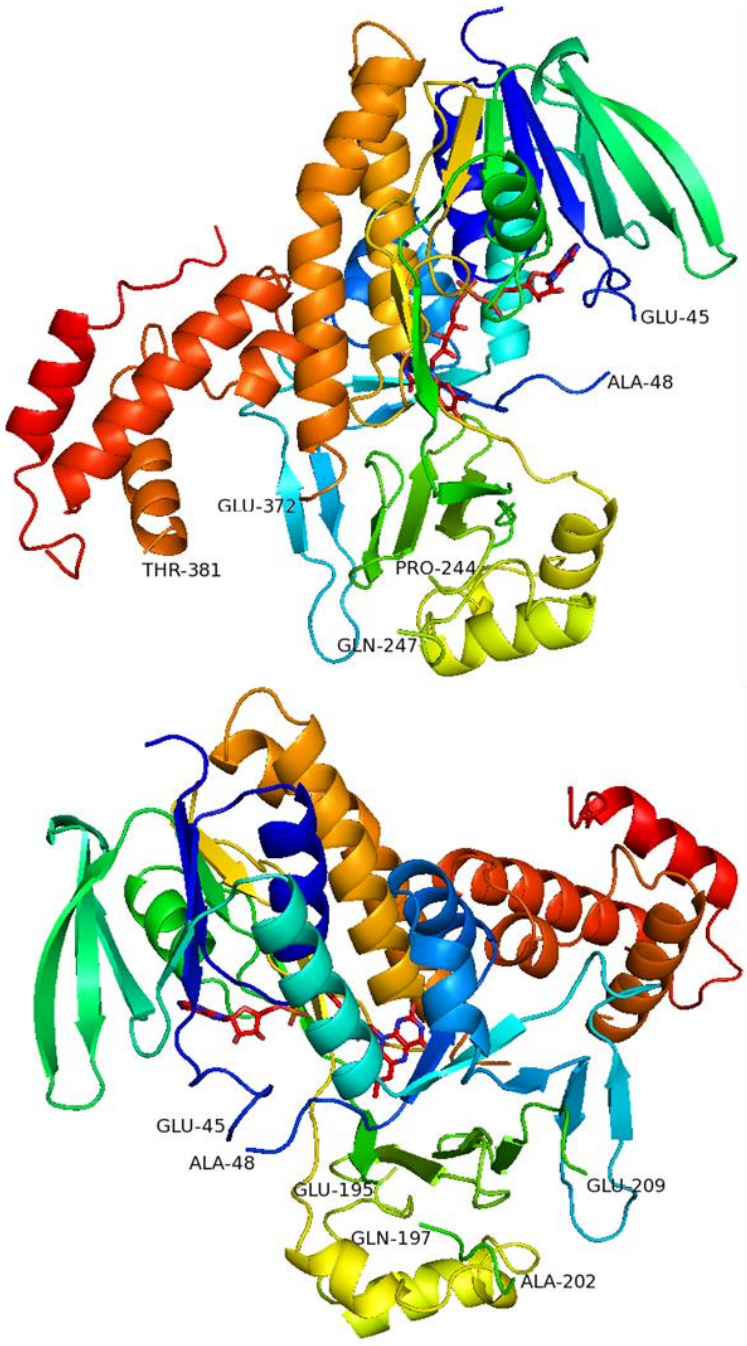

Figure 4.15: Two views of N369S *Pf*KMO* Chain A in cartoon form to represent the secondary structure elements coloured with N-terminal in blue and C-terminal in red. The FAD cofactor is in red to contrast with the colours in the main domain. The residues at each end of a break in Chain A where there is no electron density are labelled.

There are slight differences between the structure of N369S *Pf*KMO* and *Pf*KMO* in the absence of substrate including the positions of residues from 195 – 250 that appear to be the

result of the electron density map of N369S *Pf*KMO* being of lesser quality in this region, and it is difficult to position some of the residues with such a high degree of certainty. Throughout the structure the vast majority of sidechains that are completely visible in the electron density map of N369S *Pf*KMO* are in the same orientation as those in the structure of *Pf*KMO* in the absence of substrate.

The structure of N369S *Pf*KMO* is similar to those of *Pf*KMO* in the absence of substrate (Table 4.5), structures which are in the *open* conformation observed when no ligand is bound in the active site resulting in movement of the C-terminal domain away from the main domain of the protein. As this structure was obtained in the presence of NaCl, it is slightly more similar to the *Pf*KMO* structure in the absence of substrate crystallised in the presence of NaCl compared to that crystallised with sodium tartrate present.

	rmsd (Å)
*Pf*KMO* in the absence of substrate, with NaCl, Chain A	0.33
*Pf*KMO* in the absence of substrate, no NaCl, Chain A	0.47
*Pf*KMO* with L-kynurenine	0.90

Table 4.5: The rmsd values obtained in a pairwise comparison of N369S *Pf*KMO* Chain A in the absence of substrate with the structures of *Pf*KMO* in absence of L-kynurenine with and without the presence of NaCl and the structure of *Pf*KMO* with L-kynurenine bound. The values were obtained using PDBeFold. [178]

There are very few differences in the active site of N369S *Pf*KMO* compared to *Pf*KMO* with NaCl in the absence of substrate (Figure 4.16). There is a slight difference in the positions of F319 and H320 similar to that seen with Y404F *Pf*KMO* (Section 4.2.3). There is also a change in the orientation of S369 relative to N369 so that the sidechain occupies a very similar position to that in the structure of *Pf*KMO* in the absence of both NaCl and substrate. The change in the position of the F319 carbonyl means that there is no interaction between this carbonyl and S369 unlike in the *Pf*KMO* structure with NaCl where an interaction between N369 and this carbonyl is possible.

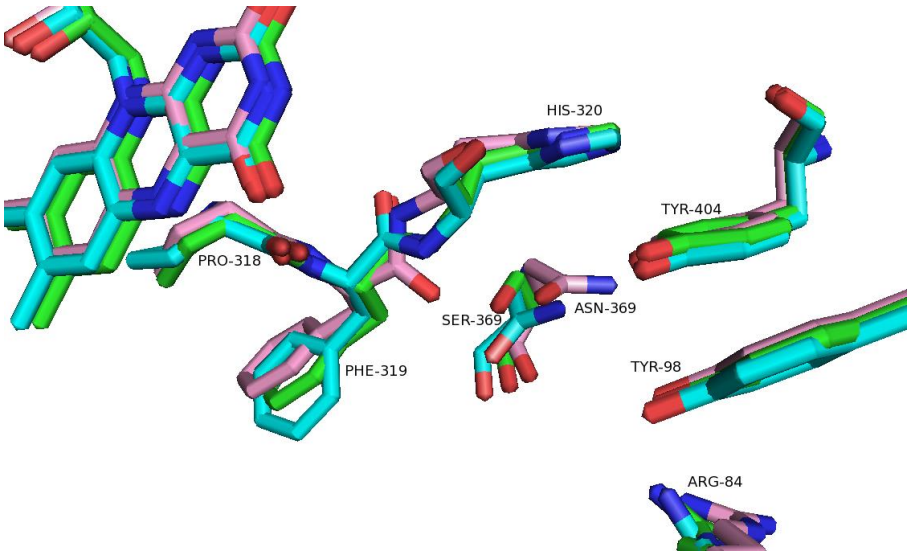

Figure 4.16: Selected active site residues in N369S *Pf*KMO* (green) overlaid with residues in *Pf*KMO* in the absence of substrate (cyan) and *Pf*KMO* with NaCl in the absence of substrate (lilac). Other active site residues have been omitted for clarity. The differences that are due to the N369S mutation rather than the presence of NaCl (comparing the green and lilac residues) are changes to the positions of Arg84, Phe319, the amide bond between Phe319 and His320, and Ser369 which is orientated in a different direction than Asn369 in the *Pf*KMO* structure with NaCl in the absence of substrate.

The mutation N369S has had very little effect on the structure of *Pf*KMO* in the absence of substrate as no major changes were observed when comparing the structure of N369S *Pf*KMO* with that of *Pf*KMO* in the absence of substrate. This finding is consistent with the kinetic results for N369S *Pf*KMO* where there is little change in either the K_M or k_{cat} values obtained.

4.2.3 Structure of N369S *Pf*KMO* with 3,4-dichlorobenzoylalanine

Crystals of N369S *Pf*KMO* with the substrate analogue, 3,4-dichlorobenzoylalanine bound in the active site were grown using the hanging drop vapour diffusion method at 4 ºC. The drop contained a 1:1 mixture of the purified protein and the well solution. The well solution consisted of 0.1 M HEPES pH 7.0 buffer, 10 mM NaCl, 8% PEG 4K, 8% glycerol, 10% isopropanol and 1 mM 3,4-dichlorobenzoylalanine. The crystal was sequentially exposed to

well solutions containing 10% and 20% ethylene glycol before being flash-frozen in liquid N_2.

Data were collected on the i03 beamline at the Diamond Light Source, Oxfordshire. The data was collected with an oscillation of 0.3º over a rotation of 180º and an exposure time of 0.3s/image, beam wavelength of 0.976 Å and beam wavelength of 0.976 Å and intensity of 40%. The images were processed using *iMosflm* and *Scala* as described in Section 2.7.4. The space group was found to be $I4_122$ with unit cell dimensions of a = b = 150.1 Å, c = 274.0 Å, $\alpha = \beta = \gamma = 90º$ (full details in Appendix 2 Table A2.3) and the data had a resolution of 3.98 Å. *Molrep* was used to generate the model of the structure using the *Pf*KMO* structure with L-kynurenine bound as a model. The structure was refined using *Refmac5* and edited using *Coot* after each refinement times with a final R_{factor} of 0.2610 and R_{free} of 0.3362. 3,4-dichlorobenzoylalanine was added to the model in *Coot* after generating the three-dimensional coordinates and library of restraints using *PRODRG*.

The high value of R_{free} and the resolution of this structure mean that while it is useful for providing some information on the general similarities and any major differences between N369S *Pf*KMO* with 3,4-dichlorobenzoylalanine bound and the structure of *Pf*KMO* with L-kynurenine, it is not a reliable guide to subtle differences in the protein structure caused by the N369S mutation.

At this resolution, many of the sidechains of N369S *Pf*KMO* were not visible in the electron density map. Using *Coot* with data at this resolution was problematic and there are a large number of outliers on the Ramachandran plot (18%) which deteriorated with successive refinement using *Refmac5*. While it would be possible to examine every residue using *Coot* and alter the angles to remove Ramachandran outliers and to create the likely secondary structure elements, actual improvements to data quality are only likely to be made by growing crystals in different conditions. Efforts were made to increase the resolution of data obtained using crystals grown in similar conditions, but these were unsuccessful.

The electron density map did clearly indicate the approximate positions of residues in the protein chain and comparing N369S *Pf*KMO* to the structure of *Pf*KMO*, the main chain as represented in cartoon form (Figure 4.17) is similar. There are significant differences though in the secondary structure which is probably caused by the issues with the data rather than changes caused by the mutation. These difference are that in N369S *Pf*KMO* there are residues which would be expected to be part of an α-helix or β-sheet but are in a loop, a

notable example of this are the β-sheets of the Rossmann fold which are not β-sheets in the N369S *Pf*KMO* structure.

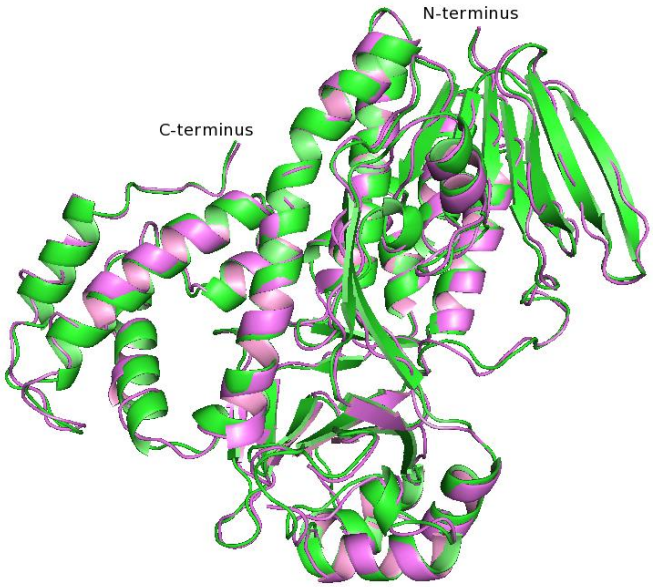

Figure 4.17: Overlay of the secondary structures represented in cartoon form of N369S *Pf*KMO* (purple) with 3,4-dichlorobenzoylalanine potentially bound in the active site and *Pf*KMO* (green) with L-kynurenine bound in the active site. The two structures are similar but there are regions of loops in the N369S *Pf*KMO* where there are β-sheets or α-helices in the *Pf*KMO* structure. These differences are probably due to the quality of the structure rather than major conformational changes as the kinetic results show that the mutation N369S does not have a significant effect on *Pf*KMO*.

A comparison of the structure of N369S *Pf*KMO* in the presence of 3,4-dichlorobenzoylalanine to those of *Pf*KMO* in the presence and absence of L-kynurenine confirms that this structure resembles more closely the structure of *Pf*KMO* with L-kynurenine (Table 4.6). The rmsd values obtained were lower than expected probably due to the low quality of this structure caused by the low resolution. This result supports the hypothesis that 3,4-dichlorobenzoylalanine is bound in this N369S *Pf*KMO* structure as the *open* conformation is observed here and for the *Pf*KMO* structure with L-kynurenine.

	rmsd (Å)
*Pf*KMO* with L-kynurenine	0.84
*Pf*KMO* in the absence of substrate, Chain A	1.13

Table 4.6: The rmsd values obtained in a pairwise comparison of N369S *Pf*KMO* with 3,4-dichlorobenzoylalanine with the structures of *Pf*KMO* in the presence and absence of L-kynurenine. The values were obtained using PDBeFold. [178] These values are lower than those above in Table 4.5 which probably reflects the poor quality of this structure rather than more significant structural changes.

There is some electron density that suggests the presence of the ligand in the active site, but this was in close proximity to residues P318 – H320 so it was not possible to model 3,4-dichlorobenzoylalanine into the active site of N369S *Pf*KMO* (Figure 4.18). As this structure is in the closed conformation and the mutation has little effect on the K_M value compared to *Pf*KMO*, it is probable that ligand is bound but that at this resolution it is not possible to see conclusive evidence for its presence in the active site.

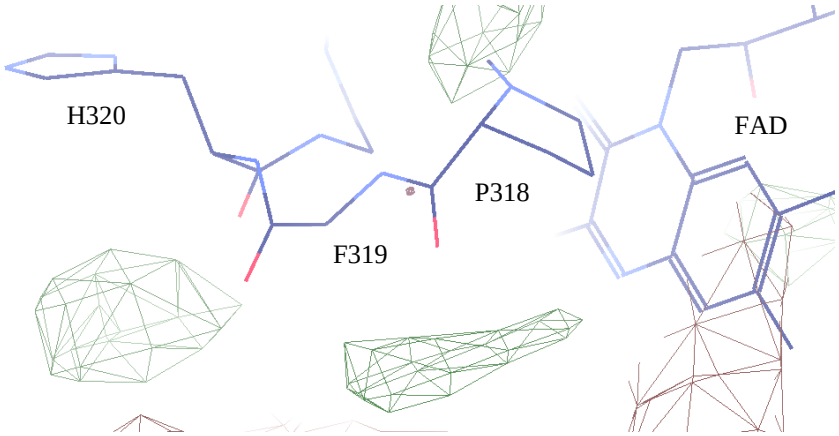

Figure 4.18: F_o-F_c for the structure of N369S *Pf*KMO* refined in the absence of ligand in the active site contoured at 3.00 σ. There are areas (green, positive) that may be due to the presence of 3,4-dichlorobenzoylalanine but there is not sufficient evidence to accurately determine the position and orientation of the ligand.

In the structure of N369S *Pf*KMO*, there are no conformational changes in close proximity to the N369S mutation but S369 is orientated in a different direction and would therefore not be involved in any interactions with the substrate or with R84 unlike N369 (Figure 4.19). [143]

There are few differences between the active site of this structure and that of *Pf*KMO* with L-kynurenine but because of the poor resolution of this structure, no conclusions can be drawn. As N369S *Pf*KMO* is an active enzyme, this would suggest that the loss of any interactions involving N369 are not particularly critical for the enzyme to function effectively; however, with the poor resolution of this structure it is not possible to be certain of the reliability of the position of the N369 sidechain.

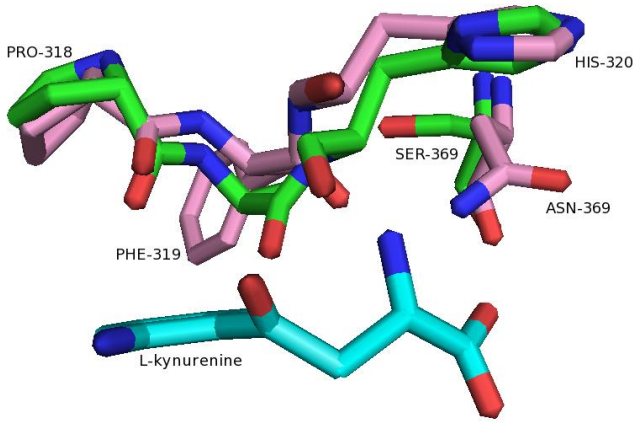

Figure 4.19: In the structure of N369S *Pf*KMO* in the presence of 3,4-dichlorobenzoylalanine (green), Ser369 is orientated towards the backbone of residues Pro318 – His320. In the structure of *Pf*KMO* (lilac) in the presence of L-kynurenine (cyan), the position of Asn369 allows for an interaction between this residue and L-kynurenine which cannot form when the mutation is made. The carbonyl of His320 is closer to the amide of L-kynurenine in the *Pf*KMO* structure although the significance of this difference is unclear due to the low resolution of the N369S *Pf*KMO* structure.

The structure of N369S *Pf*KMO* with 3,4-dichlorobenzoylalanine is not particularly high quality and has a resolution of 3.98 Å. There are only a few conclusions that can be drawn from this structure, including the overall similarity between this structure and *Pf*KMO* with L-kynurenine suggesting that the N369S mutation has not had a significant effect.

4.4 R84

4.4.1 R84A *Pf*KMO*

The mutation R84A was introduced to the *Pf*KMO* gene using the QuikChange II kit and the R84A *Pf*KMO* protein was expressed and purified using the methods described in Chapter 2 and the UV-visible spectrum was obtained (Figure 4.20). This mutation made the protein inactive and no enzyme activity was detected using the assay described in Section 2.5.2 which detects the change in absorbance as NADPH is converted to $NADP^+$.

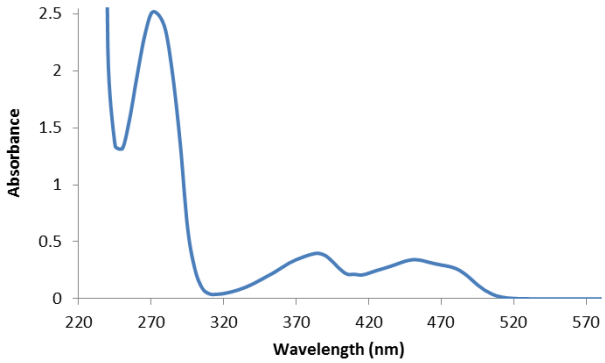

Figure 4.20: UV-visible spectrum of 27.7 µM R84A *Pf*KMO*.

This is consistent with the information gained from the structure of *Pf*KMO* as this residue interacts with the carboxylate group of L-kynurenine and is likely to be involved in one of the most important interactions for substrate binding. In addition, R84 appears to interact with N369 and is also involved in the interactions responsible for the C-terminal domain movement observed when substrate binds. [143] By making the non-conservative mutation to an alanine none of these interactions can be maintained and therefore it is not surprising that the enzyme activity is not detected using the assay. This loss of activity is also consistent with the mutation R83A made in *S. cerevisiae* KMO. [142]

4.4.2 Kinetic analysis of R84K *Pf*KMO*

The protein R84K *Pf*KMO* was expressed and purified using the methods described in Chapter 2 after the mutation was made in the gene using the megaprimer PCR method. The UV-visible spectrum of R84K *Pf*KMO* was obtained after purification (Figure 4.21).

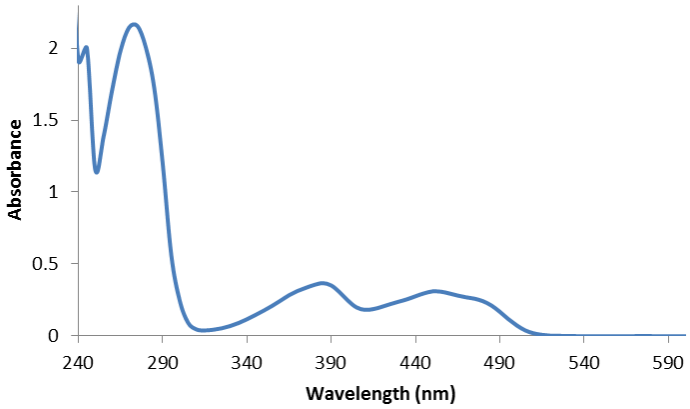

Figure 4.21: UV-visible spectrum of 25.1 µM R84K *Pf*KMO*.

The values of K_M and k_{cat} could not be determined using the kinetic assay in Section 2.5.2 as a change in absorbance could not be detected suggesting that the enzyme is inactive. This would suggest that the role of R84 is critical for enzyme function as suggested above in Section 4.4.1 as even a conservative mutation to R84K results in inactive protein. Although a lysine residue could potentially be involved in some of the interactions thought to be formed by R84, it is possible that K84 is not able to form strong interactions with either the carboxylate moiety of L-kynurenine or E372, an interaction hypothesised to be critical for conformational change between the *open* and *closed* conformations of *Pf*KMO*. The inactivity of R84K *Pf*KMO* could be caused by the mutation having an significant effect on the structure of the protein so this protein was crystallised to further understand the role of this apparently critical residue.

4.4.3 Structure of R84K *Pf*KMO*

Crystals of R84K *Pf*KMO* were obtained by hanging drop vapour diffusion at 4 ºC. The drop contained a 1:1 mixture of the purified protein and the well solution which consisted of 0.1 M HEPES buffer, pH 7.0, 14% PEG 4K, 7.5% glycerol, 10 mM NaCl, 10% isopropanol and 1 mM L-kynurenine. Although L-kynurenine was present, only substrate-free crystals were obtained and in the absence of L-kynurenine significant precipitation was observed in the hanging drops. The data were collected on the i02 beamline at the Diamond Light Source, Oxfordshire. The data were collected with an oscillation of 0.2º over a rotation of 120º with exposure time of 0.2 s/image. The beam wavelength was 1.00 Å and intensity was 65%.

The diffraction images collected were processed using *iMosflm* and *Scala* as discussed in Section 2.7.4 and the resolution was determined to be 2.45 Å. The space group is $P2_122_1$, the same as the other structures obtained with no ligand bound in the active site, and there were four R84K *Pf*KMO* molecules, one chloride found near the FAD of each *Pf*KMO* and 274 water molecules in the asymmetric unit. The unit cell dimensions were found to be a = 105.5 Å, b = 133.7 Å and c = 187.6 Å with angles $\alpha = \beta = \gamma = 90^o$ (the processing statistics are listed in Table A2.4 in Appendix 2). Molecular replacement was carried out using *Molrep* and the model was refined using *Refmac5* using rigid body refinement and subsequent rounds of restrained refinement and TLS refinement with editing carried out manually in *Coot* after each refinement in *Refmac5*. The final R_{factor} was 0.2225 and R_{free} = 0.2794.

The structure of R84K *Pf*KMO* with no substrate bound in the active site has many similarities with that of *Pf*KMO*. The FAD cofactor is non-covalently bound in the main domain of the protein and the C-terminal domain is observed in the *open* conformation (Figure 4.22). While some of the residue sidechains in this structure could not be observed clearly in the electron-density map, the structure of R84K *Pf*KMO* contains residues from Asn6 to Ser461 without any breaks in two of the chains, with only a maximum of six residues missing in the other two molecules.

Figure 4.22: The structure of one of the chains of R84K *Pf*KMO* represented in cartoon form to show the secondary structure. The protein chain colour is blue at the N-terminus and red at the C-terminus with the FAD cofactor shown in red.

Comparing the structure of R84K *Pf*KMO* to the structures of *Pf*KMO* obtained in previous work confirmed that R84K *Pf*KMO* was most similar to the structures obtained in the absence of L-kynurenine, which were also crystallised in the *open* conformation with the C-terminal domain further from the main domain (Table 4.7). There are some differences observed between the structures of R84K *Pf*KMO* and *Pf*KMO* in the absence of substrate particularly in the region close to the start of the C-terminal domain, thought to have to be caused by the presence of NaCl in the growth conditions and are therefore not a result of the R84K mutation. [143] This is reflected in the difference between the rmsd values for R84K *Pf*KMO* compared to *Pf*KMO* in the absence of L-kynurenine with and without NaCl in the crystallisation conditions.

	rmsd (Å)
*Pf*KMO* in the absence of substrate, with NaCl, Chain A	0.42
*Pf*KMO* in the absence of substrate, no NaCl, Chain A	0.62
*Pf*KMO* with L-kynurenine	0.87

Table 4.7: The rmsd values obtained in a pairwise comparison of R84K *Pf*KMO* Chain A in the absence of substrate with the structures of *Pf*KMO* in absence of L-kynurenine with and without NaCl and the structure of *Pf*KMO* with L-kynurenine bound. The values were obtained using PDBeFold. [178]

The sidechain of K84 is completely visible in the active site of three of the four R84K *Pf*KMO* molecules in the active site. K84 is located in the active site but not in the same position as R84 in the *Pf*KMO* structure with NaCl in the absence of substrate (Figure 4.23).

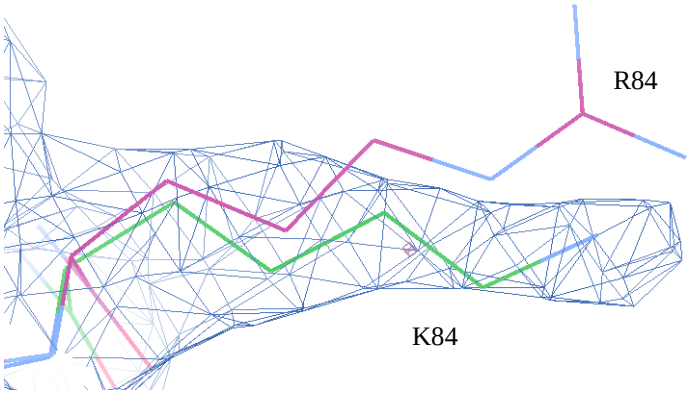

Figure 4.23: The $2F_o$-F_c map (blue) contoured at 1.00 σ for R84K *Pf*KMO* Chain A (blue) with the model of K84 (green) with R84 from the structure of *Pf*KMO* in the absence of substrate in the presence of NaCl (purple).

The other differences observed in the R84K *Pf*KMO* active is a very slight change in the position of the sidechain of N369 (Figure 4.24) and the carbonyl of F319.

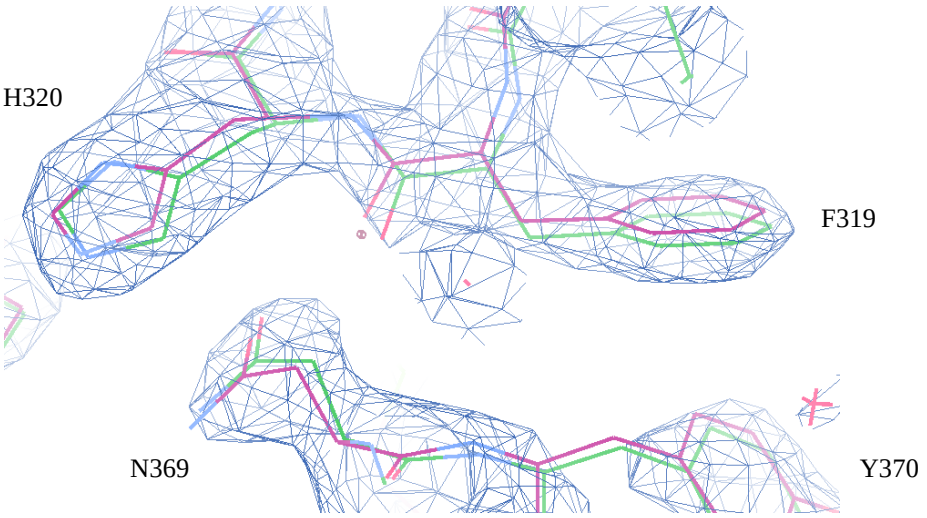

Figure 4.24: The $2F_o$-F_c map for R84K *Pf*KMO* (blue) contoured at 1.50 σ with the model of the structure (green) and the structure of *Pf*KMO* in the absence of substrate (NaCl) (purple).

In the active site of R84K *Pf*KMO*, there are very few differences that can be observed between this structure and that of *Pf*KMO* in the absence of substrate with or without NaCl (Figure 4.25). There only difference is a slight change in the position of K84 compared to R84 where K84 is further from the active site. This structure differs from Y404F *Pf*KMO* (Section 4.2.3) and N369S *Pf*KMO* (Section 4.3.2) in that this is the only structure obtained with F319 and H320 in the same position as the structure of *Pf*KMO* with NaCl in the absence of substrate. This degree of similarity between the structure of R84K *Pf*KMO* and *Pf*KMO* in the absence of substrate was unexpected given the lack of activity observed with R84K *Pf*KMO*.

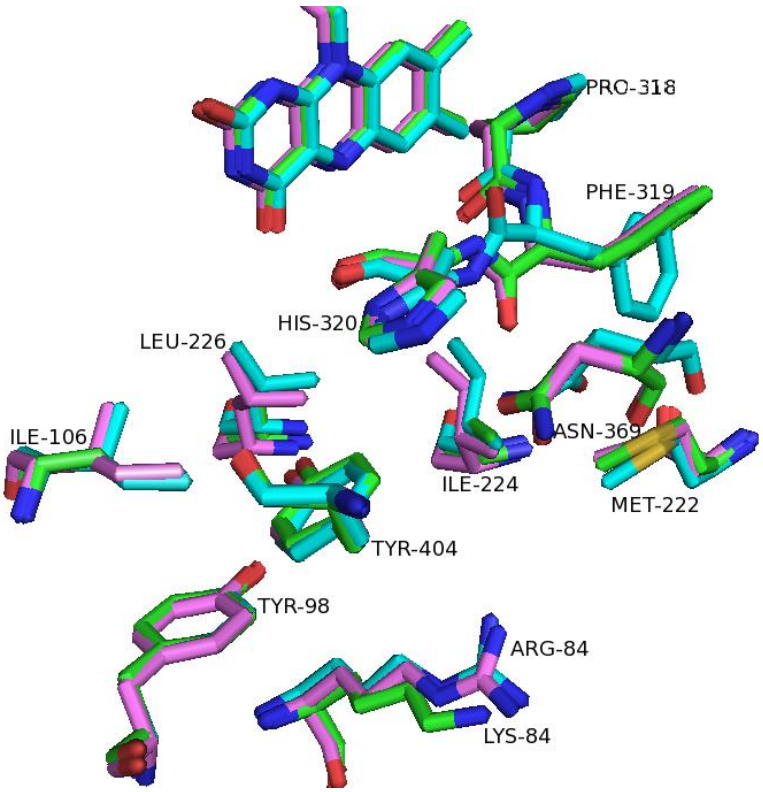

Figure 4.25: Residues in the active site of R84K *Pf*KMO* (green) overlaid with those in the structures of *Pf*KMO* in the absence of substrate (cyan) and *Pf*KMO* with NaCl in the absence of substrate (lilac). The structure of R84K *Pf*KMO* closely resembles that of *Pf*KMO* with NaCl except in the position of Lys84 which is moved further from the active site than Arg84.

4.5 Summary

The characterisation of the active site of *Pf*KMO* has focussed on three residues identified in the crystal structure as being potentially important in substrate binding. These were Y404, hypothesised to form a hydrogen bond with the substrate, N369 thought to interact with the carboxylate moiety of L-kynurenine and R84 considered important for substrate binding and conformational change. These residues were studied using active site mutants which were purified and then characterised kinetically and structurally to identify and explain any

changes in *Pf*KMO* properties. Further mutations had been planned; however, it was not possible to successfully make them during this project.

Residue Y404 was investigated with two mutations, Y404A and Y404F. Y404A *Pf*KMO* was found to be inactive indicating that a non-conservative change is not tolerated at this position. Y404F *Pf*KMO* was active and kinetic data showed a raised K_M suggesting that Y404 forms a hydrogen bond with the carboxylate moiety of L-kynurenine that is involved in substrate binding but is not essential. The structure of Y404F *Pf*KMO* was obtained in the $P2_122_1$ space group in the *open* conformation and only slight changes were observed between this structure and that of *Pf*KMO* in the absence of substrate. The structure was also obtained in the $I4_122$ space group at a poor resolution and there was not sufficient data to accurately determine the position of L-kynurenine.

The conservative mutation N369S was made to investigate the role of N369 and was observed to have little effect on the kinetic properties of this enzyme. The structure of N369S *Pf*KMO* was obtained without substrate binding in the active site and was similar to that of *Pf*KMO* with a slight change in the position of S369 which could allow the formation of hydrogen bond interaction with the carbonyl of F319. The structure of N369S *Pf*KMO* was also obtained in the presence of the effector 3,4-dichlorobenzoylalanine This compound is structurally similar to L-kynurenine but cannot be hydroxylated by KMO. The structure was similar to that of *Pf*KMO* with L-kynurenine bound but due to the poor resolution there was inconclusive evidence for the position of the ligand in the active site and few conclusions could be drawn from this structure.

R84 is thought to form one of the most important interactions for substrate binding and is also implicated in the control of the conformational changes from *open* to *closed* that occur when substrate or small ligands are bound in the active site. In the *closed* conformation R84 is part of a network of interactions that connect the active site to the C-terminal domain and mutating this residue was expected to have a significant effect on the enzyme properties. The mutation R84A caused *Pf*KMO* to lose all measurable activity. The conservative mutation R84K was also made and no activity was detected with R84K *Pf*KMO* in the kinetic assay. The structure of R84K in the *open* conformation was obtained but was remarkably similar to that of *Pf*KMO* with no change in the conformation observed but a slight difference in the position of K84 away from the active site suggesting that this mutation may significantly compromise the ability of *Pf*KMO* to bind L-kynurenine.

This information is the result of the first investigation of the role of R84, N369 and Y404 in the active site of *Pf*KMO* and supports hypotheses made about the role of active site residues from previous structures of *Pf*KMO* in the presence and absence of L-kynurenine. N369 is not particularly important for substrate binding although it is located just over 3 Å from the carboxylate moiety of L-kynurenine (Figure 4.26). Y404 is over 4 Å from L-kynurenine, from the structure of *Pf*KMO* with L-kynurenine bound, however, this residue does appear to form a hydrogen bond with the carboxylate moiety that is important for the affinity of the enzyme for the substrate. R84 appears to be the key residue in the active site, important for binding L-kynurenine and also implicated in the conformational change observed on substrate binding and with even a conservative mutation at this residue, the ability of *Pf*KMO* to hydroxylate L-kynurenine is severely affected.

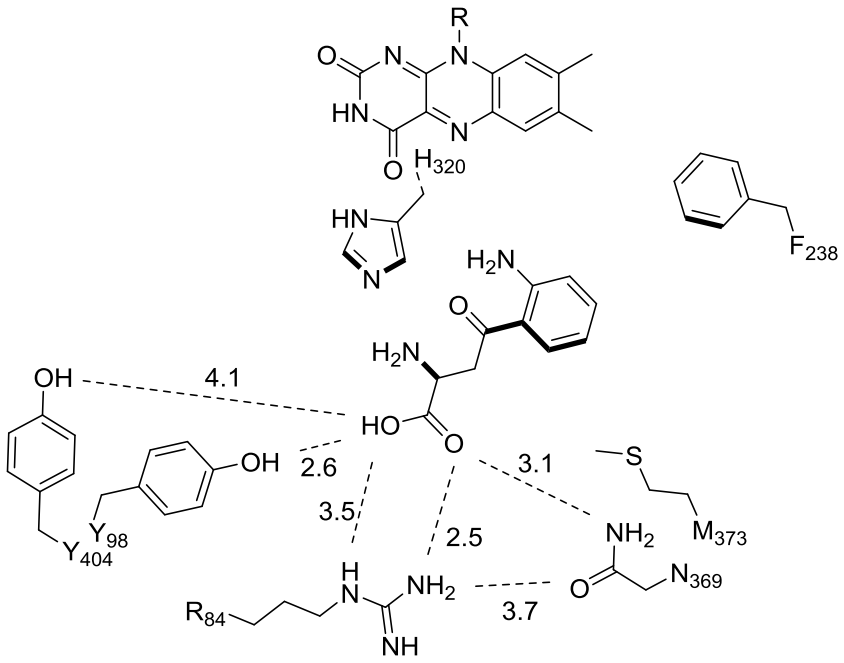

Figure 4.26: Schematic of the active site of *Pf*KMO* with L-kynurenine bound in the active site. The aromatic ring binds in close proximity to the isoalloxazine moiety of the FAD cofactor. The carboxylate moiety of L-kynurenine is able to interact with active site residues including R84, Y98, N369 and Y404.

By studying these residues, information on the interactions important to substrate binding has been gained and this has complemented the previous structural work on *Pf*KMO* confirming some of the hypotheses about the role of residues in the active site and providing a more detailed understanding of this enzyme.

Chapter 5: Investigating the Role of Histidine 320

5.1 Role of H320 in the active site

H320 is located in the active site of *Pf*KMO* on a loop close to the isoalloxazine moiety of the FAD cofactor, and the substrate L-kynurenine (Figure 5.1). From this structure of *Pf*KMO*, H320 was not expected to be critical for substrate binding as the closest distance from this residue to L-kynurenine is 3.9 Å. The distances between H320 and the surrounding residues in vicinity of the active site are also quite large suggesting that there are not significant interactions between them.

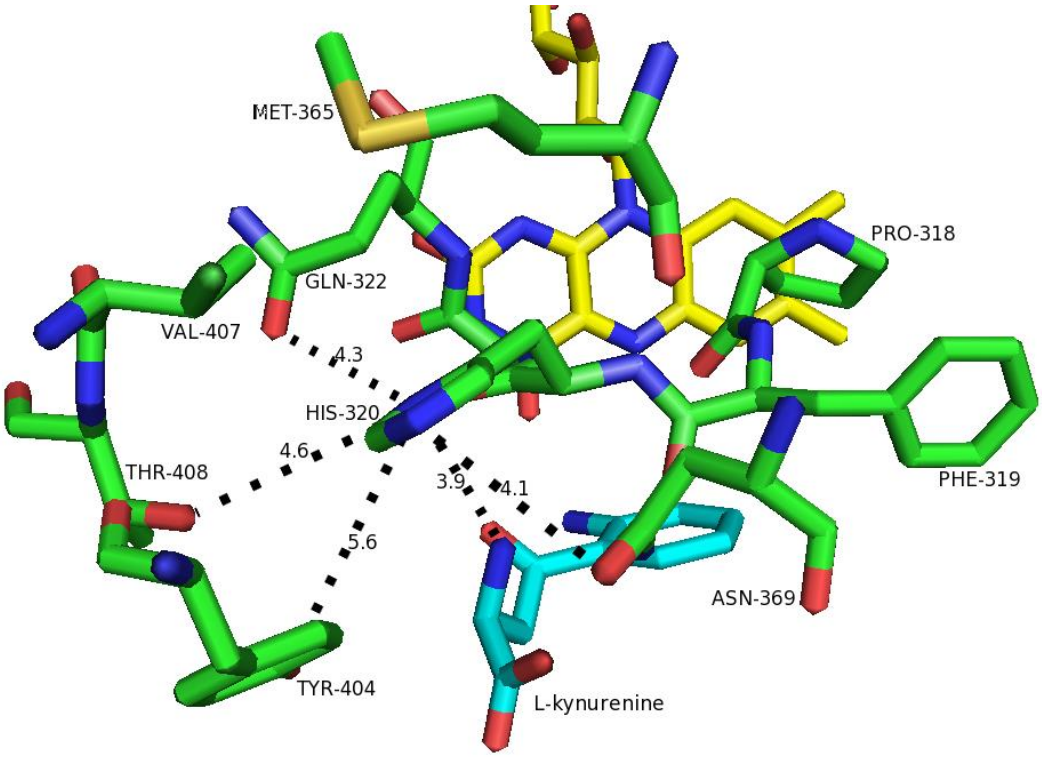

Figure 5.1: View of H320 in the active site of *Pf*KMO* with FAD cofactor (yellow) and L-kynurenine (cyan). Distances from the H320 to the nearest residues and L-kynurenine are indicated and quoted in Å.

H320 is of significant interest because from inspection of the crystal structure it is the only residue in the active site of *Pf*KMO which is not conserved in the human enzyme (Figure 5.2). This means that any changes in *Pf*KMO kinetic behaviour on mutating this residue to the phenylalanine residue present in the human enzyme could indicate possible differences between the human and *Pf*KMO enzymes that are relevant to substrate binding and inhibitor design.

```
humanKMO        MDSSVIQRKKVAVIGGGLVGSLQACFLAKRNFQIDVYEAREDTRVATFTRG--RSINLAL 58
ScKMO           ------MSESVAIIGAGLVGCLAALAFSKEGYNVTLYDFRQDPRLDTTKNKNLKSINLAI 54
PfKMO           -MTATDNARQVTIIGAGLAGTLVARLLARNGWQVNLFERRPDPRIETGARG--RSINLAL 57
                       ..*::**.**.* * *  :::..::: ::: * *.*: *  .   :*****:

humanKMO        SHRGRQALKAVG--LEDQIVSQGIPMRARMIHSLSGKKSAIPYG-TKSQYILSVSRENLN 115
ScKMO           SARGIDALKSIDPDACEHILQDMIPMKGRMIHDLKGRQESQLYG-LHGEAINSINRSVLN 113
PfKMO           AERGAHALRLAG--LEREVLAEAVMMRGRMVHVPGTPPNLQPYGRDDSEVIWSINRDRLN 115
                : ** .**:  .     .:: : : *:.**:*      .   **  ..: * *:.*. **

humanKMO        KDLLTAAEKYPNVKMHFNHRLLKCNPEEG---MITVLGSD-KVPKDVTCDLIVGCDGAYS 171
ScKMO           NSLLDELEKS-TTELKFGHKLVKIEWTDDKQICHFAIGEDLKAPHTEKYDFVIGCDGAYS 172
PfKMO           RILLDGAEAA-GASIHFNLGLDSVDFARQRLTLSNVSGER----LEKRFHLLIGADGCNS 170
                . **   *    ..::*.  * . :          . *.          .:::*.**. *

humanKMO        TVRSHLMKKPRFDYSQQYIPHGYMELTIPP-------KNGDYAMEPNYLHIWPRNTFMMI 224
ScKMO           ATRSQMQRKVEMDFSQEYMNLRYIELYIPPTEEFKPNYGGNFAIAPDHLHIWPRHKFMLI 232
PfKMO           AVRQAMASVVDLGEHLETQPHGYKELQITP------EASAQFNLEPNALHIWPHGDYMCI 224
                :.*. :     :.   :     * ** *.*        ..:: : *: *****:  :* *

humanKMO        ALPNMNKSFTCTLFMPFEE--------FEKLLTSN-DVVDFFQKYFPDAIPLIGEKLLVQ 275
ScKMO           ALANSDGSFTSTFFGSKDQ--------ISDLITSKSRVREFLIKNFPDIINIMDLDDAVK 284
PfKMO           ALPNLDRSFTVTLFLHHQSPAAQPASPCFAQLVDGHAARRFFQRQFPDLSPMLDS--LEQ 282
                **.* : *** *:*   :.            :..   .  *: : ***   ::.     :

humanKMO        DFFLLPAQPMISVKCSSFHFKS-HCVLLGDAAHAIVPFFGQGMNAGFEDCLVFDELMDKF 334
ScKMO           RFITYPKESLVCVNCKPYDVPGGKAILLGDAAHAMVPFYGQGMNCGFEDVRILMALLKKH 344
PfKMO           DFEHHPTGKLATLRLTTWHVGG-QAVLLGDAAHPMVPFHGQGMNCALEDAVALAEHLQSA 341
                 *   *   :  :. ..:.. . :.:*******.:***.*****..:**   :   :..

humanKMO        SNDLSLCLPVFSRLRIPDDHAISDLSMYNYIEMRAHVNSSWFIFQKNMERFLHAIMPSTF 394
ScKMO           SGDRSRAFTEYTQTRHKDLVSITELAKRNYKEMSHDVTSKRFLLRKKLDALFSIIMKDKW 404
PfKMO           ADNAS-ALAAFTAQRQPDALAIQAMALENYVEMSSKVASPTYLLERELGQIMAQRQPTRF 400
                :.: * .:. ::  *  *  :*  ::  ** **  .* *  :::.:::  ::       :

humanKMO        IPLYTMVTF-SRIRYHEAVQRWHWQKKVINKGLFFLGSLIAISSTYLLIHYMSPRSFLCL 453
ScKMO           IPLYTMISFRSDISYSRALERAGKQTRILKFLESLTLGMLSIGGYKLFKFLTRERS---- 460
PfKMO           IPRYSMVTF-SRLPYAQAMARGQIQEQLLKFAVANHSDLTSINLDAVEHEVTRCLPPLSH 459
                ** *:*::* * : * .*: *   * ::::       .: :*.   :        .

humanKMO        RRPWNWIAHFRNTTCFPAKAVDSLEQISNLISR 486
ScKMO           ---------------------------------
PfKMO           LC------------------------------- 461
```

Figure 5.2: Sequence alignment of the KMO gene sequences from *Pseudomonas fluorescens* (*Pf*KMO), *S. cerevisiae* (*Sc*KMO) and *Homo sapiens* (humanKMO). The residues in the active site of *Pf*KMO* and the aligned residues are highlighted in yellow, except for H320 which is highlighted in red. The UniProt codes for *Homo sapiens* and *S. cerevisiae* KMO are O15229 and A0A0C5LRM7 respectively. The sequences were found using BLAST and the alignment was made using ClustalW.

The equivalent of residue H320 is a tyrosine (Y323) in the *S. cerevisiae* KMO enzyme and in the crystal structures of this enzyme it can be seen the loop containing Y323 and surrounding residues is in the same position as that containing H320 in *Pf*KMO* (Figure 5.3). [142,143] The tyrosine is orientated in a different direction than H320F with the ring and carboxylate pointing out of the active site away from the inhibitor UPF 648. The *S. cerevisiae* structure is of a truncated KMO and is disordered from residue 359 onwards in the presence of UPF 648 so the position of F320 in H320F *Pf*KMO* may not resemble that of Y323 in *S. cerevisiae* KMO.

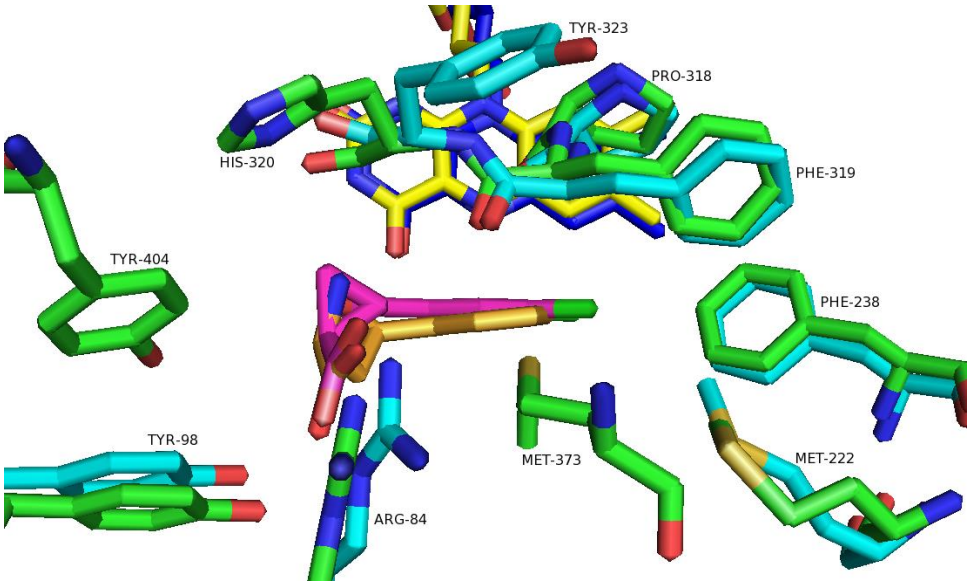

Figure 5.3: Overlay of active site residues in *Pf*KMO* (green) with FAD cofactor (yellow) and L-kynurenine (orange) and *S. cerevisiae* KMO (cyan) with FAD cofactor (blue) and UPF 648 (magenta). The labels refer to the number of that residue in the *Pf*KMO sequence with the exception of Y323. Some residues have been omitted for clarity. Constructed using PDB 4J36 and *Pf*KMO*. [142,143]

In constructing and studying H320F *Pf*KMO* the aim is to determine the extent to which this residue interacts with L-kynurenine bound in the active site and whether it contributes to the catalytic efficiency. By assaying H320F *Pf*KMO* with novel inhibitor compounds and comparing the results to those with *Pf*KMO*, potential differences in inhibitor binding in the active site that might be likely to occur in the human enzyme can be observed and this would give further confidence to the use of *Pf*KMO* in testing for inhibitor molecules that would hopefully have applications after drug development in conditions affecting human patients.

5.2 Kinetic Analysis of H320F

5.2.1 Michaelis-Menten kinetics

The mutation H320F was introduced using the QuikChange PCR method and the H320F *Pf*KMO* protein was expressed and purified using the methods described in Chapter 2. The UV-visible spectrum of H320F *Pf*KMO* was obtained (Figure 5.4).

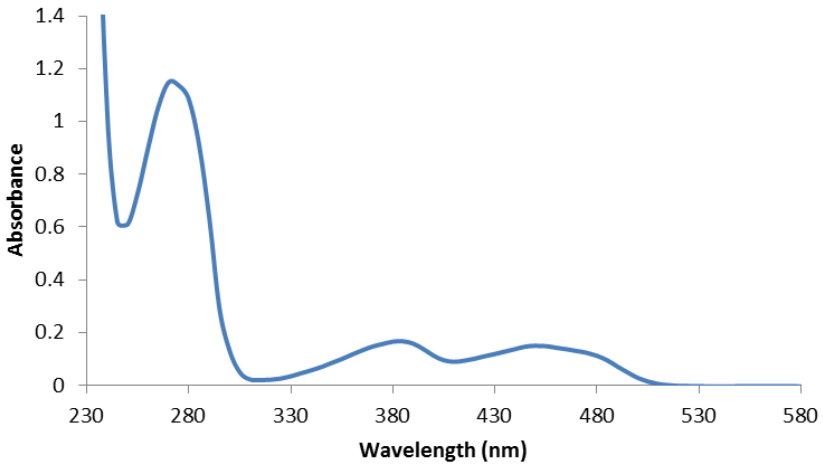

Figure 5.4: UV-visible spectrum of H320F *Pf*KMO*. The concentration of this sample was determined to be 12.2 µM from an absorbance measurement of 0.15 at 450 nm where *Pf*KMO* has a molar extinction coefficient, ε, of 12300 $M^{-1}cm^{-1}$.

The protein was assayed as described in Section 2.5.2 in triplicate to determine the K_M and k_{cat} values to determine the effects of the mutation and the data were analysed using Origin 8.5.1 (Figure 5.5).

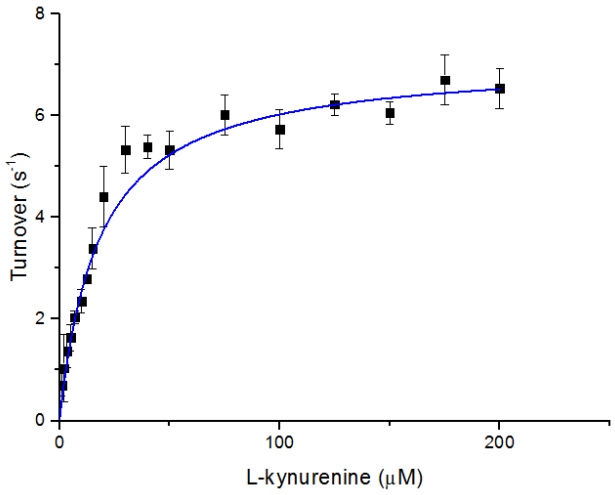

Figure 5.5: Plot of L-kynurenine concentration against turnover used to determine the value of K_M and k_{cat}. The graph was made in Origin 8.5.1 and the curve fitted using the Michaelis-Menten equation.

Compared to the values obtained for *Pf*KMO*, it can be seen that H320F *Pf*KMO* has a slightly raised K_M and very slightly lowered k_{cat} value, which suggests that the mutation has slightly decreased substrate affinity (Table 5.1). [143] This shows that this mutation has not had such a major effect on enzyme properties unlike mutations of residues involved in substrate binding (Chapter 4).

	K_M (μM)	k_{cat} (s^{-1})	k_{cat}/K_M ($s^{-1}\mu M^{-1}$)
*Pf*KMO*	8.8 ± 1.5	8.9 ± 1.1	1.01
H320F *Pf*KMO*	18.0 ± 1.2	7.1 ± 0.2	0.39

Table 5.1: The kinetic parameters, K_M and k_{cat}, and the catalytic efficiency determined for H320F *Pf*KMO* from the results of the assay described in Section 2.5.2 compared to those values obtained for *Pf*KMO* in previous work. [143]

5.2.2 Inhibition Assays

Three similar inhibitor compounds (Figure 5.6) were assayed with H320F *Pf*KMO* using the inhibition assay described in Section 2.5.3. These compounds are all known to be potent

inhibitors of *Pf*KMO* and were evaluated with the H320F variant as a means of further analysing the role of this residue.

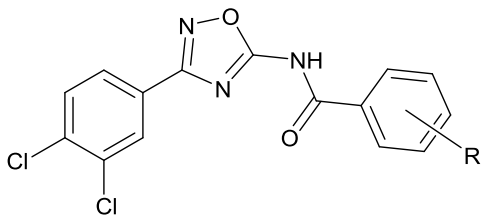

Figure 5.6: General structure of the inhibitor compounds tested on H320F *Pf*KMO*.

The results obtained from the inhibition assays contain a number of interesting trends (Table 5.2, with inhibition data in Appendix 3). All the K_i values obtained with H320F *Pf*KMO* are significantly higher, a greater effect than might have been expected given the small change in K_M observed with this enzyme compared to *Pf*KMO*.

The trend in the potency of the inhibitor compounds is not the same for H320F *Pf*KMO* as it is for *Pf*KMO*. For H320F *Pf*KMO* the most potent inhibitor is GM862, followed by GM855 and GM843 which have very similar K_i values. This is different to the trend for *Pf*KMO* where GM855 with the large *meta*- substituent has a markedly lower K_i value than the other two inhibitors which have a similar effect, with GM843 having a slightly lower K_i value than GM862. The most potent inhibitors of *Pf*KMO* have been shown to contain large *meta* substituents and have 4-OMe substitution (Chapter 3).

Compound	R	H320F *Pf*KMO* K_i value (nM)	*Pf*KMO* K_i Value (nM)
GM862	3-OMe, 4-OH	253.2 ± 30.3	82.4 ± 10.0
GM843	3-OH, 4-OMe	418.8 ± 57.7	73.3 ± 9.7
GM855	3-OCH_2CO_2Et, 4-OMe	394.1 ± 30.9	19.8 ± 8.7

Table 5.2: K_i values obtained for three novel KMO inhibitors tested against H320F *Pf*KMO* and *Pf*KMO* with full data presented in Appendix 2.

From these data alone, comparing the K_i values for GM843 and GM855 assayed with H320F *Pf*KMO*, it can be seen that a large *meta* substituent does not result in a significant change in the K_i value. It appears that the area of the inhibitor molecule more important for potency

is the *para* substituent and that with H320F *Pf*KMO* there is a slight preference for 4-OH compared to 4-OMe which was not observed in earlier work with *Pf*KMO*. [143]

This change in the trend in K_i values is interesting as these substituents are on a part of the molecule which is known not to bind in the active site. This suggests that the mutation may have resulted in more changes to the enzyme than might have been expected due to the loss of an interaction between H320 and the inhibitor molecules. To investigate potential interactions the previously obtained structure of *Pf*KMO* with GM760 was compared with the structure of *Pf*KMO* with GM859 (Figure 5.7). [143] The amide carbonyl of GM760 is in closer proximity to H320 than that of GM859 but the shortest distances between H320 and GM760 over 3.5 Å. This suggests that strong interactions are not formed between H320F and the inhibitors but those inhibitors that bind in a similar position to GM760 are in closer proximity to H320 than those that bind in a similar position to GM859. Unfortunately no crystals of H320F *Pf*KMO* with inhibitor compounds could be obtained.

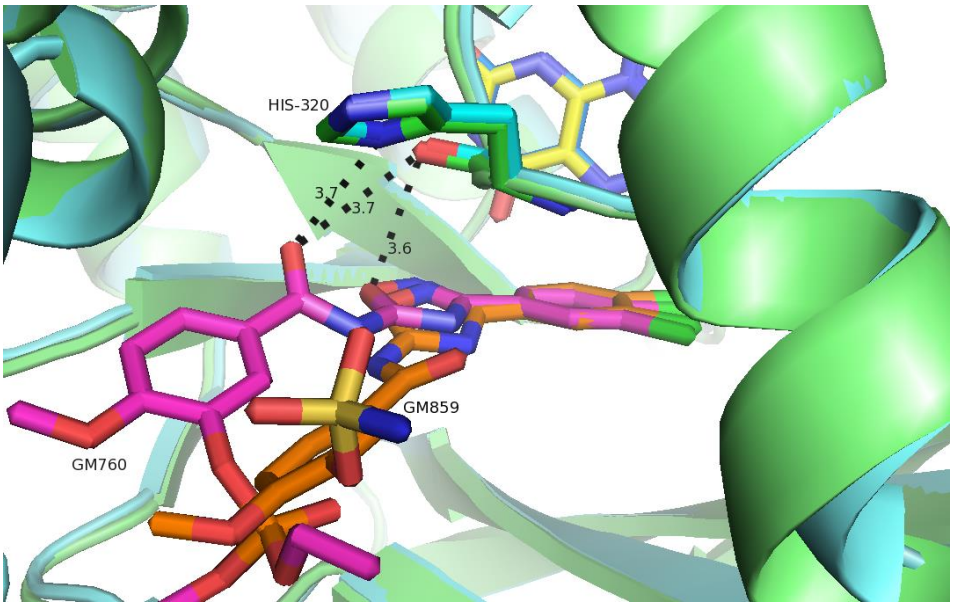

Figure 5.7: Overlay of the structures of *Pf*KMO* (green) with GM760 (pink) and FAD cofactor (yellow) and that of *Pf*KMO* (cyan) with GM859 (orange) and FAD cofactor (blue). Distances between GM760 and H320 are indicated in Å.

5.3 Structure of H320F *Pf*KMO*

5.3.1 Initial attempts to crystallise H320F *Pf*KMO*

The first attempts to obtain a model of the structure of H320F *Pf*KMO* used similar conditions to those used in obtaining the structure of *Pf*KMO*. H320F *Pf*KMO* crystals were only obtained in the presence of L-kynurenine, and unlike the other *Pf*KMO* proteins with active site mutations, no crystals in the $P2_122_1$ space group were obtained.

Several attempts were made to obtain a data set of sufficient quality to make a good model but all the data collected was low resolution. The crystals all belonged to the $I4_122$ space group (likely to contain L-kynurenine in the active site) and the resolution limit of each dataset was over 4 Å with very large B-factors, which meant that it was not possible to obtain the structure from crystals grown in these conditions.

5.3.2 High resolution structure of H320F *Pf*KMO*

New conditions for growing crystals of *Pf*KMO were shared by industrial collaborators who had had success in obtaining the structure of *Pf*KMO at a higher resolution in the space group $P2_1$. These new conditions were used as a starting point for the crystallisation of H320F *Pf*KMO* and crystals of H320F *Pf*KMO*, both in the presence and absence of L-kynurenine, were obtained from which the structure of H320F *Pf*KMO* was successfully solved (by Mark Taylor and Lindsay McGregor, members of the Mowat group).

5.3.3 H320F *Pf*KMO* in the presence of L-kynurenine

The structure of H320F *Pf*KMO* crystallised in the $P2_1$ space group in the presence of L-kynurenine has a resolution of 1.9 Å which is the highest obtained for a *Pf*KMO* structure in the presence of substrate. The R_{merge} was 0.039 overall (data processing statistics in Appendix 2, Table A2.5). This model has two H320F *Pf*KMO* and 866 waters in the asymmetric unit. There was insufficient evidence in the electron density map to determine the position of L-kynurenine.

The structure of H320F *Pf*KMO* in the presence of the substrate is similar to the structure of *Pf*KMO* with L-kynurenine bound (Figure 5.8). The H320F *Pf*KMO* structure contains a main domain and a C-terminal domain and has the non-covalently bound FAD present in a very similar position to that of the *Pf*KMO* structure. The overlay of the two structures in cartoon forms shows only a few differences in the two structures including the loop from residue 45-54 which is a flexible region visible in to the right of the protein as shown below (deep blue) and is the only region where there is a significant change in the position of residues visible in this overlay representation although there are some minor differences in the position of the helices of the C-terminal domain.

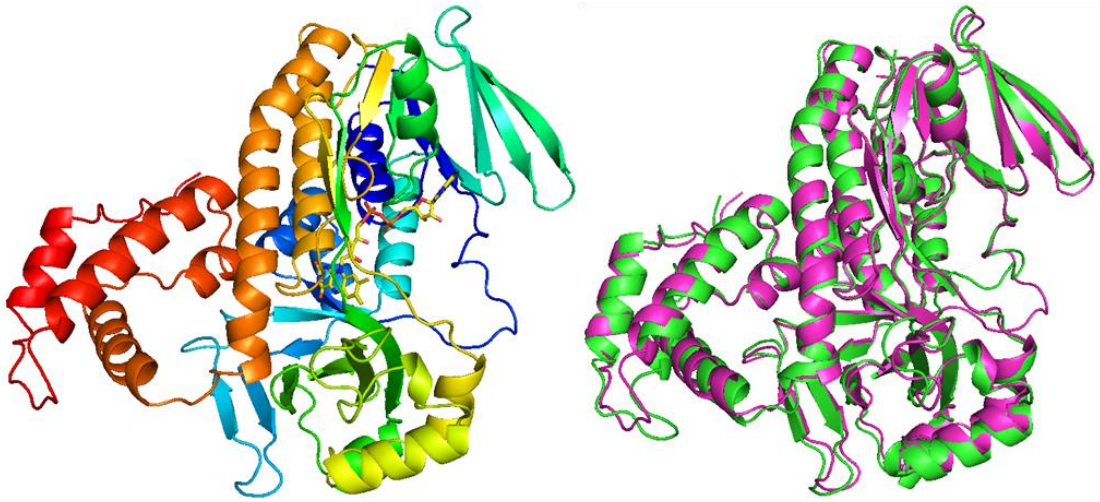

Figure 5.8: The structure of H320F *Pf*KMO* as a cartoon form with the N-terminus in deep blue and C-terminus in red is on the left. The FAD cofactor is shown in stick form in yellow. On the right is an overlay of the H320F *Pf*KMO* structure (magenta) with the *Pf*KMO* with L-kynurenine bound (green) with the FAD cofactors omitted for clarity.

The active sites of H320F *Pf*KMO* and L-kynurenine bound *Pf*KMO* have many similarities, with many of the hydrophobic residues in almost exactly the same positions. H320 and F320 occupy very similar positions in the active site (Figure 5.9), as do N369 and R84 but there are significant differences in the position of the two tyrosine residues which are thought to interact with the substrate, Y98 and Y404. It is difficult to comment on the significance of this as the evidence for the presence of L-kynurenine in active site of H320F *Pf*KMO* is not conclusive (Figure 5.10).

Y404 appears to have moved significantly closer to the carboxylate moiety of L-kynurenine with the distance from the hydroxyl to the carboxylate group decreasing from 4.1 Å to 2.8 Å in the H320F *Pf*KMO* structure, assuming that the substrate is present and that it binds in the same position. There is a distance of 1.8 Å between the hydroxyl groups of Y404 in each structure. Y98 has moved further away from the active site in the H320F *Pf*KMO* with a 1.1 Å distance between the hydroxyl groups of this residue in both structures.

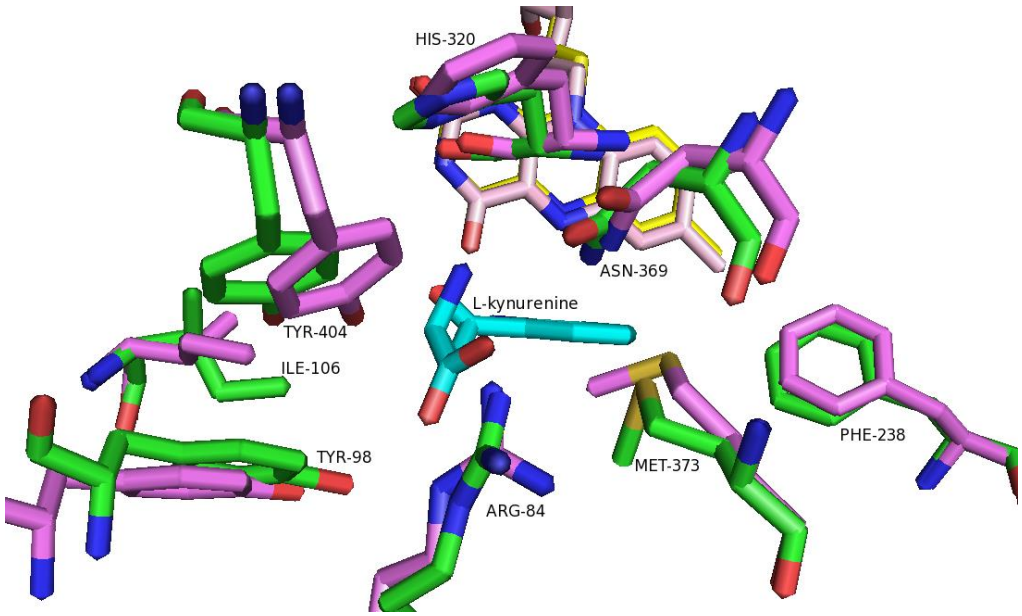

Figure 5.9: An overlay view of some active site residues in *Pf*KMO* (green) with L-kynurenine (cyan) bound and H320F *Pf*KMO* (magenta). The FAD cofactors from these structures are yellow and pink respectively. There is no unambiguous L-kynurenine molecule bound in the H320F *Pf*KMO* that can be shown.

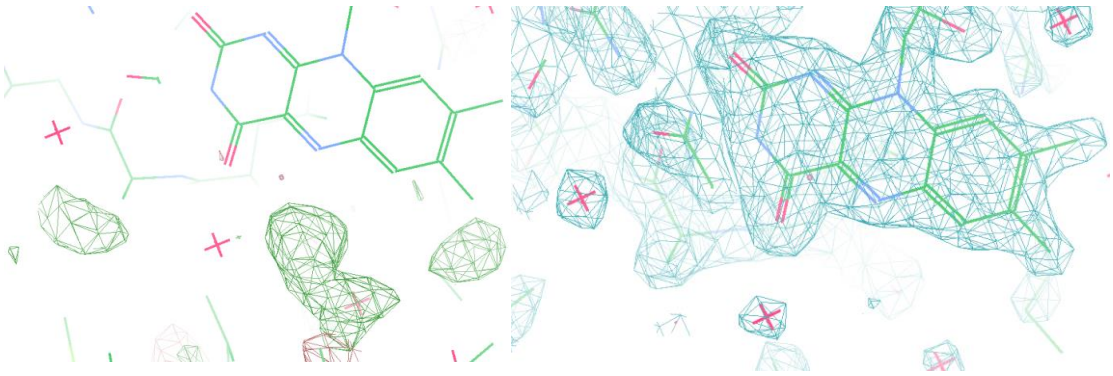

Figure 5.10: The F_o-F_c map (left; green) contoured at 2.99 σ and the $2F_o$-F_c map (right, blue) contoured at 1.5 σ of H320F *Pf*KMO* in the presence of L-kynurenine. In the area where L-kynurenine is expected to bind, with the isoalloxazine moiety of the FAD cofactor visible to the right of this area, solvent molecules have been modelled into the active site but no area of unmodelled density that corresponds to L-kynurenine can be located in the F_o-F_c map.

5.4.4 H320F *Pf*KMO* in the absence of substrate

The structure of H320F *Pf*KMO* in the absence of ligand in the active site was obtained with a resolution of 1.81 Å in the $P2_1$ space group. The asymmetric unit contained two H320F *Pf*KMO* and 383 waters (data statistics listed in Appendix 2 Table 2.5).

The structures of H320F *Pf*KMO* in the absence of substrate contains a number of differences with both the structure of *Pf*KMO* in the absence of substrate and the structure of H320F *Pf*KMO* in the presence of L-kynurenine. Compared with the structure of *Pf*KMO* in the absence of substrate (Figure 5.11) the structures are similar with a slight difference in the position of the helices of the C-terminal domain and a movement of the loop containing residues F319 and F320.

In a comparison of the structures of H320F *Pf*KMO* crystallised in the presence and absence of substrate (Figure 5.12) there is a difference in the position of the C-terminal domain which moves away from the main domain to an *open* conformation in the active site, the residues 372 to 378 are a helix in the presence of L-kynurenine and a loop in the absence of substrate, and there is a previously unseen movement of the loop containing F320 in the two structures which is not observed in *Pf*KMO* structures with the position of this region of the structure unique to H320F *Pf*KMO*.

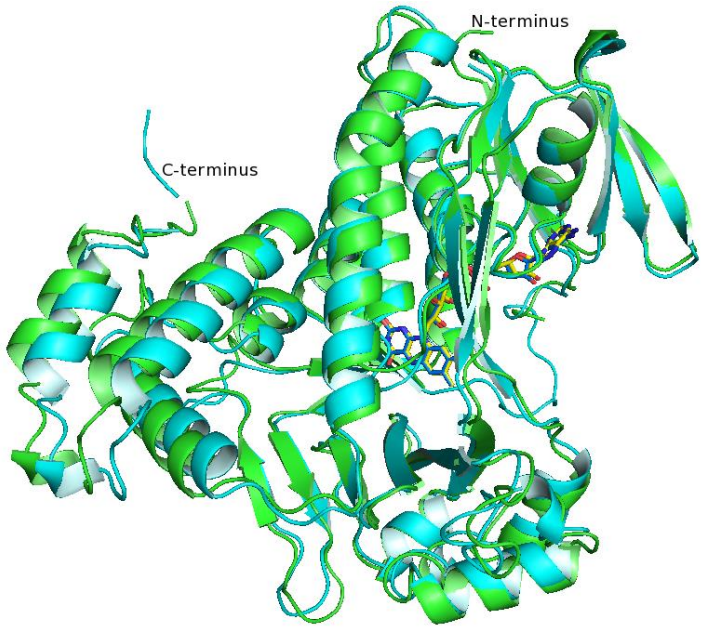

Figure 5.11: Overlay comparing the structure of H320F *Pf*KMO* in the absence of substrate (cyan with blue FAD cofactor) with that of *Pf*KMO* (green with yellow FAD cofactor).

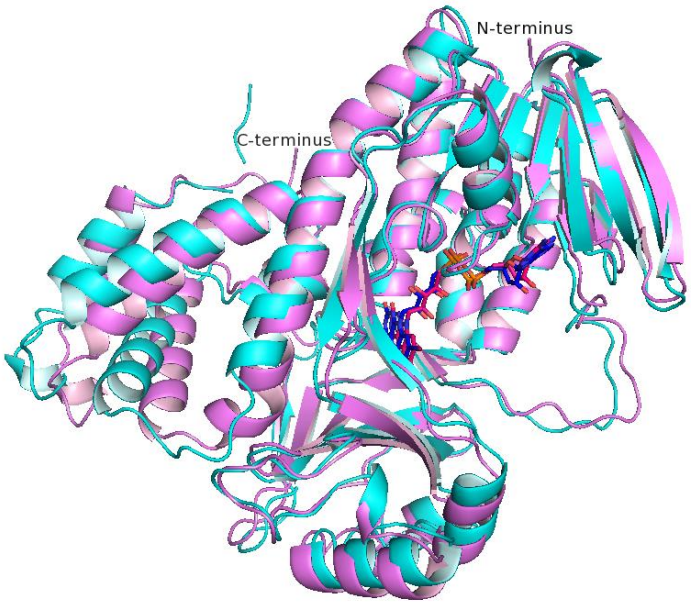

Figure 5.12: Structural changes in the event of substrate binding. H320F *Pf*KMO* in the absence of L-kynurenine (cyan) with FAD cofactor (blue) is shown overlaid with the structure of H320F *Pf*KMO* in the presence of L-kynurenine (purple) with FAD cofactor (pink).

The structure of the active site residues of H320F *Pf*KMO* in the absence of L-kynurenine contains some significant differences to that of *Pf*KMO* (Figure 5.13). As seen with the structures in the presence of substrate in Section 5.3.2 above, there is a difference in the positions of the tyrosine residues with Y404 appearing further into the active site and Y98 further away. There also appears to be a slight difference in the position of R84. The most significant change is in the region of H320. This loop in H320F *Pf*KMO* is in a different position, affecting residues F319 and F320, with the F320 sidechain in the active site in a position that it could not occupy in the presence of substrate which supports the theory that L-kynurenine is bound in the other structure although this could not confirmed.

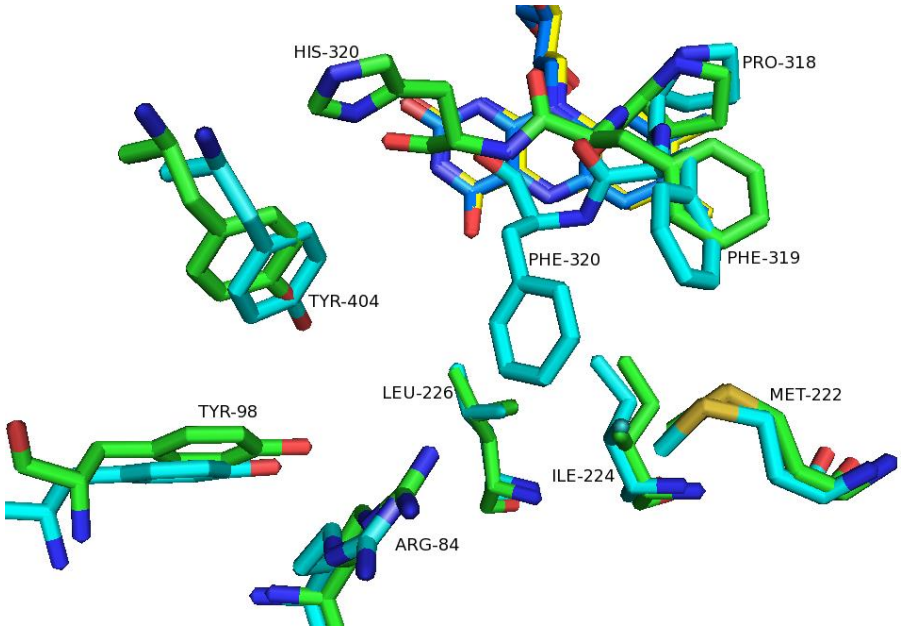

Figure 5.13: The active sites in the absence of L-kynurenine of both *Pf*KMO* (green) with FAD cofactor (yellow) and H320F *Pf*KMO* (cyan) with FAD cofactor (blue).

The structural differences between H320F *Pf*KMO* in the presence and absence of L-kynurenine suggests that the movement of this loop is a conformational change that occurs in response to substrate binding in the active site (Figure 5.14). This conformational change in the loop is not observed in any other *Pf*KMO* structure but a conformational change in this region does occur in *S. cerevisiae* KMO (Figure 1.17). Other changes that can be observed between the two structures including the movement of R84 away from the active site in the absence of substrate and a change in the position of N369 which is moved out

from the active site in the absence of L-kynurenine are differences that are all expected given the changes observed in *Pf*KMO* when substrate binds.

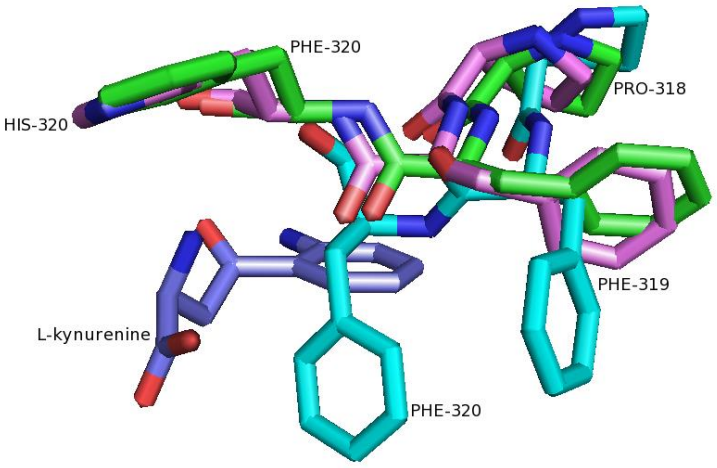

Figure 5.14: Conformational change in active site residues 318 – 320 in H320F *Pf*KMO* in the presence and absence of L-kynurenine shown through the comparison of *Pf*KMO* (purple) with L-kynurenine (purple), H320F *Pf*KMO* in the presence of L-kynurenine (green) and H320F *Pf*KMO* in the absence of L-kynurenine (cyan).

5.5 Conclusion

H320 is the only residue in the active site of *Pf*KMO* that is not conserved in the human enzyme and investigation of this residue helps to validate results gained from studying *Pf*KMO* as a source of insights into the chemistry of human KMO and development of inhibitors that could be used to inhibit human KMO.

From the structure of *Pf*KMO*, H320 is almost 4 Å from L-kynurenine and is not expected to have a significant effect on substrate binding, confirmed by the slight increase in K_M observed with H320F *Pf*KMO*. The results of the inhibition assays showed that there was a slight increase in all the K_i values and the trend in the K_i values observed for H320F *Pf*KMO* is different with GM862 being the most potent of this group of inhibitors unlike the results with *Pf*KMO* where this is the least potent of the group which is difficult to fully explain from these data alone.

The structure of H320F *Pf*KMO* crystallised in both the presence and absence of L-kynurenine has been obtained using new conditions provided by collaborators, although the electron density of the substrate is unclear. These structures revealed that when substrate binds to H320F *Pf*KMO* there is a conformational change affecting the loop around F320 resulting in F320 being in a similar position to H320 only when substrate is bound, but when substrate is absent F320 occupies space in the active site.

Chapter 6: Conclusions and Future Work

KMO is one of three enzymes that metabolises L-kynurenine as part of the kynurenine pathway of tryptophan metabolism. It is a Class A flavoprotein aromatic hydroxylase and converts L-kynurenine to 3-hydroxykynurenine in a reaction that requires NADPH, a non-covalently bound FAD cofactor and oxygen. The mechanism of KMO has been shown in previous kinetic studies to be similar to those of other related flavoproteins including PHBH.

There has been significant interest in characterising this enzyme and over the last three years the first KMO structures have been solved of the enzymes from *Pseudomonas fluorescens* and *Saccharomyces cerevisiae*. KMO inhibition has been identified as a potentially beneficial therapeutic strategy in a number of conditions including Huntington's disease, Alzheimer's disease and acute pancreatitis. In studies on animal models of Huntington's disease and Alzheimer's disease KMO inhibition has been shown to have a beneficial effect preventing further neurodegeneration.

The previously solved structures of *Pf*KMO* revealed a conformational change that occurs on the binding of substrate where the C-terminal domain is in an *open* conformation in the absence of substrate positioned further from the main domain of the protein and in a *closed* conformation in presence of substrate. The *closed* conformation requires a network of interactions between the substrate, R84, E372, Y382 and R386. In previous work E372, Y382 and R386 have been mutated and with the disruption of these interactions, substrate is still able to bind but the C-terminal domain is between the *closed* and *open* conformations.

This work also provided identification of all of the active site residues and it was possible to identify potential interactions between L-kynurenine and *Pf*KMO* that were important for substrate binding. Characterisation of the active site of *Pf*KMO* has been undertaken in this thesis with investigation of Y404, N369 and R84. The role of Y404 was investigated using the mutations Y404A, which resulted in an inactive protein, and Y404F which has a slightly raised K_M. Y404F *Pf*KMO* was crystallised without substrate in the active site revealing no major conformational change with slight changes in the position of some active site residues including F404. Y404F *Pf*KMO* was also crystallised in the $I4_122$ space group although there was not sufficient electron density to conclusively determine the position of L-kynurenine. A slight change in the orientation of F404 relative to Y404 was observed. This

supports the hypothesis that Y404 forms a hydrogen bond with the carboxylate moiety of L-kynurenine without which the affinity of *Pf*KMO* for the substrate is slightly affected but this interaction is not critical for catalysis and does not significantly affect the structure.

N369 was hypothesised to interact with the substrate and was investigated through the mutation N369S, which had only a very slight effect on the kinetic properties. N369S *Pf*KMO* was crystallised with no substrate bound in the active site and a few slight changes to the positions of S369, F319 and H320 were observed. The structure was obtained in the presence of 3,4-dichlorobenzoylalanine at a poor resolution so it was not possible to determine the position of the ligand in the active site. No major conformational changes were observed and not many of the sidechains of residues could be included in the structure. This would suggest that N369 is not is not critically important despite being in close proximity to the substrate and other active site residues.

R84 is one of the more interesting residues in the active site as not only does it interact with the substrate but it appears to be extremely important for controlling conformational change in *Pf*KMO*. R84A *Pf*KMO* was found to be inactive. No activity could be detected for R84K *Pf*KMO* although the K_M is expected to be greatly affected by this mutation so perhaps extremely high enzyme concentrations would be required to observe activity. The structure of R84K *Pf*KMO* without substrate bound was extremely similar to that of *Pf*KMO*. A potential reason for the lack of activity observed with R84K *Pf*KMO* could be that this enzyme cannot easily achieve the change from the *open* to the *closed* conformation.

This study is the first characterisation of active site residues in *Pf*KMO* and compliments the previous structural work by confirming the importance of some of these residues in substrate binding, such Y404. The evidence obtained from studying R84A and R84K *Pf*KMO* showed for the first time how important this residue for enzyme function with loss of activity observed with even a conservative mutation. From this, it is hypothesised that the ability of *Pf*KMO* to control the conformational change from *open* to *closed* upon substrate binding is critically important and depends on the interactions between R84 and both the substrate and the other residues involved in the conformational change.

There are other residues in the active site, including Y98, which may be important for substrate binding and should be investigated. The kinetic and structural data obtained in this thesis would be complimented using isothermal titration calorimetry to obtain thermodynamic data which would confirm and strengthen the hypotheses made about the role of specific active site residues in substrate binding. The new conditions used to obtain

the structure of H320F *Pf*KMO* could be used to obtain better resolution structures of mutated enzymes, particularly in the presence of L-kynurenine, and this may provide further insights into the effect of each mutation.

In the absence of structural information many of the KMO inhibitors studied previously, including m-nitrobenzoylalanine and 3,4-dichlorobenzoylalanine, were based on the structure of L-kynurenine and are also effectors. Effectors bind to KMO allowing NADPH to reduce the FAD cofactor but as these compounds are not substrates and cannot be hydroxylated, there is decay of the unstable hydroperoxyflavin with release of H_2O_2 into the surrounding environment. A more promising inhibitor Ro 61-8048 has been shown to be efficacious in animal models of disease.

In our group, we have investigated a series of novel potent inhibitors which do not act as effectors. In previous work it has been shown that parts of these compounds bind in the active site but due to their size, they do not entirely fit within it. In this thesis the final set of these compounds was assayed with *Pf*KMO* and were shown to all have K_i values in the nanomolar range. The substituents on the ring outside the active site were found to affect the potency and large substituents were well tolerated with GM855 and GM849 being the most potent of this group. The structures of *Pf*KMO* with three of these inhibitors bound were obtained using sitting drop vapour diffusion methods. GM859 was seen clearly in the structure and a potential interaction was observed between E372 and the sulfonamide moiety of the inhibitor which is the probable reason why this inhibitor is particularly potent (Figure 6.1). With the other inhibitors, GM862 and GM849, that were crystallised with *Pf*KMO* it was more difficult to find the aromatic ring furthest from the active site.

These novel compounds are the most potent inhibitors of *Pf*KMO* currently known. The potency of these compounds appears to arise from their ability to form several interactions with *Pf*KMO* and also because they prevent the enzyme from forming the *closed* conformation as they are so large they do not fit entirely within the active site. This is likely to be the reason that these are true inhibitors rather than effectors and also confirms the vital importance of conformational dynamics for *Pf*KMO* supporting both previous work with *Pf*KMO* and the characterisation of R84 in this work.

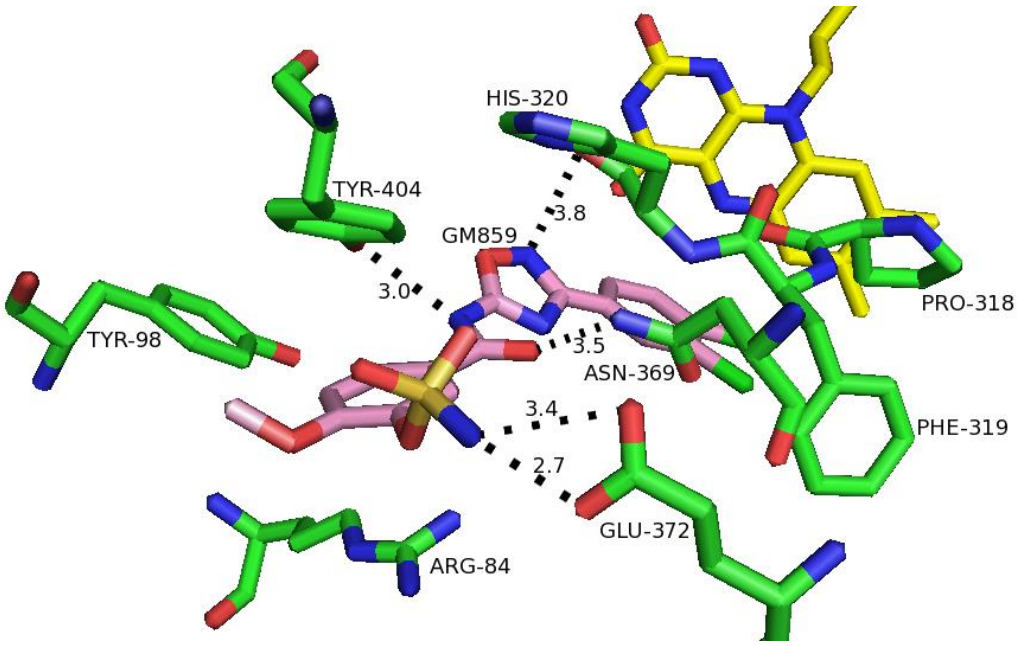

Figure 6.1: View of GM859 bound in the active site of *Pf*KMO* with the FAD cofactor shown to the back of the active site close to the 3,4-dichlorosubstituted aromatic ring. The sulfonamide interacts with Glu372 and displaces Arg84 which causes *Pf*KMO* to stay in the *open* conformation despite the presence of a ligand in the active site. Distances are indicated in Å.

These inhibitors are very promising compounds and to assess whether they may lead to the development of clinically useful compounds, they should be assayed with the human KMO enzyme.

Three of these inhibitors were assayed with H320F *Pf*KMO* where the only residue in the active site which is not conserved between these residues was mutated to the phenylalanine, which is the residue found in the human enzyme. The K_i assay results suggest that the inhibitors are not as potent with H320F *Pf*KMO* but they still inhibit the enzyme and, in the absence of substrate, no NADPH consumption was observed. This indicates that these inhibitors may perform well in assays with the human enzyme although these experiments would need to be carried out.

H320F *Pf*KMO* was found to have similar values of K_M and k_{cat} to *Pf*KMO* suggesting that this residue is not important for substrate binding. The structure of H320F *Pf*KMO* was obtained (with collaboration of other members of the Mowat research group) in the presence

and absence of L-kynurenine. The evidence of the presence of substrate in the active site was not unambiguous but a conformational change is observed from the structures of H320F *Pf*KMO* involving residues F319 and F320 probably caused by substrate binding and this may be an important feature of the human enzyme.

The characterisation of the active site of *Pf*KMO* undertaken in this thesis has contributed to the understanding of KMO. The study of residues in the active site has identified interactions important for substrate binding. Characterisation of H320F *Pf*KMO* has led to the identification of a conformational change which could occur in the human enzyme and novel potent inhibitor compounds have been assayed and shown to bind in the active site of *Pf*KMO*.

References

1 Schwarcz R, Bruno JP, Muchowski PJ, Wu HQ. Kynurenines in the mammalian brain: when physiology meets pathology. *Nat Rev Neurosci* 2012; **13**: 465-77.

2 Stone TW, Darlington LG. The kynurenine pathway as a therapeutic target in cognitive and neurodegenerative disorders. *Br J Pharmacol* 2013; **169**: 1211-27.

3 Vécsei L, Szalárdy L, Fülöp F, Toldi J. Kynurenines in the CNS: recent advances and new questions. *Nat Rev Drug Discov* 2013; **12**: 64-82.

4 Stone TW, Darlington LG. Endogenous kynurenines as targets for drug discovery and development. *Nat Rev Drug Discov* 2002; **1**: 609-20.

5 Amori L, Guidetti P, Pellicciari R, Kajii Y, Schwarcz R. On the relationship between the two branches of the kynurenine pathway in the rat brain in vivo. *J Neurochem* 2009; **109**: 316-25.

6 Vamos E, Pardutz A, Klivenyi P, Toldi J, Vecsei L. The role of kynurenines in disorders of the central nervous system: possibilities for neuroprotection. *J Neurol Sci* 2009; **283**: 21-7.

7 Chiarugi A, Calvani M, Meli E, Traggiai E, Moroni F. Synthesis and release of neurotoxic kynurenine metabolites by human monocyte-derived macrophages. *J Neuroimmunol* 2001; **120**: 190-8.

8 Lugo-Huitrón R, Blanco-Ayala T, Ugalde-Muñiz P, Carrillo-Mora P, Pedraza-Chaverrí J, Silva-Adaya D, Maldonado PD, Torres I, Pinzón E, Ortiz-Islas E, López T, García E, Pineda B, Torres-Ramos M, Santamaría A, La Cruz VP. On the antioxidant properties of kynurenic acid: free radical scavenging activity and inhibition of oxidative stress. *Neurotoxicol Teratol* 2011; **33**: 538-47.

9 Perkins MN, Stone TW. An iontophoretic investigation of the actions of convulsant kynurenines and their interaction with the endogenous excitant quinolinic acid. *Brain Res* 1982; **247**: 184-7.

10 Prescott C, Weeks AM, Staley KJ, Partin KM. Kynurenic acid has a dual action on AMPA receptor responses. *Neurosci Lett* 2006; **402**: 108-12.

11 Rózsa E, Robotka H, Vécsei L, Toldi J. The Janus-face kynurenic acid. *J Neural Transm* 2008; **115**: 1087-91.

12 Hilmas C, Pereira EF, Alkondon M, Rassoulpour A, Schwarcz R, Albuquerque EX. The brain metabolite kynurenic acid inhibits alpha7 nicotinic receptor activity and increases non-alpha7 nicotinic receptor expression: physiopathological implications. *J Neurosci* 2001; **21**: 7463-73.

13 Moroni F, Russi P, Lombardi G, Beni M, Carlà V. Presence of kynurenic acid in the mammalian brain. *J Neurochem* 1988; **51**: 177-80.

14 Stone TW, Stoy N, Darlington LG. An expanding range of targets for kynurenine metabolites of tryptophan. *Trends Pharmacol Sci* 2013; **34**: 136-43.

15 Pocivavsek A, Wu HQ, Potter MC, Elmer GI, Pellicciari R, Schwarcz R. Fluctuations in endogenous kynurenic acid control hippocampal glutamate and memory. *Neuropsychopharmacology* 2011; **36**: 2357-67.

16 Forrest CM, Mackay GM, Oxford L, Millar K, Darlington LG, Higgins MJ, Stone TW. Kynurenine metabolism predicts cognitive function in patients following cardiac bypass and thoracic surgery. *J Neurochem* 2011; **119**: 136-52.

17 Moroni F, Cozzi A, Sili M, Mannaioni G. Kynurenic acid: a metabolite with multiple actions and multiple targets in brain and periphery. *J Neural Transm* 2012; **119**: 133-9.

18 DiNatale BC, Murray IA, Schroeder JC, Flaveny CA, Lahoti TS, Laurenzana EM, Omiecinski CJ, Perdew GH. Kynurenic acid is a potent endogenous aryl

hydrocarbon receptor ligand that synergistically induces interleukin-6 in the presence of inflammatory signaling. *Toxicol Sci* 2010; **115**: 89-97.
19 Opitz CA, Litzenburger UM, Sahm F, Ott M, Tritschler I, Trump S, Schumacher T, Jestaedt L, Schrenk D, Weller M, Jugold M, Guillemin GJ, Miller CL, Lutz C, Radlwimmer B, Lehmann I, von Deimling A, Wick W, Platten M. An endogenous tumour-promoting ligand of the human aryl hydrocarbon receptor. *Nature* 2011; **478**: 197-203.
20 Prendergast GC. Cancer: Why tumours eat tryptophan. *Nature* 2011; **478**: 192-4.
21 Wang J, Simonavicius N, Wu X, Swaminath G, Reagan J, Tian H, Ling L. Kynurenic acid as a ligand for orphan G protein-coupled receptor GPR35. *J Biol Chem* 2006; **281**: 22021-8.
22 Stone TW, Perkins MN. Quinolinic acid: a potent endogenous excitant at amino acid receptors in CNS. *Eur J Pharmacol* 1981; **72**: 411-2.
23 Guillemin GJ. Quinolinic acid, the inescapable neurotoxin. *FEBS J* 2012; **279**: 1356-65.
24 Chiarugi A, Meli E, Moroni F. Similarities and differences in the neuronal death processes activated by 3OH-kynurenine and quinolinic acid. *J Neurochem* 2001; **77**: 1310-8.
25 Santamaría A, Ríos C. MK-801, an N-methyl-D-aspartate receptor antagonist, blocks quinolinic acid-induced lipid peroxidation in rat corpus striatum. *Neurosci Lett* 1993; **159**: 51-4.
26 Stípek S, Stastný F, Pláteník J, Crkovská J, Zima T. The effect of quinolinate on rat brain lipid peroxidation is dependent on iron. *Neurochem Int* 1997; **30**: 233-7.
27 Rahman A, Ting K, Cullen KM, Braidy N, Brew BJ, Guillemin GJ. The excitotoxin quinolinic acid induces tau phosphorylation in human neurons. *PLoS One* 2009; **4**: e6344.
28 Lugo-Huitrón R, Ugalde Muñiz P, Pineda B, Pedraza-Chaverrí J, Ríos C, Pérez-de la Cruz V. Quinolinic acid: an endogenous neurotoxin with multiple targets. *Oxid Med Cell Longev* 2013; **2013**: 104024.
29 Zwilling D, Huang SY, Sathyasaikumar KV, Notarangelo FM, Guidetti P, Wu HQ, Lee J, Truong J, Andrews-Zwilling Y, Hsieh EW, Louie JY, Wu T, Scearce-Levie K, Patrick C, Adame A, Giorgini F, Moussaoui S, Laue G, Rassoulpour A, Flik G, Huang Y, Muchowski JM, Masliah E, Schwarcz R, Muchowski PJ. Kynurenine 3-monooxygenase inhibition in blood ameliorates neurodegeneration. *Cell* 2011; **145**: 863-74.
30 Colín-González AL, Maldonado PD, Santamaría A. 3-Hydroxykynurenine: an intriguing molecule exerting dual actions in the central nervous system. *Neurotoxicology* 2013; **34**: 189-204.
31 Eastman CL, Guilarte TR. The role of hydrogen peroxide in the in vitro cytotoxicity of 3-hydroxykynurenine. *Neurochem Res* 1990; **15**: 1101-7.
32 Goldstein LE, Leopold MC, Huang X, Atwood CS, Saunders AJ, Hartshorn M, Lim JT, Faget KY, Muffat JA, Scarpa RC, Chylack LT, Bowden EF, Tanzi RE, Bush AI. 3-Hydroxykynurenine and 3-hydroxyanthranilic acid generate hydrogen peroxide and promote alpha-crystallin cross-linking by metal ion reduction. *Biochemistry* 2000; **39**: 7266-75.
33 Hiraku Y, Inoue S, Oikawa S, Yamamoto K, Tada S, Nishino K, Kawanishi S. Metal-mediated oxidative damage to cellular and isolated DNA by certain tryptophan metabolites. *Carcinogenesis* 1995; **16**: 349-56.
34 Korlimbinis A, Hains PG, Truscott RJ, Aquilina JA. 3-Hydroxykynurenine oxidizes alpha-crystallin: potential role in cataractogenesis. *Biochemistry* 2006; **45**: 1852-60.
35 Backhaus C, Rahman H, Scheffler S, Laatsch H, Hardeland R. NO scavenging by 3-hydroxyanthranilic acid and 3-hydroxykynurenine: N-nitrosation leads via oxadiazoles to o-quinone diazides. *Nitric Oxide* 2008; **19**: 237-44.

36 Leipnitz G, Schumacher C, Dalcin KB, Scussiato K, Solano A, Funchal C, Dutra-Filho CS, Wyse AT, Wannmacher CM, Latini A, Wajner M. In vitro evidence for an antioxidant role of 3-hydroxykynurenine and 3-hydroxyanthranilic acid in the brain. *Neurochem Int* 2007; **50**: 83-94.
37 Colín-González AL, Maya-López M, Pedraza-Chaverrí J, Ali SF, Chavarría A, Santamaría A. The Janus faces of 3-hydroxykynurenine: Dual redox modulatory activity and lack of neurotoxicity in the rat striatum. *Brain Res* 2014.
38 Giorgini F, Huang SY, Sathyasaikumar KV, Notarangelo FM, Thomas MA, Tararina M, Wu HQ, Schwarcz R, Muchowski PJ. Targeted deletion of kynurenine 3-monooxygenase in mice: a new tool for studying kynurenine pathway metabolism in periphery and brain. *J Biol Chem* 2013; **288**: 36554-66.
39 KNOX WE, MEHLER AH. The conversion of tryptophan to kynurenine in liver. I. The coupled tryptophan peroxidase-oxidase system forming formylkynurenine. *J Biol Chem* 1950; **187**: 419-30.
40 Forouhar F, Anderson JL, Mowat CG, Vorobiev SM, Hussain A, Abashidze M, Bruckmann C, Thackray SJ, Seetharaman J, Tucker T, Xiao R, Ma LC, Zhao L, Acton TB, Montelione GT, Chapman SK, Tong L. Molecular insights into substrate recognition and catalysis by tryptophan 2,3-dioxygenase. *Proc Natl Acad Sci U S A* 2007; **104**: 473-8.
41 Pilotte L, Larrieu P, Stroobant V, Colau D, Dolusic E, Frédérick R, De Plaen E, Uyttenhove C, Wouters J, Masereel B, Van den Eynde BJ. Reversal of tumoral immune resistance by inhibition of tryptophan 2,3-dioxygenase. *Proc Natl Acad Sci U S A* 2012; **109**: 2497-502.
42 Pantouris G, Mowat CG. Antitumour agents as inhibitors of tryptophan 2,3-dioxygenase. *Biochem Biophys Res Commun* 2014; **443**: 28-31.
43 Uyttenhove C, Pilotte L, Théate I, Stroobant V, Colau D, Parmentier N, Boon T, Van den Eynde BJ. Evidence for a tumoral immune resistance mechanism based on tryptophan degradation by indoleamine 2,3-dioxygenase. *Nat Med* 2003; **9**: 1269-74.
44 Muller AJ, DuHadaway JB, Donover PS, Sutanto-Ward E, Prendergast GC. Inhibition of indoleamine 2,3-dioxygenase, an immunoregulatory target of the cancer suppression gene Bin1, potentiates cancer chemotherapy. *Nat Med* 2005; **11**: 312-9.
45 Mándi Y, Vécsei L. The kynurenine system and immunoregulation. *J Neural Transm* 2012; **119**: 197-209.
46 Connor TJ, Starr N, O'Sullivan JB, Harkin A. Induction of indolamine 2,3-dioxygenase and kynurenine 3-monooxygenase in rat brain following a systemic inflammatory challenge: a role for IFN-gamma? *Neurosci Lett* 2008; **441**: 29-34.
47 Alberati-Giani D, Cesura AM. Expression of the kynurenine enzymes in macrophages and microglial cells: regulation by immune modulators. *Amino Acids* 1998; **14**: 251-5.
48 Phillips RS. Structure and mechanism of kynureninase. *Arch Biochem Biophys* 2014; **544**: 69-74.
49 Lima S, Kumar S, Gawandi V, Momany C, Phillips RS. Crystal structure of the Homo sapiens kynureninase-3-hydroxyhippuric acid inhibitor complex: insights into the molecular basis of kynureninase substrate specificity. *J Med Chem* 2009; **52**: 389-96.
50 Maitrani C, Phillips RS. Substituents effects on activity of kynureninase from Homo sapiens and Pseudomonas fluorescens. *Bioorg Med Chem* 2013; **21**: 4670-7.
51 Guidetti P, Okuno E, Schwarcz R. Characterization of rat brain kynurenine aminotransferases I and II. *J Neurosci Res* 1997; **50**: 457-65.
52 Guidetti P, Amori L, Sapko MT, Okuno E, Schwarcz R. Mitochondrial aspartate aminotransferase: a third kynurenate-producing enzyme in the mammalian brain. *J Neurochem* 2007; **102**: 103-11.

53 Yu P, Li Z, Zhang L, Tagle DA, Cai T. Characterization of kynurenine aminotransferase III, a novel member of a phylogenetically conserved KAT family. *Gene* 2006; **365**: 111-8.
54 Rossi F, Garavaglia S, Montalbano V, Walsh MA, Rizzi M. Crystal structure of human kynurenine aminotransferase II, a drug target for the treatment of schizophrenia. *J Biol Chem* 2008; **283**: 3559-66.
55 Guidetti P, Hoffman GE, Melendez-Ferro M, Albuquerque EX, Schwarcz R. Astrocytic localization of kynurenine aminotransferase II in the rat brain visualized by immunocytochemistry. *Glia* 2007; **55**: 78-92.
56 Rossi F, Han Q, Li J, Rizzi M. Crystal structure of human kynurenine aminotransferase I. *J Biol Chem* 2004; **279**: 50214-20.
57 Han Q, Robinson H, Li J. Crystal structure of human kynurenine aminotransferase II. *J Biol Chem* 2008; **283**: 3567-73.
58 Han Q, Robinson H, Cai T, Tagle DA, Li J. Biochemical and structural properties of mouse kynurenine aminotransferase III. *Mol Cell Biol* 2009; **29**: 784-93.
59 A novel gene containing a trinucleotide repeat that is expanded and unstable on Huntington's disease chromosomes. The Huntington's Disease Collaborative Research Group. *Cell* 1993; **72**: 971-83.
60 Guidetti P, Luthi-Carter RE, Augood SJ, Schwarcz R. Neostriatal and cortical quinolinate levels are increased in early grade Huntington's disease. *Neurobiol Dis* 2004; **17**: 455-61.
61 Beal MF, Matson WR, Storey E, Milbury P, Ryan EA, Ogawa T, Bird ED. Kynurenic acid concentrations are reduced in Huntington's disease cerebral cortex. *J Neurol Sci* 1992; **108**: 80-7.
62 Schwarcz R, Okuno E, White RJ, Bird ED, Whetsell WO. 3-Hydroxyanthranilate oxygenase activity is increased in the brains of Huntington disease victims. *Proc Natl Acad Sci U S A* 1988; **85**: 4079-81.
63 Sathyasaikumar KV, Stachowski EK, Amori L, Guidetti P, Muchowski PJ, Schwarcz R. Dysfunctional kynurenine pathway metabolism in the R6/2 mouse model of Huntington's disease. *J Neurochem* 2010; **113**: 1416-25.
64 Pearson SJ, Reynolds GP. Increased brain concentrations of a neurotoxin, 3-hydroxykynurenine, in Huntington's disease. *Neurosci Lett* 1992; **144**: 199-201.
65 Guidetti P, Reddy PH, Tagle DA, Schwarcz R. Early kynurenergic impairment in Huntington's disease and in a transgenic animal model. *Neurosci Lett* 2000; **283**: 233-5.
66 Heng MY, Detloff PJ, Wang PL, Tsien JZ, Albin RL. In vivo evidence for NMDA receptor-mediated excitotoxicity in a murine genetic model of Huntington disease. *J Neurosci* 2009; **29**: 3200-5.
67 Giorgini F, Guidetti P, Nguyen Q, Bennett SC, Muchowski PJ. A genomic screen in yeast implicates kynurenine 3-monooxygenase as a therapeutic target for Huntington disease. *Nat Genet* 2005; **37**: 526-31.
68 Guidetti P, Bates GP, Graham RK, Hayden MR, Leavitt BR, MacDonald ME, Slow EJ, Wheeler VC, Woodman B, Schwarcz R. Elevated brain 3-hydroxykynurenine and quinolinate levels in Huntington disease mice. *Neurobiol Dis* 2006; **23**: 190-7.
69 Campesan S, Green EW, Breda C, Sathyasaikumar KV, Muchowski PJ, Schwarcz R, Kyriacou CP, Giorgini F. The kynurenine pathway modulates neurodegeneration in a Drosophila model of Huntington's disease. *Curr Biol* 2011; **21**: 961-6.
70 Giorgini F, Möller T, Kwan W, Zwilling D, Wacker JL, Hong S, Tsai LC, Cheah CS, Schwarcz R, Guidetti P, Muchowski PJ. Histone deacetylase inhibition modulates kynurenine pathway activation in yeast, microglia, and mice expressing a mutant huntingtin fragment. *J Biol Chem* 2008; **283**: 7390-400.

71 Stone TW, Forrest CM, Stoy N, Darlington LG. Involvement of kynurenines in Huntington's disease and stroke-induced brain damage. *J Neural Transm* 2012; **119**: 261-74.
72 Tauber E, Miller-Fleming L, Mason RP, Kwan W, Clapp J, Butler NJ, Outeiro TF, Muchowski PJ, Giorgini F. Functional gene expression profiling in yeast implicates translational dysfunction in mutant huntingtin toxicity. *J Biol Chem* 2011; **286**: 410-9.
73 Schwarcz R, Guidetti P, Sathyasaikumar KV, Muchowski PJ. Of mice, rats and men: Revisiting the quinolinic acid hypothesis of Huntington's disease. *Prog Neurobiol* 2010; **90**: 230-45.
74 Reinhart PH, Kelly JW. Treating the periphery to ameliorate neurodegenerative diseases. *Cell* 2011; **145**: 813-4.
75 Guillemin GJ, Brew BJ, Noonan CE, Takikawa O, Cullen KM. Indoleamine 2,3 dioxygenase and quinolinic acid immunoreactivity in Alzheimer's disease hippocampus. *Neuropathol Appl Neurobiol* 2005; **31**: 395-404.
76 Heyes MP, Achim CL, Wiley CA, Major EO, Saito K, Markey SP. Human microglia convert l-tryptophan into the neurotoxin quinolinic acid. *Biochem J* 1996; **320 (Pt 2)**: 595-7.
77 Widner B, Leblhuber F, Walli J, Tilz GP, Demel U, Fuchs D. Tryptophan degradation and immune activation in Alzheimer's disease. *J Neural Transm* 2000; **107**: 343-53.
78 Majláth Z, Toldi J, Vécsei L. The potential role of kynurenines in Alzheimer's disease: pathomechanism and therapeutic possibilities by influencing the glutamate receptors. *J Neural Transm* 2014; **121**: 881-9.
79 Fillit H, Ding WH, Buee L, Kalman J, Altstiel L, Lawlor B, Wolf-Klein G. Elevated circulating tumor necrosis factor levels in Alzheimer's disease. *Neurosci Lett* 1991; **129**: 318-20.
80 Yamamoto M, Kiyota T, Horiba M, Buescher JL, Walsh SM, Gendelman HE, Ikezu T. Interferon-gamma and tumor necrosis factor-alpha regulate amyloid-beta plaque deposition and beta-secretase expression in Swedish mutant APP transgenic mice. *Am J Pathol* 2007; **170**: 680-92.
81 Misztal M, Skangiel-Kramska J, Niewiadomska G, Danysz W. Subchronic intraventricular infusion of quinolinic acid produces working memory impairment--a model of progressive excitotoxicity. *Neuropharmacology* 1996; **35**: 449-58.
82 Saito K, Nowak TS, Markey SP, Heyes MP. Mechanism of delayed increases in kynurenine pathway metabolism in damaged brain regions following transient cerebral ischemia. *J Neurochem* 1993; **60**: 180-92.
83 Cozzi A, Carpenedo R, Moroni F. Kynurenine hydroxylase inhibitors reduce ischemic brain damage: studies with (m-nitrobenzoyl)-alanine (mNBA) and 3,4-dimethoxy-[-N-4-(nitrophenyl)thiazol-2yl]-benzenesulfonamide (Ro 61-8048) in models of focal or global brain ischemia. *J Cereb Blood Flow Metab* 1999; **19**: 771-7.
84 Carpenedo R, Meli E, Peruginelli F, Pellegrini-Giampietro DE, Moroni F. Kynurenine 3-mono-oxygenase inhibitors attenuate post-ischemic neuronal death in organotypic hippocampal slice cultures. *J Neurochem* 2002; **82**: 1465-71.
85 Darlington LG, Mackay GM, Forrest CM, Stoy N, George C, Stone TW. Altered kynurenine metabolism correlates with infarct volume in stroke. *Eur J Neurosci* 2007; **26**: 2211-21.
86 Lavebratt C, Olsson S, Backlund L, Frisén L, Sellgren C, Priebe L, Nikamo P, Träskman-Bendz L, Cichon S, Vawter MP, Osby U, Engberg G, Landén M, Erhardt S, Schalling M. The KMO allele encoding Arg452 is associated with psychotic features in bipolar disorder type 1, and with increased CSF KYNA level and reduced KMO expression. *Mol Psychiatry* 2014; **19**: 334-41.

87 Wonodi I, Stine OC, Sathyasaikumar KV, Roberts RC, Mitchell BD, Hong LE, Kajii Y, Thaker GK, Schwarcz R. Downregulated kynurenine 3-monooxygenase gene expression and enzyme activity in schizophrenia and genetic association with schizophrenia endophenotypes. *Arch Gen Psychiatry* 2011; **68**: 665-74.
88 Holtze M, Saetre P, Engberg G, Schwieler L, Werge T, Andreassen OA, Hall H, Terenius L, Agartz I, Jönsson EG, Schalling M, Erhardt S. Kynurenine 3-monooxygenase polymorphisms: relevance for kynurenic acid synthesis in patients with schizophrenia and healthy controls. *J Psychiatry Neurosci* 2012; **37**: 53-7.
89 Mole DJ, McFerran NV, Collett G, O'Neill C, Diamond T, Garden OJ, Kylanpaa L, Repo H, Deitch EA. Tryptophan catabolites in mesenteric lymph may contribute to pancreatitis-associated organ failure. *Br J Surg* 2008; **95**: 855-67.
90 Steinberg W, Tenner S. Acute pancreatitis. *N Engl J Med* 1994; **330**: 1198-210.
91 Johnson CD, Abu-Hilal M. Persistent organ failure during the first week as a marker of fatal outcome in acute pancreatitis. *Gut* 2004; **53**: 1340-4.
92 Pawlak D, Tankiewicz A, Mysliwiec P, Buczko W. Tryptophan metabolism via the kynurenine pathway in experimental chronic renal failure. *Nephron* 2002; **90**: 328-35.
93 Pawlak K, Domaniewski T, Mysliwiec M, Pawlak D. Kynurenines and oxidative status are independently associated with thrombomodulin and von Willebrand factor levels in patients with end-stage renal disease. *Thromb Res* 2009; **124**: 452-7.
94 Justinova Z, Mascia P, Wu HQ, Secci ME, Redhi GH, Panlilio LV, Scherma M, Barnes C, Parashos A, Zara T, Fratta W, Solinas M, Pistis M, Bergman J, Kangas BD, Ferré S, Tanda G, Schwarcz R, Goldberg SR. Reducing cannabinoid abuse and preventing relapse by enhancing endogenous brain levels of kynurenic acid. *Nat Neurosci* 2013; **16**: 1652-61.
95 Richter A, Hamann M. The kynurenine 3-hydroxylase inhibitor Ro 61-8048 improves dystonia in a genetic model of paroxysmal dyskinesia. *Eur J Pharmacol* 2003; **478**: 47-52.
96 Crozier KR, Moran GR. Heterologous expression and purification of kynurenine-3-monooxygenase from Pseudomonas fluorescens strain 17400. *Protein Expr Purif* 2007; **51**: 324-33.
97 van Berkel WJ, Kamerbeek NM, Fraaije MW. Flavoprotein monooxygenases, a diverse class of oxidative biocatalysts. *J Biotechnol* 2006; **124**: 670-89.
98 Huijbers MM, Montersino S, Westphal AH, Tischler D, van Berkel WJ. Flavin dependent monooxygenases. *Arch Biochem Biophys* 2014; **544**: 2-17.
99 Chaiyen P, Fraaije MW, Mattevi A. The enigmatic reaction of flavins with oxygen. *Trends Biochem Sci* 2012; **37**: 373-80.
100 Eppink MH, Schreuder HA, Van Berkel WJ. Identification of a novel conserved sequence motif in flavoprotein hydroxylases with a putative dual function in FAD/NAD(P)H binding. *Protein Sci* 1997; **6**: 2454-8.
101 Montersino S, Tischler D, Gassner GT, van Berkel WJH. Catalytic and Structural Features of Flavoprotein Hydroxylases and Epoxidases. *Advanced Synthesis & Catalysis* 2011; **353**: 2301-19.
102 Palfey BA, Basu R, Frederick KK, Entsch B, Ballou DP. Role of protein flexibility in the catalytic cycle of p-hydroxybenzoate hydroxylase elucidated by the Pro293Ser mutant. *Biochemistry* 2002; **41**: 8438-46.
103 Schreuder HA, Prick PA, Wierenga RK, Vriend G, Wilson KS, Hol WG, Drenth J. Crystal structure of the p-hydroxybenzoate hydroxylase-substrate complex refined at 1.9 A resolution. Analysis of the enzyme-substrate and enzyme-product complexes. *J Mol Biol* 1989; **208**: 679-96.
104 Gatti DL, Palfey BA, Lah MS, Entsch B, Massey V, Ballou DP, Ludwig ML. The mobile flavin of 4-OH benzoate hydroxylase. *Science* 1994; **266**: 110-4.

105 Ortiz-Maldonado M, Entsch B, Ballou DP. Oxygen reactions in p-hydroxybenzoate hydroxylase utilize the H-bond network during catalysis. *Biochemistry* 2004; **43**: 15246-57.
106 Moran GR, Entsch B, Palfey BA, Ballou DP. Mechanistic insights into p-hydroxybenzoate hydroxylase from studies of the mutant Ser212Ala. *Biochemistry* 1999; **38**: 6292-9.
107 van Berkel W, Westphal A, Eschrich K, Eppink M, de Kok A. Substitution of Arg214 at the substrate-binding site of p-hydroxybenzoate hydroxylase from Pseudomonas fluorescens. *Eur J Biochem* 1992; **210**: 411-9.
108 Entsch B, Cole LJ, Ballou DP. Protein dynamics and electrostatics in the function of p-hydroxybenzoate hydroxylase. *Arch Biochem Biophys* 2005; **433**: 297-311.
109 Wang J, Ortiz-Maldonado M, Entsch B, Massey V, Ballou D, Gatti DL. Protein and ligand dynamics in 4-hydroxybenzoate hydroxylase. *Proc Natl Acad Sci U S A* 2002; **99**: 608-13.
110 Cole LJ, Gatti DL, Entsch B, Ballou DP. Removal of a methyl group causes global changes in p-hydroxybenzoate hydroxylase. *Biochemistry* 2005; **44**: 8047-58.
111 Cole LJ, Entsch B, Ortiz-Maldonado M, Ballou DP. Properties of p-hydroxybenzoate hydroxylase when stabilized in its open conformation. *Biochemistry* 2005; **44**: 14807-17.
112 Ballou DP, Entsch B, Cole LJ. Dynamics involved in catalysis by single-component and two-component flavin-dependent aromatic hydroxylases. *Biochem Biophys Res Commun* 2005; **338**: 590-8.
113 Moran GR, Entsch B, Palfey BA, Ballou DP. Evidence for flavin movement in the function of p-hydroxybenzoate hydroxylase from studies of the mutant Arg220Lys. *Biochemistry* 1996; **35**: 9278-85.
114 Frederick KK, Palfey BA. Kinetics of proton-linked flavin conformational changes in p-hydroxybenzoate hydroxylase. *Biochemistry* 2005; **44**: 13304-14.
115 Lah MS, Palfey BA, Schreuder HA, Ludwig ML. Crystal structures of mutant Pseudomonas aeruginosa p-hydroxybenzoate hydroxylases: the Tyr201Phe, Tyr385Phe, and Asn300Asp variants. *Biochemistry* 1994; **33**: 1555-64.
116 Frederick KK, Ballou DP, Palfey BA. Protein dynamics control proton transfers to the substrate on the His72Asn mutant of p-hydroxybenzoate hydroxylase. *Biochemistry* 2001; **40**: 3891-9.
117 Palfey BA, Moran GR, Entsch B, Ballou DP, Massey V. Substrate recognition by "password" in p-hydroxybenzoate hydroxylase. *Biochemistry* 1999; **38**: 1153-8.
118 Gatti DL, Entsch B, Ballou DP, Ludwig ML. pH-dependent structural changes in the active site of p-hydroxybenzoate hydroxylase point to the importance of proton and water movements during catalysis. *Biochemistry* 1996; **35**: 567-78.
119 Ortiz-Maldonado M, Cole LJ, Dumas SM, Entsch B, Ballou DP. Increased positive electrostatic potential in p-hydroxybenzoate hydroxylase accelerates hydroxylation but slows turnover. *Biochemistry* 2004; **43**: 1569-79.
120 Moran GR, Entsch B, Palfey BA, Ballou DP. Electrostatic effects on substrate activation in para-hydroxybenzoate hydroxylase: studies of the mutant lysine 297 methionine. *Biochemistry* 1997; **36**: 7548-56.
121 Neujahr HY, Gaal A. Phenol hydroxylase from yeast. Purification and properties of the enzyme from Trichosporon cutaneum. *Eur J Biochem* 1973; **35**: 386-400.
122 Xu D, Ballou DP, Massey V. Studies of the mechanism of phenol hydroxylase: mutants Tyr289Phe, Asp54Asn, and Arg281Met. *Biochemistry* 2001; **40**: 12369-78.
123 Enroth C. High-resolution structure of phenol hydroxylase and correction of sequence errors. *Acta Crystallogr D Biol Crystallogr* 2003; **59**: 1597-602.
124 Enroth C, Neujahr H, Schneider G, Lindqvist Y. The crystal structure of phenol hydroxylase in complex with FAD and phenol provides evidence for a concerted

conformational change in the enzyme and its cofactor during catalysis. *Structure* 1998; **6**: 605-17.

125 Chaiyen P, Ballou DP, Massey V. Gene cloning, sequence analysis, and expression of 2-methyl-3-hydroxypyridine-5-carboxylic acid oxygenase. *Proc Natl Acad Sci U S A* 1997; **94**: 7233-8.

126 Chaiyen P, Brissette P, Ballou DP, Massey V. Reaction of 2-methyl-3-hydroxypyridine-5-carboxylic acid (MHPC) oxygenase with N-methyl-5-hydroxynicotinic acid: studies on the mode of binding, and protonation status of the substrate. *Biochemistry* 1997; **36**: 13856-64.

127 McCulloch KM, Mukherjee T, Begley TP, Ealick SE. Structure of the PLP degradative enzyme 2-methyl-3-hydroxypyridine-5-carboxylic acid oxygenase from Mesorhizobium loti MAFF303099 and its mechanistic implications. *Biochemistry* 2009; **48**: 4139-49.

128 Chaiyen P, Sucharitakul J, Svasti J, Entsch B, Massey V, Ballou DP. Use of 8-substituted-FAD analogues to investigate the hydroxylation mechanism of the flavoprotein 2-methyl-3-hydroxypyridine-5-carboxylic acid oxygenase. *Biochemistry* 2004; **43**: 3933-43.

129 Tian B, Strid Å, Eriksson LA. Catalytic roles of active-site residues in 2-methyl-3-hydroxypyridine-5-carboxylic acid oxygenase: an ONIOM/DFT study. *J Phys Chem B* 2011; **115**: 1918-26.

130 Chaiyen P, Brissette P, Ballou DP, Massey V. Unusual mechanism of oxygen atom transfer and product rearrangement in the catalytic reaction of 2-methyl-3-hydroxypyridine-5-carboxylic acid oxygenase. *Biochemistry* 1997; **36**: 8060-70.

131 Lindqvist Y, Koskiniemi H, Jansson A, Sandalova T, Schnell R, Liu Z, Mäntsälä P, Niemi J, Schneider G. Structural basis for substrate recognition and specificity in aklavinone-11-hydroxylase from rhodomycin biosynthesis. *J Mol Biol* 2009; **393**: 966-77.

132 Ryan KS, Howard-Jones AR, Hamill MJ, Elliott SJ, Walsh CT, Drennan CL. Crystallographic trapping in the rebeccamycin biosynthetic enzyme RebC. *Proc Natl Acad Sci U S A* 2007; **104**: 15311-6.

133 Howard-Jones AR, Walsh CT. Staurosporine and rebeccamycin aglycones are assembled by the oxidative action of StaP, StaC, and RebC on chromopyrrolic acid. *J Am Chem Soc* 2006; **128**: 12289-98.

134 Greenhagen BT, Shi K, Robinson H, Gamage S, Bera AK, Ladner JE, Parsons JF. Crystal structure of the pyocyanin biosynthetic protein PhzS. *Biochemistry* 2008; **47**: 5281-9.

135 Hiromoto T, Fujiwara S, Hosokawa K, Yamaguchi H. Crystal structure of 3-hydroxybenzoate hydroxylase from Comamonas testosteroni has a large tunnel for substrate and oxygen access to the active site. *J Mol Biol* 2006; **364**: 878-96.

136 Montersino S, Orru R, Barendregt A, Westphal AH, van Duijn E, Mattevi A, van Berkel WJ. Crystal structure of 3-hydroxybenzoate 6-hydroxylase uncovers lipid-assisted flavoprotein strategy for regioselective aromatic hydroxylation. *J Biol Chem* 2013; **288**: 26235-45.

137 Crozier-Reabe KR, Phillips RS, Moran GR. Kynurenine 3-monooxygenase from Pseudomonas fluorescens: substrate-like inhibitors both stimulate flavin reduction and stabilize the flavin-peroxo intermediate yet result in the production of hydrogen peroxide. *Biochemistry* 2008; **47**: 12420-33.

138 Alberati-Giani D, Cesura AM, Broger C, Warren WD, Röver S, Malherbe P. Cloning and functional expression of human kynurenine 3-monooxygenase. *FEBS Lett* 1997; **410**: 407-12.

139 Breton J, Avanzi N, Magagnin S, Covini N, Magistrelli G, Cozzi L, Isacchi A. Functional characterization and mechanism of action of recombinant human kynurenine 3-hydroxylase. *Eur J Biochem* 2000; **267**: 1092-9.

140 Hirai K, Kuroyanagi H, Tatebayashi Y, Hayashi Y, Hirabayashi-Takahashi K, Saito K, Haga S, Uemura T, Izumi S. Dual role of the carboxyl-terminal region of pig liver L-kynurenine 3-monooxygenase: mitochondrial-targeting signal and enzymatic activity. *J Biochem* 2010; **148**: 639-50.
141 Wilson K, Mole DJ, Binnie M, Homer NZ, Zheng X, Yard BA, Iredale JP, Auer M, Webster SP. Bacterial expression of human kynurenine 3-monooxygenase: solubility, activity, purification. *Protein Expr Purif* 2014; **95**: 96-103.
142 Amaral M, Levy C, Heyes DJ, Lafite P, Outeiro TF, Giorgini F, Leys D, Scrutton NS. Structural basis of kynurenine 3-monooxygenase inhibition. *Nature* 2013; **496**: 382-5.
143 Wilkinson M. Structural Dynamics and Ligand Binding in Kynurenine-3-Monooxygenase. In: *Chemistry*), Vol. Doctor of Philosophy: University of Edinburgh, 2013.
144 Matthews BW. Solvent content of protein crystals. *J Mol Biol* 1968; **33**: 491-7.
145 Lowe DM, Gee M, Haslam C, Leavens B, Christodoulou E, Hissey P, Hardwicke P, Argyrou A, Webster SP, Mole DJ, Wilson K, Binnie M, Yard BA, Dean T, Liddle J, Uings I, Hutchinson JP. Lead discovery for human kynurenine 3-monooxygenase by high-throughput RapidFire mass spectrometry. *J Biomol Screen* 2014; **19**: 508-15.
146 Winkler D, Beconi M, Toledo-Sherman LM, Prime M, Ebneth A, Dominguez C, Muñoz-Sanjuan I. Development of LC/MS/MS, high-throughput enzymatic and cellular assays for the characterization of compounds that inhibit kynurenine monooxygenase (KMO). *J Biomol Screen* 2013; **18**: 879-89.
147 Moroni F, Russi P, Gallo-Mezo MA, Moneti G, Pellicciari R. Modulation of quinolinic and kynurenic acid content in the rat brain: effects of endotoxins and nicotinylalanine. *J Neurochem* 1991; **57**: 1630-5.
148 Pellicciari R, Natalini B, Costantino G, Mahmoud MR, Mattoli L, Sadeghpour BM, Moroni F, Chiarugi A, Carpenedo R. Modulation of the kynurenine pathway in search for new neuroprotective agents. Synthesis and preliminary evaluation of (m-nitrobenzoyl)alanine, a potent inhibitor of kynurenine-3-hydroxylase. *J Med Chem* 1994; **37**: 647-55.
149 Carpenedo R, Chiarugi A, Russi P, Lombardi G, Carlà V, Pellicciari R, Mattoli L, Moroni F. Inhibitors of kynurenine hydroxylase and kynureninase increase cerebral formation of kynurenate and have sedative and anticonvulsant activities. *Neuroscience* 1994; **61**: 237-43.
150 Russi P, Alesiani M, Lombardi G, Davolio P, Pellicciari R, Moroni F. Nicotinylalanine increases the formation of kynurenic acid in the brain and antagonizes convulsions. *J Neurochem* 1992; **59**: 2076-80.
151 Natalini B, Mattoli L, Pellicciari R, Carpenedo R, Chiarugi A, Moroni F. Synthesis and activity of enantiopure (S) (m-nitrobenzoyl) alanine, potent kynurenine-3-hydroxylase inhibitor. *Bioorganic & Medicinal Chemistry Letters* 1995; **5**: 1451-4.
152 Speciale C, Wu HQ, Cini M, Marconi M, Varasi M, Schwarcz R. (R,S)-3,4-dichlorobenzoylalanine (FCE 28833A) causes a large and persistent increase in brain kynurenic acid levels in rats. *Eur J Pharmacol* 1996; **315**: 263-7.
153 Giordani A, Pevarello P, Cini M, Bormetti R, Greco F, Toma S, Speciale C, Varasi M. 4-Phenyl-4-oxo-butanoic acid derivatives inhibitors of kynurenine 3-hydroxylase. *Bioorg Med Chem Lett* 1998; **8**: 2907-12.
154 Drysdale MJ, Hind SL, Jansen M, Reinhard JF. Synthesis and SAR of 4-aryl-2-hydroxy-4-oxobut-2-enoic acids and esters and 2-amino-4-aryl-4-oxobut-2-enoic acids and esters: potent inhibitors of kynurenine-3-hydroxylase as potential neuroprotective agents. *J Med Chem* 2000; **43**: 123-7.
155 Röver S, Cesura AM, Huguenin P, Kettler R, Szente A. Synthesis and biochemical evaluation of N-(4-phenylthiazol-2-yl)benzenesulfonamides as high-affinity inhibitors of kynurenine 3-hydroxylase. *J Med Chem* 1997; **40**: 4378-85.

156 Feng Y, Bowden BF, Kapoor V. Ianthellamide A, a selective kynurenine-3-hydroxylase inhibitor from the Australian marine sponge Ianthella quadrangulata. *Bioorg Med Chem Lett* 2012; **22**: 3398-401.
157 L M, ML M. Die Kinetik der Invertinwirkung. *Biochemische Zeitschrift* 1913; **49**.
158 DIXON M. The determination of enzyme inhibitor constants. *Biochem J* 1953; **55**: 170-1.
159 Cornish-Bowden A. A simple graphical method for determining the inhibition constants of mixed, uncompetitive and non-competitive inhibitors. *Biochem J* 1974; **137**: 143-4.
160 Kakkar T, Boxenbaum H, Mayersohn M. Estimation of Ki in a competitive enzyme-inhibition model: comparisons among three methods of data analysis. *Drug Metab Dispos* 1999; **27**: 756-62.
161 Chayen NE. Methods for separating nucleation and growth in protein crystallisation. *Prog Biophys Mol Biol* 2005; **88**: 329-37.
162 Rhodes G. *Crystallography Made Crystal Clear: a guide for users of macromolecular models*, Third edn.: Academic Press, Elsevier, 2006.
163 Vagin A, Teplyakov A. MOLREP: an Automated Program for Molecular Replacement. In: *Journal of Applied Crystallography*), Vol. 30, 1997: 1022-5.
164 Sarkar G, Sommer SS. The "megaprimer" method of site-directed mutagenesis. *Biotechniques* 1990; **8**: 404-7.
165 Liu H, Naismith JH. An efficient one-step site-directed deletion, insertion, single and multiple-site plasmid mutagenesis protocol. *BMC Biotechnol* 2008; **8**: 91.
166 Leslie AG, Powell HR. Processing diffraction data with mosflm. In: *Evolving methods in macromolecular crystallography* (Read RJ, Sussman JL, eds): Springer Netherlands, 2007: 41-51.
167 Collaborative Computational Project Nm. The CCP4 suite: programs for protein crystallography. *Acta Crystallogr D Biol Crystallogr* 1994; **50**: 760-3.
168 Evans P. Scaling and assessment of data quality. *Acta Crystallogr D Biol Crystallogr* 2006; **62**: 72-82.
169 Evans PR. An introduction to data reduction: space-group determination, scaling and intensity statistics. *Acta Crystallogr D Biol Crystallogr* 2011; **67**: 282-92.
170 Emsley P, Lohkamp B, Scott WG, Cowtan K. Features and development of Coot. *Acta Crystallogr D Biol Crystallogr* 2010; **66**: 486-501.
171 Murshudov GN, Skubák P, Lebedev AA, Pannu NS, Steiner RA, Nicholls RA, Winn MD, Long F, Vagin AA. REFMAC5 for the refinement of macromolecular crystal structures. *Acta Crystallogr D Biol Crystallogr* 2011; **67**: 355-67.
172 Schüttelkopf AW, van Aalten DM. PRODRG: a tool for high-throughput crystallography of protein-ligand complexes. *Acta Crystallogr D Biol Crystallogr* 2004; **60**: 1355-63.
173 Debreczeni J, Emsley P. Handling ligands with Coot. *Acta Crystallogr D Biol Crystallogr* 2012; **68**: 425-30.
174 DeLano WL. The PyMOL Molecular Graphics System. In), 1.5 edn.: Schrödinger LLC.
175 Leatherbarrow RJ. *GraFit* Version 3.0. In). Staines, U.K.: Erithacus Software Ltd., 1992.
176 Kjeldsen AE. Screening and characterisation of KMO inhibitors. In: *Chemistry*), Vol. M(Chem) Chemistry with Industrial Experience: University of Edinburgh, 2013.
177 Lipinski CA, Lombardo F, Dominy BW, Feeney PJ. Experimental and computational approaches to estimate solubility and permeability in drug discovery and development settings. *Adv Drug Deliv Rev* 2001; **46**: 3-26.

178 Krissinel E, Henrick K. Secondary-structure matching (SSM), a new tool for fast protein structure alignment in three dimensions. *Acta Crystallogr D Biol Crystallogr* 2004; **60**: 2256-68.
179 Hasegawa H, Holm L. Advances and pitfalls of protein structural alignment. *Curr Opin Struct Biol* 2009; **19**: 341-8.

Appendix 1: Sequencing Data

The success of making a mutation in the *Pf*KMO gene was confirmed by submitting samples for Sanger sequencing as described in Section 2.1.8. The results are listed below for each sample with Sample 1 being the sample containing the T7 Promotor primer and Sample 2 containing the T7 Terminator primer presented as the reverse complement.

Y404A

Sample 1:

cgaggggtggcccgcaacggctggcaggtcaacctgttcgagcgacgccccgacccgcgcatcgaaa
ccggcgcccgggggcgctccatcaacctggcgctggccgaacgaggcgcccatgccttgcgtttggcc
gggctagagcgcgaagtactggcagaagcggtgatgatgcgcgggcgcatggtgcatgtgcccggcac
gccccccaacctgcagccatacgggcgtgatgacagcgaggtgatctggtcgatcaatcgggatcgct
tgaaccgcattttgctcgacggcgccgaagcggccggcgcgagtatccacttcaacctggggctcgac
agcgtggactttgcgcgccaacgcctgaccctcagcaacgtgtcgggggagcgcctggagaaacgctt
ccatctgctgatcggcgccgatggctgcaactcggcggtgcgccaggccatggccagcgtcgtcgacc
tgggcgagcacctggaaaccccagcccccatggctaccaggaaactgcagatcactcccgaggcccaa
cgcgcaattcaaccctggagcccaacgccctgcatatctgggccccatgggcgactaccatggtgcat
tccccctggcccaccctgggaccgcagcttcacggt

Sample 2:

ggcggaacctggaaccgcagcttcacggtaacgttgttctgcatcaccagagccgggcggcacaaacc
cgccagccccgtctttggcgcaactggtggatgggcatgcccgcgcgaaggtttttttccagcgccagt
tccccgacctgtcaccgatgctcgacagcctggagcaagacttcgagcaccaccccaccggcaagctc
gcaaccctgcgcctgaccacctggcatgtcggcggccaggccgtgctgctgggcgatgcggcccatcc
catggtgccgttccatggccagggcatgaactgtgcactggaagacgccgtagccctcgccgaacacc
tgcaatcggccgccgacaacgccagcgcactcgcggcgttcaccgcccagcgccaacccgatgcgttg
gcgatccaggccatggccctggaaaactacgtggagatgagcagtaaagtggccagccccacctactt
gctggagcgcgaactgggccaaatcatggcccagcgccaaccgacgcgttttatcccgcgtgccagca

tggtcaccttcagccgcctgccctacgcccaggcaatggctcgcgggcagatccaggagcaactgctg
aaattcgcagtggccaaccacagtcacctt

Y404F

Sample 1:

aataattttgtttactttaagaaggagatatacatatgactgctacagacaacgctcgtcaagtcacc
attatcggcgcagggctcgccggaaccctggtcgcgcgcctgctggcccgcaacggctggcaggtcaa
cctgttcgagcgacgccccgacccgcgcatcgaaaccggcgcccgggggcgctccatcaacctggcgc
tggccgaacgaggcgcccatgccttgcgtttggccgggctagagcgcgaagtactggcagaagcggtg
atgatgcgcgggcgcatggtgcatgtgcccggcacgccccccaacctgcagccatacgggcgtgatga
cagcgaggtgatctggtcgatcaatcgggatcgcttgaaccgcattttgctcgacggcgccgaagcgg
ccggcgcgagtatccacttcaacctggggctcgacagcgtggactttgcgcgccaacgcctgaccctc
agcaacgtgtcgggggagcgcctggagaaacgcttccatctgctgatcggcgccgatggctgcaactc
ggcggtgcgccaggccatggccagcgtcgtcgacctgggcgagcacctggaaacccagccccatggct
acaaggaactgcagatcactcccgaggccagcgcgcaattcaacctggagcccaacgccctgcatatc
tggccccatggcgactacatgtgcatcgccctgccgaacctggaccgcagcttcacggtgacgttgtt
cctgcatcaccagagcccggcggcacaacccgccagcccgtcttttgcgcaactggtggatgggcatg
ccgcgcgaaggtttttccagcgccagttccccgacctgtcaccgatgctcgacagcctggagcaagac
ttcgagcaccacccccaccggcaagctcgcaaccctgcgcctgaccacctgggcatgtcggcggccag
gccgtgctgctgggcgatgcggcccatcccatggtgccgttccatggccagggcatgaactgtgcact
ggaggacgtccgtagccctcggcgaacacctgcattcgccgccgaaaacgccagcgcactcgcggcgt
tcaccgcccacgccacccgatgcgttgggcaatccaggccatggccctggaaactaccgtggaatgag
accataagtgcagcccactctcttggttggaagcgccactggtgctcaaatcatgtgctcgacgc

Sample 2:

catggtactggtgccggcacgtccccccaactgcagccaacagggcgatagaaagcgaagtaatctg
gtccgatcaatcgggatcgcttgaaccgcaattggctggaacggcgcccgaagcggccggccgcgagt
attccacttcaacctggggctcgacaggcggtggactttgccggccaacgctgaccctcagcaacgtg
ttcggggaagcgcctggaggaacgctcccatctgctgatcggcgccgatggctgcaactcggcggtgc
gccaggccatgcccagcgtcgtcgacctgggcgagcacctggaaacccagccccatggctacaaggaa
ctgcagatcactcccgaggccagcgcgcaattcaacctggagcccaacgccctgcatatctggcccca
tggcgactacatgtgcatcgccctgccgaacctggaccgcagcttcacggtgacgttgttcctgcatc

accagagcccggcggcacaacccgccagcccgtcttttgcgcaactggtggatgggcatgccgcgcga
aggtttttccagcgccagttccccgacctgtcaccgatgctcgacagcctggagcaagacttcgagca
ccaccccaccggcaagctcgcaaccctgcgcctgaccacctggcatgtcggcggccaggccgtgctgc
tgggcgatgcggcccatcccatggtgccgttccatggccagggcatgaactgtgcactggaagacgcc
gtagccctcgccgaacacctgcaatcggccgccgacaacgccagcgcactcgcggcgttcaccgccca
gcgccaacccgatgcgttggcgatccaggccatggccctggaaaactacgtggagatgagcagtaaag
tggccagccccacctacttgctggagcgcgaactgggccaaatcatggcccagcgccaaccgacgcgt
tttatcccgcgtttcagcatggtcaccttcagccgcctgccctacgcccaggcaatggctcgcgggca
gatccaggagcaactgctgaaattcgcagtggccaatcacagcgacctgacctcgatcaacctcgacg
ccgtggagcacgaagtgacccgctgcctgccacccttgagccacctgagctgactcgagcagatccgg
ctgctaacaaagcccgaa

N369S

Sample 1:

ccattatcggcgcagggctcgccggaaccctggtcgcgcgcctgctggcccgcaacggctggcaggtc
aacctgttcgagcgacgccccgacccgcgcatcgaaaccggcgcccgggggcgctccatcaacctggc
gctggccgaacgaggcgcccatgccttgcgtttggccgggctagagcgcgaagtactggcagaagcgg
tgatgatgcgcgggcgcatggtgcatgtgcccggcacgccccccaacctgcagccatacgggcgtgat
gacagcgaggtgatctggtcgatcaatcgggatcgcttgaaccgcattttgctcgacggcgccgaagc
ggccggcgcgagtatccacttcaacctggggctcgacagcgtggactttgcgcgccaacgcctgaccc
tcagcaacgtgtcgggggagcgcctggagaaacgcttccatctgctgatcggcgccgatggctgcaac
tcggcggtgcgccaggccatggccagcgtcgtcgacctgggcgagcacctggaaacccagccccatgg
ctacaaggaactgcagatcactcccgaggccagcgcgcaattcaa

Sample 2:

tggttgagaccgcgtttttgtctgaacgggccgaagcggccggcgcggagttaccacttcaacctggg
ggctgacagcgtggactttgcgcgccaacgcttgacccttcagcaacgtggtcgggggggagggcctgg
agaacgcttccattctgctgatcggcgccgaaggactgcaactgggcggtgcgccaagccatggccag
cgtcgtcgacctgggcgagcacctggaaacccagccccatggctacaaggaactgcagatcactcccg
aggccagcgcgcaattcaaccttggagcccaacgccctgcatatctggccccatggcgactacatgtg
catcgccctgccgaacctggaccgcagcttcacggtgacgttgttcatgcatcaccagagcccggcgg
cacaacccgccagcccgtctttttgcgcaactggtggatgggcatgccgcgcgaaggtttttccagcg

ccagttccccgacctgtcaccgatgctcgacagcctggagcaagacttcgagcaccaccccaccggca
agctcgcaaccctgcgcctgaccacctggcatgtcggcggccaggccgtgctgctgggcgatgcggcc
catcccatggtgccgttccatggccagggcatgaactgtgcactggaagacgccgtagccctcgccga
acacctgcaatcggccgccgacaacgccagcgcactcgcggcgttcaccgcccagcgccaacccgatg
cgttggcgatccaggccatggccctggaaagctacgtggagatgagcagtaaagtggccagccccacc
tacttgctggagcgcgaactgggccaaatcatggcccagcgccaaccgacgcgttttatcccgcgtta
cagcatggtcaccttcagccgcctgccctacgcccaggcaatggctcgcgggcagatccaggagcaac
tgctgaaattcgcagtggccaaccacagcgacctgacctcgatcaacctcgacgccgtggagcacgaa
gt

R84A

Sample 1:

ttttgtttactttaagaaggagatatacatatgactgctacagacaacgctcgtaagtcaccattatc
ggcgcagggctcgccggaaccctggtcgcgcgcctgctggcccgcaacggctggcaggtcaacctgtt
cgagcgacgccccgacccgcgcatcgaaaccggcgcccgggggcgctccatcaacctggcgctggccg
aacgaggcgcccatgccttgcgtttggccgggctagagcgcgaagtactggcagaagcggtgatgatg
cgtggggccatggtgcatgtgcccggcacgccccccaacctgcagccatacgggcgtgatgacagcga
ggtgatctggtcgatcaatcgggatcgcttgaaccgcattttgctcgacggcgccgaagcggccggcg
cgagtatccacttcaacctggggctcgacagcgtggactttgcgcgccaacgcctgaccctcagcaac
gtgtcgggggagcgcctggagaaacgcttccatctgctgatcggcgccgatggctgcaactcggcggt
gcgccaggccatggccagcgtcgtcgacctgggcgagcacctggaaacccagccccatggctacaagg
aactgcagatcactcccgaggccagcgcgcaattcaacctggagcccaacgccctgcatatctggccc
catggcgactacatgtgcatcgccctgccgaacctggaccgcagcttcacggtgacgttgttcctgca
tcaccagagcccggcggcacaacccgccagcccgtcttttgcgcaactggtggatgggcatgccgcgc
gaaggtttttcccagcgccagtttcccgacctgtcaccgatgctcgacagcctggagcaagacttcga
gcaccaccccaccggcaagctcgcaaccctgcgcctgaccacctggcatgtcggcggccaggccgtgc
tgctggcgatgcggcccatcccatggtggccgttccatggcccagggcatgaactgtgcacctgaaga
ccgtcgtagcccttcgtcgaacactgcaattcgggcgccgacaacgcccaggcgcactcgtggcgttc
accgcccaaggcgcccatccgatggcgttggcgaatcggccaaggccttggaaacctaacgtgggaga
tgagcaggtactgtgtcagccccccctactgtctggaagccgaactgtcccaatctcacattggccga
gcgcgacaagcgagacgagcgtactc

R84K

Sample 1:

tcagcggaatttcctctagaataattttgtttactttaagaaggagatatacatatgactgctacaga
caacgctcgtcaagtcaccattatcggcgcagggctcgccggaaccctggtcgcgcgcctgctggccc
gcaacggctggcaggtcaacctgttcgagcgacgccccgacccgcgcatcgaaaccggcgcccggggg
cgctccatcaacctggcgctggccgaacgaggcgcccatgccttgcgtttggccgggctagagcgcga
agtactggcagaagcggtgatgatgcgtgggaaaatggtgcatgtgcccggcacgccccccaacctgc
agccatacgggcgtgatgacagcgaggtgatctggtcgatcaatcgggatcgcttgaaccgcattttg
ctcgacggcgccgaagcggccggcgcgagtatccacttcaacctggggctcgacagcgtggactttgc
gcgccaacgcctgaccctcagcaacgtgtcgggggagcgcctggagaaacgcttccatctgctgatcg
gcgccgatggctgcaactcggcggtgcgccaggccatggccagcgtcgtcgacctgggcgagcacctg
gaaacccagccccatggctacaaggaactgcagatcactcccgaggccagcgcgcaattcaacctgga
gcccaacgccctgcatatctggccccatggcgactacatgtgcatcaccctgccgaacctggaccgca
gcttcacggtgac

Sample 2:

gacggcatcgcatgcgcgccggcgacgagtatgcaacttcaccttggggctcggacaggctgtgaact
ttggcgccgcaacgcctgaccctcaggaacgtgttcgggggaggcgcctggagaaacgcttccatctg
ctgatcggcgccgatggctgcaactcggcggtgcgccaggcccatgcccagcgtcgtcgacctgggcg
agcacctggaaacccagccccatggctacaaggaactgcagatcactcccgaggccagcgcgcaattc
aacctggagcccaacgccctgcatatctggccccatggcgactacatgtgcatcgccctgccgaacct
ggaccgcagcttcacggtgacgttgttcctgcatcaccagagcccggcggcacaacccgccagcccgt
cttttgcgcaactggtggatgggcatgccgcgcgaaggtttttccagcgccagttccccgacctgtca
ccgatgctcgacagcctggagcaagacttcgagcaccaccccaccggcaagctcgcaaccctgcgcct
gaccacctggcatgtcggcggccaggccgtgctgctgggcgatgcggcccatcccatggtgccgttcc
atggccagggcatgaactgtgcactggaagacgccgtagccctcgccgaacacctgcaatcggccgcc
gacaacgccagcgcactcgcggcgttcaccgcccagcgccaacccgatgcgttggcgatccaggccat
ggccctggaaaactacgtggagatgagcagtaaagtggccagccccacctacttgctggagcgcgaac
tgggccaaatcatggcccagcgccaaccgacgcgttttatcccgcgttacagcatggtcaccttcagc
cgcctgccctacgcccaggcaatggctcgcgggcagatccaggagcaactgctgaaattcgcagtggc
caaccacagcgacctgacctcgatcaacctcgacgccgtggagcacgaagtgacccgctgcctgccac
ccttgagccacctgagctgactcgagcagatccggctgctaacaaagcccgaaagaa

H320F

Sample 1 (low quality):

ccccttgaaattcctctaaaaataattttgtttactttaagaaggagatatacatatgactgctacag
acaacgctagttaagtgaccattatcggcgcagggctcgccggatccctggctgcgcgcctgctggcc
cgcaacggctggcaggtcaacctgttcgagcgacgccccgacccgcgcatccaaaccggcgcccgggg
gcgctccatcaacctggcgctggccgaacgaggcgcccatgccttgcgtttggccgggctagagcgcg
aagtactggcagaagcggtgatgatgcgcgggcgcttggtgcatgtgtccggcacgccccccaacctg
aaaccttacgggcgtgatgacagcgaggtgatatggtcaatcaatccggatcgcttgaacc

Sample 2:

tgcatatttgggccccatggcgactaccatgtgcatcgccctgccgaacctggaccgcagcttcacgg
tgacgttgtcctgcatcaccagagcccggcggcacaacccgccagcccgtttttgcgcaatggtgga
tgggcaggccgcgcgaaggtttttccagcgccagttccccgacctgtcaccgatgctcgacagcctg
gagcaagacttcgagcaccactccaccggcaagctcgcaaccctgcgcctgaccacctggcatgtcgg
cggccaggccgtgctgctgggcgatgcggcccatcccatggtacccttctttggccaaggcatgaact
gtgcactggaagacgccgtagccctcgcagaacacctgcaatcggccgccgacaacgccagcgcactc
gcggcgttcaccgcccagcgccaacccgatgcgttggcgatccaggccatggccctggaaaactacgt
ggagatgagcagtaaagtggccagccccacctacttgctggagcgcgaactgggccaaatcatggccc
agcgccaaccgacgcgttttatcccgcgttacagcatggtcaccttcagccgcctgccttacgcccag
gcaatggctcgcgggcagatccaggagcaactgctgaaattcgcagtggccaaccacagcgacccg

Appendix 2: Crystallography Data

*Pf*KMO* with inhibitors bound

Inhibitor bound	GM862	GM849	GM859
Space group	$P6_122$	$P6_122$	$P6_122$
Cell dimensions a = b, c (Å) α = β, γ (º)	 117.0, 418.1 90, 120	 116.7, 419.2 90, 120	 117.0, 419.2 90, 120
Resolution (Å)	34.84 – 1.98 (2.09 – 1.98)	64.54 – 3.26 (3.44 – 3.26)	36.92 – 2.6 (2.74 – 2.6)
R_{merge}	0.213 (0.606)	0.195 (0.421)	0.224 (0.543)
Mean I/σ(I)	10.8 (4.2)	11.7 (6.8)	10.1 (4.4)
Completeness (%)	99.9 (99.8)	100.0 (100.0)	100.0 (100.0)
Multiplicity	11.6 (11.9)	11.1 (9.7)	11.8 (11.7)
R_{free}	0.2183	0.1904	0.2025
R_{factor}	0.2561	0.2858	0.2628
Number of reflections	178080	39009	76545
rmsd bond lengths (Å)	0.0193	0.0134	0.0133
rmsd bond angles (º)	1.9220	1.6869	1.7143
Ramachandran outliers (%)	0.38		1.58

Table A2.1: Data collection and refinement statistics for inhibitor bound *Pf*KMO* crystals. The values in brackets are for the higher resolution shell.

Y404F *Pf*KMO*

	Substrate free	L-kynurenine bound
Space group	$P2_122_1$	$I4_122$
Cell dimensions a, b, c (Å) α = β = γ (º)	 103.6, 133.8, 190.6 190	 149.5, 149.5, 271.3 90
Resolution (Å)	43.43 – 2.7 (2.85 – 2.7)	57.07 – 3.95 (4.16 – 3.95)
R_{merge}	0.077 (0.288)	0.109 (0.992)
Mean I/σ(I)	9.9 (3.3)	13.6 (2.4)
Completeness (%)	98.2 (98.5)	100.0 (100.0)
Multiplicity	3.6 (3.7)	11.8 (12.7)
R_{free}	0.2154	0.2602
R_{factor}	0.2853	0.2914
Number of reflections	96915	17436
rmsd bond lengths (Å)	0.0131	0.0100
rmsd bond angles (º)	1.7101	1.4646
Ramachandran outliers (%)	2.97	10.49

Table A2.2: Data collection and refinement statistics for Y404F *Pf*KMO* crystals. The values in brackets are for the higher resolution shell.

N369S *Pf*KMO*

	Substrate free	3,4-dichlorobenzoylalanine bound
Space group	$P2_122_1$	$I4_122$
Cell dimensions a, b, c (Å) α = β = γ (º)	 104.8, 134.00, 188.3 90	 150.08, 150.08, 274.05 90
Resolution (Å)	43.44 - 2.38 (2.51- 2.38)	57.54 - 3.98 (4.20 - 3.98)
R_{merge}	0.065 (0.582)	0.076 (0.395)
Mean I/σ(I)	13.0 (2.3)	15.2 (5.3)
Completeness (%)	99.5 (99.6)	100.0 (100.0)
Multiplicity	4.2 (4.2)	10.1 (10.5)
R_{factor}	0.2290	0.2610
R_{free}	0.2752	0.3362
Number of reflections	143640	17436
rmsd bond lengths (Å)	0.0146	0.0116
rmsd bond angles (º)	1.6771	1.7603
Ramachandran outliers (%)	2.59	18.04

Table A2.3: Data collection and refinement statistics for N369S *Pf*KMO* crystals. The values in brackets are for the higher resolution shell.

R84K *Pf*KMO*

	Substrate free
Space group	$P2_122_1$
Cell dimensions a, b, c (Å) α = β = γ (º)	 105.53, 133.74, 187.60 90
Resolution (Å)	35.35 – 2.45 (2.58 – 2.45)
R_{merge}	0.053 (0.358)
Mean I/σ(I)	15.0 (3.5)
Completeness (%)	99.2 (99.4)
Multiplicity	4.2 (4.3)
R_{free}	0.2225
R_{factor}	0.2794
Number of reflections	130438
rmsd bond lengths (Å)	0.0137
rmsd bond angles (º)	1.6899
Ramachandran outliers (%)	2.83

Table A2.4: Data collection and refinement statistics for the R84K *Pf*KMO* crystal. The values in brackets are for the higher resolution shell.

H320F *Pf*KMO*

	Substrate free	With L-kynurenine
Space group	$P2_1$	$P2_1$
Cell dimensions a, b, c (Å) α, β, γ (º)	 68.26, 45.99, 74.99 90, 104, 90	 69.50, 51.89, 136.48 90, 104.11, 90
Resolution (Å)	33.11 – 1.81 (1.91 – 1.81)	34.75 – 1.90 (2.01 – 1.90)
R_{merge}	0.038 (0.089)	0.039 (0.078)
Mean I/σ(I)	17.8 (8.8)	17.5 (9.1)
Completeness (%)	98.4 (95.1)	99.2 (96.9)
Multiplicity	2.7 (2.5)	2.9 (2.6)
R_{free}	0.1548	0.1752
R_{factor}	0.2007	0.2260
Number of reflections	58094	104428
rmsd bond lengths (Å)	0.0183	0.0182
rmsd bond angles (º)	1.8853	2.1067
Ramachandran outliers (%)	0.67	1.55

Table A2.5: Data collection and refinement statistics for the H320F *Pf*KMO* crystal. The values in brackets are for the higher resolution shell.

Appendix 3: Inhibition Data

*Pf*KMO* inhibited by GM843

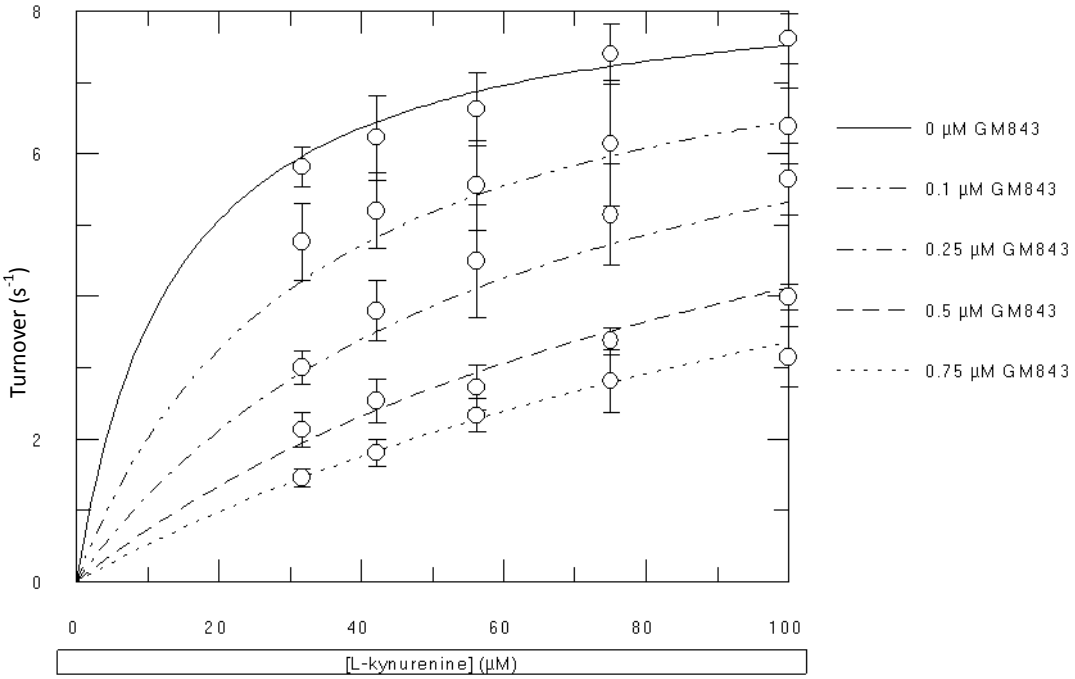

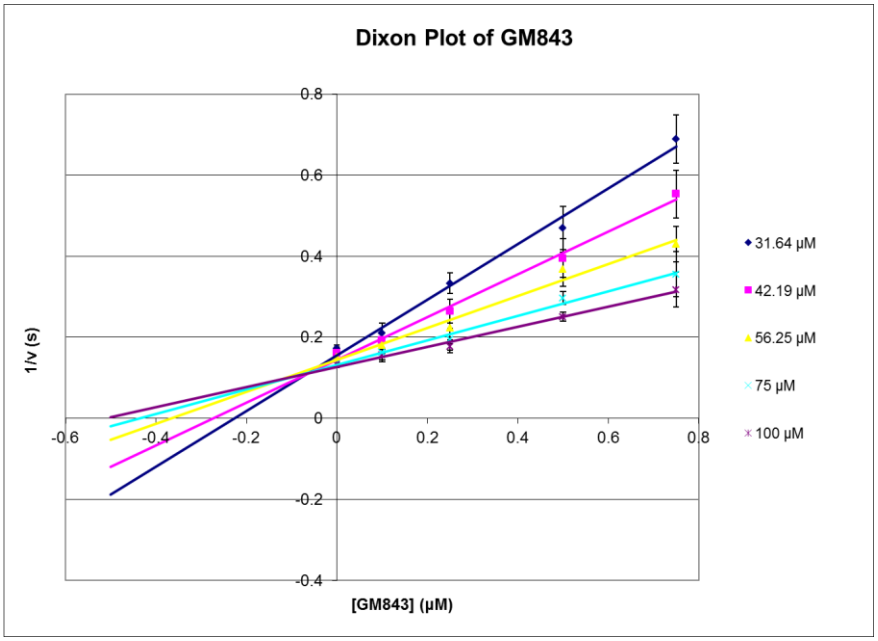

*Pf*KMO* inhibited by GM849

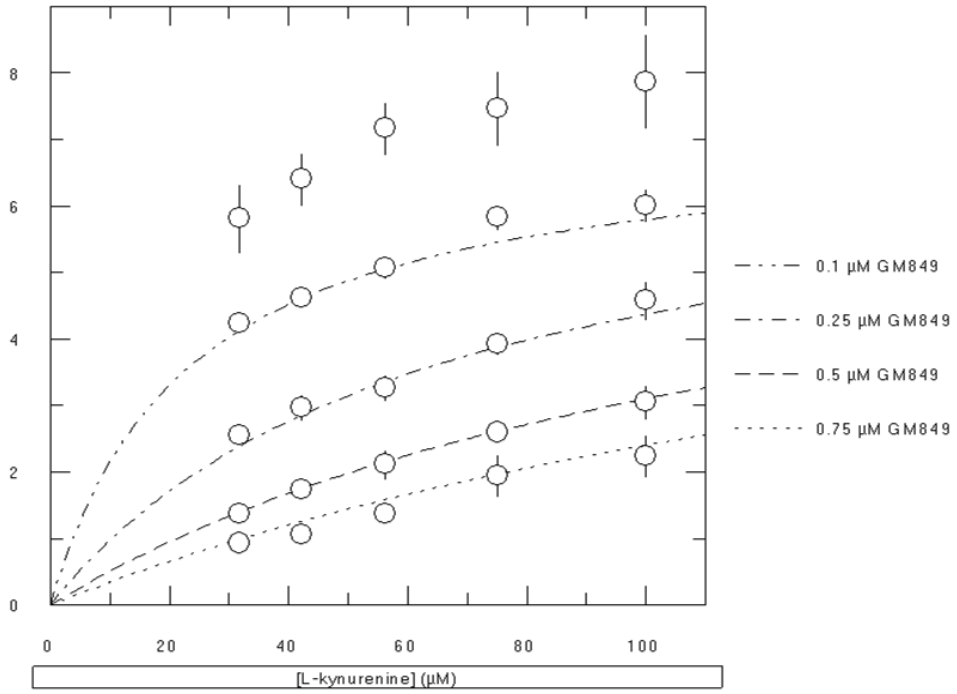

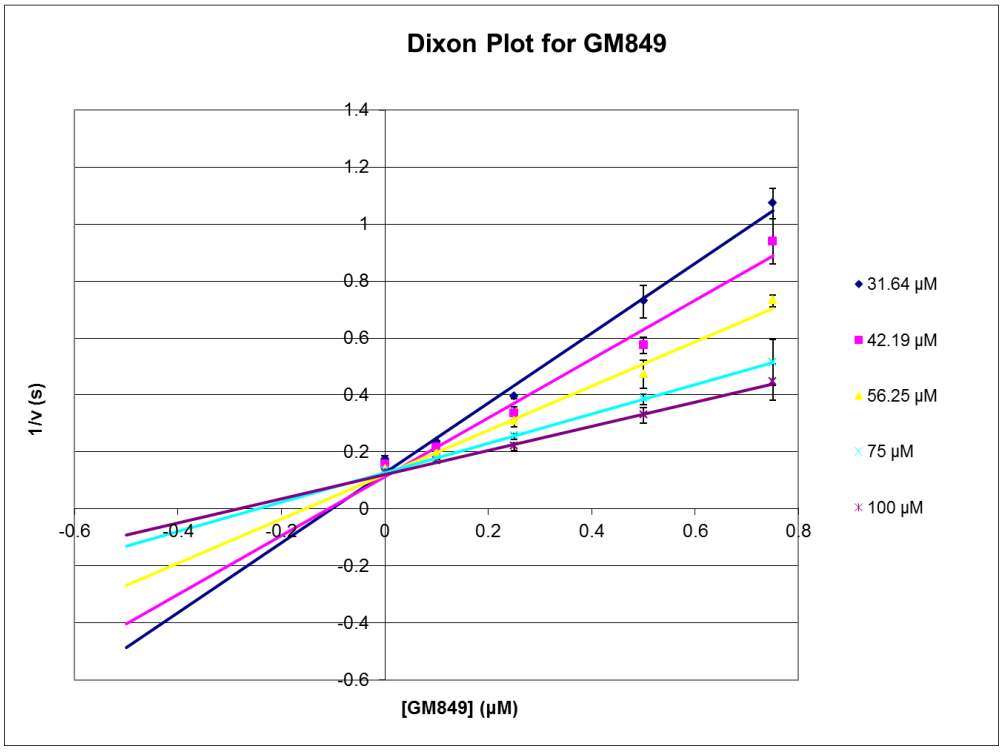

*Pf*KMO* inhibited by GM855

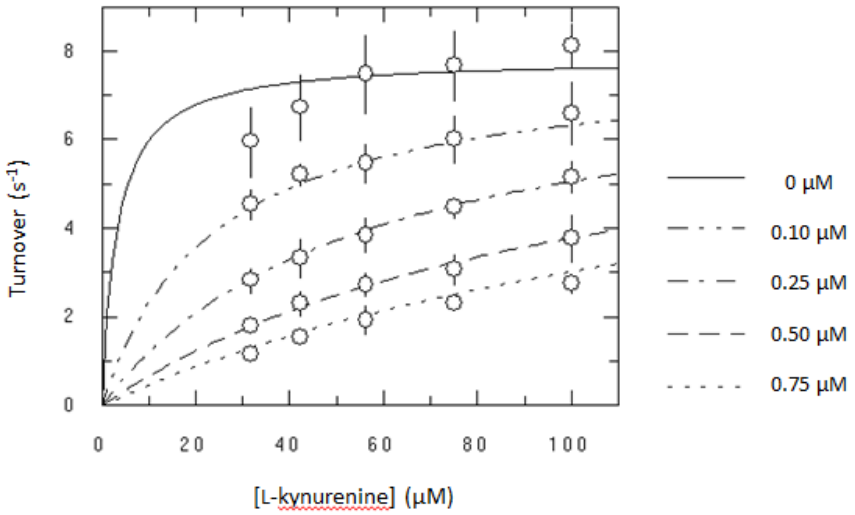

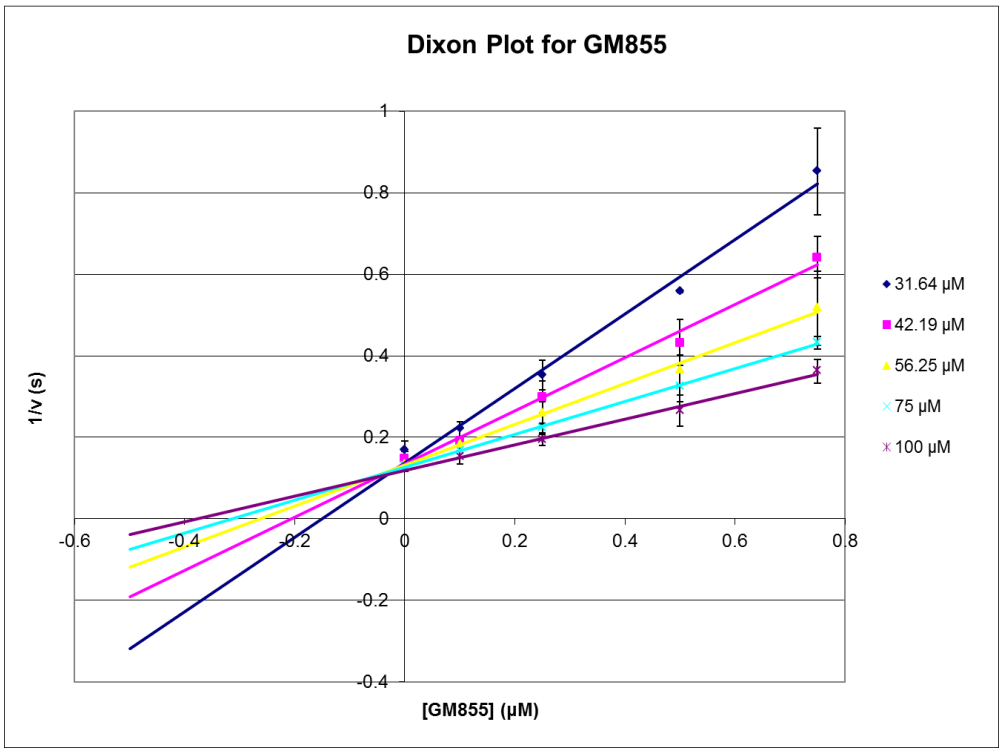

*Pf*KMO* inhibited by GM859

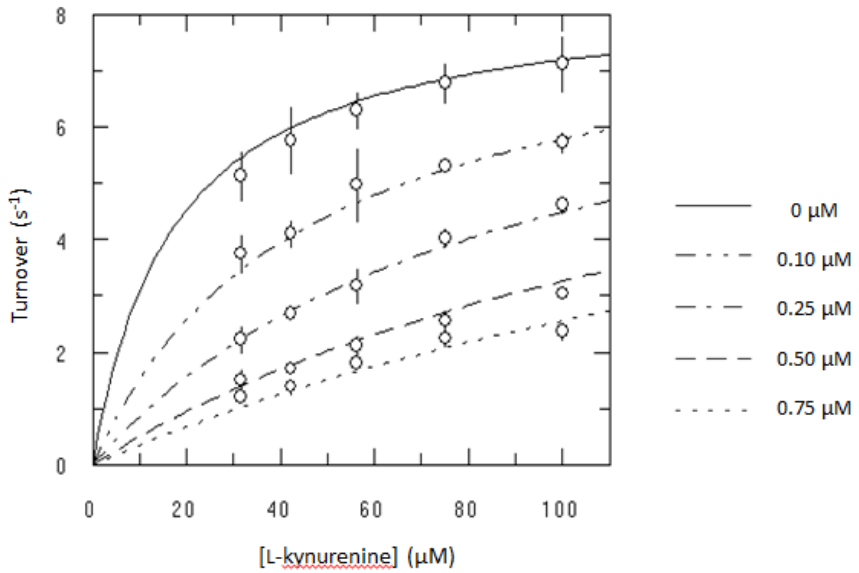

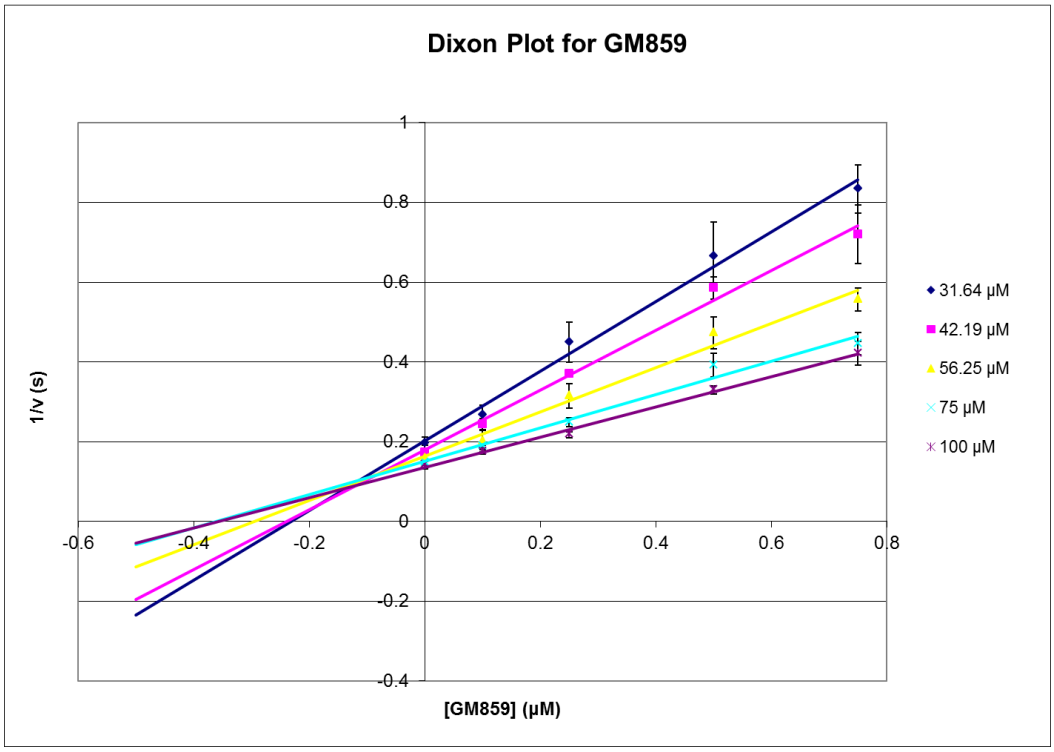

*Pf*KMO* inhibited by GM862

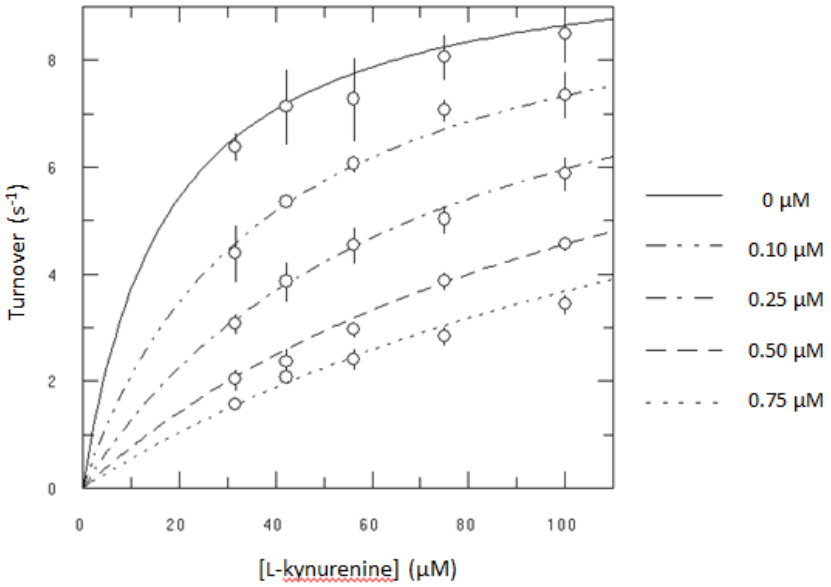

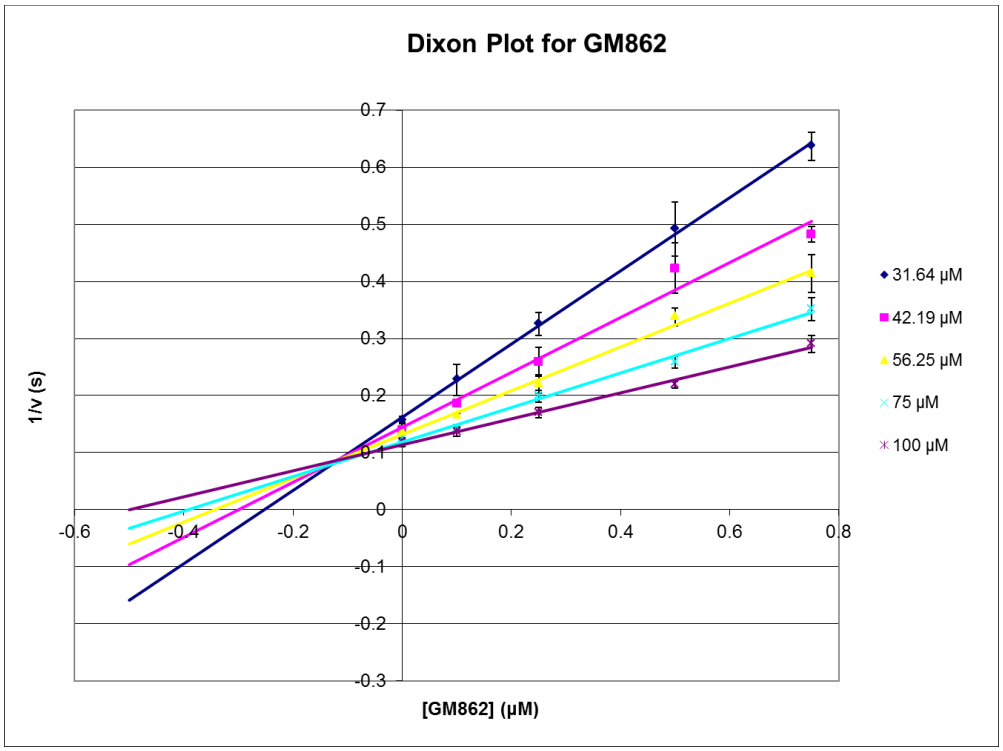

H320F *Pf*KMO* inhibited by GM843

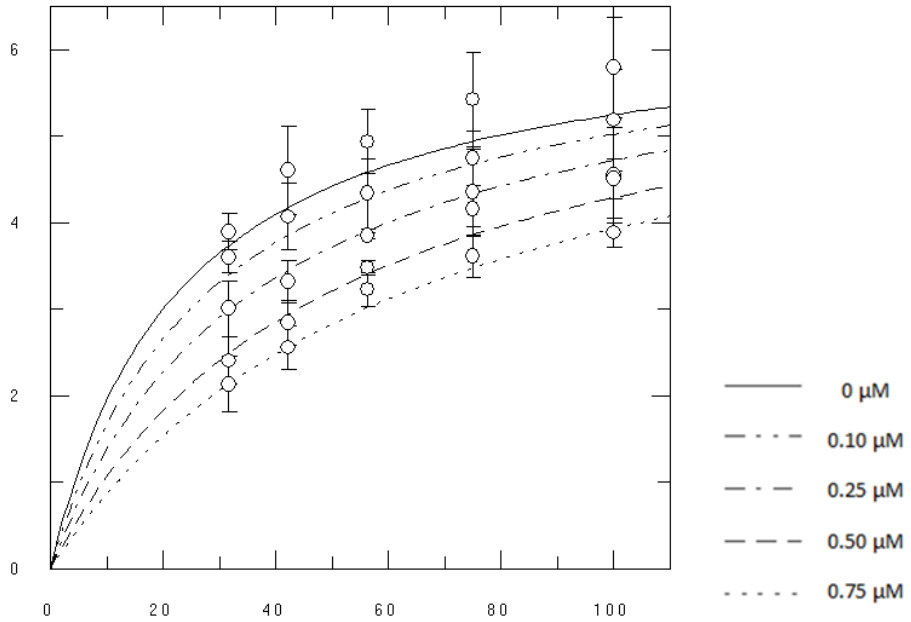

[L-kynurenine (µM)]

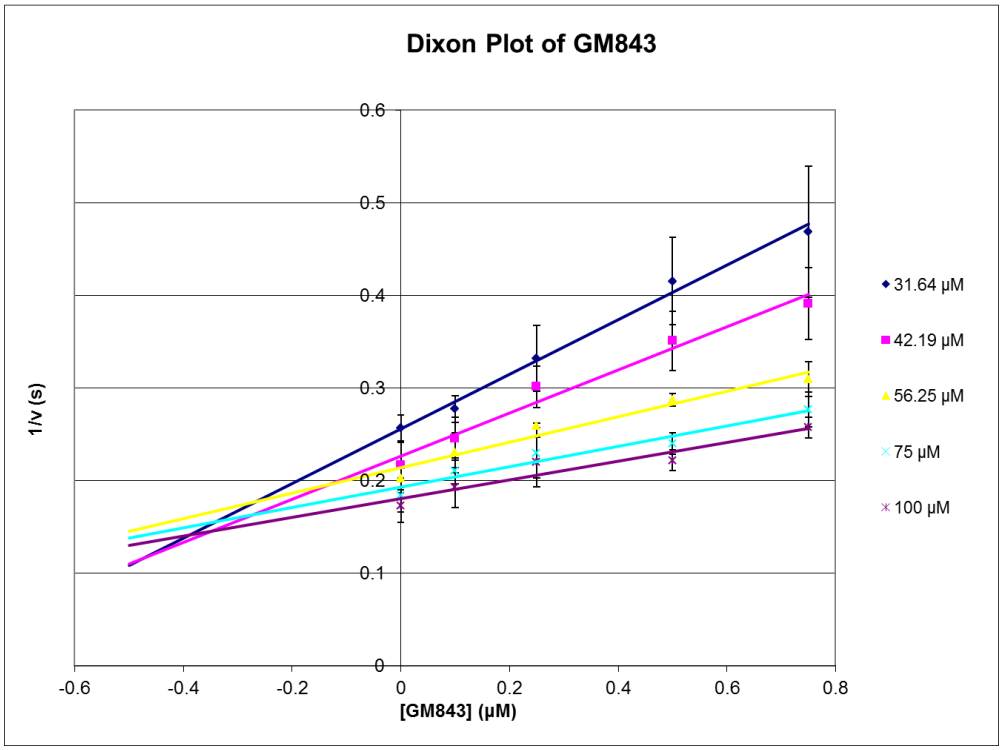

H320F *Pf*KMO* inhibited by GM855

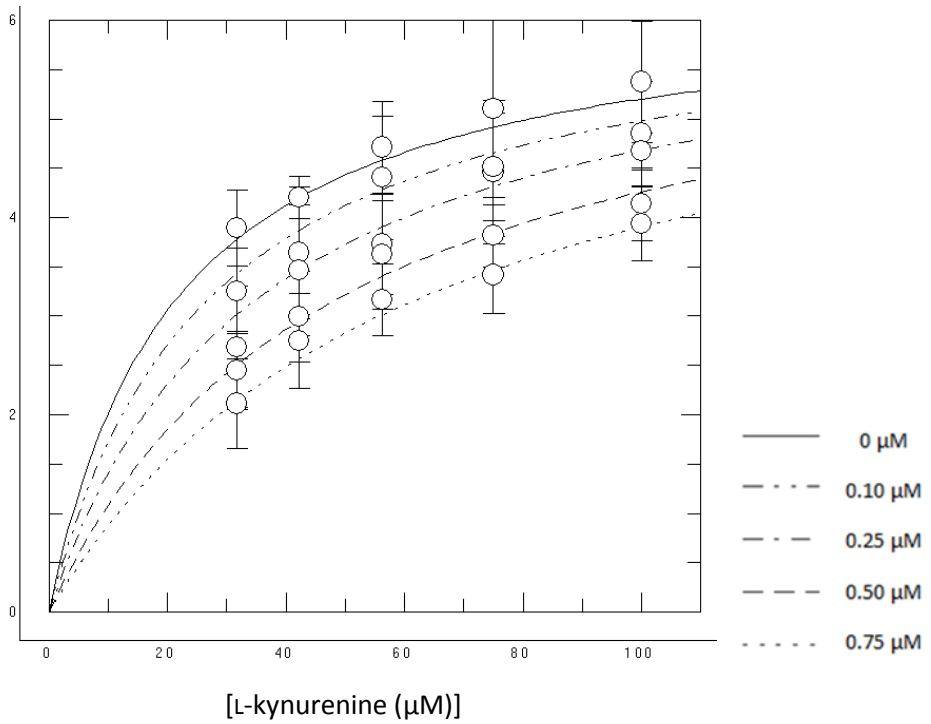

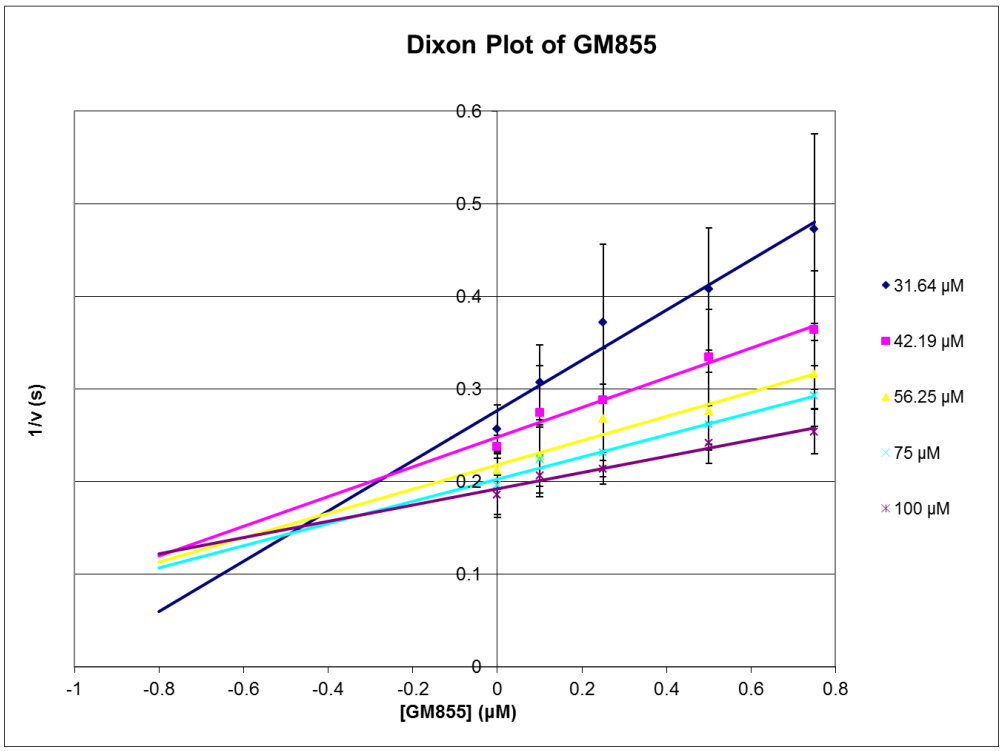

H320F *Pf*KMO* inhibited by GM859